MDC E0666

HIGH TEMPERATURE INSULATION MATERIALS FOR RERADIATIVE THERMAL PROTECTION SYSTEMS

FINAL REPORT

MCDONNELL DOUGLAS ASTRONAUTICS COMPANY - EAST

MCDONNELL DOUGLAS

(NASA-CR-123945) HIGH TEMPERATURE INSULATION MATERIALS FOR RERADIATIVE THERMAL PROTECTION SYSTEMS Final Report, 30 T.A. Hughes (McDonnell-Douglas Astronautics Co.) 19 Jul. 1972 171 p

N73-12957

Unclas
G3/33 16644

ABSTRACT

Results are presented of a two year program to evaluate packaged thermal insulations for use under a metallic radiative TPS of a shuttle orbiter vehicle. Evaluations demonstrated their survival for up to 100 mission reuse cycles under shuttle acoustic and thermal loads with peak temperatures of 1000°F, 1800°F, 2000°F, 2200°F and 2500°F. The specimens were composed of low density refractory fiber felts, packaged in thin gage metal foils. In addition, studies were conducted on the venting requirements of the packages, salt spray resistance of the metal foils, and the thermal conductivity of many of the insulations as a function of temperature and ambient air pressure. New data is also presented on the radiant energy transport through insulations, and back-scattering coefficients were experimentally determined as a function of source temperature.

FOREWORD

This report was prepared by McDonnell Douglas Astronautics Company - East, under Contract NAS 8-26115, National Aeronautics and Space Administration, Marshall Space Flight Center, Alabama. The work was performed under the direction of the Materials Division of the Astronautics Laboratory, with Mr. H. M. King acting as Contracting Officer's Representative.

The author acknowledges the assistance of R. J. Morford, T. M. Whitley, C. R. Johnson, G. L. Lacanski, and the many personnel of the Space Simulation Laboratory and Acoustics Laboratory. The valuable experimental work of R. M. F. Linford, R. J. Schmitt and C. F. Dillow of the Applied Optics Laboratory was greatly appreciated.

TABLE OF CONTENTS

LIST OF PAGES

Title Page
ii thru iv
1 thru 166

1.0 SUMMARY

The objective of this two year program was the development and evaluation of high temperature insulations and packaging materials for use under the radiative metal heat shield of a reusable shuttle vehicle. The insulation was to be capable of surviving the thermal loads and the acoustic/vibration loads associated with launch and reentry, for a minimum of 20 missions, and an ultimate goal of 100 missions. Minimum weight and cost were also important criteria. During the course of the program a total of 2700 specimen-cycles were completed, simulating launch acoustics/vibration and reentry heating to peak temperatures ranging from 1000°F to 2500°F. The 100 mission goal was achieved in 2200°F mission simulation, and with the insulations, but not the packages, in the 2500°F tests. In the latter case the packaging materials showed a life of 50 simulated missions, and provided indications that 100 missions is achievable with about 50% heavier coated columbium package material thickness. The test specimens for 1000° and 1800°F peak temperature service were tested for 80 cycles, and appeared fully capable of meeting the 100 mission goal.

The insulation concept used in this program was typically low density refractory fiber felts, enclosed in thin metal foil packages. The evaluation program also included the vent requirements for the packages, and techniques for inhibiting the entry of moisture through the vents.

An ancillary study was made to examine the potential for the reduction of thermal conductivity of HCF reusable surface insulation and led to significant new information on the role of infra-red transmission in high temperature insulations. I-R transmission studies were conducted on a number of insulations, in addition to HCF, and a more accurate mathematical model of radiation contribution to thermal conductivity was developed.

The results of the insulation evaluation program demonstrated the following capabilities:

Packaging Materials: For service up to 1000°F, titanium foil, 2 mils thick was satisfactory; for service to 2000°F, Inconel* 702, 3 mils thick, is preferred, but it degrades under heavy salt depositions. For slightly lower temperatures (1800°F), Hastelloy X and Inconel 601 were satisfactory, but did not appear to have the temperature overshoot capability of Inconel 702. Of the superalloys, only TD-NiCr (3 mil) provided good service at 2200°F. For 2500°F service, coated columbium gave good service for 50 missions, and indications were that longer life

*Registered trade names are listed in the Appendix.

could be achieved with greater thicknesses than employed here (5 mil columbium prior to coating).

Insulation Materials: For service up to 1000°F, most of the glass fiber felts provided acceptable service, though AA fiber products below 1.0 lb/ft^3 and B fiber products below 2.0 lbs/ft^3 density might present handling problems. For service up to 1800°F, silica fiber felts such as Astroquartz and Refrasil A-100 have performed satisfactorily for 80 reuses; Dynaflex was unsatisfactory only at low density, 3 lb/ft^3. Microquartz at 3.5 lbs/ft^3 density displayed some shrinkage that creates reservations about its use. Flexible Min-K demonstrated satisfactory performance to peak temperatures of 2200°F, and would be a desirable material for volume limited application. An experimental fibrous felt, Fiberfrax SKX had excellent performance at 2200° and 2500° peak temperatures. Astroquartz had surprisingly good dimensional stability to temperatures as high as 2500°F.

Venting and Moisture Entry: It was determined that a vent area of about 0.023% of the insulation surface area per inch of thickness of insulation is adequate. This would restrict deflections of the surface of 20 x 20 in. corrugation stiffened packages to 0.25 in. under conditions of ascent and reentry pressure changes. The use of 400 x 400 mesh wire cloth over the vent openings was found to be very effective in restricting moisture entry.

As part of a thermal analysis program, the thermal conductivity of a number of the felts used in this program was measured at several levels of pressure. This type of data has generally been lacking for these materials.

The complete details of the first year of study under this program have been previously reported in Reference (1). Many of the details of test equipment and procedures are reviewed in this final report, but for detailed information on the first year of study, Reference (1) should be consulted.

2.0 INTRODUCTION

The thermal protection system (TPS) is one of the most important space shuttle systems, and has a large impact on weight, development cost, and operating cost. It is also one of the major contributors to the uncertainties in weight and reuse predictions. In the metallic radiative TPS approach, the high temperature insulation, which must be placed between the metal heat shield panel and the primary structure, is an essential item.

The primary requirements for shuttle TPS insulation as defined in the scope of work for this contract were that it have the lowest density and thermal conductivity consistent with mechanical durability and thermal stability to withstand repetitive exposure to the shuttle operating environments, including acoustic, vibrational and thermal loads. Since the radiative skin is not likely to be weathertight, the insulation must not absorb moisture, or it must be protected from it. The insulation was to be capable of withstanding at least 20 cycles of exposure to nominal ascent and reentry conditions with an ultimate goal of withstanding 100 cycles of exposure.

The two year study described herein was performed to compare insulation materials and packaging techniques, and to provide information and data to assist the shuttle program in the selection and design of thermal insulations. To accomplish this, selected insulations were cyclically exposed to the shuttle environment of acoustic/vibration loads and thermal exposure at reduced pressure. The insulation concepts examined were generally low density refractory fiber felts (1 to 12 lb/ft^3) enclosed or packaged in thin gage, oxidation resistant metal foil, and rigid blocks, either in metal foil packages or incorporating a water-resistant refractory coating. The metal foil packaging concept has many advantages, including effective support and containment of light, nonrigid felts, protection from moisture, and versatile means of attachment to the structure. An impermeable package, such as metal foil, however, must be vented to accommodate the rapid pressure changes associated with launch and reentry.

The evaluation program was conducted by mounting five specimens (20 x 4 in) in a fixture, subjecting the assembly to multiple cycles of launch acoustics or vibration at ambient room temperature, and then to multiple thermal cycles at 10 torr pressure. During the initial evaluations all specimens were either 1.5 or 2.0 inches thick, and no attempt was made to optimize thicknesses. Later in the test

program, however, flight weight specimens designed for specific temperature constraints were evaluated.

The environmental definition for establishing the test parameters initially reflected the then current primary interest in the low cross-range orbiter. As the program progressed, however, the primary interest shifted to the high cross-range orbiter, and which influenced principally the thermal test profile. In establishing our thermal profile we had given considerable weight to the possible long cross-range reentries, and therefore the change in emphasis did not cause any perturbations to the program.

Ancillary studies were also made of compositional refinements to reduce the thermal conductivity of HCF reusable surface insulation. This included an in-depth study of the contribution of infra-red "shine-through" to the overall conductance of high temperature insulations. This provided guidance for reducing the conductivity of HCF and contributed to the understanding of the effects of I-R transmission in any high temperature insulation.

During the first year of this program, the thermal test equipment for insulation evaluation was designed and built, the test environment defined, and testing was conducted at the peak temperature of 1800°F and 2200°F. The tests at 1800°F (80 cycles) were highly successful. However, in the 2200°F testing, the superalloy packaging materials were generally inadequate, except for one metal, TD-NiCr. During the second year of the program, testing was continued at 2200°F and extended to 2500°F, and 1000°F. The evaluations were concluded with test specimens designed to provide a 300°F maximum temperature on an aluminum structure behind the insulation, while the radiative skin was cycled up to the given maximum service temperature.

Also during the second year, studies were made of the venting necessary to prevent the packages from deforming excessively under the ascent and reentry pressure changes, and of techniques to reduce moisture entry through the vents.

Insulations employed in shuttle service will experience the main heat pulse under conditions of low air pressure, and for which little thermal conductivity data is available. To rectify this situation, the thermal conductivity of a number of promising materials was measured at several levels of air pressure.

3.0 PACKAGED INSULATIONS

During the second year of this program, simulated shuttle mission cycle tests were conducted on a variety of insulations and metal foil packaging with maximum service temperatures of 1000°F, 2200°F, and 2500°F. In addition, flight configuration packages were designed and tested in which realistic thicknesses were employed to obtain a 300°F maximum temperature on an aluminum structure mounted behind the insulation package, with a variety of insulation densities and thicknesses. The problem of venting the package to accommodate rapid pressure changes, and prevent moisture intrusion was also studied. The results of these tests are described in the sections which follow. Ancillary studies on the salt spray resistance of the packaging materials, their emittance after thermal exposure, and the thermal conductivity of a number of low density insulations are also described. The latter were measured as a function of ambient air pressure and mean temperature.

3.1 Environment Simulation and Test Procedures - The test procedures employed for evaluation of packaged insulations during the second year of the contract subjected the specimens to a block of 10 cycles of launch acoustics, followed by a block of 10 cycles of reentry thermal exposure. This procedure was a minor change from the procedure employed during the first year of the program (Ref 1), in which the environments were applied in blocks of 5 cycles, and in which vibration was employed in alternate blocks in lieu of acoustics. Experience during the first year indicated that the acoustic exposure was more severe in its effects than the mechanical vibration.

The most severe acoustic loads occur during the ascent phase, in conjunction with a very modest heating period. During reentry, the situation is reversed, a severe thermal pulse of considerable duration, and with a moderate acoustic load. To simulate these environments, the test specimens were subjected to acoustic/vibration loads at ambient room temperature and pressure, and to thermal loads at reduced atmospheric pressure, reflecting the low ambient pressures associated with the high altitude of entry.

3.1.1 Acoustics Environment - The major source of mechanical excitation on the shuttle vehicle is the noise from the main propulsion engines, which results in an acoustic load on the TPS skin. The acoustic environment experienced by the internal insulation is modulated by the vehicle skin, though the degree of modulation is uncertain. In addition, response of the skin to the acoustic excitation

may be transmitted to the insulation via the structural supports in the form of mechanical vibration.

Peak lift-off noise external to the aft portion of the booster was estimated from empirical considerations to be 169 dB (0.82 lbf/in^2), and the transonic buffeting near the booster-orbiter interface, 155 dB (0.164 lbf/in^2). The most significant excitation ends before appreciable heating of the insulation occurs. Peak noise external to the orbiter is estimated to be 0.33 lbf/in^2 (161 dB), at lift-off, decaying to 0.13 lbf/in^2 (153 dB). Because the use of internal TPS insulation was expected to be primarily in the orbiter, the maximum power available from the test equipment (156 dB) was considered adequate for evaluation purposes. It was assumed that the mated vehicles would pass through Mach 1.0 at about 30 seconds, after which time the vehicles would be essentially free of the acoustic noise field.

Reentry acoustic excitation for the orbiter was estimated to be 113 dB (0.0013 lbf/in^2), or less than 0.2% of that occurring during launch. This peak occurs about 10 minutes after peak reentry heating when the surface temperature has cooled considerably. The estimate for noise level during reentry was based on data from the ASSET reentry (Ref 2) and from the NASA-Langley wing stall flutter and buffet response study (Ref 3).

The acoustic noise spectrum specified for test purposes is shown in the table below, and was applied for 300 seconds in each test, representing 10 launch cycles.

RANDOM ACOUSTIC NOISE SPECTRUM

Octave Band Hz	dB Re 0.002 dynes/cm^2 rms	Tolerance dB
23.8 - 47.2	133.7	+6, -2
47.2 - 92	139.3	+6, -2
94 - 188	142.7	+5, -1
183 - 375	146.8	+4, -1
375 - 750	150.7	+4, -1
750 - 1500	144.0	+5, -1
1500 - 3000	139.7	+6, -2
3000 - 6000	133.2	+6, -2
Overall	154.0	+4, -0

The noise source consisted of a Wyle WAS-3000 airstream modulator coupled to an exponential horn having a 50 Hz low frequency cut-off. The modulator was rated at 10,000 acoustic watts. A general view of the acoustic test arrangement is shown in Figure 1. The 20 inch dimension of the specimens was purposely placed in the vertical plane to simulate launch orientation and which provides for representative excitation and resultant settling of the insulation.

The acoustic spectrum and power level achieved during testing was monitored with a reference microphone. Representative data is shown in Figure 2 along with the tolerance permitted under the approved plan. A traverse across the opening of the exponential horn indicated that the spectrum-power level was uniform across the face within the tolerance band.

3.1.2 Thermal Environment - A wide range of time-temperature histories are possible, depending on the various shuttle trajectories, vehicle body stations, and configurations. For the purposes of this test program, one general profile was selected that would adequately test the response of the insulation to its environment, be reasonably representative of current and foreseeable heat pulses, and be economical in test time.

From an insulation materials viewpoint, the precise shape of the thermal pulse is not as important as the time at or above various temperatures. However, the initial heating rate should be representative of the actual thermal shock the insulation will experience in service. By utilizing a generalized time-temperature profile that was not unique to any specific trajectory or body station, insulation performance comparison could also be applicable to a broader range of uses.

An analysis was made of the various heat pulses that would be encountered by shuttle orbiters, and which provided a basis for the simplified thermal profile for test purposes. This profile was most strongly influenced by the long cross-range delta orbiter. Details of this analysis were reported in Ref 1.

The time-temperature profiles used in the current year's testing are illustrated in Figure 3, and are comparable to the ones used in the previous year's testing (Ref 1).

It was not possible to define closely the ambient pressure of the atmosphere surrounding the insulation, due to lack of adequate data on heat shield air leakage rates. Prior to entry into the atmosphere, the insulation will be in a high vacuum environment, and the pressure environment external to the vehicle will build up at a slower rate than the thermal pulse. However, the rate at which the

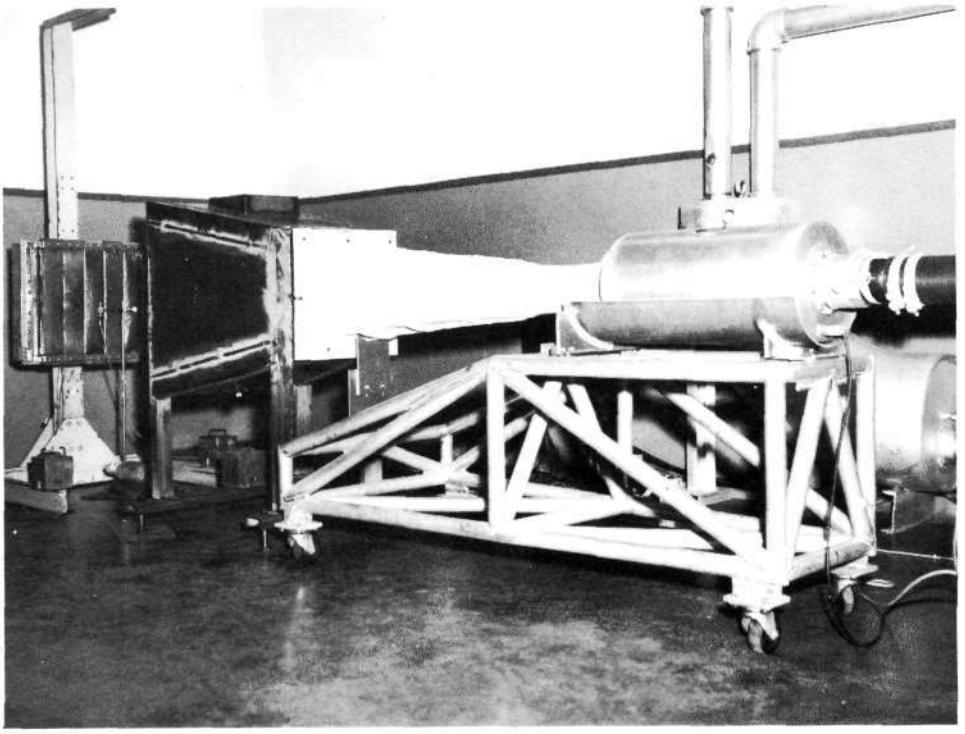

457-1127

ACOUSTIC TEST SET-UP WITH SPECIMENS IN PLACE

Figure 1

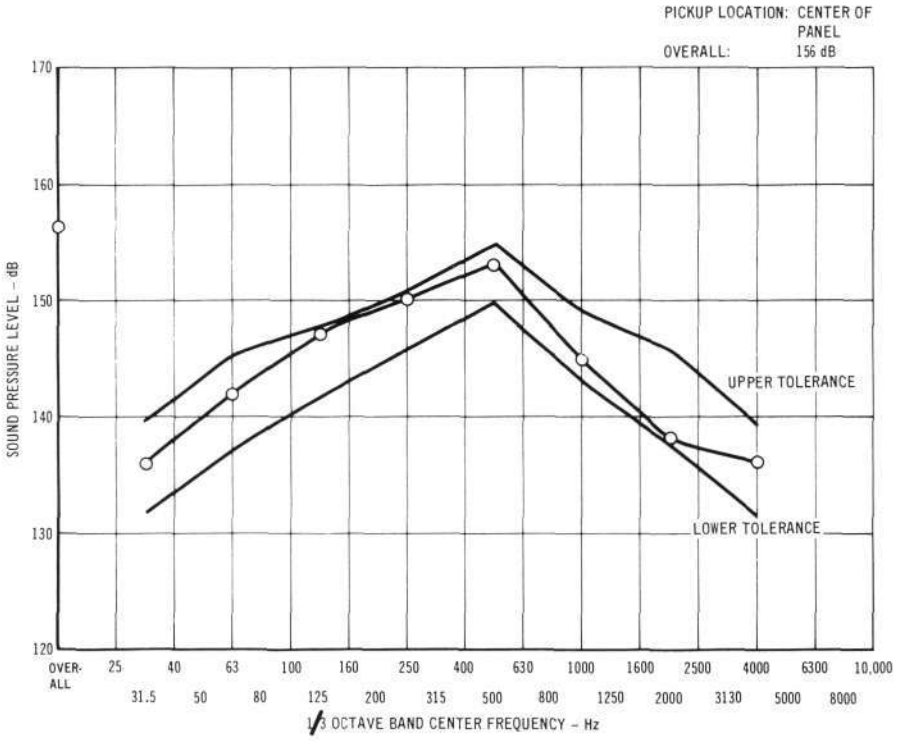

457-1126

OCTAVE BAND SPL DISTRIBUTION

Figure 2

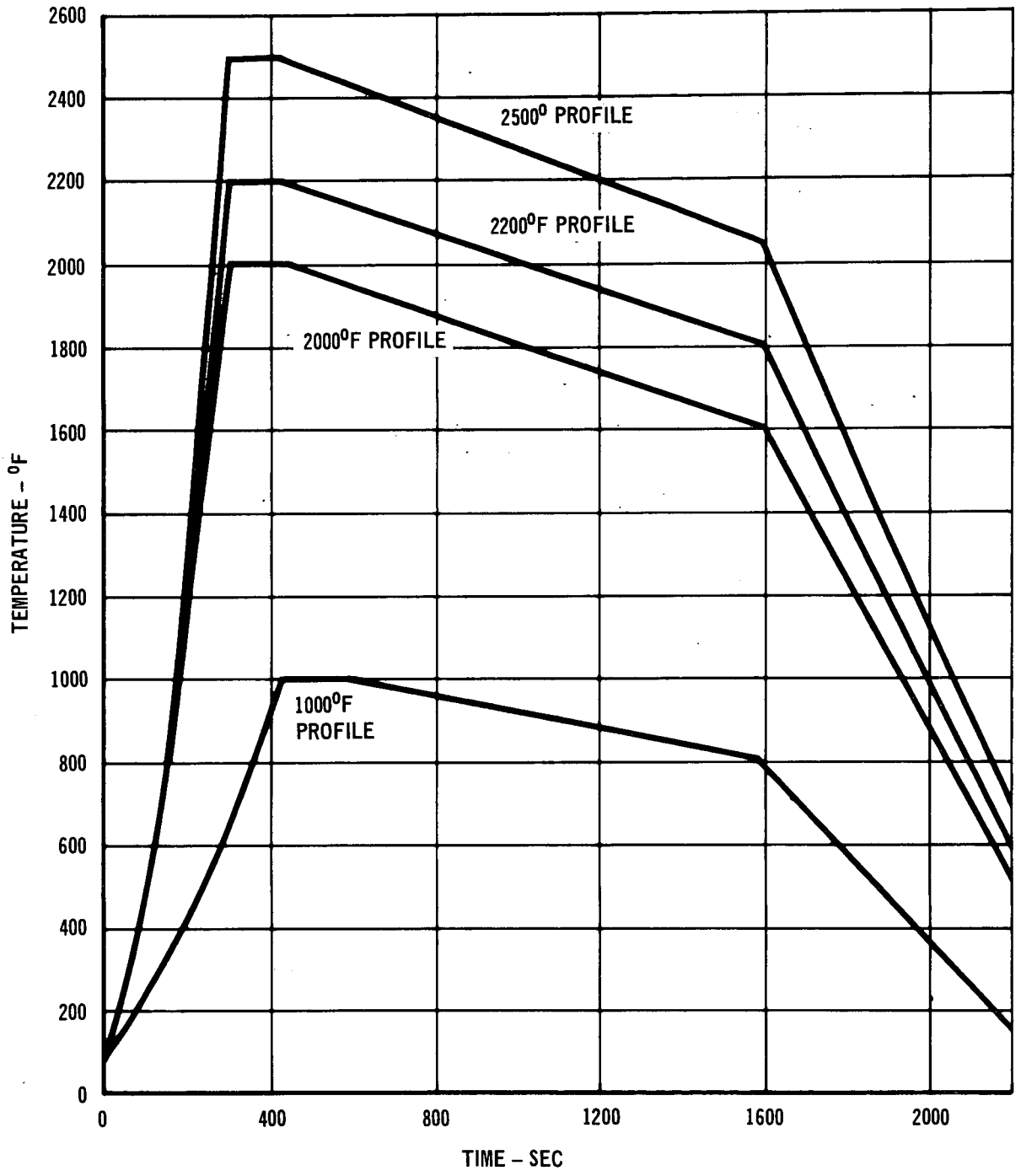

457–3118

TIME–TEMPERATURE PROFILES FOR THERMAL TESTING

Figure 3

increased air density penetrates into the insulation could not be predicted accurately. For test purposes, we utilized a constant pressure of 10 torr.

The equipment for providing the thermal pulse to the specimens at low air pressures is the same as previously described in Ref 1. The heater was essentially a coated columbium plate radiating to the specimens, with the entire assembly mounted in a vacuum chamber. The columbium plate, usually referred to as a susceptor plate, was itself heated by radiation from 24 graphite resistance heaters. The susceptor plate simulated the metallic skin of the radiative TPS and also served to close off the graphite heater cavity from the specimen area. The graphite heaters were bathed in low pressure nitrogen to prevent oxidation, while the specimens were in a fresh flowing air atmosphere to permit oxidation of the metal foil packaging. A sketch of the test arrangement is shown in Figure 4, and exterior views of the chamber in Figures 5 and 6. A more detailed description of the thermal test facility has been reported in References 1 and 4.

This heater system has demonstrated its effectiveness and reliability. During the course of this program it has been used for over 800 thermal cycles without significant problems. Graphite elements have been replaced only as preventative maintenance.

3.1.3 Test Specimens - The basic test specimens consisted of low density felts enclosed in thin gage metal foil packages. The specimens were 3.85 inches wide, 20 inches long, and 1.5 inches thick. The usual metal foil package was a simple box shape with the hot and cool skins extended to provide tabs for mounting in the test fixture; however, other package configurations were also tested, as described later. The cool face of the box and the end closures were attached by spot welding. In many cases the necessary width of flat sheet for forming the boxes was obtained by seam welding narrow strips. To permit the package to breathe during pressure changes in the vacuum chamber, holes were provided in the cool face.

Three thermocouples were installed in each specimen near the center. One was about 0.1 inch from the hot surface, the second one at the center of the thickness, and the third about 0.1 inch from the cool surface. The position of the thermocouples has to be qualified because in inserting the thermocouples, there was no assurance that they would not drift to one side or the other. After assembly, the package was x-rayed to determine the final position of the junction.

The flight configuration test specimens were 10 x 20 in., larger than the basic test specimens, and of sufficient thickness to provide realistic service temperatures at the cool side. These specimens were also more thorough instrumented. They are described in greater detail in Section 3.6.

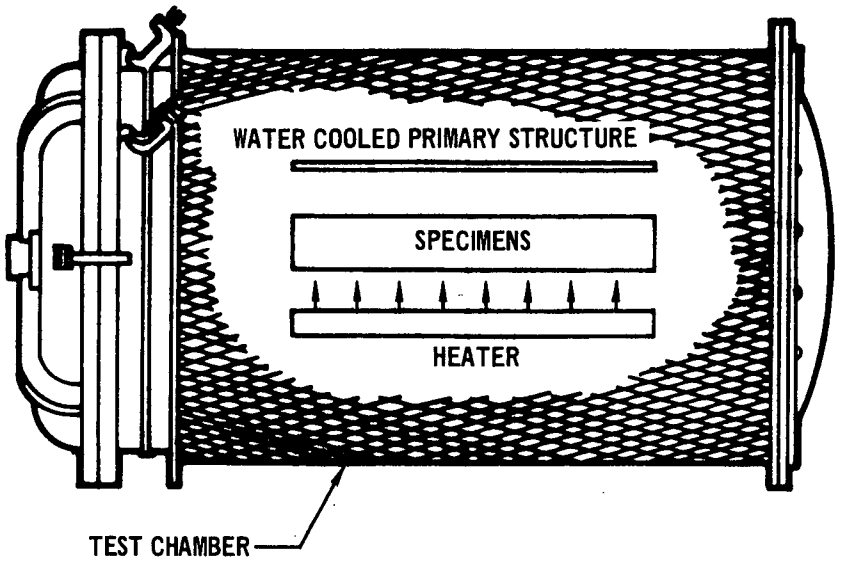

457-3119

THERMAL TEST SETUP

Figure 4

3.2 Venting and Moisture Condensation Studies - During ground operations of the shuttle vehicle and during flights within the atmosphere, the vehicle will be occasionally exposed to moisture, which may penetrate through joints or other openings in the vehicle skin. In addition, prior to launch, it likely will be exposed to fluctuating ambient temperatures and high humidity, and with cryogenic propellant on-board, a high potential for cryogenic condensation will be present. Prevention of moisture entry into the insulation is important because in addition to its effect on the physical properties of the insulation, it can also introduce a high amount of unneeded mass to the vehicle which might seriously affect its payload capability. The ideal construction of packaged insulation to prevent moisture intrusion would be the use of hermetically sealed packages. This has never been seriously considered, of course, as it would impose a severe weight penalty in structural requirements for the metal foil packages.

The approach taken in this program has been to allow the package to breathe through vents to accommodate the changes in ambient pressure during launch and reentry, but with vent area restricted to a minimum to prevent excessive moisture entry.

3.2.1 Venting Studies - The venting study approach used in this program was:

- o Allowable pressure differential on the package was based on the permissible package deflection (ballooning and compression)
- o Launch and reentry time/pressure profile was used

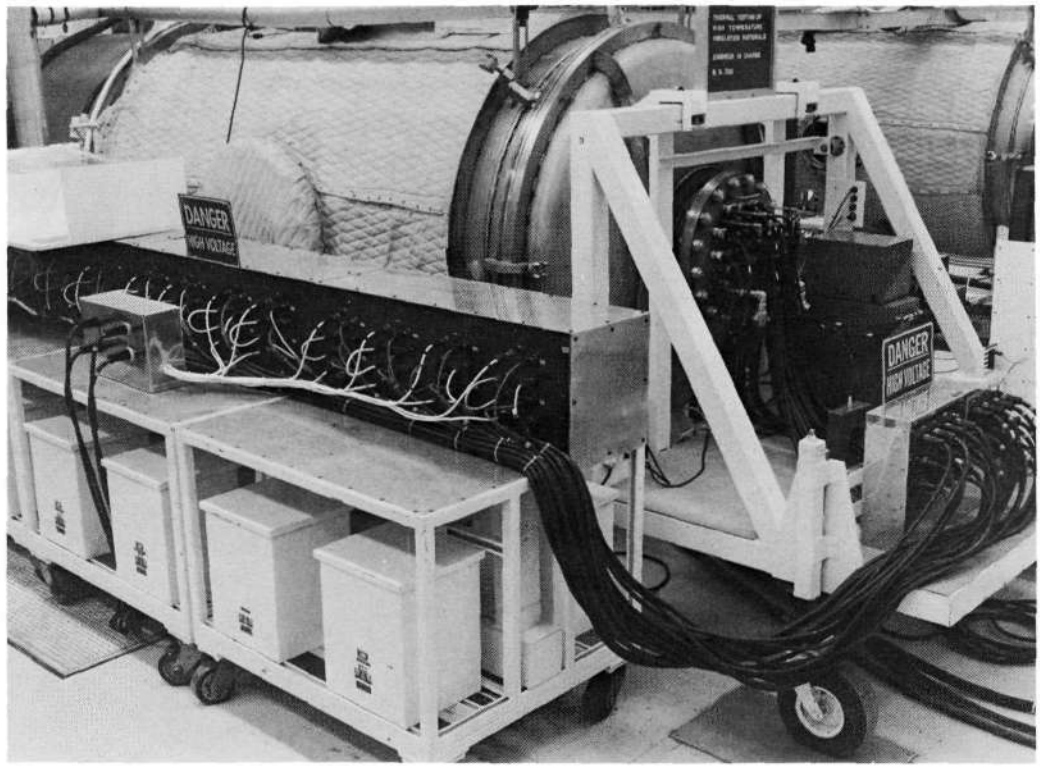

Figure 5

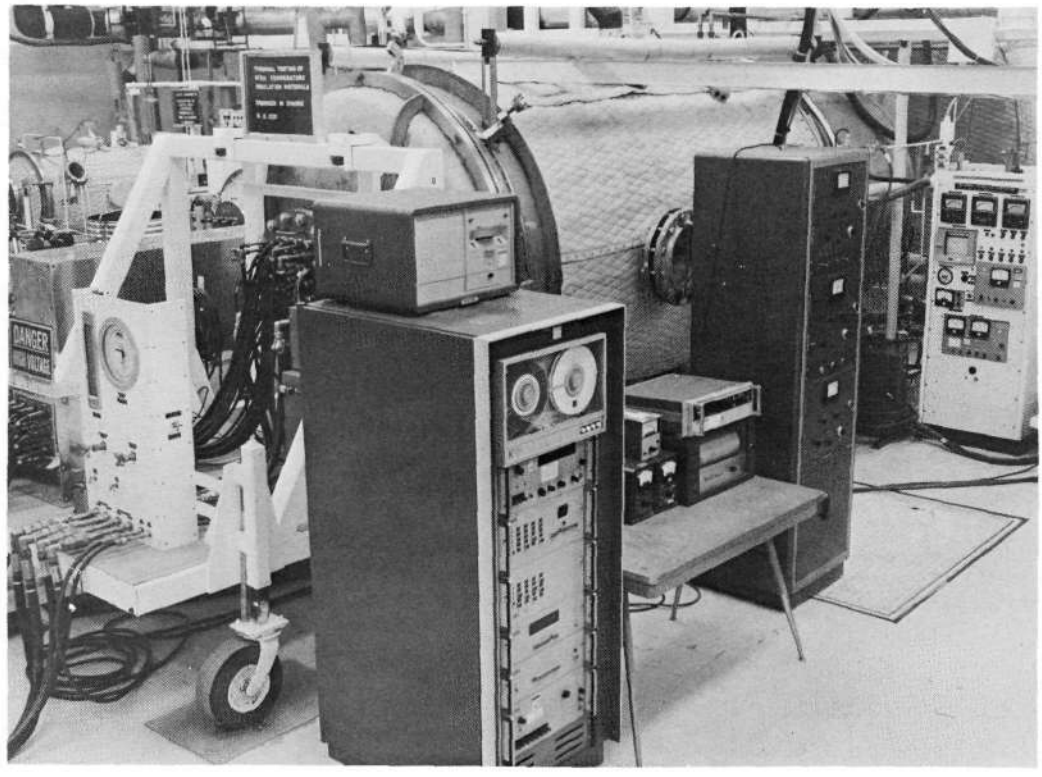

VIEWS OF VACUUM CHAMBER FOR THERMAL TEST WITH INSTRUMENTATION AND CONTROLS

457-1132

Figure 6

- o Vent area required to provide low pressure differentials was calculated
- o Verification testing was used to define the number and size of orifices, and total vent area.

Subsequent testing included moisture migration through the vents under representative ambient temperature/humidity conditions with cryogenic temperatures on the cool side of the insulation package. A technique for restricting moisture intrusion through the vents was also examined.

The vent requirements were based on a proposed prototype package design in which the hot surface of the package was corrugated to resist long term 10g loads during reentry maneuvers. The corrugations limited hot surface displacements to 0.25 inch under the specified load, assuming an insulation package 20 by 20 inches. The corrugations were 0.25 inch peak-to-peak amplitude and 1.25 inch wavelength, formed as intersecting circular arcs. To limit displacement under ascent decompression and entry compression to the same maximum deflection, maximum permissible pressure differential was calculated to be 0.07 psi. The pressure differentials were based on the proposed launch and entry trajectories for a delta wing orbiter with 1100 N.M. cross-range capability with modulated angle of attack during reentry. The altitude, velocity, and ambient pressure histories used are shown in Figures 7 and 8.

To prevent the pressure differential across the package face from exceeding the established amount (0.07 psi), the required vent area was calculated based on the simulated flight pressure history (discussed below) assuming isentropic subsonic flow through the vent orifices, with a discharge coefficient of 0.61. The pressure external to the package was assumed to be the same as that experienced by the outer skin of the TPS (i.e., pressure aft of the bow shock during reentry) with no time lag or reduction in pressure caused by leakage through the outer skin.

The maximum pressure differential was found to occur during ascent, approximately 60 seconds after launch. Figure 9 shows the estimated maximum differential pressure as a function of orifice area divided by package volume. Figure 9 shows that for a package 20 x 20 x 3 inches thick, a minimum orifice area of 0.054 square inch is required, which would be equivalent to a single hole 0.262 inch diameter. Based on experience on earlier parts of the program, this area was expected to be inadequate.

3.2.2 Vent Tests - For test purposes, the ascent and entry simulation pressure-time profile shown in Figure 10 was utilized. This was derived from the predicted delta wing orbiter pressure history (Figure 8) except that the lengthy

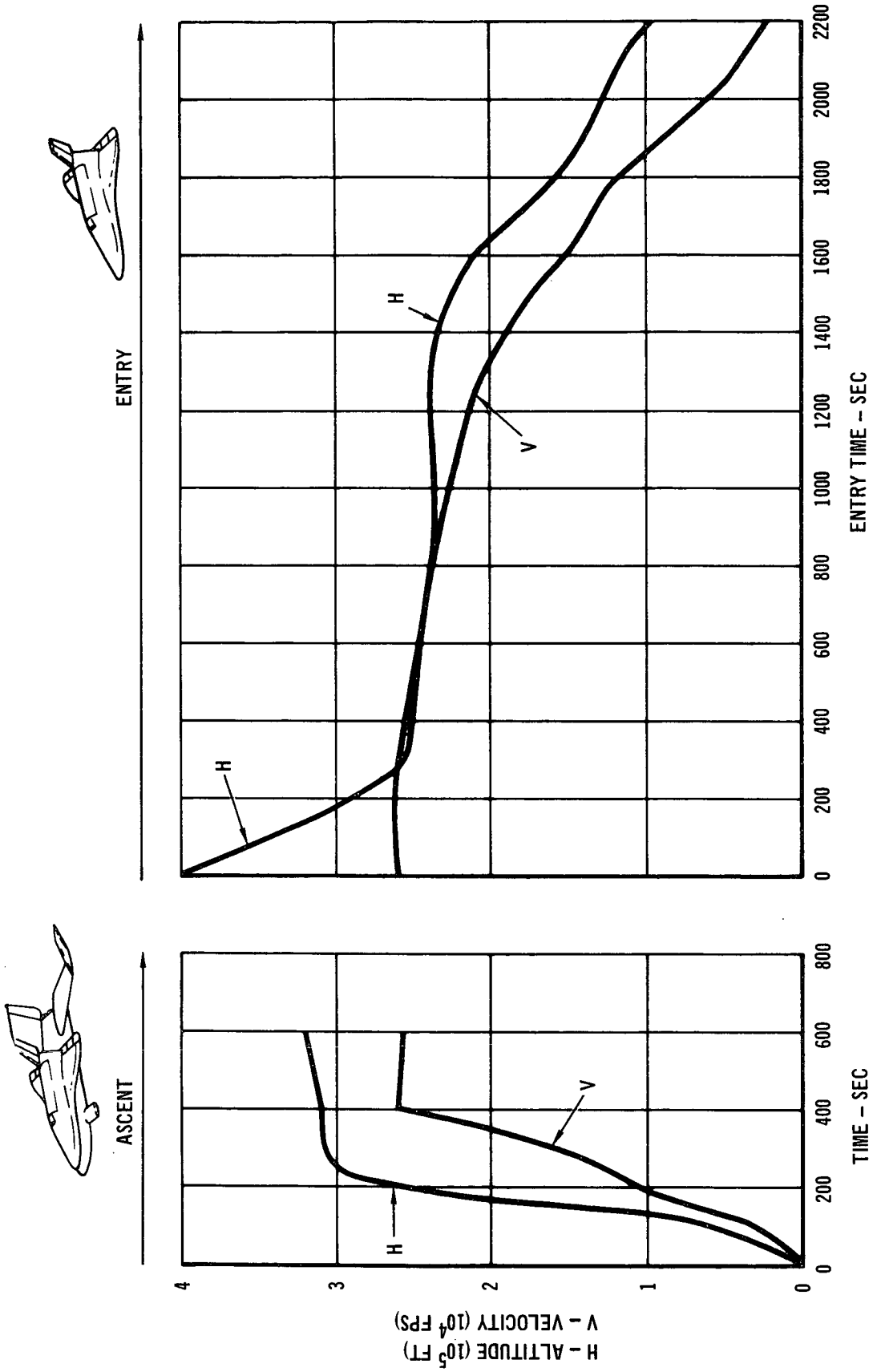

LAUNCH AND ENTRY TRAJECTORIES FOR THE DELTA WING ORBITER

457-1841

Figure 7

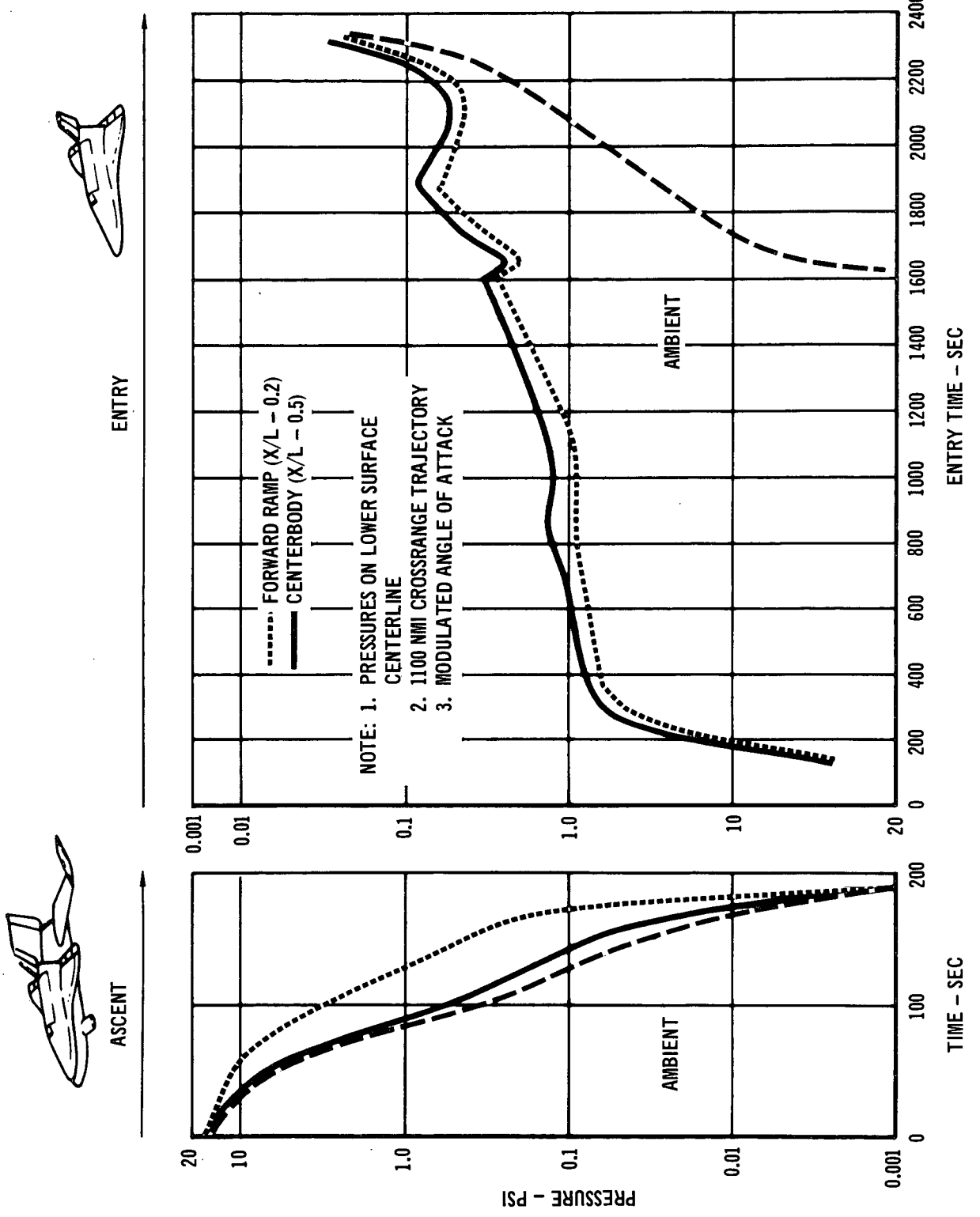

DELTA WING ORBITER LOWER SURFACE PRESSURES

Figure 8

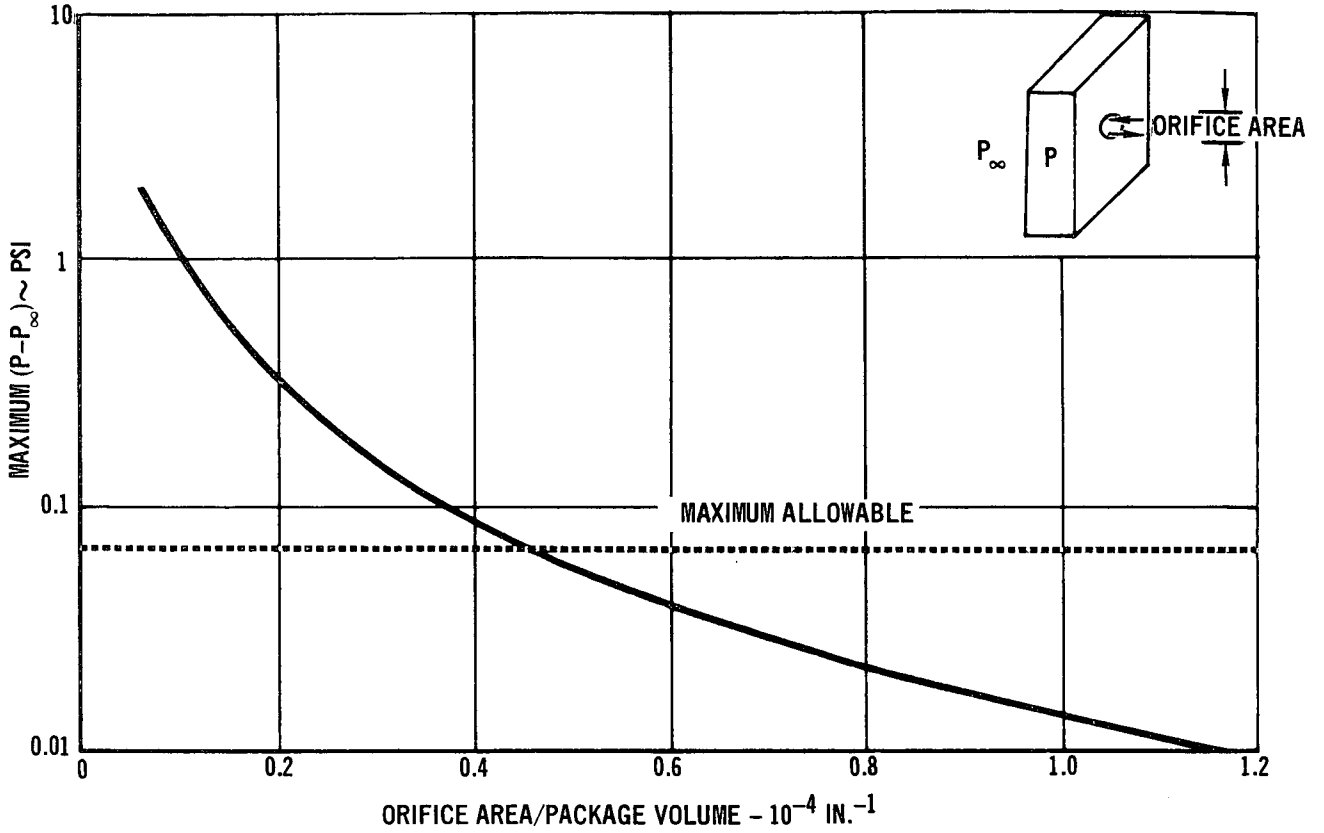

457-3120

MAXIMUM ASCENT DIFFERENTIAL PRESSURE

Figure 9

period of small rate or pressure change during the entry (from 300 to 2200 sec, Figure 8) was omitted, and the minimum ambient pressure was not taken below 1 torr. At that low level of total pressure, the pressure difference is insignificant.

The vent tests were conducted in a 5.5 foot diameter space simulation chamber equipped with a viewing port. This chamber was similar to the one used for thermal testing, but had a higher vacuum pumping capacity to allow shuttle ascent pressure change simulation. The test specimen was a 20" x 20" x 3" thick package made of 2 mil Hastelloy X with a corrugated "hot side". The 3 inch thickness was chosen as representative of expected package thicknesses in service. The package hot side was corrugated to conform with the probable prototype configuration which requires restricted deflection during 10g maneuvers. The package was filled with 6 lb/ft^3 Dynaflex insulation, which was selected to provide a realistic impedance to air flow and produce pressure drops similar to those expected in actual flight. Fiber surfaces may also contain absorbed gases at one atmosphere pressure, which could be released during evacuation, thereby affecting the package pressure.

The cold side of the package had 100 3/16" diameter vent holes. As testing

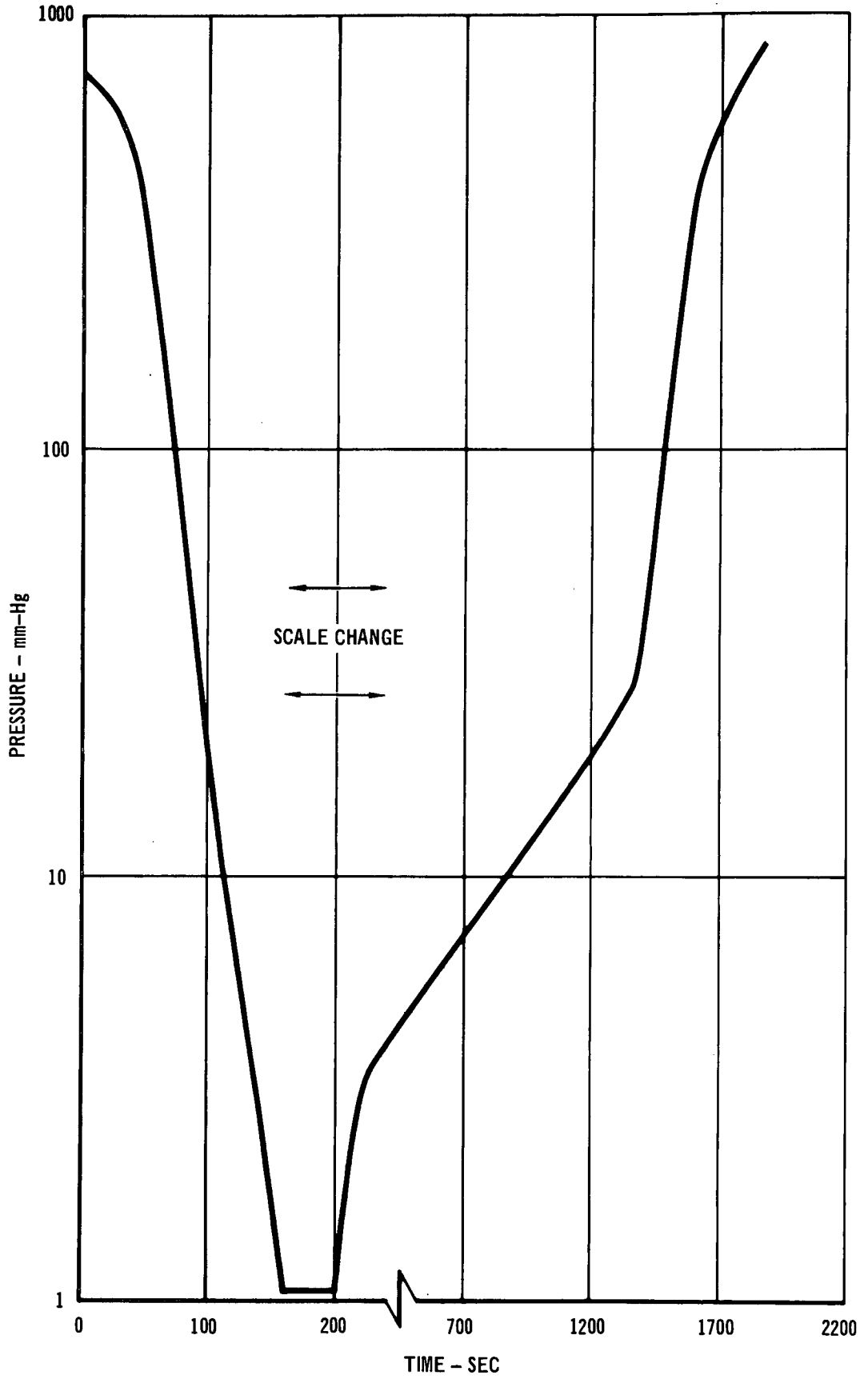

457–3121

ASCENT AND REENTRY SIMULATION PRESSURE – TIME PROFILE

Figure 10

progressed, holes were covered until the minimum number of holes for a maximum of 1/4" of hot side package deflection was obtained.

To monitor the package performance under the simulated flight pressure environments, the vacuum chamber pressure and the differential pressure between the chamber and the interior of the package were measured as well as "hot" surface deflection. An Alphatron Vacuum Gauge, Type 530, was used to measure the chamber absolute pressure (a multiple decade instrument with full scale ranges from 10^{3} to 10^{-4} torr), and a Baratron, Type 77, with a 100 torr head was used for differential pressure. The accuracy of the Alphatron was $\pm$4% of full-scale, and the Baratron $\pm$0.05% of full-scale. The "hot" surface deflection was measured by two techniques. One method employed a Physitech Optical Tracker which when centered on a high contrast optical discontinuity, will follow and record the displacement of the discontinuity. This system has a sensitivity to detect displacements as small as 0.0004 in. The alternate technique was to record the relative movement of the tracker target against a stationary string behind the target at selected time intervals (usually 2 seconds) by a motorized 35 mm Nikon camera. A digital clock was included in the camera view to provide a time base. The target, viewed by both tracking devices, was attached to the "hot" surface as shown in Figures 11 and 12. During the actual tests the test specimen, mounted on the forks attached to the vacuum chamber door, was viewed by the optical tracker and camera through a port in the wall of the vacuum chamber. In initial runs an early movement of the "hot" surface of 30 mils was detected by the optical tracker, but not by visual or photographic recording. This was caused by compression of the door seal of the chamber as the chamber was pumped down. Since the test specimen was mounted on the door, this compression was reflected as surface movement by the optical tracker though actually the entire specimen moved. The photographic records did not show this movement as the reference (a vertical string directly behind the target) was attached to the supporting frame which also moved. When an appropriate correction was made to the optical tracker data, the two methods were in agreement throughout the tests.

The design of the corrugation stiffeners for the package "hot" surface was based on intersecting circular arcs with a peak-to-peak amplitude of 0.25 inch, and a wavelength of 1.25 inches. The stiffeners were approximately 17 inches long and blended to the flat face near the ends over a distance of approximately 0.5 inch. However, the corrugations did not form as well as expected, resulting in an amplitude of about half the design value. This also resulted in much higher

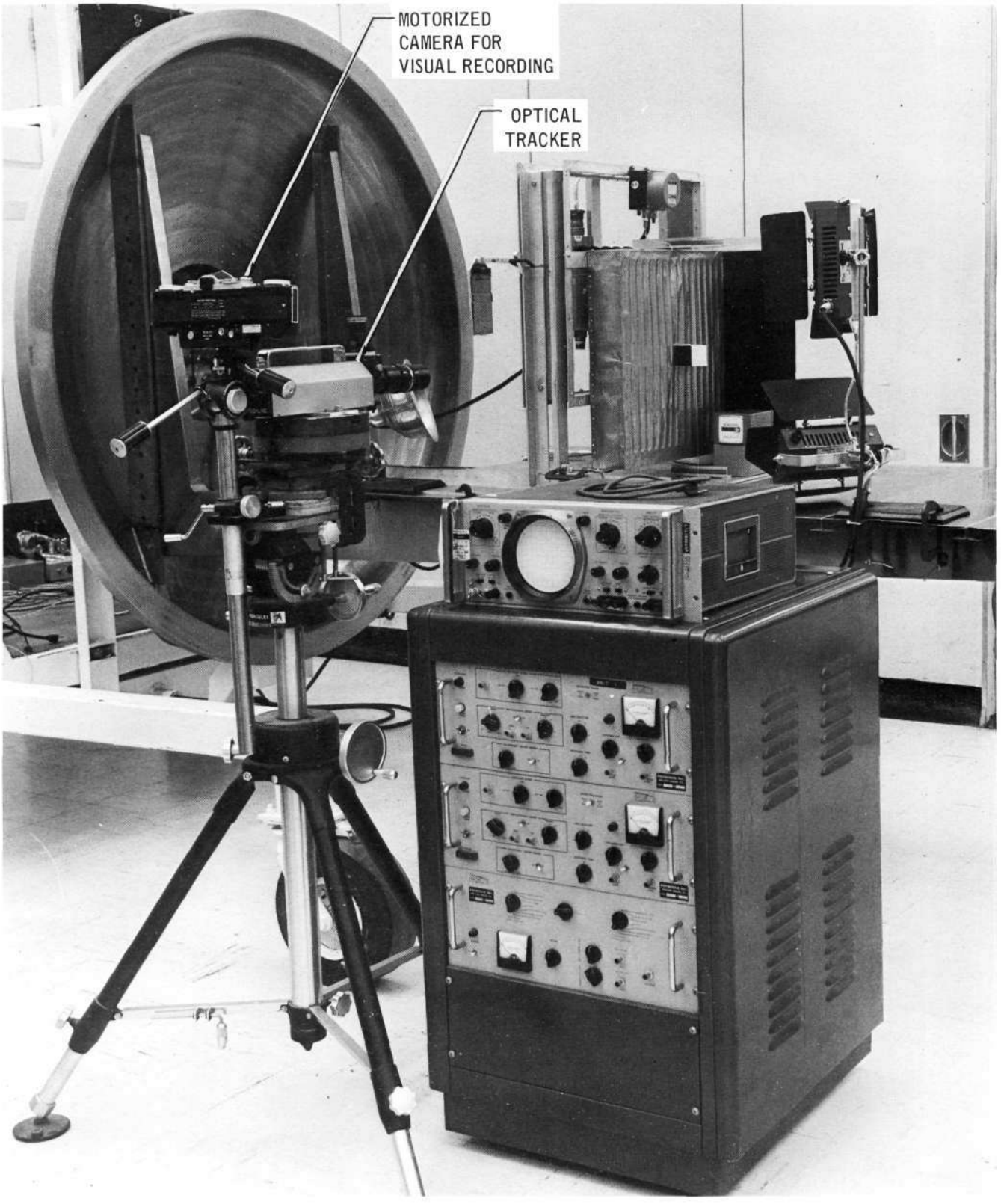

VENT TEST SET-UP – SPECIMEN WITHDRAWN FROM VACUUM CHAMBER

457 – 2380

Figure 11

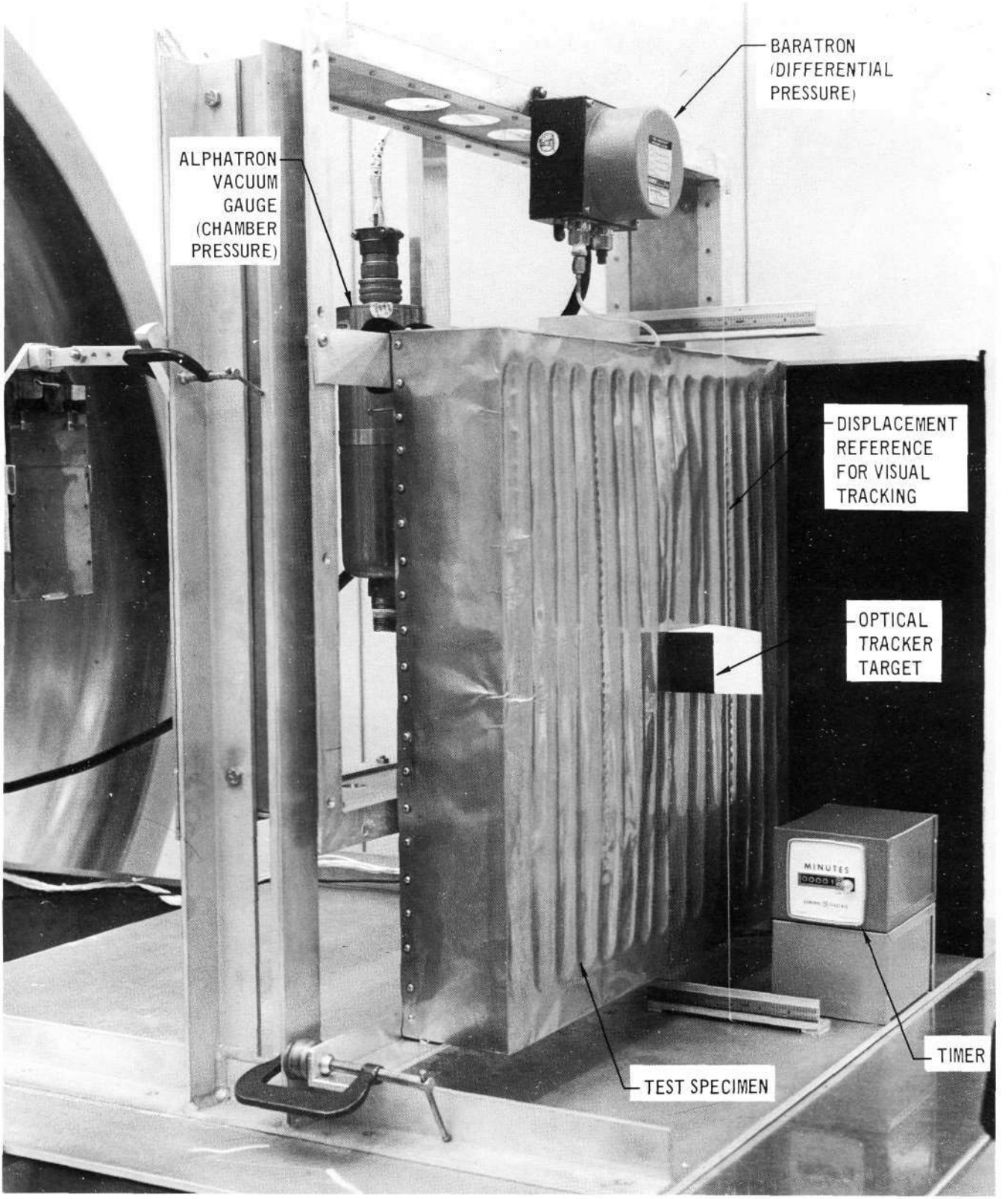

VENT TEST INSTRUMENTATION DETAILS

457 –2 38 1

Figure 12

deflections for a given pressure differential.

A summary of the open port vent tests is presented in Table I. In this series, testing was initiated with 100 - 3/16 in. diameter holes in the "cold" face. These were subsequently taped over to provide 50, 25, 10 and 5 holes. The same ascent and reentry pressure histories (Figure 10) was used in all tests. Correlation of the deflection of the stiffened "hot" surface to the total vent area is shown in Figure 13. About ten holes of 3/16 in. diameter were required to provide less than 1/4 in. deflection. The corresponding peak differential pressure with this number of holes (Table I) was about 0.20 torr. This was a considerably lower ΔP than originally expected (0.07 psi or 3.6 torr) and is attributed to: (1) not obtaining the full design depth of the corrugations, and (2) blending the corrugations to flat sheet at the ends, resulting in a much different moment of inertia.

Typical pressures, differential pressures and deflection plots are shown in Figures 14 and 15 for 10 vent holes (Test 4) for simulated ascent and reentry. It had been expected from prior calculations that maximum deflection and ΔP would occur about 60 seconds into the launch cycle. This actually occurred between 40 and 55 seconds into the simulated launch. The data also indicated that the maximum ΔP across the "hot" face did not occur simultaneously with the maximum deflection. This anomaly was due to the error in the optical tracker due to compression of the door seal. The magnitude of this error increased as pressure was reduced within the chamber and only the maximum value was applied to the data. This would alter slightly the shape of the time-deflection curve.

In Figure 14, it will be noted that considerable dispersion of the differential pressure data points occurred early in the launch cycle. This is believed to be the result of minor flow pulsations from the mechanical pumps during the high pump-down rate, with the ΔP measured by very sensitive gages (ΔP of less than 0.1 torr at a pressure of about 600 torr). When the pressure was below about 100 torr, the pulsations were well dampened.

A slight compression of the package was indicated on simulated reentry (Figure 15), which was, as anticipated, considerably lower in magnitude than the expansion during the launch cycle.

Two techniques were evaluated to provide restriction to moisture entry during static periods on the ground, due to changes in temperature and humidity and air-entrained moisture. The first technique employed Teflon pressure sensitive tape placed over the vent holes and cross-slit over the opening, with the intent that

Table I

VENT TEST DATA

TEST NO.	VENT CONFIGURATION	MAXIMUM DEFLECTION (HOT SIDE) (IN.)	PEAK DIFFERENTIAL PRESSURE (TORR)	COMMENTS
1	100–3/16 IN. DIA HOLES	–	–	VISUAL DATA ONLY – NEGLIGIBLE DEFLECTION
2	50–3/16 IN. DIA HOLES	0.08	–	35 MM PHOTOGRAPHIC DEFLECTION DATA ONLY
3	25–3/16 IN. DIA HOLES	0.13	–	35 MM PHOTOGRAPHIC DEFLECTION DATA ONLY
4	10–3/16 IN. DIA HOLES	0.21	0.20	OPTICAL TRACKER OPERATIVE AND ITS DEFLECTION AGREED WITH PHOTO DATA
5	10–3/16 IN. DIA HOLES	0.26	0.20	ALL INSTRUMENTATION PERFORMED PROPERLY. SAME AS TEST NO. 4, TO DETERMINE REPEATABILITY
6	10–3/16 IN. DIA HOLES	0.20	0.19	SAME AS TEST NO. 4, TO DETERMINE REPEATABILITY
7	5–3/16 IN. DIA HOLES	0.34	0.17	
8	10–3/8 IN. DIA PORTS COVERED WITH 5 MIL TEFLON CUT WITH A CROSS PATTERN FOR VENTING	–	0.44	TESTING TERMINATED EARLY DUE TO EXCESS DEFLECTION OF OVER 1/2 IN. THIS TEST APPARENTLY WEAKENED THE CORRUGATED SURFACE WHICH RESULTED IN INORDINATE DEFLECTIONS FROM THIS TEST ON
9	10–1/2 IN. DIA PORTS COVERED WITH 5 MIL TEFLON CUT WITH A CROSS PATTERN FOR VENTING	0.57	0.07	INSTRUMENTATION PERFORMED PROPERLY. EXTREMELY LOW DIFFERENTIAL PRESSURE AT DEFLECTION BELIEVED TO BE DUE TO PRESSURE DROP AS CORRUGATED SURFACE SNAPPED OUT
10	–	–	–	"INSTRUMENTATION CHECK" TO VERIFY DIFFERENTIAL PRESSURE READINGS – CHECKED GOOD
11	7–1/2 IN. DIA PORTS COVERED WITH 5 MIL TEFLON CUT WITH A CROSS PATTERN FOR VENTING	0.54	0.13	DEFLECTION LESS THAN WITH 10 SIMILAR PORTS. THIS INDICATES PRESSURE IS NOT SUFFICIENT TO PROPERLY OPEN THE TEFLON PARTS
12	20–3/16 IN. DIA PORTS COVERED WITH 400 MESH SCREEN (APPROX 36% OPEN AREA IN THE SCREEN)	0.62	0.12	RESULTS SHOULD NOT BE COMPARED TO DATA FROM TESTS PERFORMED PRIOR TO TEST NO. 8
13	SAME AS FOR TEST NO. 12	0.57	0.11	BASICALLY THE SAME AS TEST NO. 12 TO DETERMINE REPEATABILITY
14	10–3/16 IN. DIA PORTS COVERED WITH 400 MESH SCREEN (APPROX 36% OPEN AREA IN THE SCREEN)	0.74	0.30	DATA AS EXPECTED
15	SAME AS FOR TEST NO. 14	0.72	0.35	BASICALLY THE SAME AS TEST NO. 14
16	15–3/16 IN. DIA PORTS COVERED WITH 400 MESH SCREEN (APPROX 36% OPEN AREA IN SCREEN)	0.67	0.18	DATA AS EXPECTED – VALUES IN BETWEEN THOSE OF THE 10 AND 20 PORT TESTS
17	SAME AS FOR TEST NO. 16	0.60	0.21	DATA AS EXPECTED – VALUES IN BETWEEN THOSE OF THE 10 AND 20 PORT TESTS

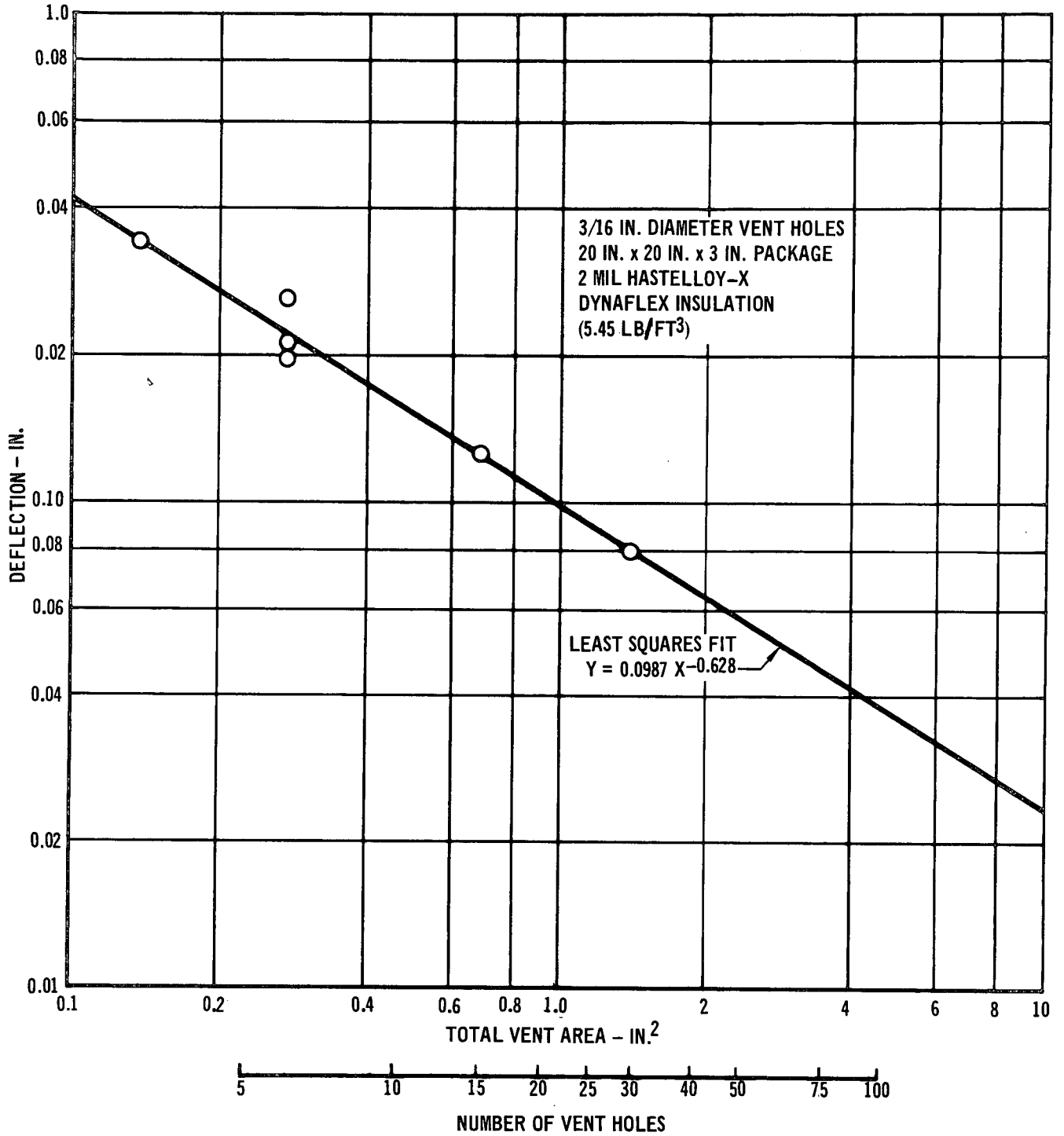

457 – 2384

"HOT SURFACE" DEFLECTION VS VENT AREA

Figure 13

C

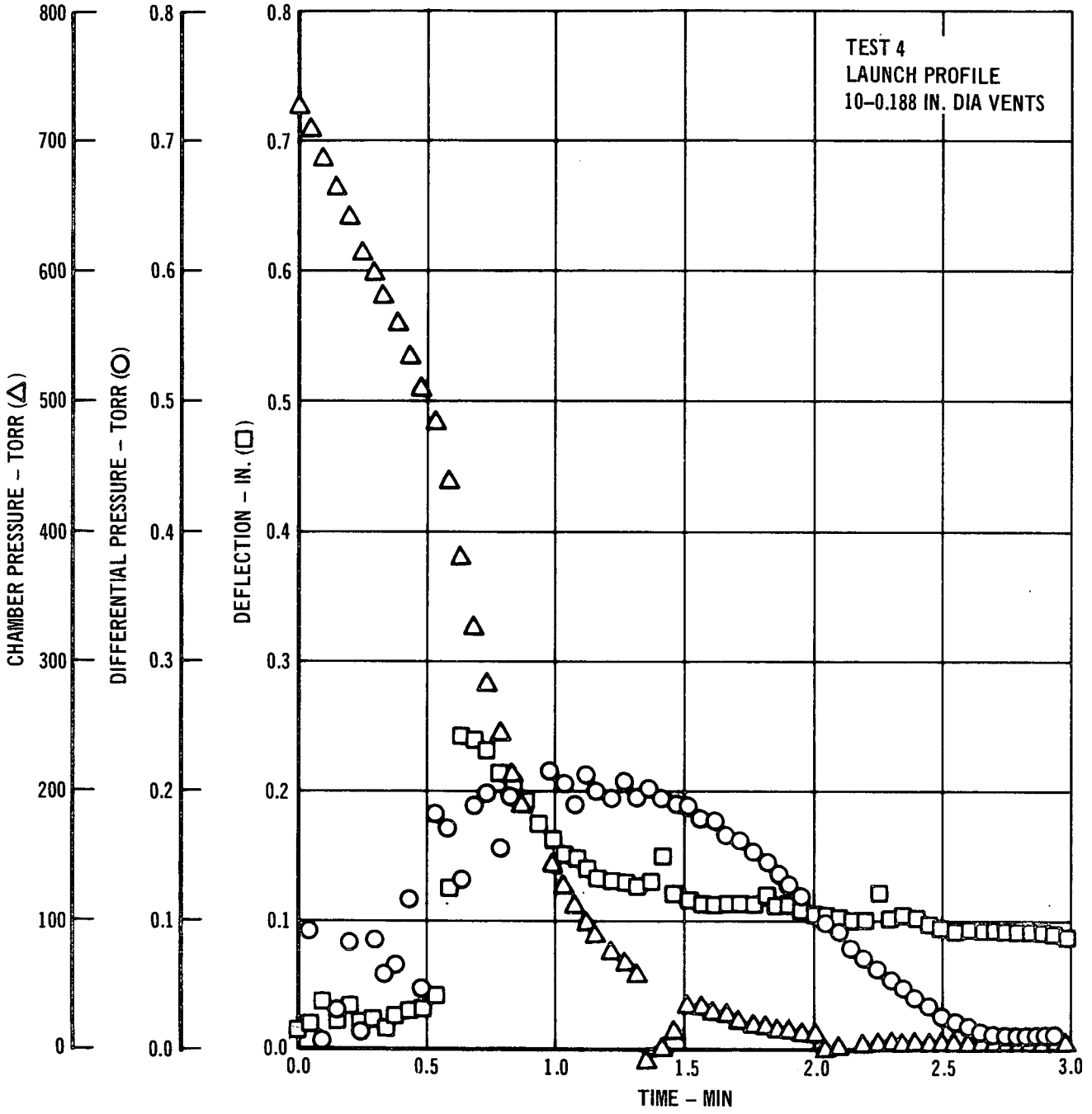

PRESSURE, DIFFERENTIAL PRESSURE, AND DEFLECTION OF HOT SURFACE UNDER SIMULATED LAUNCH

457–2385

Figure 14

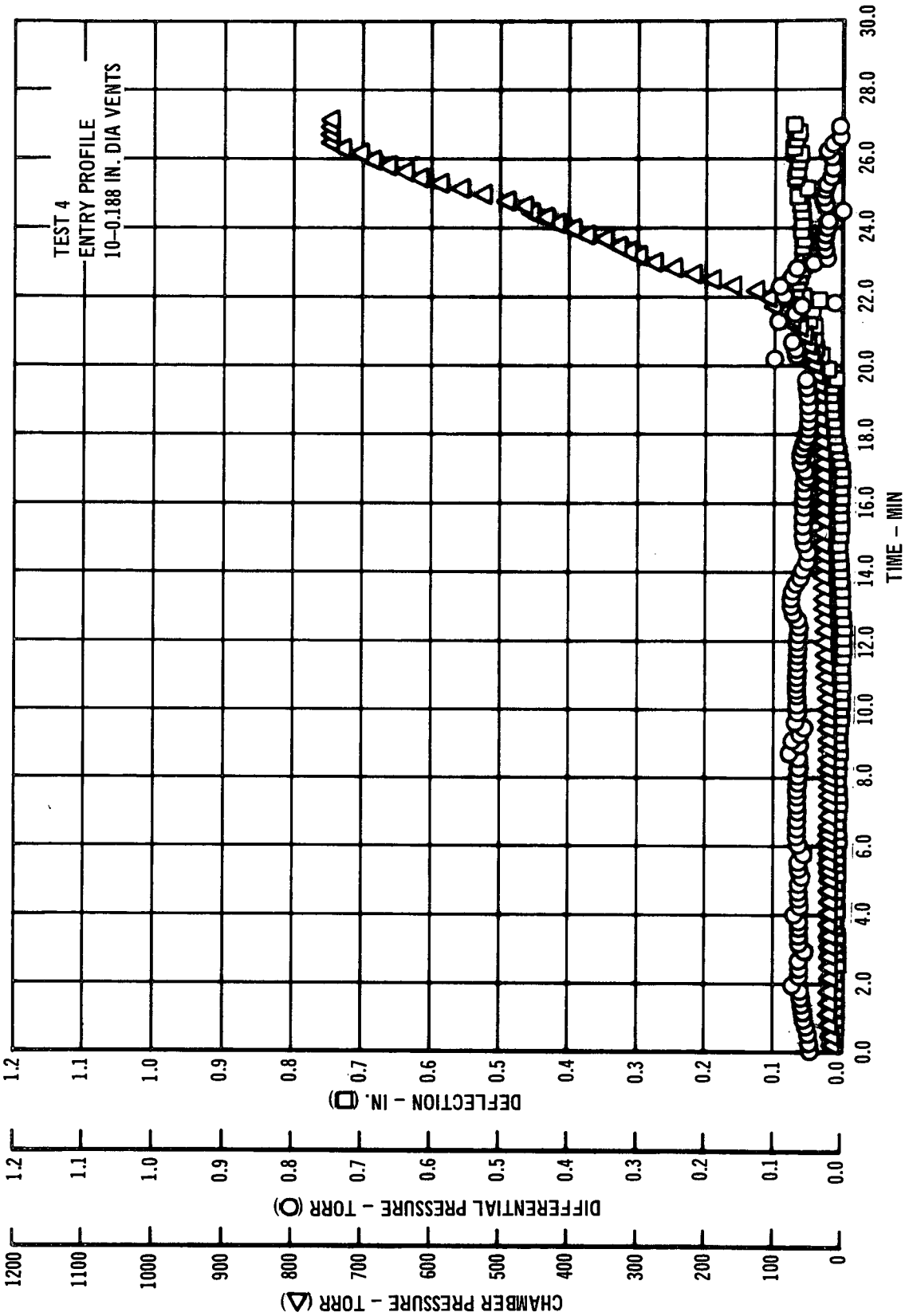

PRESSURE, DIFFERENTIAL PRESSURE, AND DEFLECTION OF HOT SURFACE UNDER SIMULATED REENTRY

457-2386

Figure 15

the hole would be closed under static pressure conditions but would readily open under a small pressure differential. However, this did not work out in practice; too much pressure differential was required to open the slits. In fact the pressure differential became so great that some of the corrugations in the face sheet snapped out. This substantially altered the response of the hot surface to pressure differentials in subsequent tests.

The other approach to restricting influx of moisture (and especially air-entrained moisture and rain in this particular approach) was to cover the vent holes with a 400 mesh wire cloth. This would serve to prevent liquid water from entering, by surface tension effects. The particular wire cloth used for testing was 400 x 400 mesh made of 1 mil stainless steel wire, with about 36% net open area. Because of the previously described alteration of the corrugated stiffeners, the surface deflection was no longer a valid criterion for effectiveness of the screened vents. However, sufficient data had been accumulated on the permissible ΔP to estimate the effectiveness of screened vents (tests 12-16 Table I). Based on ΔP comparisons, the presence of the wire cloth had negligible influence on the ΔP based on net open area.

For the corrugated stiffeners employed in these tests, the results indicate that a minimum of 10-3/16" dia. vent holes (or equivalent screened area) is required for the 20" x 20" x 3" package to restrict deflection of the stiffened face to 0.25 inch. This is equivalent to 0.023% of the surface area per inch of insulation thickness.

3.2.3 Condensation Tests - Because the presence of the vent holes allows moisture cryopumping within the insulation whenever the internal insulation is below the dewpoint (as when cryogenic propellant tanks are filled), it is necessary to know how much moisture will migrate through the vents. To determine the weight gain from moisture condensation and ice formation within an insulation package, tests were conducted on such a package mounted on a cryogenic tank wall. The insulation package used was the same one that was used for the vent tests except that the cold side was made of 32 mil aluminum. The package size was 20" x 20" x 3" and it was filled with 6 lb/ft^3 Dynaflex insulation. For venting, 16-3/16 inch diameter vents, covered with 400 mesh screen, were placed in the sides of the package 1.5 inches down from the "hot" surface. These vents were evenly spaced with 4 on each side. They were not put on the "cold" side of the package as in the vent tests because the cold side was mounted against the simulated cryogenic tank.

Two tests were conducted to determine how much moisutre accumulation would occur with the test specimen mounted on a "cold plate" at -320°F over a two-hour period with an environment of circulating air at a relative humidity of 95-100% at a temperature of 100°F. The following are the results of these two tests:

Test No.		Package Wt. (Grams)	Wt. Change from Start (Grams)
1	Beginning of test	2535.0	-
1	After 2 hour exposure	2717.0	182.0
1	After external ice removed	2538.0	3.0
2	Beginning of test	2535.0	-
2	After 2 hour exposure	2672.7	137.7
2	After external ice removed	2539.7	4.7

The weight measured at the end of the two-hour cryogenic test includes the weight of the ice formed on the outside of the package. As soon as the specimen was weighed, the external ice and frost were removed and the surface of the package wiped off as well as possible, though some moisture remained in the joints and corners. The final net increase in weight was due to ice, frost and water trapped inside the package during the cryogenic "soak". In test No. 2 the vents were taped shut immediately after the removal of the external ice in order to prevent loss of internal moisture while the outside of the packaged dried completely. The ports were not taped over in Test No. 1 which may account for the 1.7 gm greater increase in internal weight gain in the second test.

Another consideration was the effect, if any, that the icing would have on package venting. Therefore, in the third test, the test specimen was put into a 5.5 foot vacuum chamber immediately after the cryogenic soak and was subjected to the same pressure profile as that used during the vent configuration tests. The maximum "hot" surface deflection was about 0.45 inches (as determined by visual observation) which was no greater than that of similar tests without ice or water present.

These tests demonstrated that:

(1) If insulation packages are so mounted that the cool side is at cryogenic temperatures, the weight gain due to moisture and ice accumulation inside the insulation packages would not represent any appreciable weight gain to the Shuttle (less than 0.2% of the configuration tested here).

(2) Conversely, if 20" x 20" x 3" or similarly sized packages were used, a large amount of ice would be formed on the edges of the package unless

measures were taken to prevent it such as very small clearance between packages.

(3) Insulation packages mounted on the cryogenic tanks will vent properly if the vents are located in an area that will not ice over. Location of the vents in this test precluded determining venting characteristics if a hard ice formed over the vents.

3.2.4 Moisture Condensation in Insulation Packages Due to Ambient Climatic Variations - Packaged fibrous insulations may also retain moisture and create a weight problem under cyclic variations of ambient climatic conditions. Therefore, testing was conducted to determine the amount of moisture absorbed in a typical insulation package from severe climatic variations in a one week period. A Webber Model No. WF-15-0+200H environmental chamber was used to control the humidity and temperature during these tests.

The insulation package tested was the same one used in the cryogenic test. The package was box shaped with dimensions of 20" x 20" x 3" and filled with 6 PCF Dynaflex insulation. Package vents were 16-3/16 inch diameter holes in the side of the package, covered with 400 mesh screen. The vents were 1.5 inches inboard from the hot surface. These vents were evenly spaced with 4 on each side. The package was placed in the environmental chamber with the "cold" side down, and was subjected to 7 environmental cycles. Each cycle consisted of:

1 hr at 85% relative humidity, at 102°F (96° dew point)

1 hr reconditioning to lower temperature and humidity

1 hr at 50% R.H., at 52°F

1 hr reconditioning to original temperature and humidity

Both wet and dry bulb temperatures were measured during these tests and the humidity profile was determined from these readings.

The test sequence consisted of 7 cycles, and two of these 7 cycle tests were performed to establish test repeatability. A large analytic balance was used to weigh the test package. The original weight of the package was 2538.46 grams and the weight gains on the two 7 cycle tests were:

1st test - 1.63 grams

2nd test - 1.79 grams

The average weight gain was 0.00136 lb/ft^2 (0.067%w), equivalent to a total weight gain for a 12,000 ft^2 vehicle of about 16.5 pounds.

3.3 1000°F Mission Simulation - A large portion of the surface area (∿ 50%) of the orbiter vehicle will experience temperatures no higher than 1000°F. There are several ultra-low density (∿ 0.6-1.0 lb/ft^3) insulation materials available that are capable of service in the 1000°F range, and which are significantly lower in cost than materials with higher temperature capabilities. These offer excellent opportunities for lowering the weight and cost of the insulation system. Further, it should be possible to combine these materials with the higher temperature materials to provide a gradated composite insulation of lower weight.

To determine their capability to survive in the shuttle thermal and acoustic environment, ultra-low density materials were evaluated in a simulated mission environment of repeated acoustic and thermal cycles. The test insulations for this series were low density AA and B glass fiber felts, both bonded (silicone resin) and unbonded in densities varying from 0.6 to 4.0 lb/ft^3. While the insulations used in testing were all from Hitco, essentially identical products are available from other vendors, from which equivalent results could be expected.

The packages were formed of commercially pure titanium A-70 foil, 2 mils thick. Package configuration was similar to that used previously for preliminary evaluation testing (3.85" wide, 20" long, 1.5" thick), except that the hot surface incorporated corrugation stiffeners as described in Section 3.2. Also, as occurred with the Hastelloy X, the titanium A-70 was not corrugated to the full depth of the tool, and it is likely that some localized stretching of the foil may have occurred.

Three thermocouples were installed in each specimen, approximately 0.25, 0.75 and 1.25 in. from the hot surface. The thermocouples were 0.040 in. diameter metal sheathed, closed and with ungrounded junctions. To maintain the position of the thermocouples within the package, a wire was brazed to the tip of the sheath, which led to the opposite side of the package. This supported the thermocouple and provided much more reproducible data than in previous tests. However, several of the brazed joints led to thermocouple failure, and in replacing those thermocouples an improved procedure was used. This consisted of butting the sheath axially to the wire extension, wrapping the joint with 5 mil Inconel foil and resistance welding the foil and parts together. No failures have occurred with this technique, and all subsequent thermocouples were made by this method.

The specimens in the 1000°F tests were exposed to 10 consecutive cycles of acoustic environment for 30 seconds each, followed by 10 consecutive cycles of thermal testing at 10 torr air pressure. This was repeated until a total of 80 cycles had been completed. Acoustic exposure was conducted with the specimens in a vertical plane, with the 20 in. dimension in the vertical plane.

One specimen, TG-15000, 0.6 pcf, was removed from test at the end of 50 cycles due to a tear in the titanium foil (on the hot surface), which propagated further in successive acoustic cycles. This specimen was replaced in the test panel by the TG-10000 (1.0 pcf) for the remainder of the 80 cycles.

The thermal histories of each of the specimens during the first and last groups of thermal cycles are shown in Figures 16-21. The points show, respectively, the radiant panel temperature, and the three thermocouple readings within the insulation. During the course of the test it was necessary to replace a number of the thermocouples, and these are listed below. With the current technique of supporting the thermocouples from both sides of the package, replacing the thermocouple resulted in minimal change in position or thermal response.

THERMOCOUPLE REPLACEMENT

	At Cycle No		
Specimen	Hot Side	Center	Cool Side
TG-15000 - 0.60 pcf	31	31	--
TG-15000 - 1.0 pcf	21	21	21 & 41
TG-15000 - 2.0 pcf	--	--	--
FA-Batt - 4.0 pcf	41	--	--
FB-1 Batt- 2.0 pcf	--	--	--
TG-10000 - 1.0 pcf	11	21	--

It can be noted from Figures 16-21 that very little change occurred in the thermal histories of the individual specimens over the number of cycles tested. As would be expected, the lower density insulations permitted changes in the panel temperature almost immediately at the cool surface; the time delay increased with material density. The effect of density is also reflected in the differences in peak temperatures recorded by the hot and cool side thermocouples (at whatever time they occurred) as shown by the following table.

MATERIAL AND NOMINAL DENSITY	ACTUAL DENSITY lbs/ft^3	SURFACE DENSITY lbs/ft^2	$T_{1_{max}} - T_{3_{max}}$ °F
TG 15000 $_3$ 0.6 lb/ft^3	0.54	0.0675	260
TG 15000 $_3$ 1.0 lb/ft^3	0.73	0.091	260
TG 15000 $_3$ 2.0 lb/ft^3	2.0	0.25	480
FA Batt $_3$ 4.0 lb/ft^3	4.2	0.525	420
FB-1 Batt $_3$ 2.0 lb/ft^3	2.0	0.25	330
TG 10000 $_3$ 1.0 lb/ft^3	0.8	0.100	210

The above tabulation can be considered only a rough comparison because it assumes all thermocouples were in the same relative positions. However it does indicate that, on a weight basis, the lower densities would provide minimum weight and that from a thermal standpoint, the finer fiber diameter products (the first four in the above tabulation) are more effective. The 4 lb/ft^3 FA Batt was not as effective as the lower density AA fiber batts as the $k\rho$ product was less favorable.

The specimens before and after the 80 cycles of testing are shown in Figures 22 and 23. The color of the titanium at the hot surface ranged from gold to an intense blue as a result of the thermal cycling. The one specimen which had received only 30 cycles as a replacement specimen (TG-10000) showed only a small amount of blue color. Data on the emittance of the titanium foil after testing is included in Section 3.8.

The specimen which was removed from testing at the end of 50 cycles due to a hole in the titanium foil hot surface displayed cracks extending from the hole (Figure 24). The hole apparently initiated at a crease across a corrugation, possibly due to overstretching during forming. Repeated exposure to acoustics caused the hole to develop, and the cracks to propagate. This specimen contained the TG-15000, 0.6 pcf glass felt. It is believed that with improved titanium forming techniques the stretching problem would not occur.

The condition of the insulations within the packages at the conclusion of the 80 cycles is illustrated in Figure 25. The 2 pcf products (TG-15000/2 and FB-1) and the 4 pcf insulation (FA Batt) displayed excellent dimensional stability,

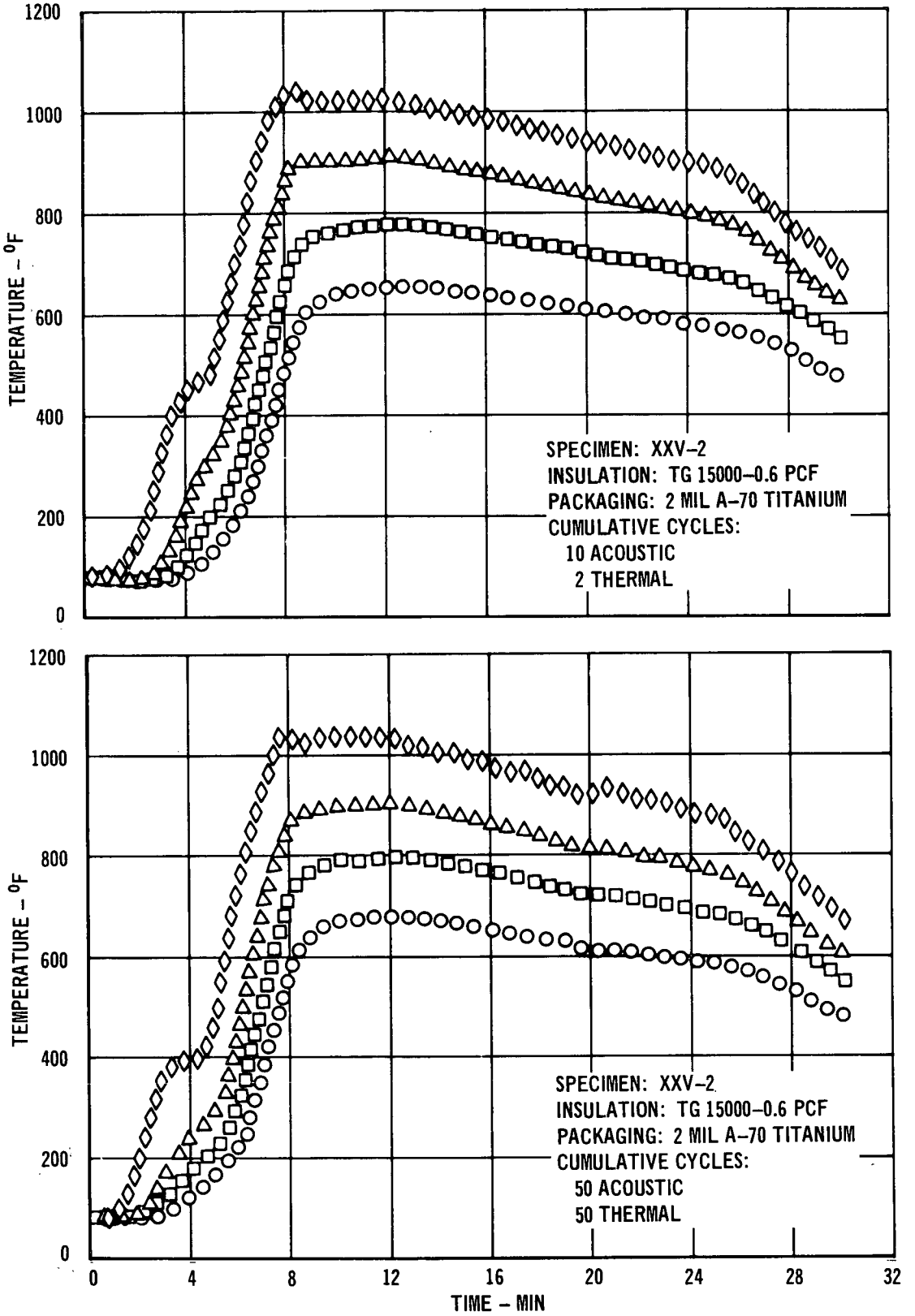

THERMAL HISTORY TG 15000–0.6 PCF
EARLY CYCLE AND LATE CYCLE
("AA" Glass with Binder)

457–2389

Figure 16

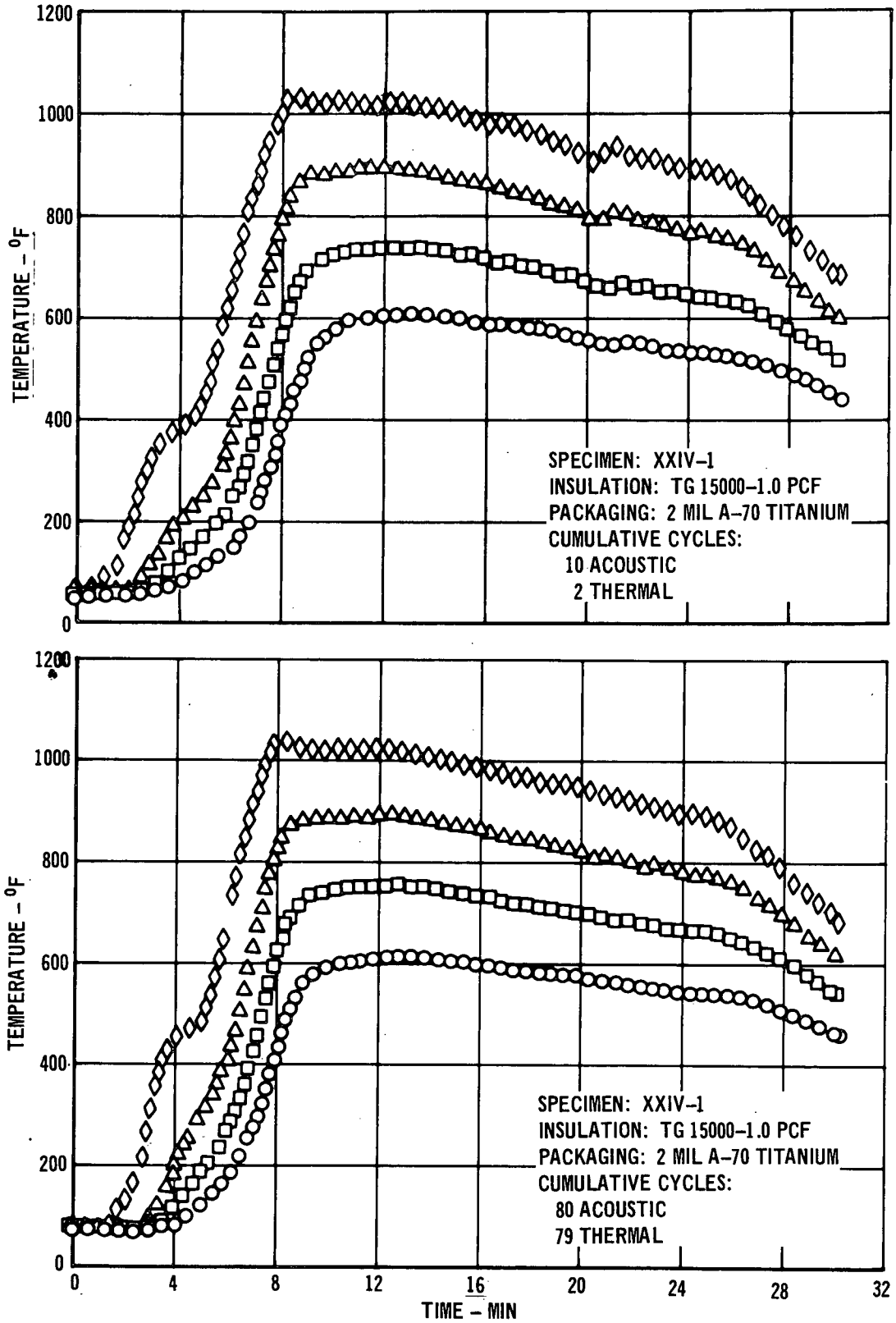

THERMAL HISTORY – TG 15000–1.0 PCF
EARLY CYCLE AND LATE CYCLE
("AA" Glass with Binder)

457-2390

Figure 17

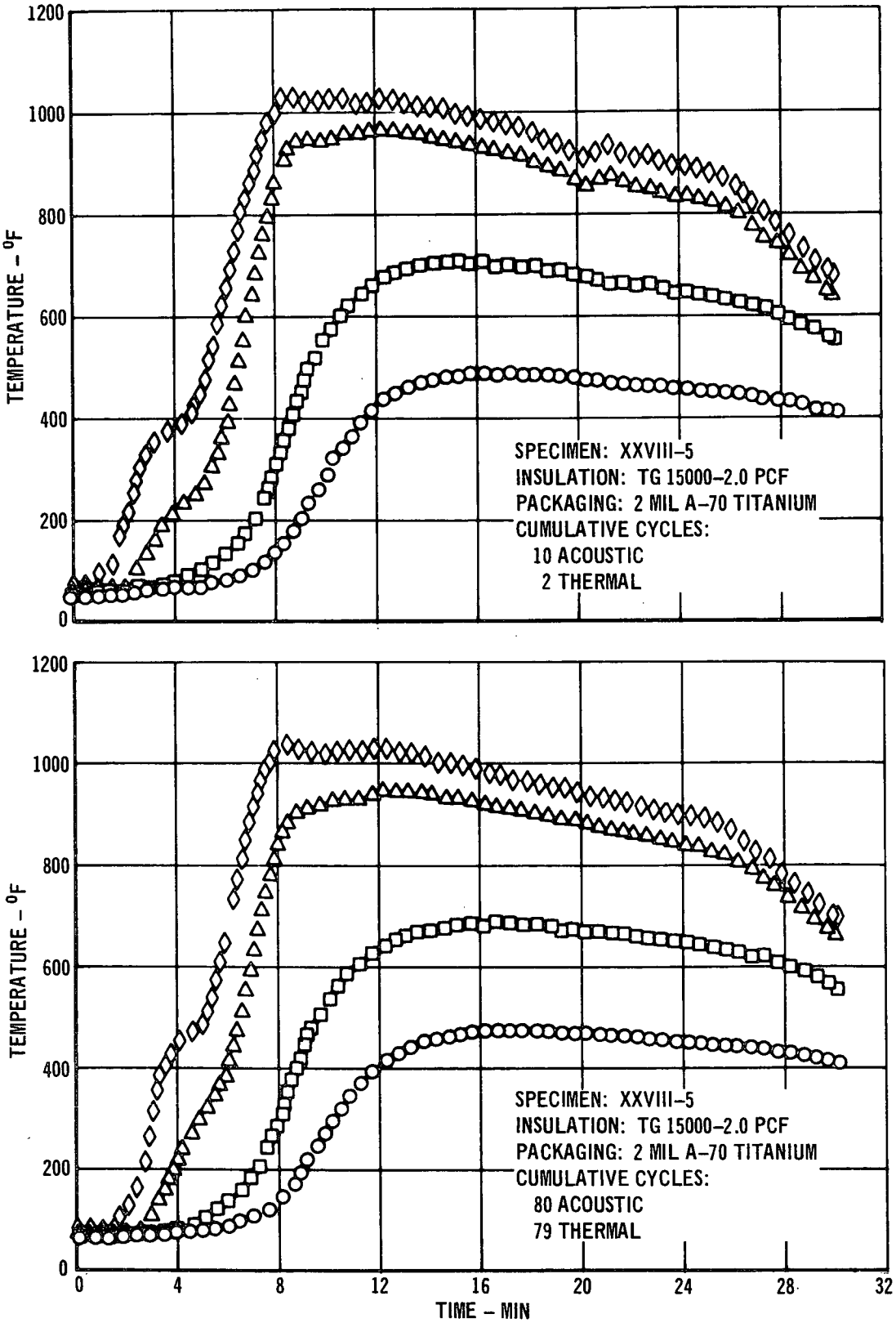

THERMAL HISTORY – TG 15000–2.0 PCF
EARLY CYCLE AND LATE CYCLE
("AA" Glass with Binder)

457–2391

Figure 18

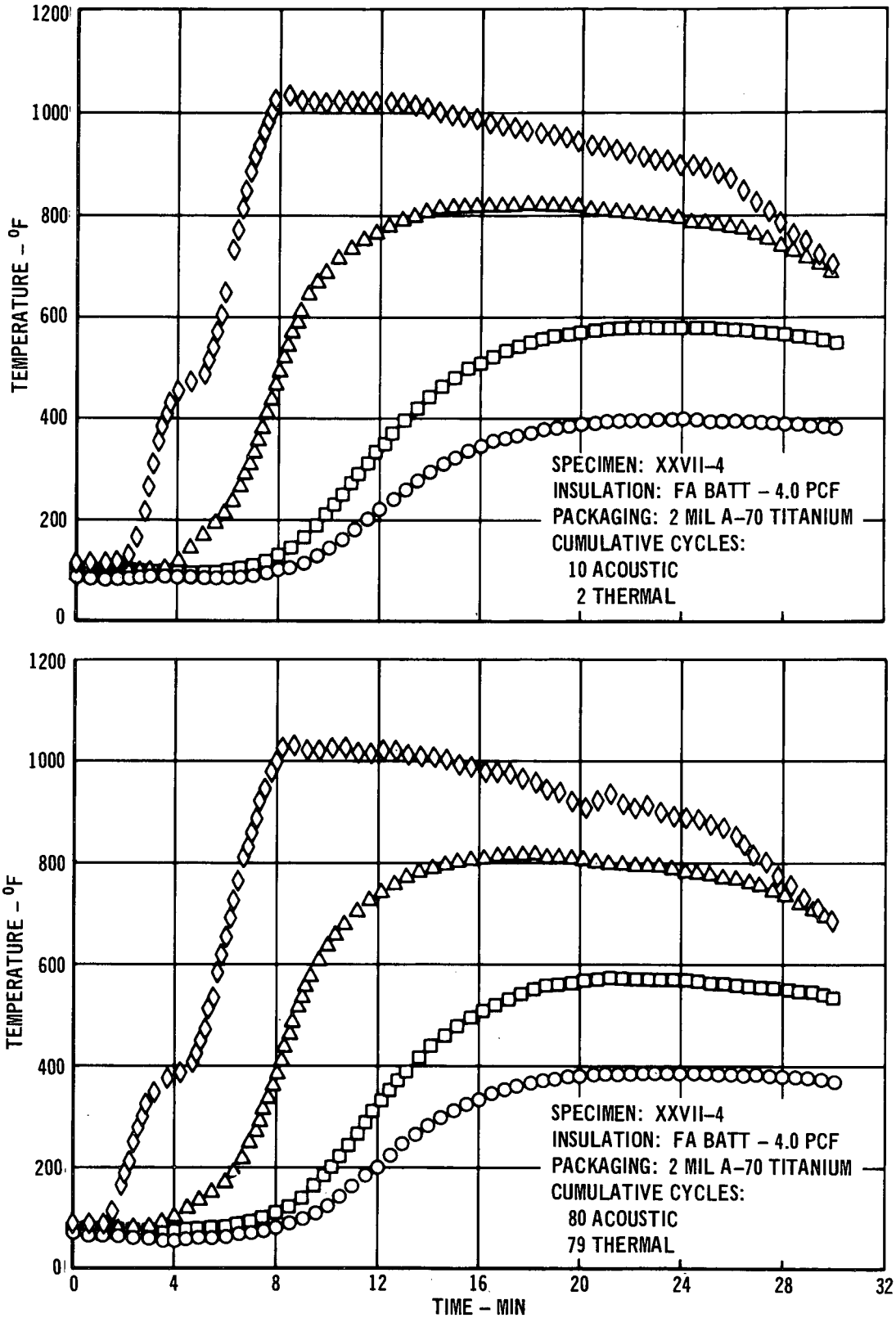

THERMAL HISTORY FA BATT – 4.0 PCF EARLY CYCLE AND LATE CYCLE
(Unbonded "AA" Glass)

457 – 2387

Figure 19

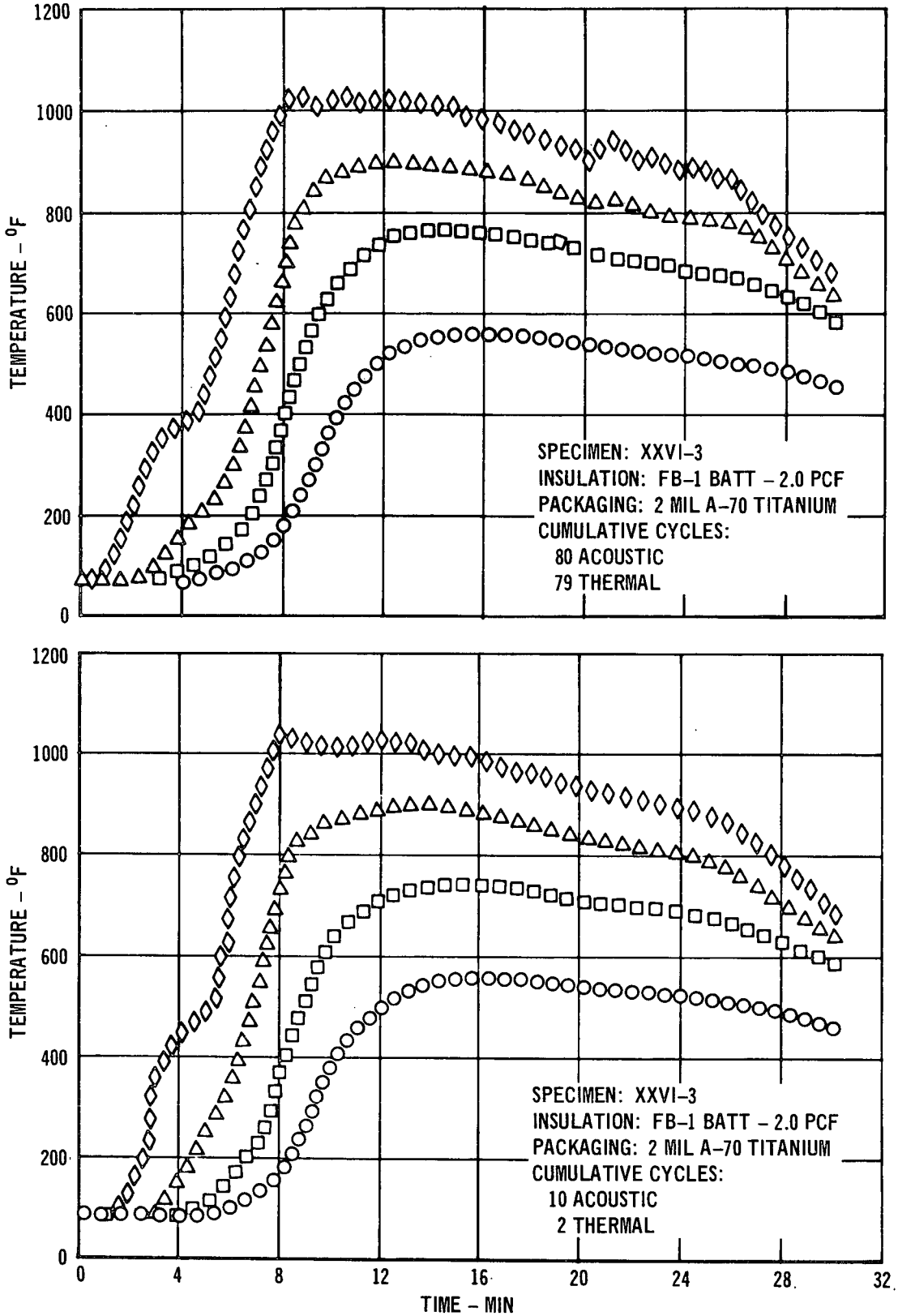

THERMAL HISTORY FB-1 BATT - 2.0 PCF
EARLY CYCLE AND LATE CYCLE
(Unbonded "B" Glass)

457 - 239 2

Figure 20

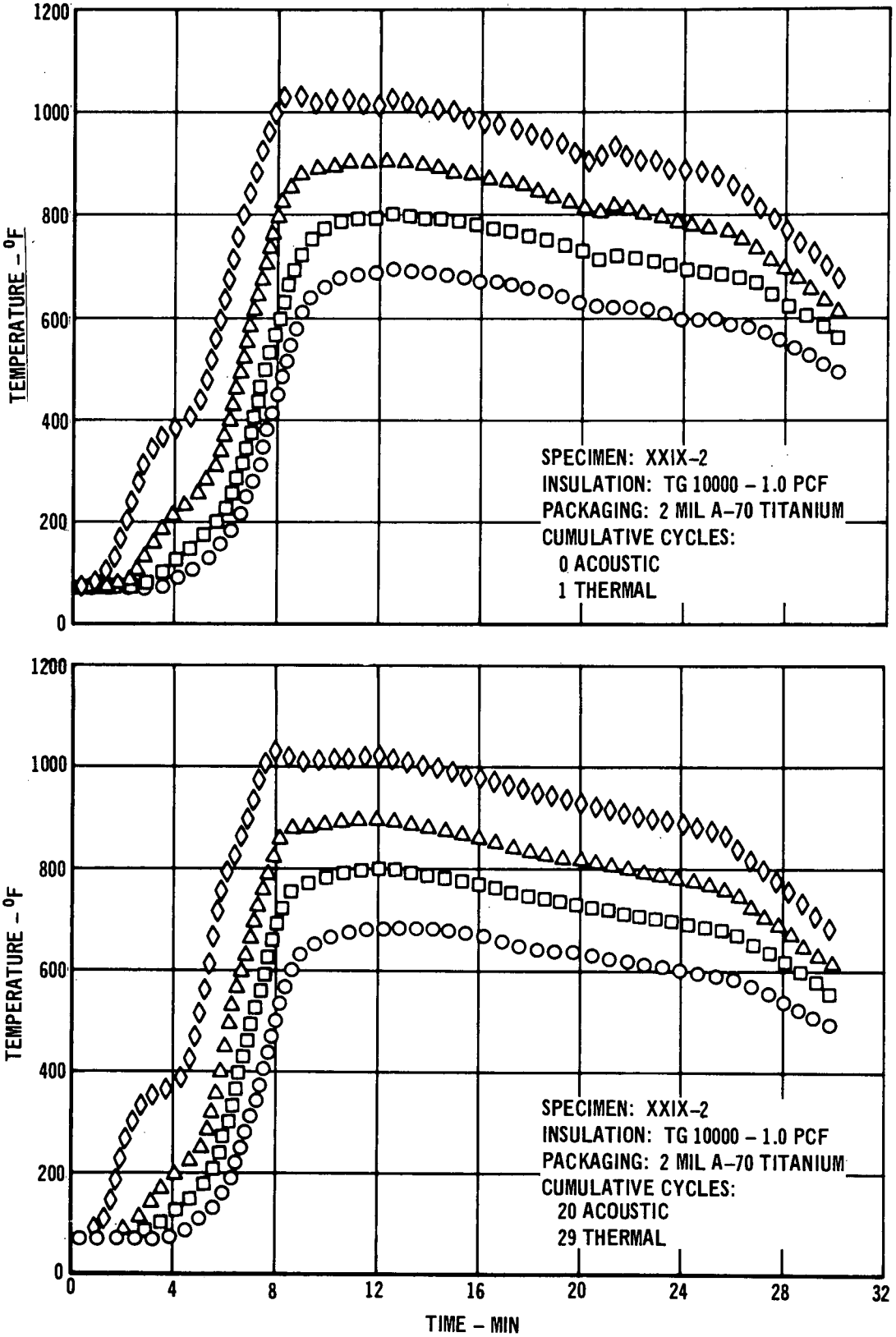

THERMAL HISTORY TG 1000 - 1.0 PCF EARLY CYCLE AND LATE CYCLE
("B" Glass with Binder)

457-2393

Figure 21

D

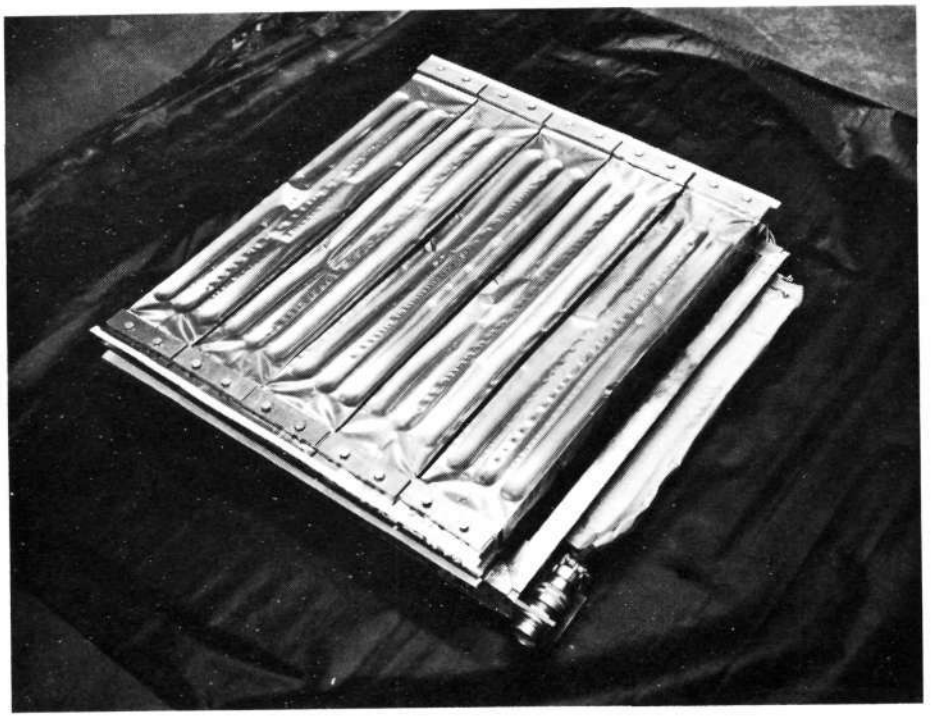

457-2395

1000 °F TEST SPECIMENS PRIOR TO TEST

Figure 22

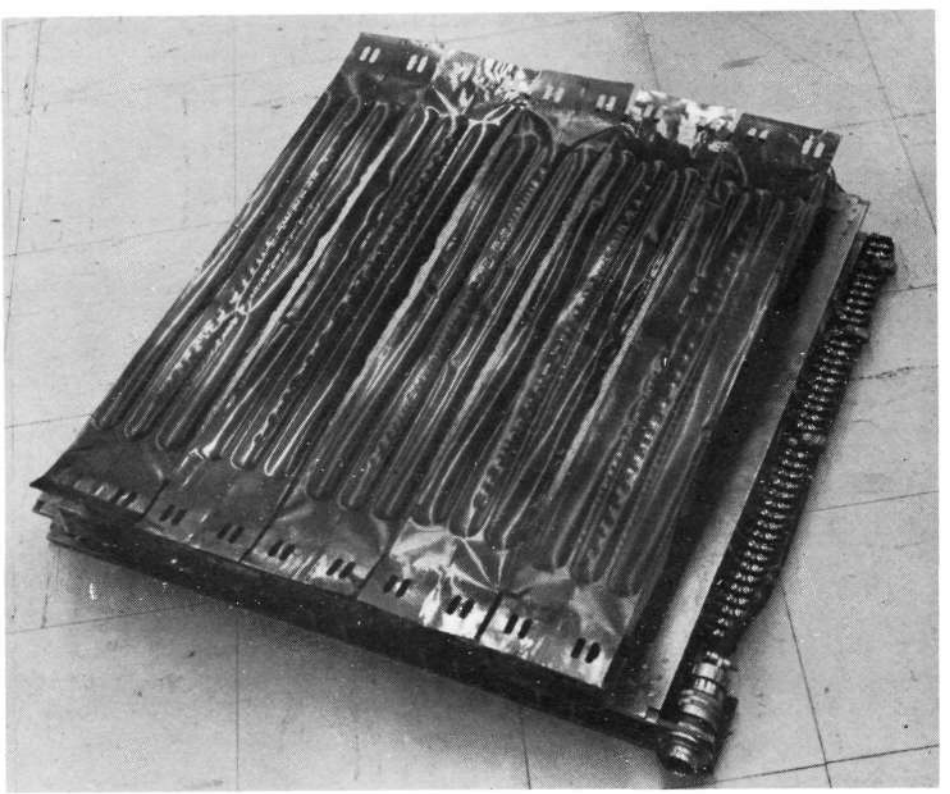

457-2394

1000 °F TEST SPECIMENS AFTER 80 CYCLES OF THERMAL AND ACOUSTIC EXPOSURE

Figure 23

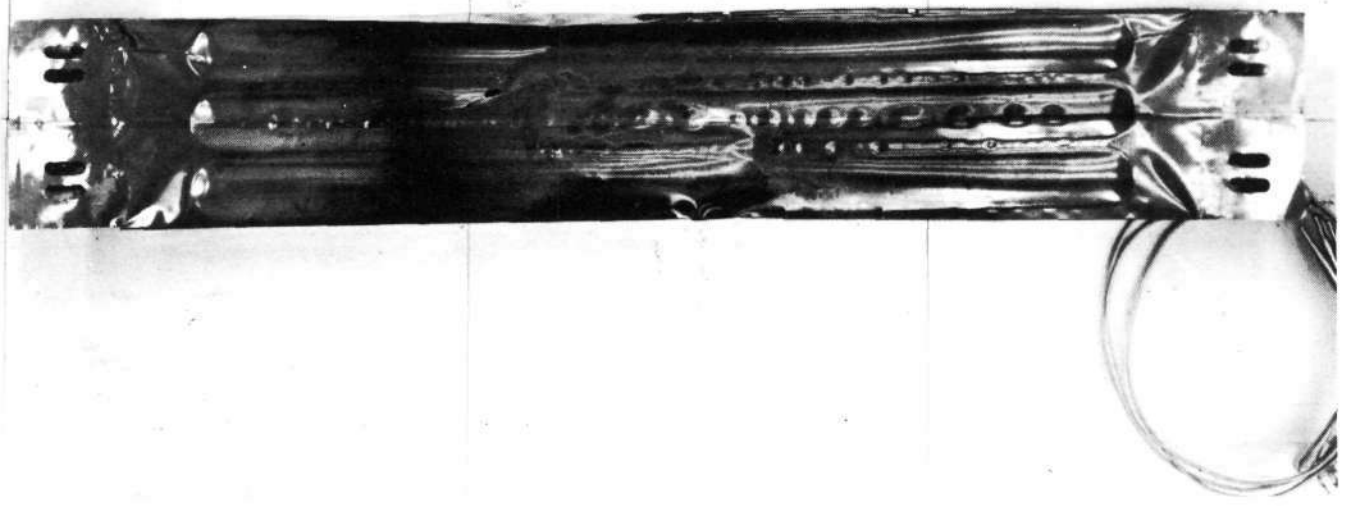

457-2396

1000 °F TEST SPECIMEN REMOVED DUE TO PACKAGE FAILURE

Figure 24

as did the 1.0 pcf TG-15000. The B fiber batt at 1.0 pcf slumped lengthwise about 3/16 inch, as did the AA fiber batt at 0.6 pcf (TG-15000/0.6). This amount of slump would probably be acceptable in service; however, the possibility exists that a greater width (such as the 20 inches contemplated for shuttle service), may allow greater slumping. While the 0.6 pcf TG-15000 performed reasonably well, its very low physical strength could present handling problems. A practical limit may be a minimum density of 1.0 pcf in the "AA" glass felts, and 2 pcf in "B" glass felts, which appear to have essentially the same resiliency.

It will be noted in Figure 25 that a void area is present in the TG-10000 batt. This was present before testing and is not a result of the cycling.

3.4 2200°F Mission Simulation - During the first year of this contract, 18 specimens were evaluated for 2200°F service. All of these, with one exception, had short lives due to failure of the superalloy metal foil packages. The one exception was a package made of TD-NiCr, using the shingle design. Because of the short lives of most of those packages, it was not possible to fully evaluate the service capabilities of the insulations themselves. During the contract extension, additional

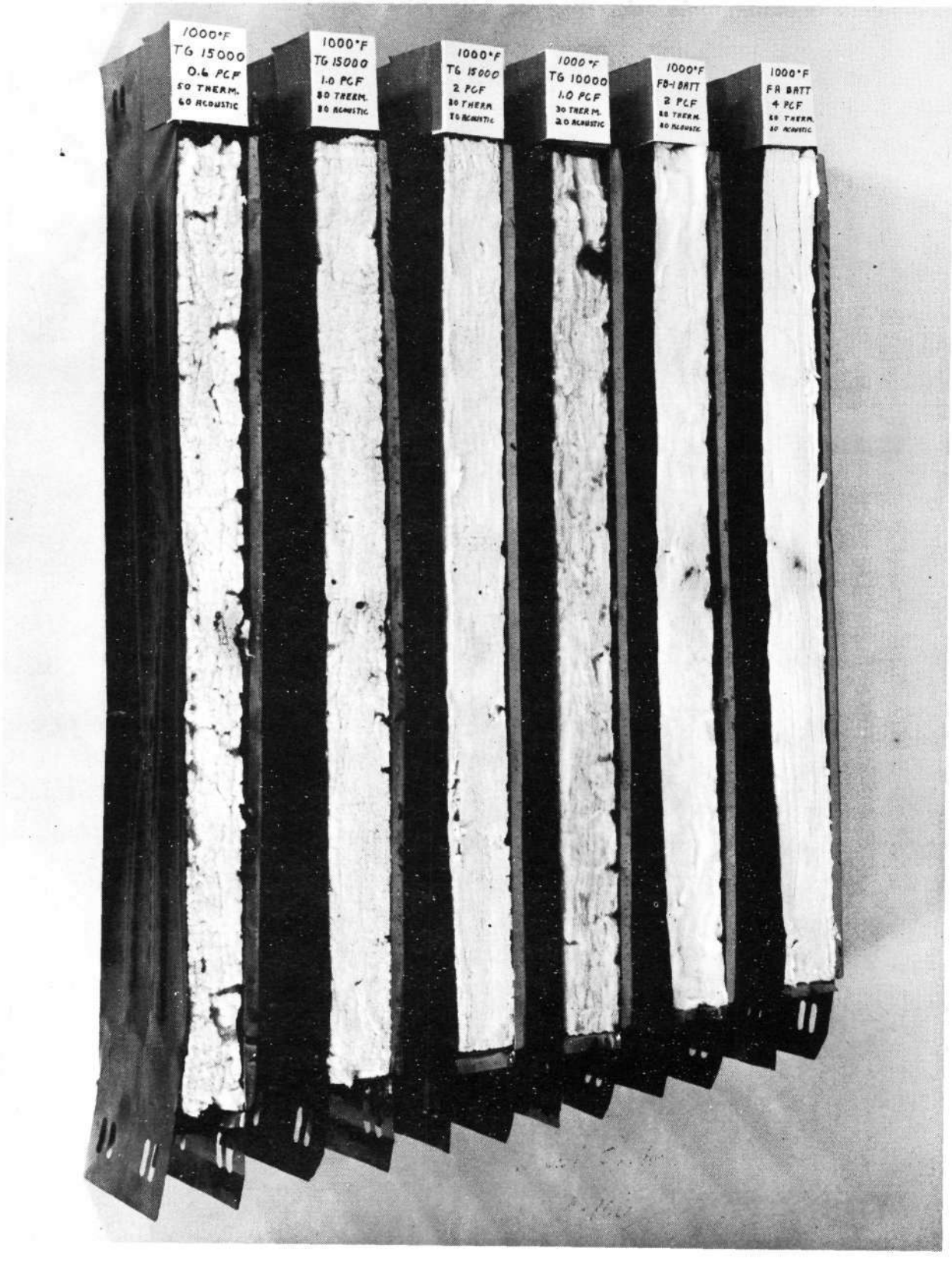

457-2397

1000 °F TEST SPECIMENS AFTER THERMAL AND ACOUSTIC TESTING

Figure 25

specimens of packaged insulations were prepared, all using 3 mil thick TD-NiCr metal foil as the packaging material, and exposing them to 100 cycles of mission simulation. The test specimens consisted of 3 mil TD-NiCr formed to a simple box design (without corrugation stiffeners), and containing various insulations. The insulations employed in the current test series are listed in Table II. Each specimen was instrumented with three thermocouples in accordance with our normal practice. The thermocouples in this test series had tip extensions so that they were supported from both sides of the package to reduce possible dislocation. During the course of this test, it was necessary to replace only one thermocouple, which is considerably better than previous experience.

3.4.1 Test Results - The test equipment and environments were similar to those employed previously and comprised launch acoustics and thermal testing to 2200°F at 10 torr flowing air pressure. The tests were conducted by exposing the specimens to alternating 10 cycles of acoustic testing and 10 cycles of thermal testing until a total of 100 cycles of each was completed.

After the first 10 thermal cycles of this series, one of the TD-NiCr packages was found to have suffered what appeared to be chemical attack in two areas of the hot face, another had sustained minor attack in two areas, and two more packages, traces of attack. The general condition of these packages immediately after the first 10 cycles is shown in Figure 26. These defects were green in color and of a glassy appearance. Since TD-NiCr had previously been cycled 100 times at 2200°F (Ref 1) without difficulty, a study was undertaken to determine the cause of these defects. The details of that study are contained in Section 3.4.2.

The severely damaged test specimen, which contained Fiberfrax paper, was replaced with a back-up specimen containing Dynaflex 1200, and testing continued. During the time the next group of 10 thermal cycles were being run, the cause of the earlier difficulty was fairly well established as physical contact of the specimen with the columbium susceptor plate. Therefore, at the end of 20 cycles, the test arrangement was modified to provide greater clearance.

The condition of the insulation packages at the conclusion of the test is shown in Figure 27. Four of the specimens show evidence of contacting the columbium heater plate, resulting in minor damage. A characteristic damage mode to all these TD-NiCr packages was small tears along the edges of the hot surface (Figure 28). These tears are believed to be the result of the high coefficient of thermal expansion of TD-NiCr, combined with the restraint imposed by the cooler sides and low elongation (3-5%) of the foil. In the previous test of TD NiCr and which was of

Table II

2200°F TEST INSULATIONS

INSULATION	DESCRIPTION	NOMINAL DENSITY PCF	AS TESTED DENSITY PCF
FIBERFRAX PAPER – 970A CARBORUNDUM CO	CERAMIC FIBER PAPER	12	10.1
SKX – FIBERFRAX BLANKET CARBORUNDUM CO	CERAMIC FIBER FELT OF 1.6 μ ALUMINA-SILICA FIBERS (EXPERIMENTAL)		7.2
IRISH REFRASIL B–1576–1 HITCO	10 μ SiO_2 FIBER FELT WITH CHROMIA ADDITION		3.1
ASTROQUARTZ MAT–550 J.P. STEVENS	7 μ SiO_2 FIBER FELT	1.0	0.94
DYNAFLEX – 900 JOHNS-MANVILLE	CERAMIC FIBER FELT 3 μ FIBERS WITH CHROMIA ADDITION	9	8.84
DYNAFLEX – 1200 JOHNS-MANVILLE	CERAMIC FIBER FELT 3 μ FIBERS WITH CHROMIA ADDITION	12	9.52
REFRASIL A–100 HITCO	SiO_2 FIBER FELT 1.3 μ FIBERS	4.3	5.2

457–2398

shingle construction (Ref 1), this mode of damage did not exist, presumably because that design allowed the hot surface more freedom to expand. It was partly because of such edge tears that the specimen containing Irish Refrasil was removed from the test at the end of 50 cycles. The other reason was to obtain comparative data on Refrasil A-100, which replaced the Irish Refrasil for the remaining 50 cycles.

The condition of the insulation installed in the packages is summarized in Table III and illustrated in Figure 29. Several aspects of the posttest condition of the insulations were unusual. A hardened layer in the felts, centered about 0.5-inch down from the hot surface, was found in varying degrees in several insulations. The felts were softer in both directions from the band of hardened material. It is believed that the band was caused by progressive devitrification of the fibers.

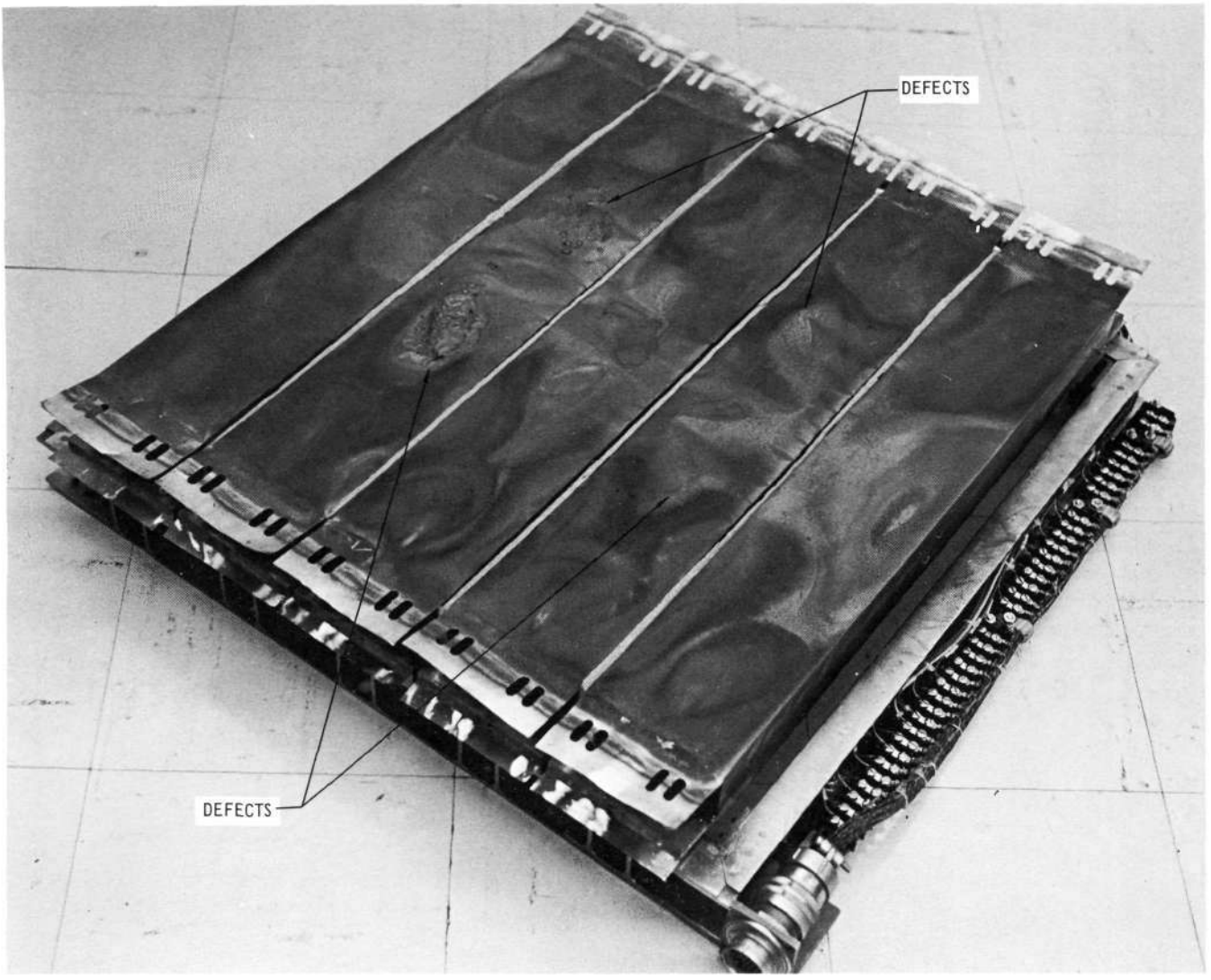

INSULATION PACKAGES AFTER 10 CYCLES AT 2200°F

457-2399

Figure 26

Both Refrasil products (A-100 and B-1576-1) displayed deterioration, but which were different in character. The A-100 had high shrinkage at the hottest layer, with succeeding layers having less shrinkage (A-100 is furnished as a felt about 0.2-inch thick). It is apparent from the posttest condition that the A-100 after shrinking in the thermal exposure, settled down to one end of the package in the acoustic test. The Refrasil B-1576-1 appears to have settled as a homgeneous felt about one-inch in the 20-inch dimension. Compaction of the felt at one end of the package only indicates that this dimensional change was primarily settling of the felt rather than thermal shrinkage.

The physical performance of the two Dynaflex specimens presented an anomaly.

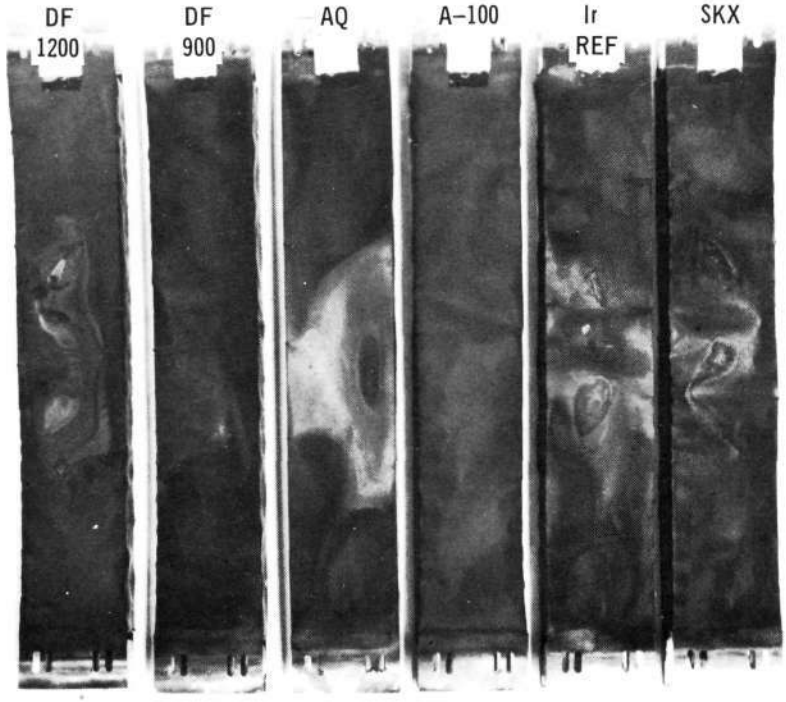

456-2783

TD-NiCr PACKAGED INSULATIONS AFTER COMPLETION OF 100 CYCLES OF MISSION SIMULATION AT 2200°F

Figure 27

457-2783

TD-NiCr PACKAGED INSULATION WITH 50 CYCLES TO 2200°F SHOWING CHARACTERISTIC EDGE TEARS

Figure 28

Table III

INSULATION CONDITIONS AFTER 2200°F THERMAL AND ACOUSTIC CYCLING

INSULATION	INSTALLED DENSITY	NO. OF CYCLES	DIMENSIONAL INTEGRITY	COMMENTS
FIBERFRAX PAPER	10.0 PCF	10	NO CHANGE	LIMITED TESTING DUE TO PACKAGE FAILURE
SKX-FIBERFRAX BLANKET	7.2 PCF	100	NO CHANGE	SLIGHT HARDENING OF BATT ABOUT 0.5 IN. DOWN FROM HOT SURFACE
IRISH REFRASIL B-1576-1	3.1 PCF	50	BATT CONDENSED ABOUT 1 IN. IN 20 IN. LENGTH. APPEARED TO BE SETTLING DUE TO ACOUSTICS	
ASTROQUARTZ MATT NO. 550	0.94 PCF	100	NO CHANGE	SLIGHT HARDENING OF FELT, BARELY DETECTABLE, ABOUT 0.5 IN. DOWN FROM HOT SURFACE
DYNAFLEX-900	8.8 PCF	100	SHRINKAGE AND/OR SETTLING, 0.4 IN. AT HOT SURFACE, 0.1 IN. AT COOL SURFACE IN 20 IN. DIMENSION	DEFINITE HARDENING OF FELT ABOUT 0.5 IN. DOWN FROM HOT SURFACE
DYNAFLEX-1200	9.5 PCF	90	NO CHANGE	DEFINITE HARDENING OF FELT ABOUT 0.5 IN. DOWN FROM HOT SURFACE
REFRASIL A-100	5.2 PCF	50	VARIED FROM LAYER TO LAYER. ABOUT 1.5 IN. SHRINKAGE IN HOTTEST LAYER, DECREASING TO ZERO ABOUT HALFWAY THROUGH TOTAL THICKNESS	

457-2760

While they were nominally 9 and 12 lb/ft^3 density, their true densities were essentially identical, 8.8 and 9.5 lb/ft^3, respectively. However, the lower density displayed a slight amount of shrinkage/settling, while the higher density material did not. It is believed that this difference in performance was not due to the small density difference, but rather to routine manufacturing variations.

Astroquartz matt continued to be a surprise with its ability to retain its form and configuration, in spite of its very low density.

The temperature histories of each specimen for their first and last cycle of thermal exposure are shown in Figures 30-36. These show the temperatures recorded at the susceptor plate and by three thermocouples within the insulation. The location of those three thermocouples varied slightly from specimen to specimen, consequently, a precise comparison of the relative thermal efficiency of the various

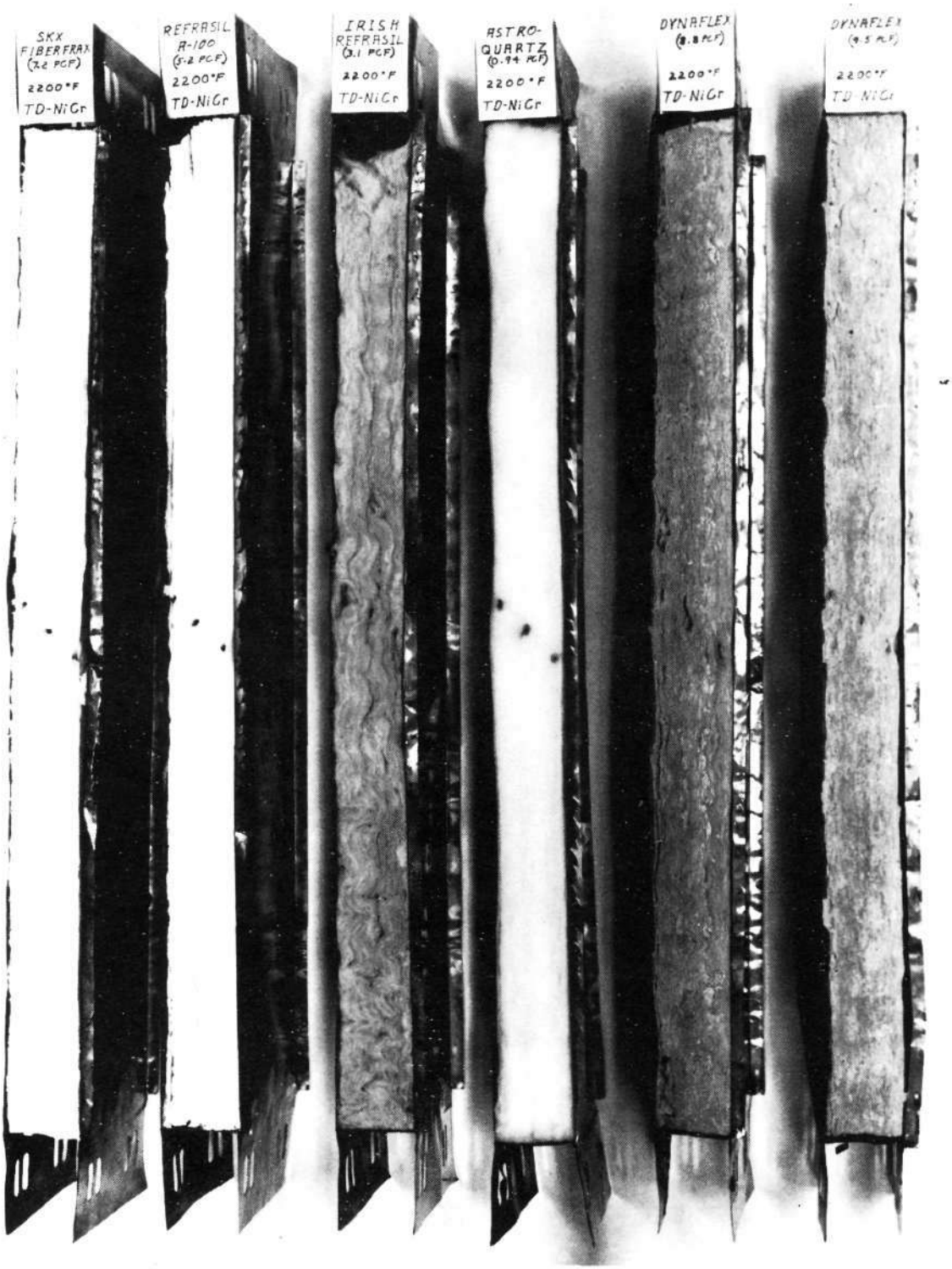

INSULATION CONDITION AFTER MISSION SIMULATION AT 2200°F

457-2784

Figure 29

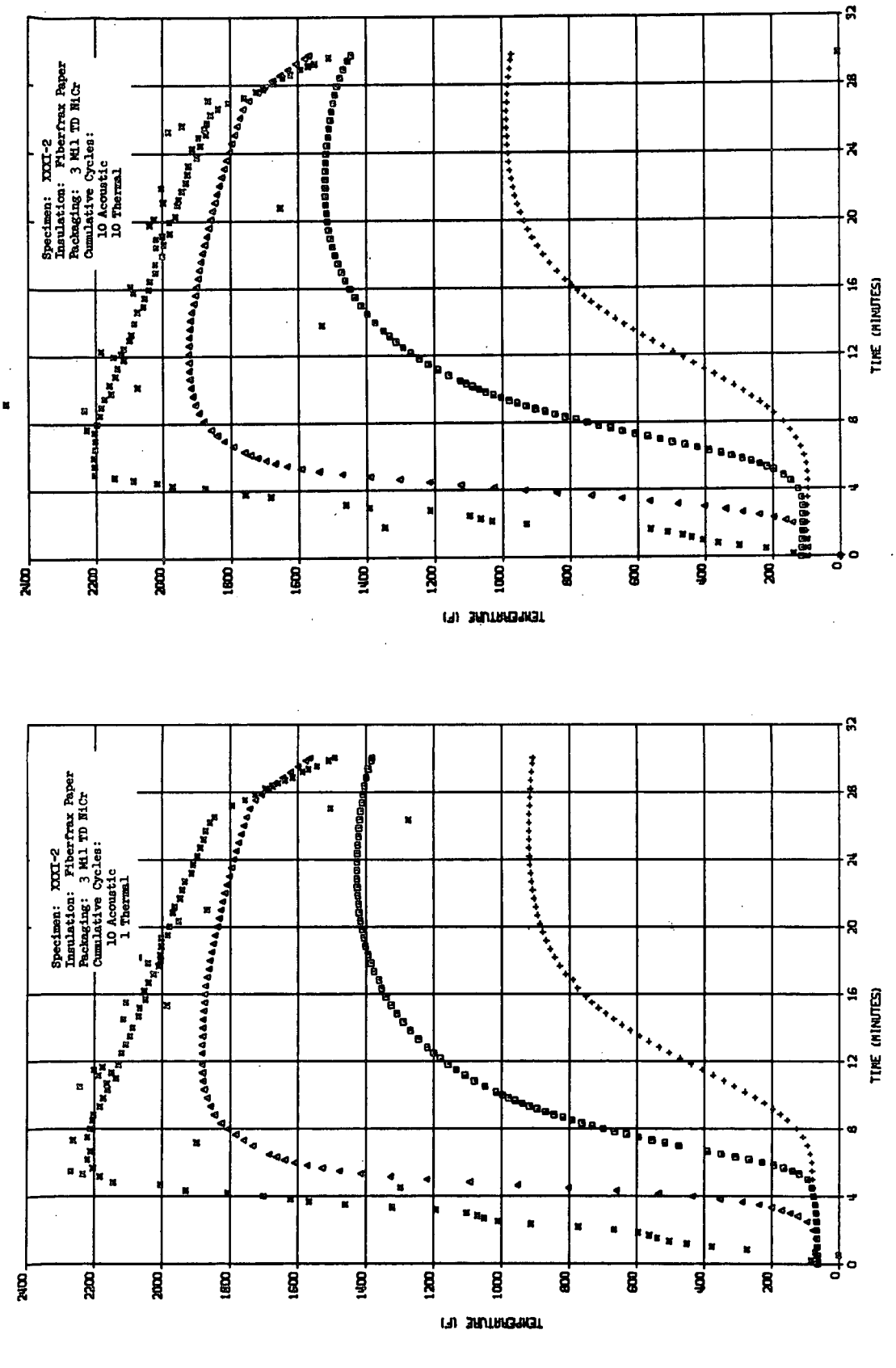

THERMAL RESPONSE OF FIBERFRAX PAPER
First and Last Cycle
2200°F Series

457-2761

Figure 30

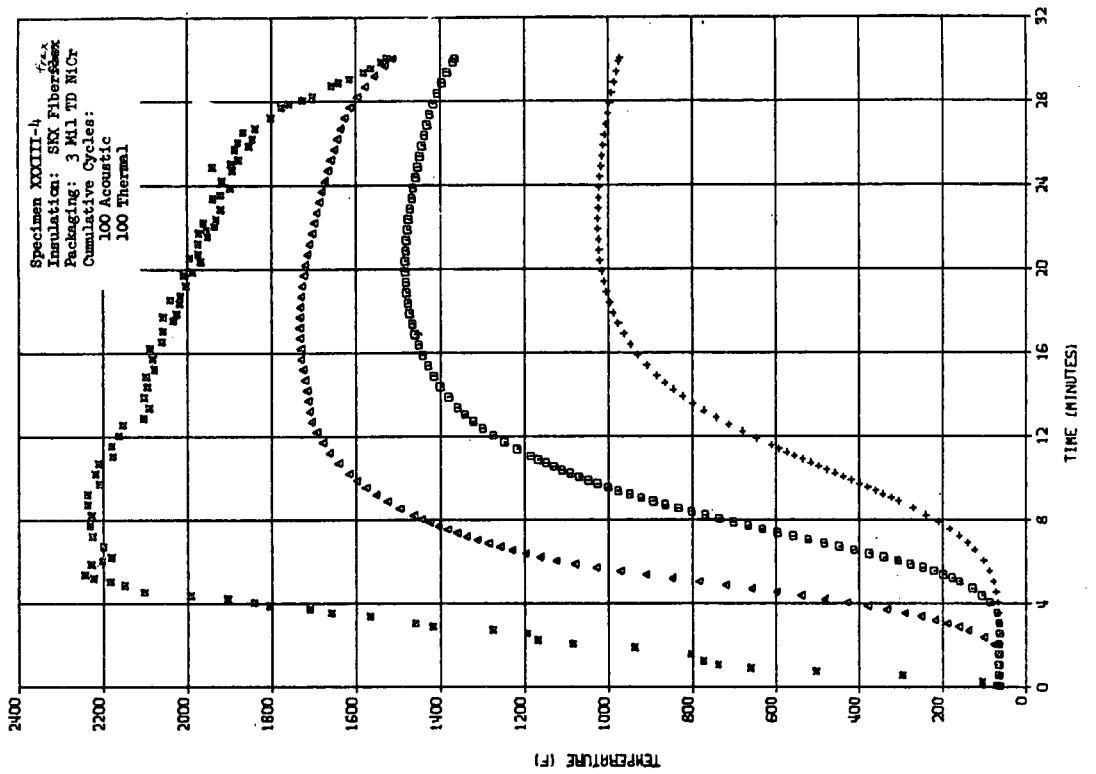

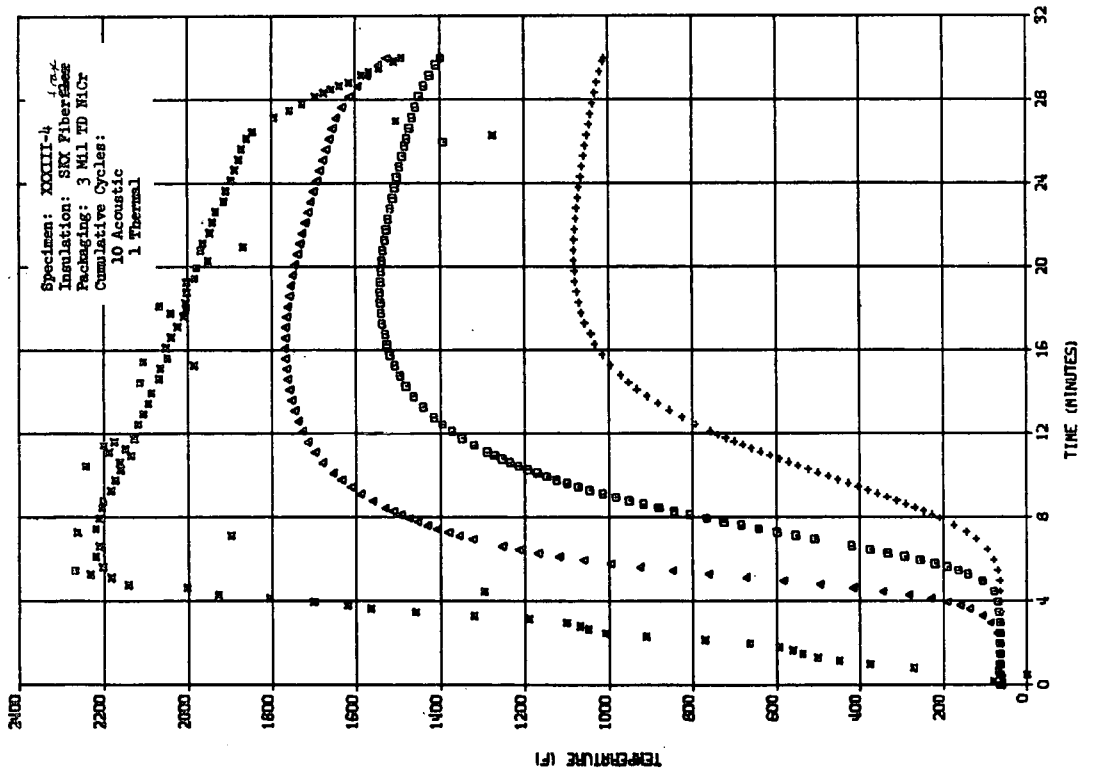

THERMAL RESPONSE OF SKX-FIBERFRAX FELT
First and Last Cycle
2200°F Series

457-2770

Figure 31

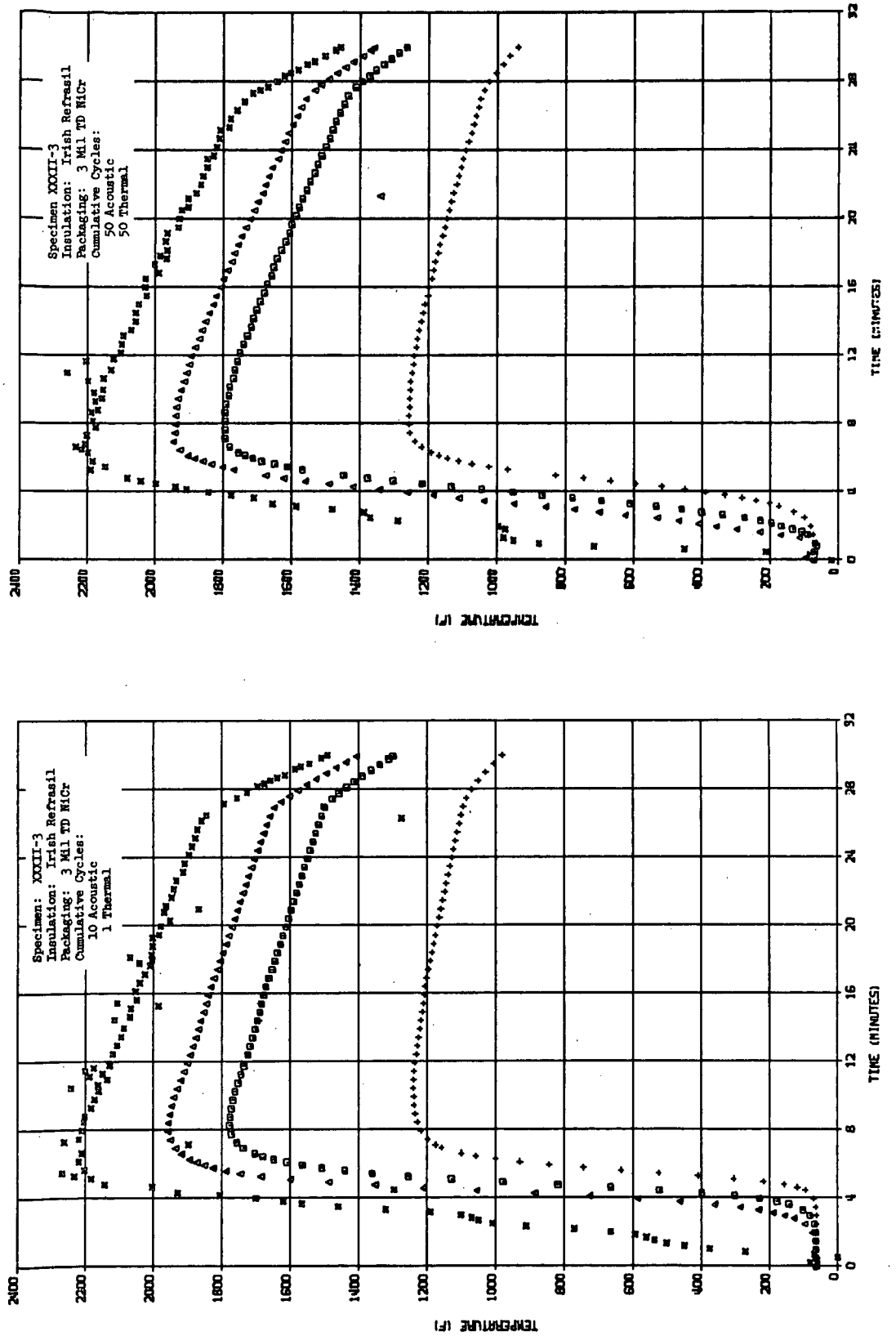

THERMAL RESPONSE OF IRISH REFRASIL B-1576
First and Last Cycle
2200°F Series

457-2752

Figure 32

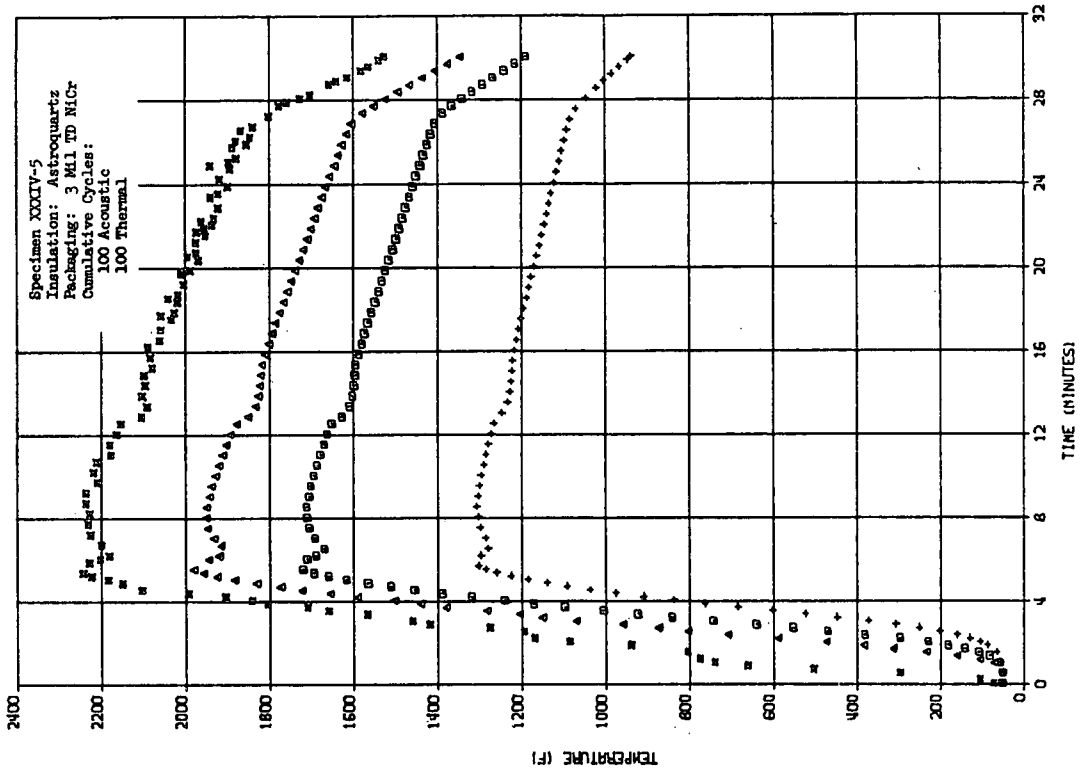

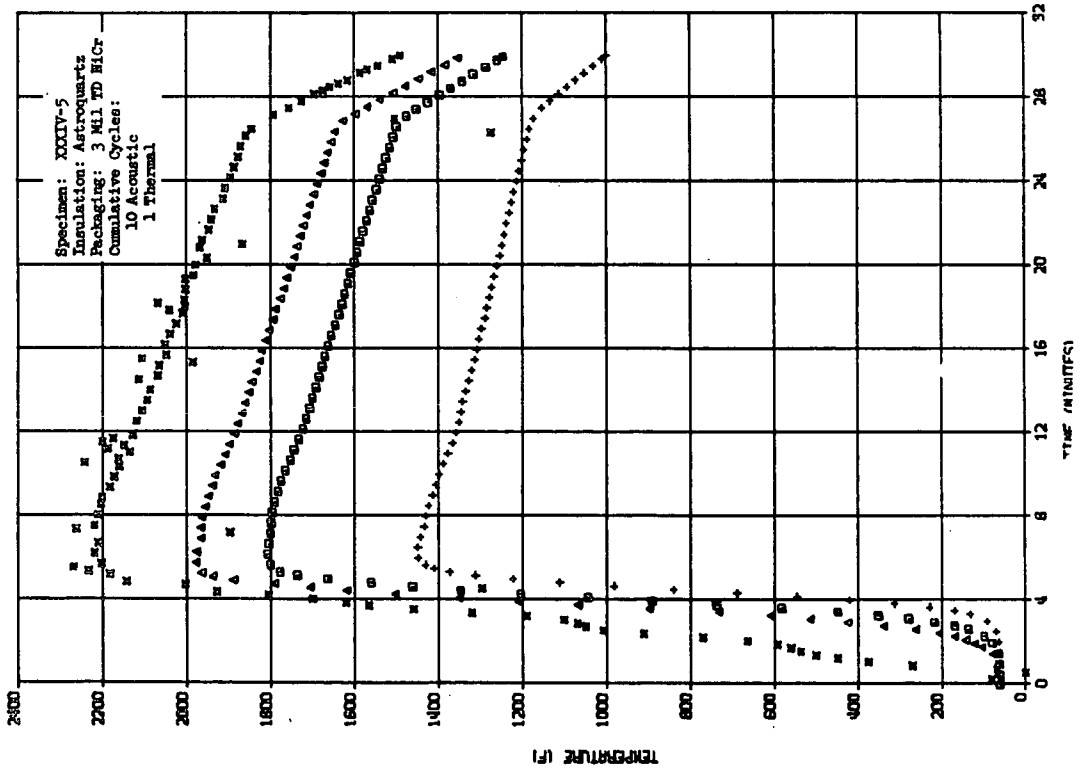

THERMAL RESPONSE OF ASTROQUARTZ
First and Last Cycle
2200°F Series

457-2771

Figure 33

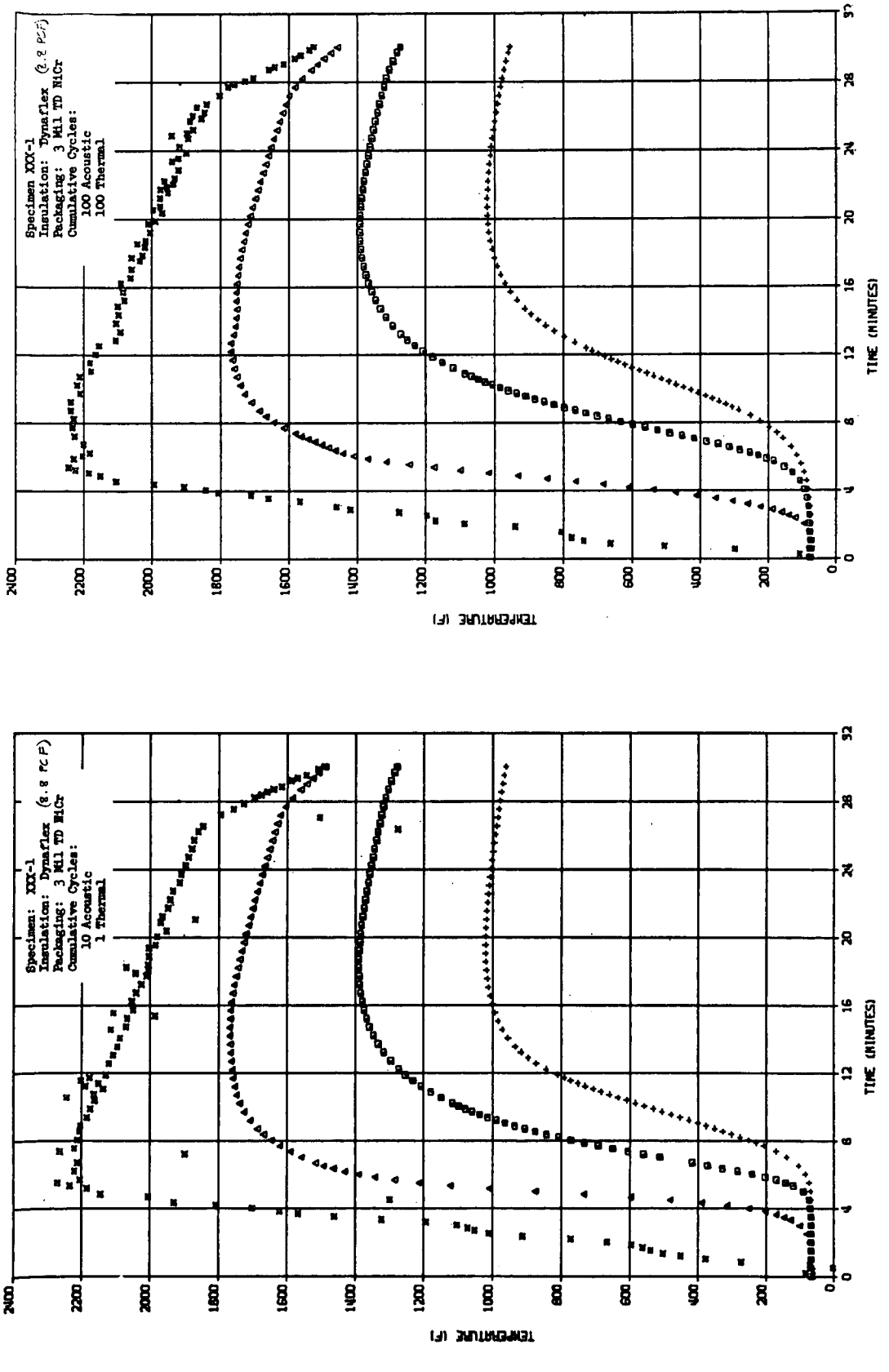

THERMAL RESPONSE OF DYNAFLEX 900
First and Last Cycle
2200°F Series

Figure 34

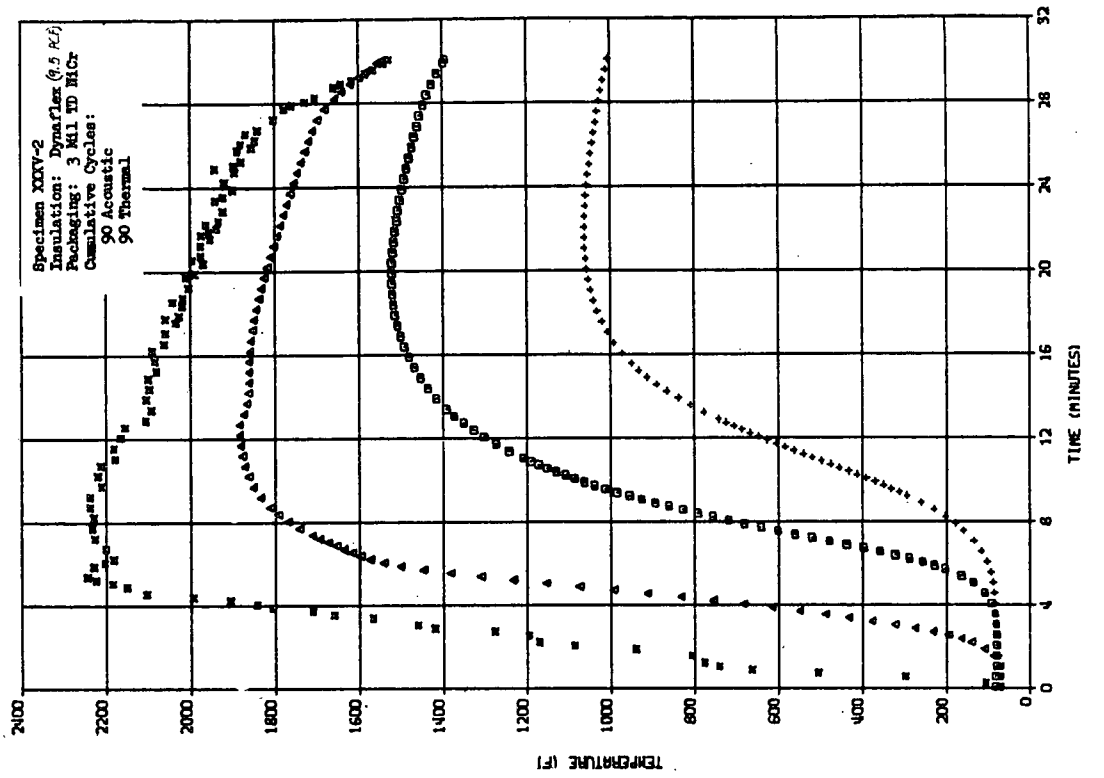

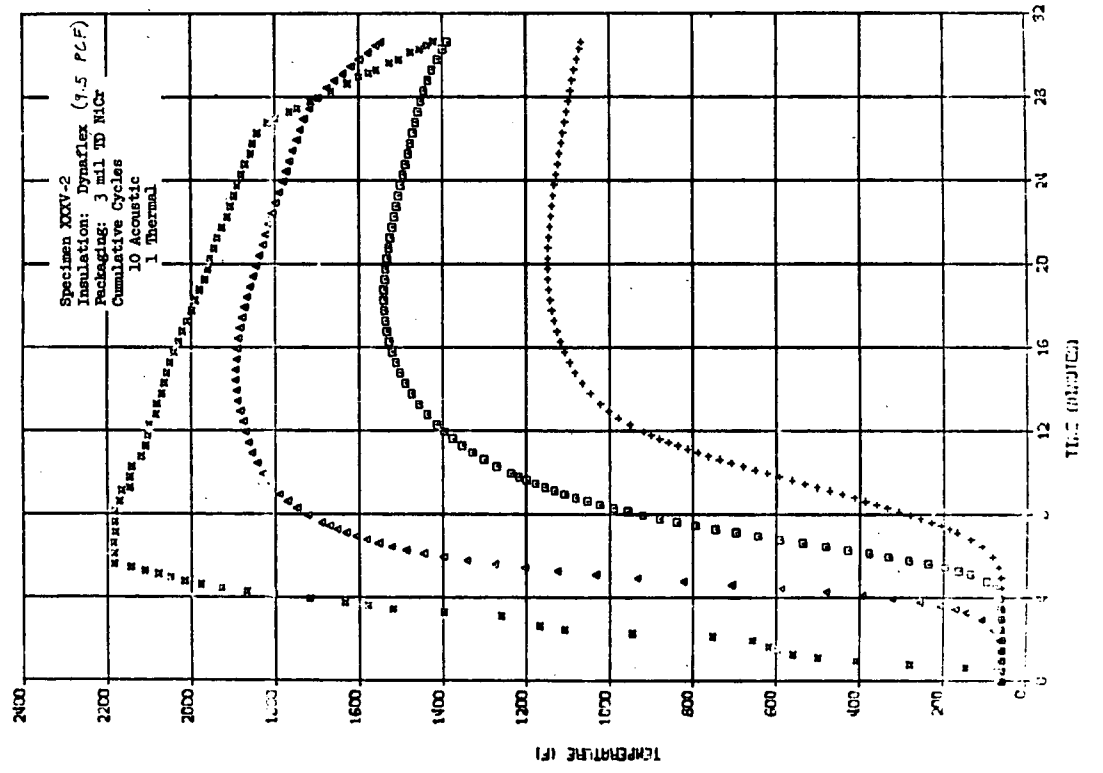

THERMAL RESPONSE OF DYNAFLEX 1200
First and Last Cycle
2200°F Series

457-2772

Figure 35

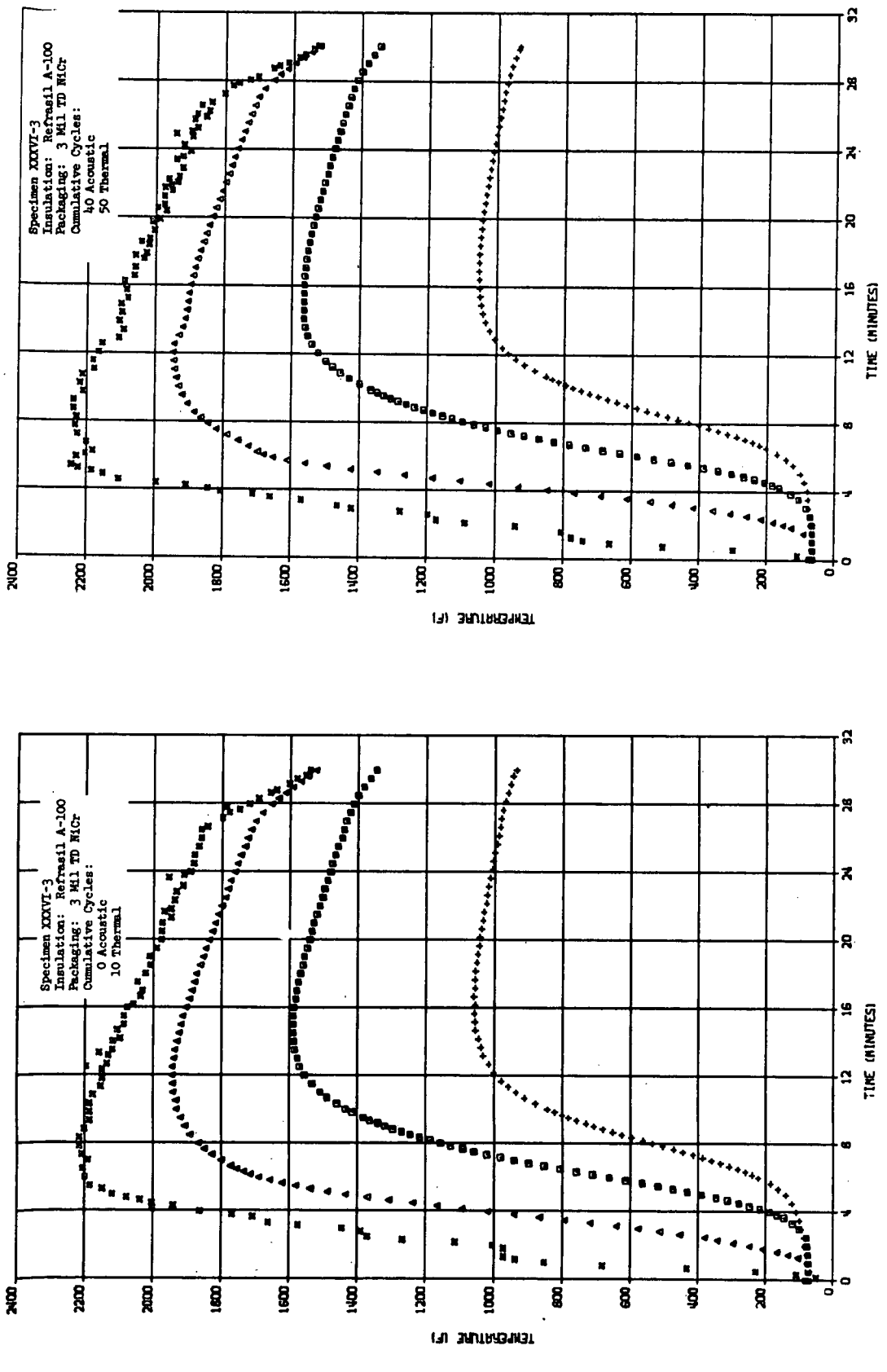

THERMAL RESPONSE OF REFRASIL A-100
First and Last Cycle
2200°F Series

457-2754

Figure 36

materials cannot be made by a simple visual comparison of cold side temperatures in Figures 30-36. However, changes in thermal performance can be indicated by changes in response to specific thermocouples within a specimen, as a function of the number of cycles. To be valid this must assume that the thermocouples did not shift position within the specimen. The installation procedure for thermocouples utilized in the current year's program has greatly reduced the probability of thermocouple movement, though it still cannot be positively guaranteed from cycle to cycle.

Figure 37 shows the peak temperatures attained by the susceptor plate and by each of the three thermocouples installed in each specimen as a function of number of cycles. For simplicity, the temperatures are shown for the tenth cycle of each sequence, except for the first sequence, where the first cycle is shown for baseline data. Random variations in temperature occurred, but no consistent pattern of change is evident. Astroquartz showed an abrupt change for one sequence (11 to 20 cycles) but in subsequent cycles recovered to essentially baseline levels. No explanation is known for this occurrence.

Review of the results of the 2200°F testing indicates:

(a) TD-NiCr has the capability of withstanding 100 cycles of thermal exposure; however, reinforcement may be necessary at hot surface corners to prevent crack propagation. Package designs that allow the hot surface to expand with minimum restriction will provide the best results.

(b) SKX blankets provide a high resistance to mechanical settling and excellent thermal performance. Astroquartz matt also provides excellent mechanical performance, however, excessive thickness may be required. Refrasil A-100 exhibited shrinkage, which while undesirable, could be tolerated. Irish Refrasil exhibited a serious settling problem that could permit unacceptable heat leaks. Dynaflex, while exhibiting generally satisfactory performance, shows variations which may cause concern.

3.4.2 Analysis of Initial Package Failure - After the first 10 thermal cycles of this series, one of the TD-NiCr packages was noted to have suffered what appeared to be chemical attack in two areas of the hot face, another had sustained minor attack. The general condition of these packages immediately after the first 10 cycles was illustrated in Figure 26. These defects were green in color and of a glassy appearance. Since TD-NiCr had previously been cycled 100 times at 2200°F without difficulty, a study was undertaken to determine the cause of these defects. Photomicrographs of selected areas of the most severely affected specimen are shown in Figure 38.

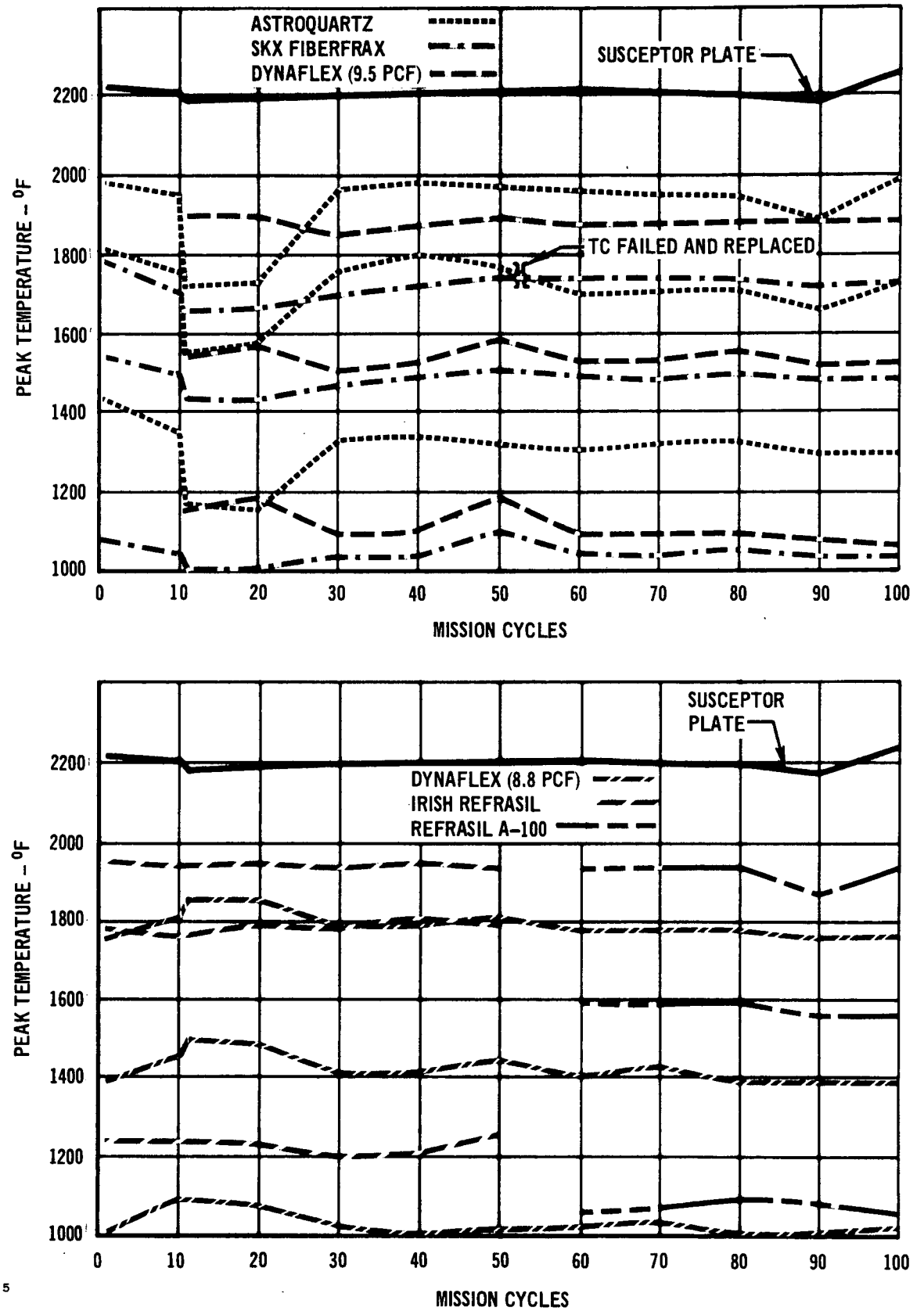

457-2765

PEAK TEMPERATURE RECORDED BY EACH THERMOCOUPLE DURING MISSION CYCLING

Figure 37

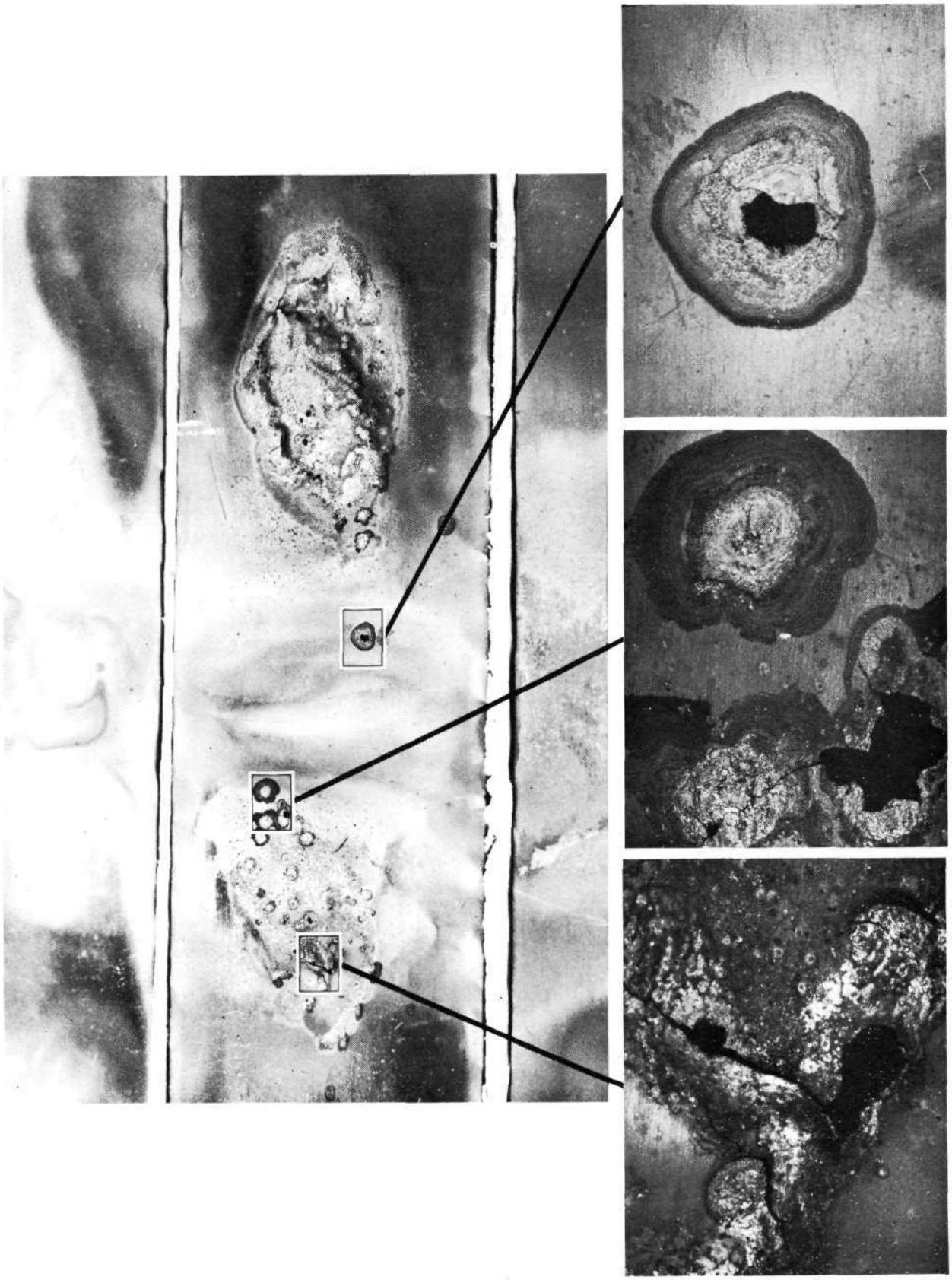

CLOSE UP OF PANEL DEFECTS
(8X REDUCED 36% IN REPRODUCTION)

457-2400

Figure 38

From Figure 26 it can be seen that these defects were present in more than one insulation package. Based on this fact it was assumed that the insulation was not at fault, and this was substantiated in subsequent testing. Subsequent examination of the test conditions revealed that prior to testing, the columbium susceptor plate had several failures of the coating and a repair coating had been sprayed on the plate. Since TD-NiCr had been cycled over the same columbium plate before without difficulty, it was believed that the repair coating was the most likely culprit. A check of the composition of the repair coating revealed that it is essentially a mixture of type 7740 Pyrex frit, Boron, and Cinelac. The Cinelac burns off at a low temperature (400°F) leaving the 7740 glass and the Boron to react with the TD-NiCr. To determine if the repair coating might react with TD-NiCr, a 0.010-in. thick sample was coated with the repair coating and cycled to 2200°F for 10 minutes under a pressure of 10 torr. Examination of this sample revealed that a reaction may have occurred but not to the extent observed with the 0.003-in. thick package material.

Since the exact cause of the failure was not immediately apparent, samples of the reacted area were subjected to a variety of tests which included atomic absorption spectroscopy, infrared spectroscopy up to 25 microns, emission spectography, x-ray diffraction and microprobe analysis. From these tests it was determined that traces were present of boron, silicon, and columbium. X-ray diffraction showed that Ni, NiO, Cr_2O_3 and ThO_2 were present. TD-NiCr is essentially a nickel base alloy with a solid solution of 20% chromium and a fine dispersion of ThO_2 (2% by wt). Therefore, the x-ray diffraction revealed that only the base metal and its oxides were present, and the emission spectograph that B, Si, and Cb were present.

The only place the boron, silicon, or columbium could have come from was the repair coating or the R512E coating (fused slurry silicide) on the columbium susceptor. Reviewing the composition of the repair coating and the original R512E columbium coating, the source of the metallic constituents found by the emission spectograph were determined to be B, B_2O_3, SiO_2, and $CbSi_2$. Once the possible compounds were determined the next step was to determine if these compounds would form low melting compounds with Ni, NiO, Cr_2O_3 or ThO_2. By examining the phase diagrams (Ref 5 and 6) of all possible combinations, it was determined that only B and B_2O_3 would react with Ni and ThO_2 to form low melting compounds. The phase diagrams for these two systems are shown in Figures 39 and 40. From the phase diagrams it can be seen that low melting compounds are formed at 200°C and at 900°C. These reactions are believed to have caused the defects in TD-NiCr.

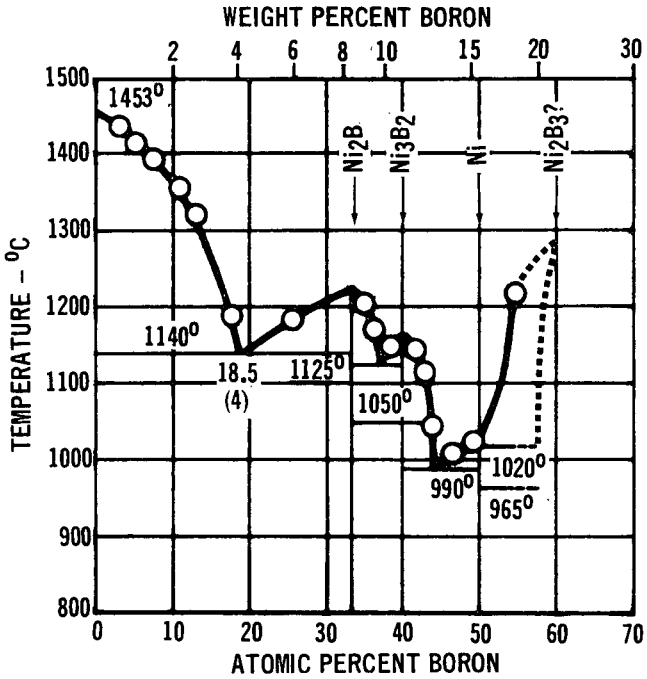

BORON – NICKEL PHASE DIAGRAM
(Reference 5)

457-2402

Figure 39

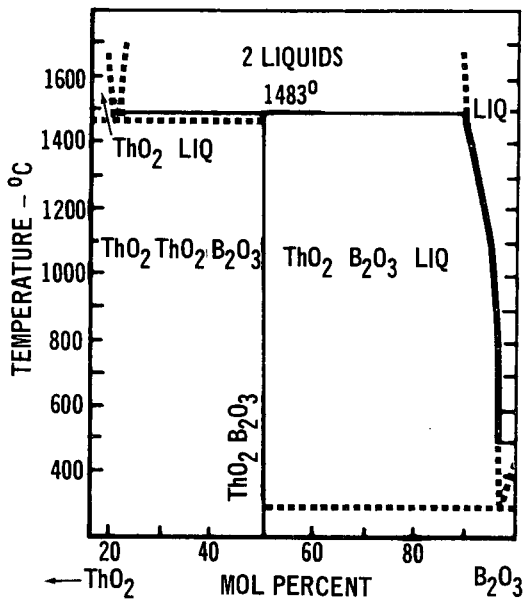

B_2O_3 – ThO_2 PHASE DIAGRAM
(Reference 6)

457-2403

Figure 40

Once the cause of the melting of the TD-NiCr had been identified, the question remained as to how the packages had contacted the repair coating since these materials do not vaporize at 10 torr. From calculations it was determined that the high thermal expansion of the TD-NiCr caused the package to deflect about 1", which was enough to cause it to touch the susceptor and become contaminated with the molten repair coating.

The mechanism by which the defects could have occurred as two isolated areas on one package is illustrated below:

457-2401

To alleviate the problem during subsequent cycles, modification was made to the test set-up to allow greater clearance between the heater susceptor and the test specimens.

3.5 2500°F Mission Simulation - The peak temperature to which a refractory metal skin of the orbiter vehicle would be exposed is generally accepted as 2500°F. While only a relatively small area of the vehicle would see this high a temperature, it is also the most technically difficult, and no less critical than other areas of the orbiter. One of the principal goals of this program was to evaluate materials for this service for 100-mission cycles.

Selection of packaging materials for 2500°F service was limited solely to refractory metal alloys with appropriate oxidation resistant coatings. Selection of coated columbium alloy for this purpose was made on the basis of separate studies of the radiative skin made by MDAC-E on the Phase A and Phase B space shuttle contracts. The specific alloy used, FS-80, was dictated not by any superiority of properties, but by availability in thin foil gages within the time span allowed by this contract.

The thickness of the vehicle radiative TPS skin where columbium would be employed was only 0.010-inch. Therefore, it was unrealistic to consider a package thickness greater than about one-half that amount. The use of coated columbium

also necessitated modifications to the package design and construction. As it is undesirable to form columbium with close faying surfaces before coating (coating may not penetrate well, leaving uncoated or poorly coated areas), the box design was changed to have a single (cool side) attach tab. Also, the cool face of the box was a sheet of Inconel-601, attached to the coated columbium box by machine screws.

The columbium box was first formed to the desired shape (top, sides and ends), with corrugation stiffening of the hot surface. The sides and end were joined by TIG welding, after which the box was coated. The FS-80 columbium used was 5 mils thick before coating and approximately 3 mils thick after the R-512E coating was applied by Sylvania. This difference was due to consumption of the columbium during coating. The net coating was approximately 1.2 mils per side. A completed test specimen is shown in Figure 41.

The insulations evaluated in the 2500°F testing were selected on the basis of earlier 2200°F testing. Results from the current 2200° testing were not yet available at the time the 2500°F specimens were prepared. Because of the higher temperature, the choice of materials was somewhat limited. Of the insulations used, only three are claimed by their vendors to be capable of 2500°F service. These are Dynaquartz, Dynaflex and Irish Refrasil B-1576. The other insulations used had potential, provided effects of devitrification were not severe.

Dynaquartz block yielded good thermal results but cracked into four pieces during vibration/acoustic testing when tested previously (Ref 1). To accommodate this potential problem and eliminate possible direct radiant interchange between hot and cold surfaces at the cracks, the Dynaquartz was installed as four individual pieces with shiplap joints, providing 1.0-inch overlap at each break. Astroquartz was installed in the package at a much higher density (4.28 pcf) than normally used ($\sim$ 1.0 pcf) in order to provide a more reasonable temperature drop through the specimen.

A listing of the insulations evaluated in the 2500°F testing is presented in Table IV with a summary of pertinent test results. Photographs of the specimens at various stages of the testing are shown in Figures 42 through 49.

Performance of the coated columbium indicated that 50 cycles can be achieved with acceptable performance with the metal and coating thickness employed here. The loss of metal that occurred after 50 cycles is believed to have originated at flaws in the coating or at thin spots, permitting localized oxidation. The localized oxidation, starting as small holes, apparently progressed outwardly to enlarge

COATED COLUMBIUM TEST PACKAGE PRIOR TO 2500°F TESTING

457-2785

Figure 41

Table IV

2500°F TEST RESULTS

INSULATION		CUMULATIVE CYCLES		MAJOR TEST EFFECTS	
MATERIAL	DENSITY (PCF)	ACOUSTIC	THERMAL	INSULATION	COATED Cb PACKAGE
ASTROQUARTZ	4.28	90	100	THE FIRST 3/4 IN. FROM THE HOT SIDE WAS HARDENED. NO SHRINKAGE (INSULATION ~19.7 IN. LONG FROM VENDOR)	SEVERAL HOLES 0.15 IN. DIAMETER OR LESS IN THE TOP OF THE PACKAGE AFTER 90 ACOUSTIC AND 100 THERMAL CYCLES
IRISH REFRASIL B1576	4.12	100	100	NO SHRINKAGE. A 1/4 IN. LAYER OF INSULATION ABOUT 0.6 IN. FROM THE HOT SURFACE WAS HARDENED	ABOUT 3% OF THE HOT FACE OF PACKAGE OXIDIZED AND GONE AFTER 100 CYCLES
SKX FIBERFRAX	7.06	100	100	FIRST 1 IN. FROM THE HOT SIDE HARDENED. UP TO 1/4 IN. SHRINKAGE IN THE FIRST 3/8 IN. FROM THE HOT SIDE	0.05 IN. DIAMETER HOLE IN THE TOP OF THE PACKAGE AFTER 30 CYCLES. ABOUT 35% OF HOT FACE OF PACKAGE OXIDIZED AND GONE AFTER 100 CYCLES
REFRASIL A-100	7.54	60	50	FIRST 3/4 IN. FROM THE HOT SIDE HARDENED. SHRINKAGE OF 1 IN. FOR DEPTH OF 0.6 IN.	OXIDATION HOLES OF 0.05 IN. DIAMETER OR LESS ON THE HOT SURFACE AFTER 60 ACOUSTIC AND 50 THERMAL CYCLES
DYNAQUARTZ	6.14	100	100	ABOUT 1/8 IN. VOID ACROSS ONE END. CRACKED COMPLETELY ACROSS IN 3 PLACES	CRACK IN 20 IN. LONG SIDE OF PACKAGE, SHOWED UP AFTER 10 CYCLES AND INCREASED TO ABOUT 1.5 IN. AFTER 100 CYCLES. ABOUT 10% OF HOT FACE OF PACKAGE OXIDIZED AND GONE AFTER 100 CYCLES
DYNAFLEX	8.76	50	50	FIRST 1 IN. FROM THE HOT SIDE HARDENED. ABOUT 1/4 IN. SPACE AT ONE END	0.1 IN. HOLE IN THE TOP OF THE PACKAGE AFTER 10 CYCLES. ABOUT 1% OF HOT FACE OF PACKAGE OXIDIZED AND GONE AFTER 50 CYCLES

457-2762

the areas in subsequent cycles as the columbium core was exposed. The net coating thickness, as determined from metallographs, was 0.6-0.8 mil on the interior of the package and 1.0-1.2 mil on the exterior. It is believed that with a slightly thicker virgin columbium and a correspondingly heavier coating, the full 100 cycles could have been achieved without major loss of metal.

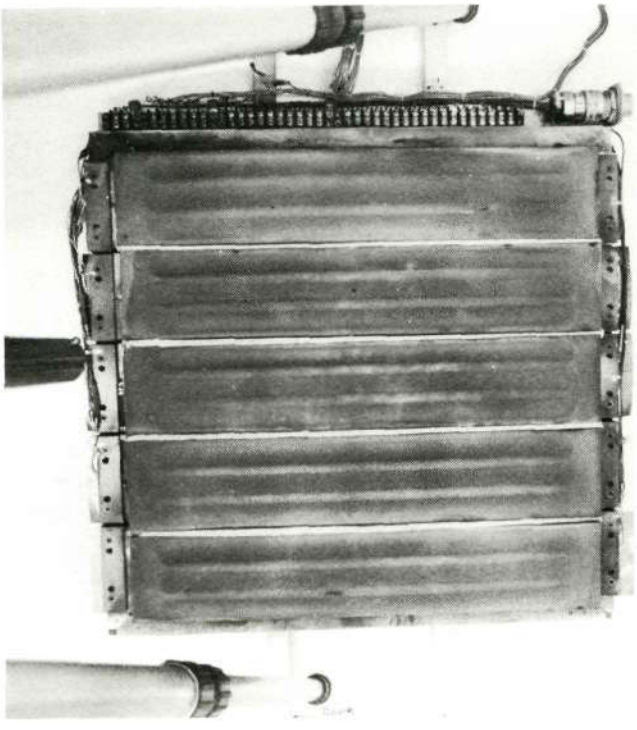

457-2786

COLUMBIUM PACKAGES AFTER 10 CYCLES (2500°F)
The Small Hole in One Package was Repaired

Figure 42

457-2787

COLUMBIUM PACKAGES AFTER 30 CYCLES (2500°F)
Cracks in the End Plates Beginning to Appear

Figure 43

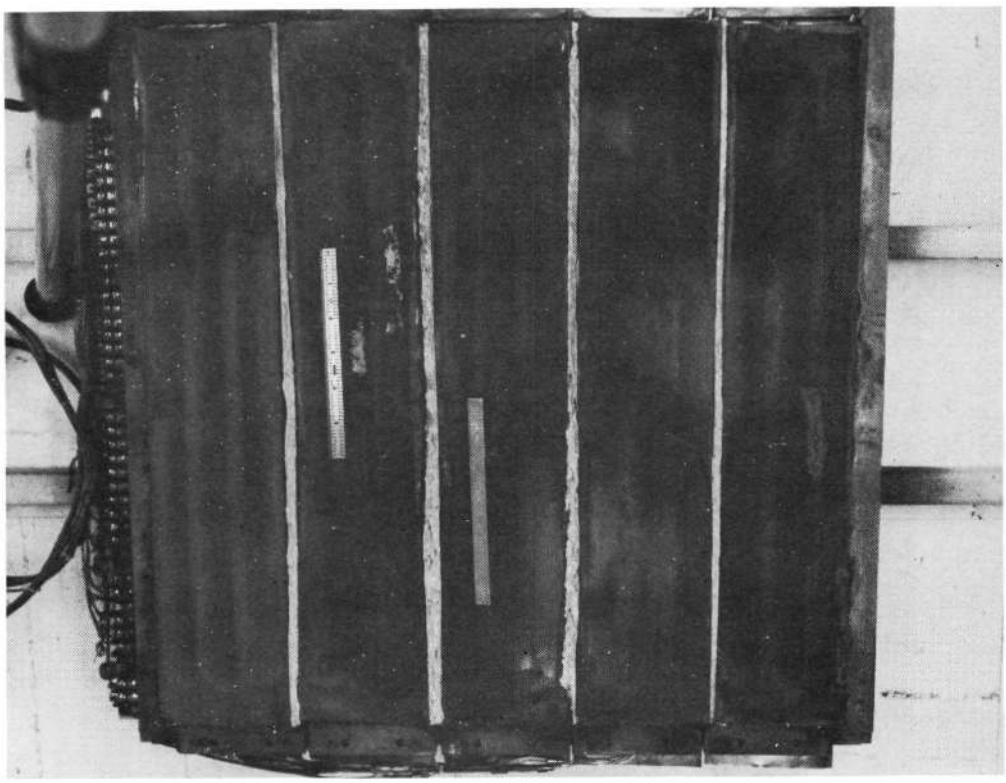

457-2788

COLUMBIUM PACKAGES AFTER 50 CYCLES (2500°F)
Oxidation Beginning to Eat Through Hot Surface – Second Package from Left Removed at this Point

Figure 44

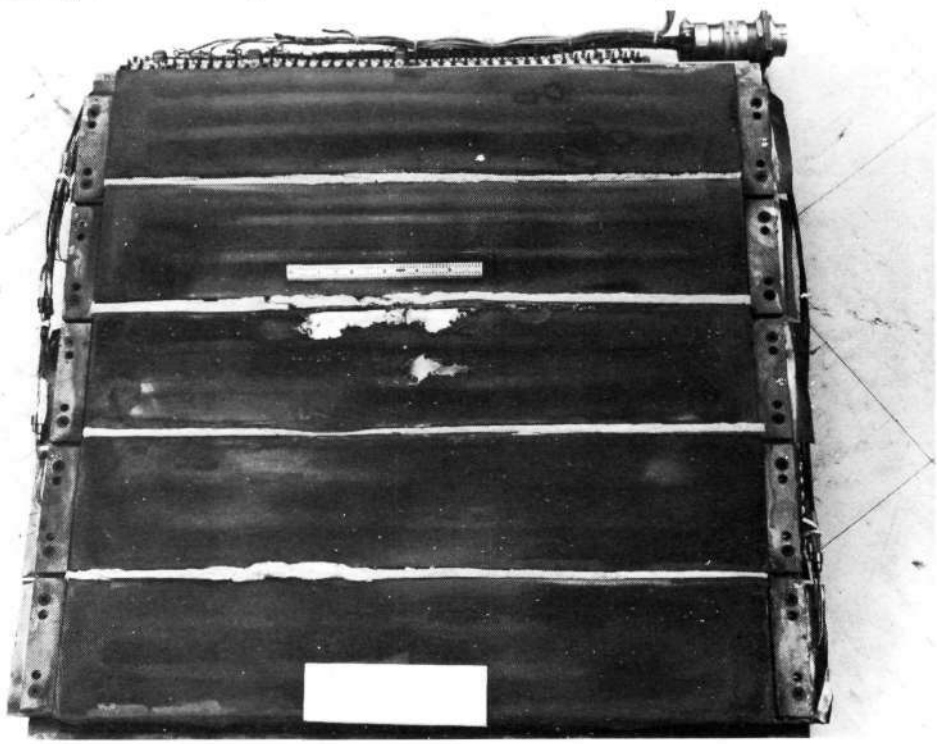

457-2789

COLUMBIUM PACKAGES AFTER 70 CYCLES (2500°F)
Growth of Area of Metal Loss is Apparent Continued in Test to Observe Consequences

Figure 45

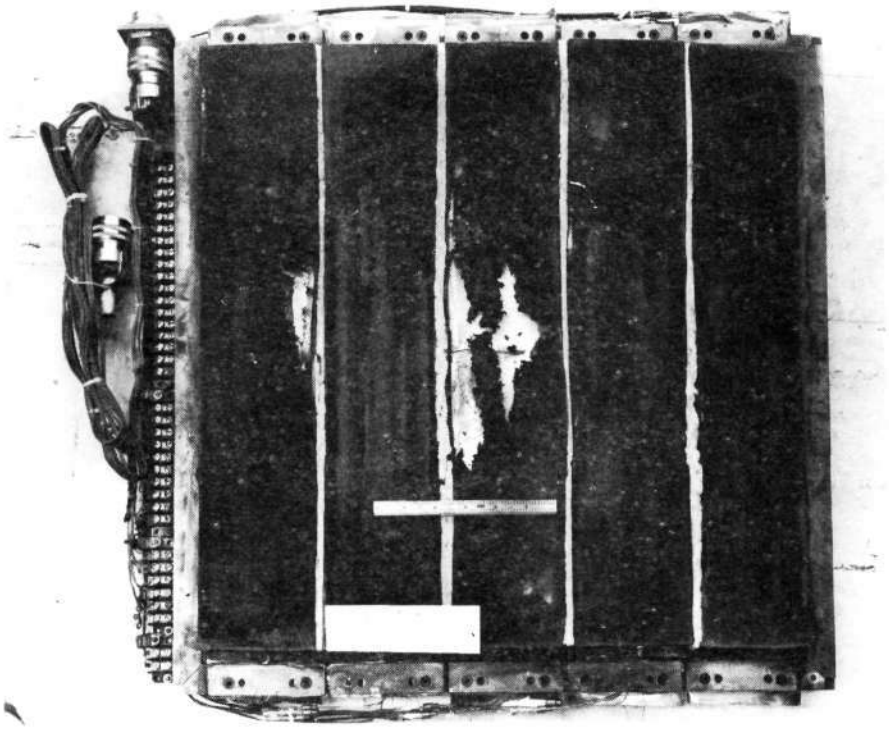

457-2790

COLUMBIUM PACKAGES AFTER 80 CYCLES (2500°F)
Note Continued Growth of Oxidation on Two Packages and Beginning on a Third

Figure 46

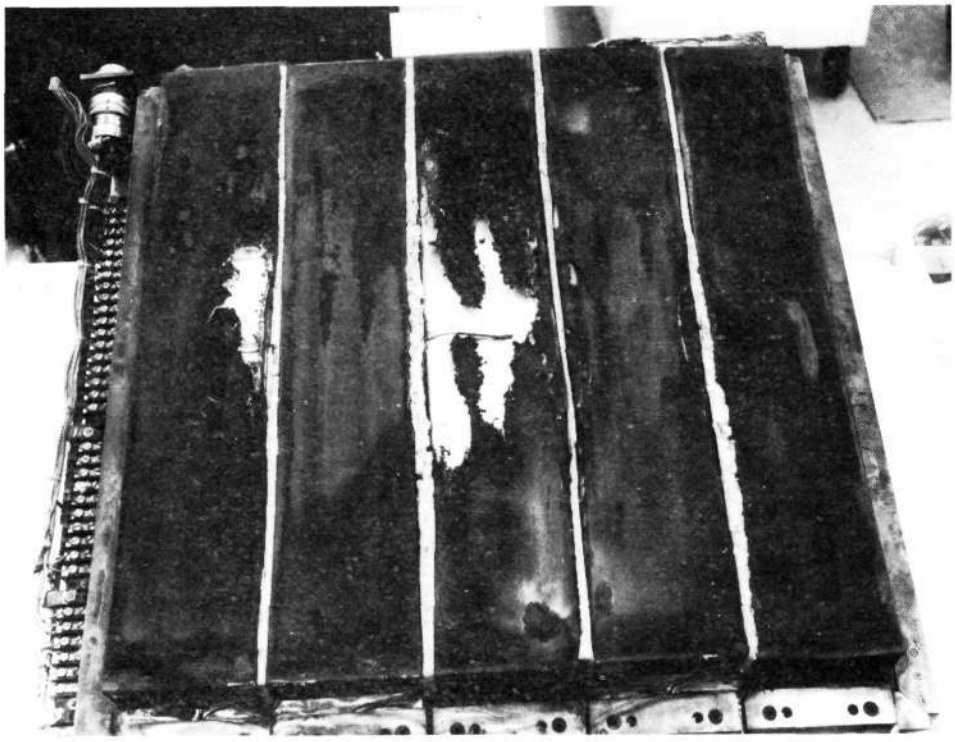

457-2791

COLUMBIUM PACKAGES AFTER 90 CYCLES
Metal Loss Continuing on Three Packages

Figure 47

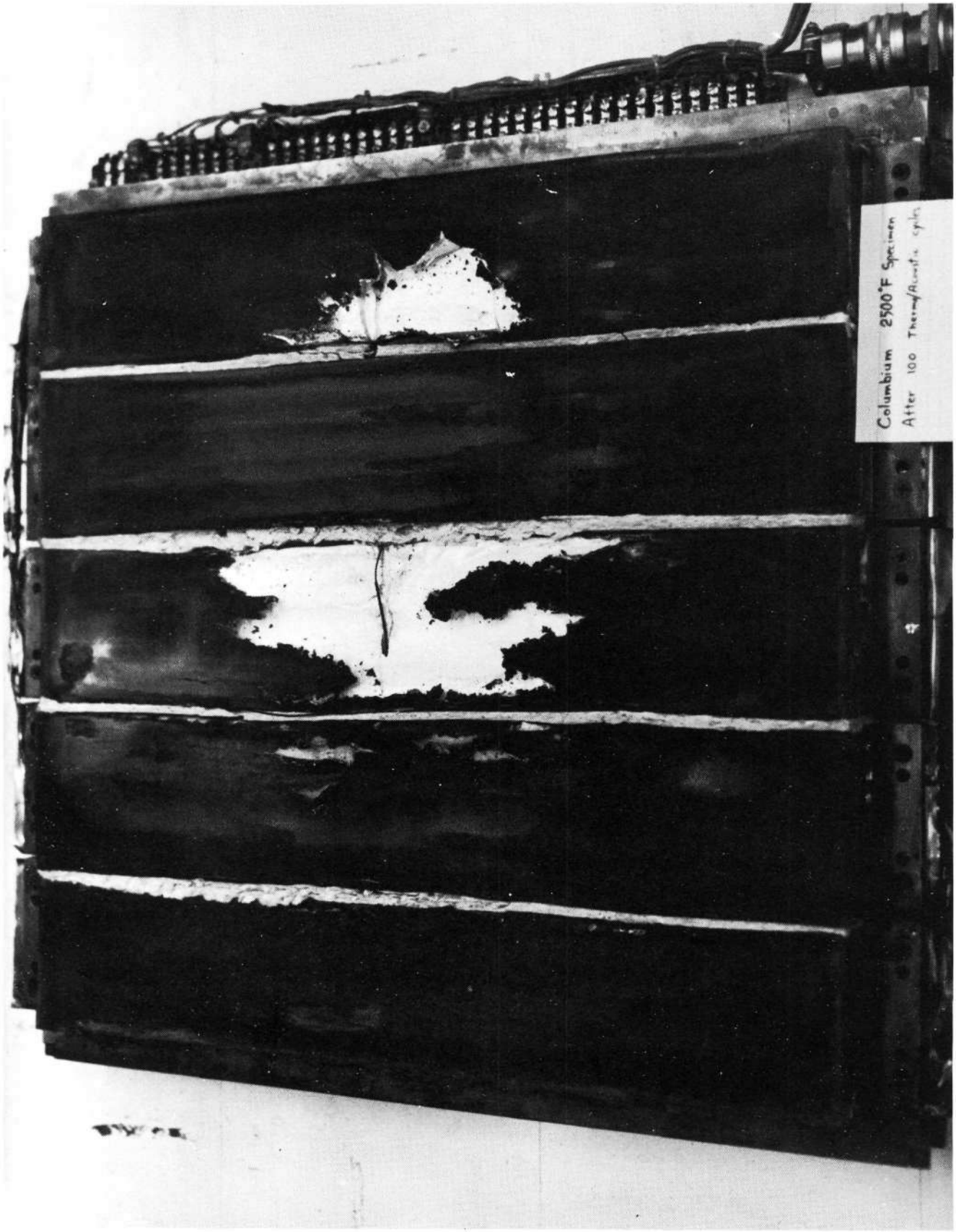

COLUMBIUM PACKAGES AFTER 100 THERMAL AND ACOUSTIC CYCLES (2500°F)
Center Package Contained SKX-Felt. Package on Far Right, Dynaquartz

457-2792

Figure 48

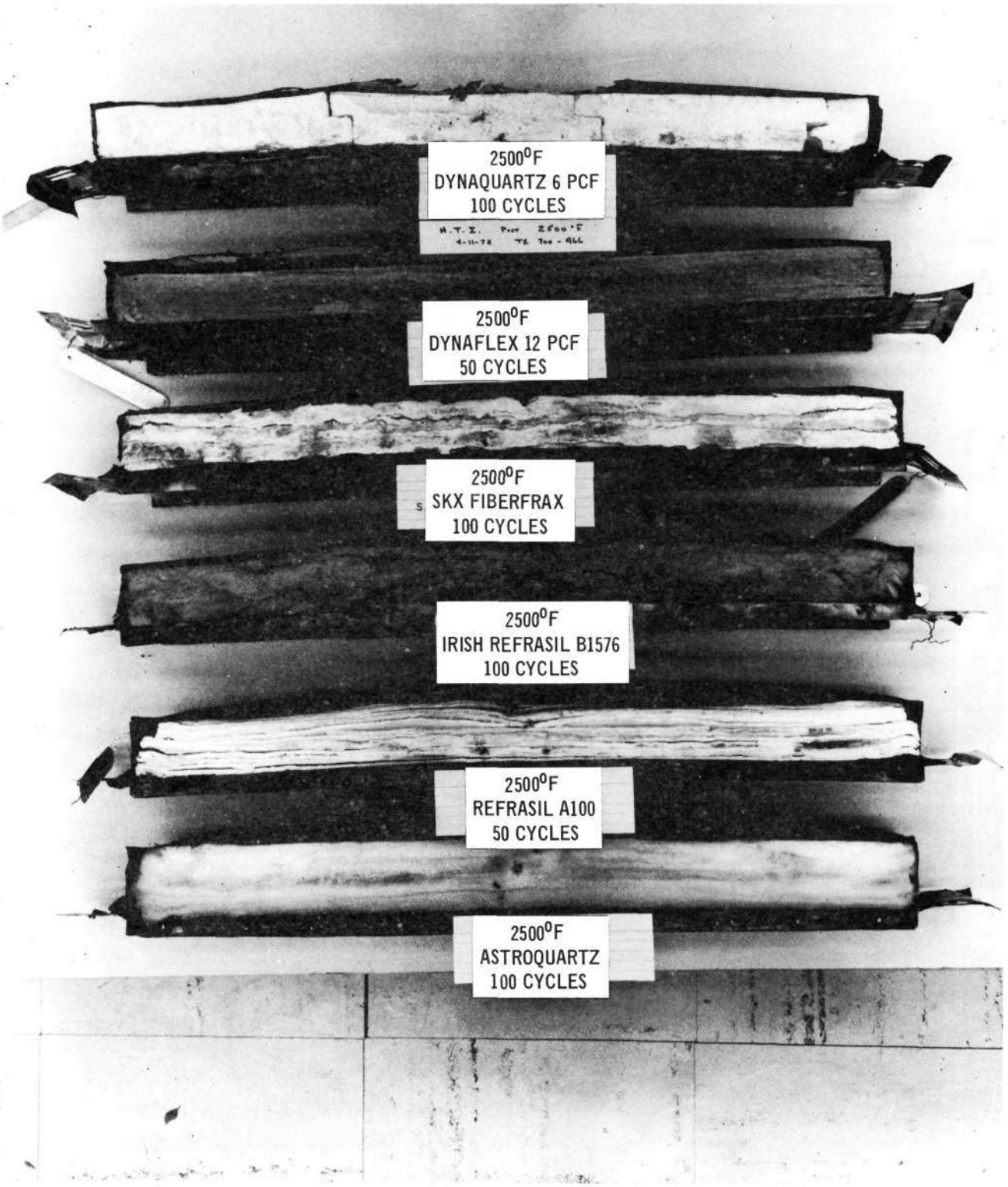

457-2782

INSULATIONS AFTER ACOUSTIC AND THERMAL TESTING AT 2500°F

Figure 49

The insulations included in this test generally showed equal or less shrinkage and settling than in the 2200°F mission simulation. Refrasil A-100, however, was an exception to this. The hot portions of the insulations were hardened to a greater degree and to a greater depth than in the 2200°F tests. This may have contributed greater resistance to settling. Irish Refrasil B-1576 displayed no settling or shrinkage, in contradiction to its performance at 2200°F. Astroquartz, installed at 4.3 pcf density, instead of the usual 1.0 pcf, again showed no dimensional change. Its heat transfer rate was notably higher than for the other materials, judging by the temperature responses. This was not an unexpected result in light of the infrared transmission characteristics of Astroquartz as described in Section 5.2 of this report.

The attempt to prevent cracking of Dynaquartz by installing it in short segments with overlapping joints was unsuccessful. It still cracked through the thickness, but provided excellent thermal performance. The SKX blanket shrank about 1/4-inch at the hot surface; the shrinkage became undetectable about 1-inch from the hot surface. It was this material which had about 35% of its surface exposed, due to loss of package hot face, during the later cycles of acoustic and thermal exposure. Dynaflex (9 pcf) settled 1/4-inch, and Refrasil A-100 shrank 1.0-inch at the hot face and showed shrinkage to a depth of 0.6-inch.

The peak temperatures recorded by each of the three thermocouples installed in the insulations are shown as a function of the number of test cycles in Figures 50 and 51. The points at which thermocouples failed and were replaced are also noted on the figures as thermocouple location could be altered by replacement. The temperature histories for the first and last thermal cycle for each specimen are shown in Figures 52-57.

Close visual examination of the test specimens was made after the completion of testing for indications of reaction between the individual insulations and the coated columbium. No evidence of reaction or lack of compatibility was detected.

Because of the apparent necessity for a thickness of coated columbium packaging material approaching that of the heat shield, there is likely to be considerable merit in an alternate design approach. This would enclose the insulation in a five-sided package, with the heat shield itself forming the sixth side. This would provide a substantial weight reduction, though it also complicates moisture proofing.

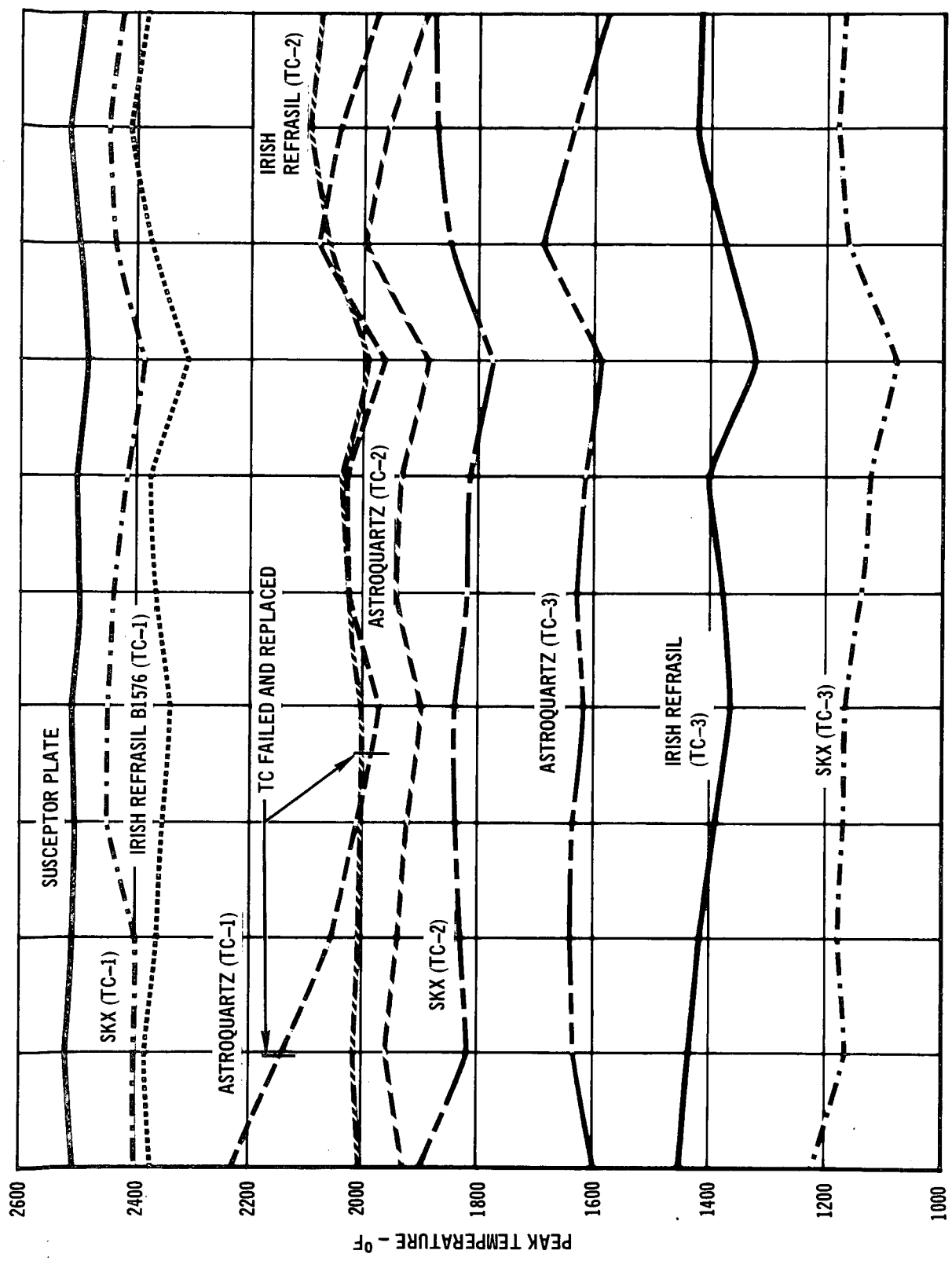

PEAK TEMPERATURES RECORDED BY SPECIMEN THERMOCOUPLES IN 2500°F MISSION SIMULATION

Figure 50

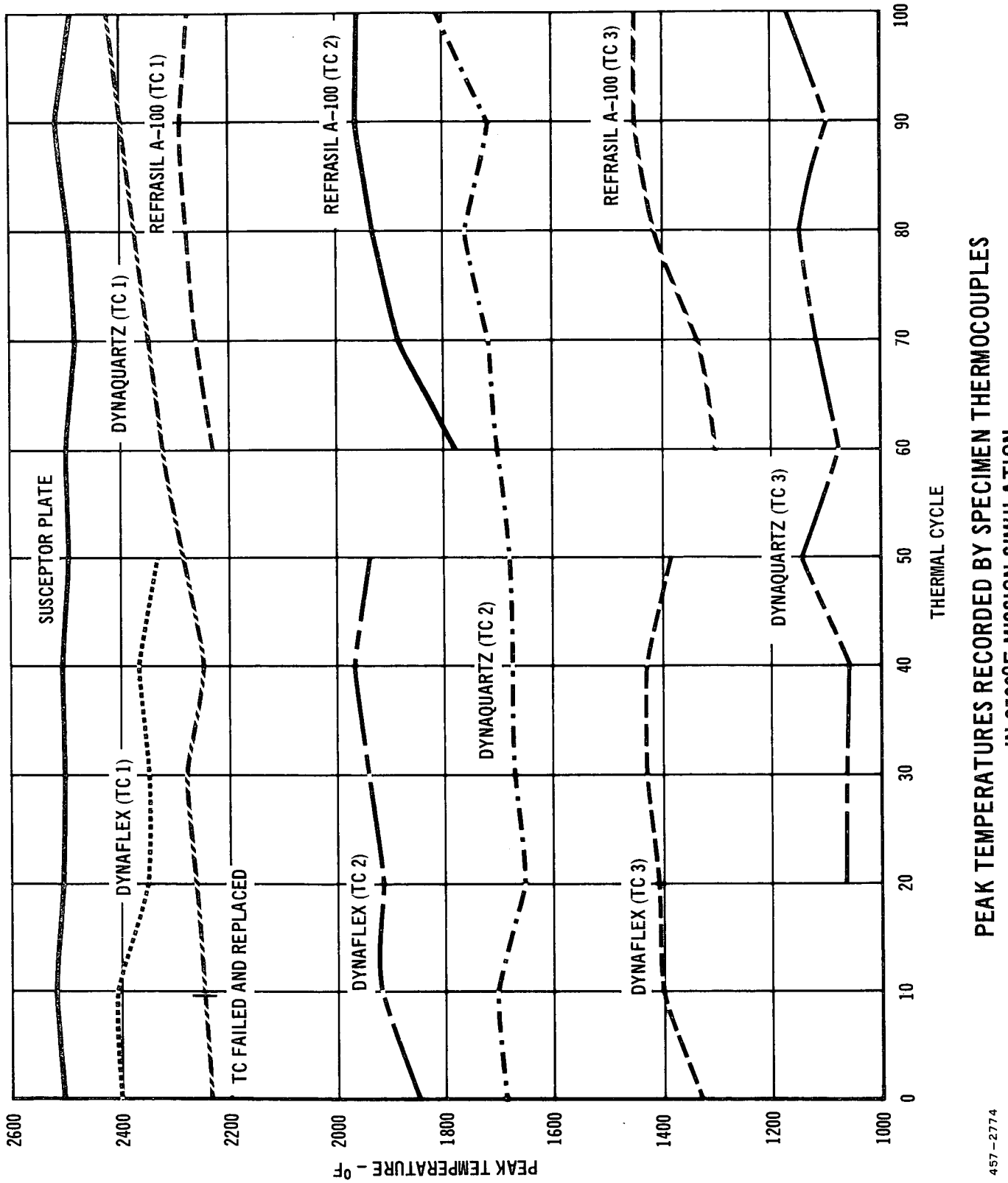

PEAK TEMPERATURES RECORDED BY SPECIMEN THERMOCOUPLES IN 2500°F MISSION SIMULATION

Figure 51

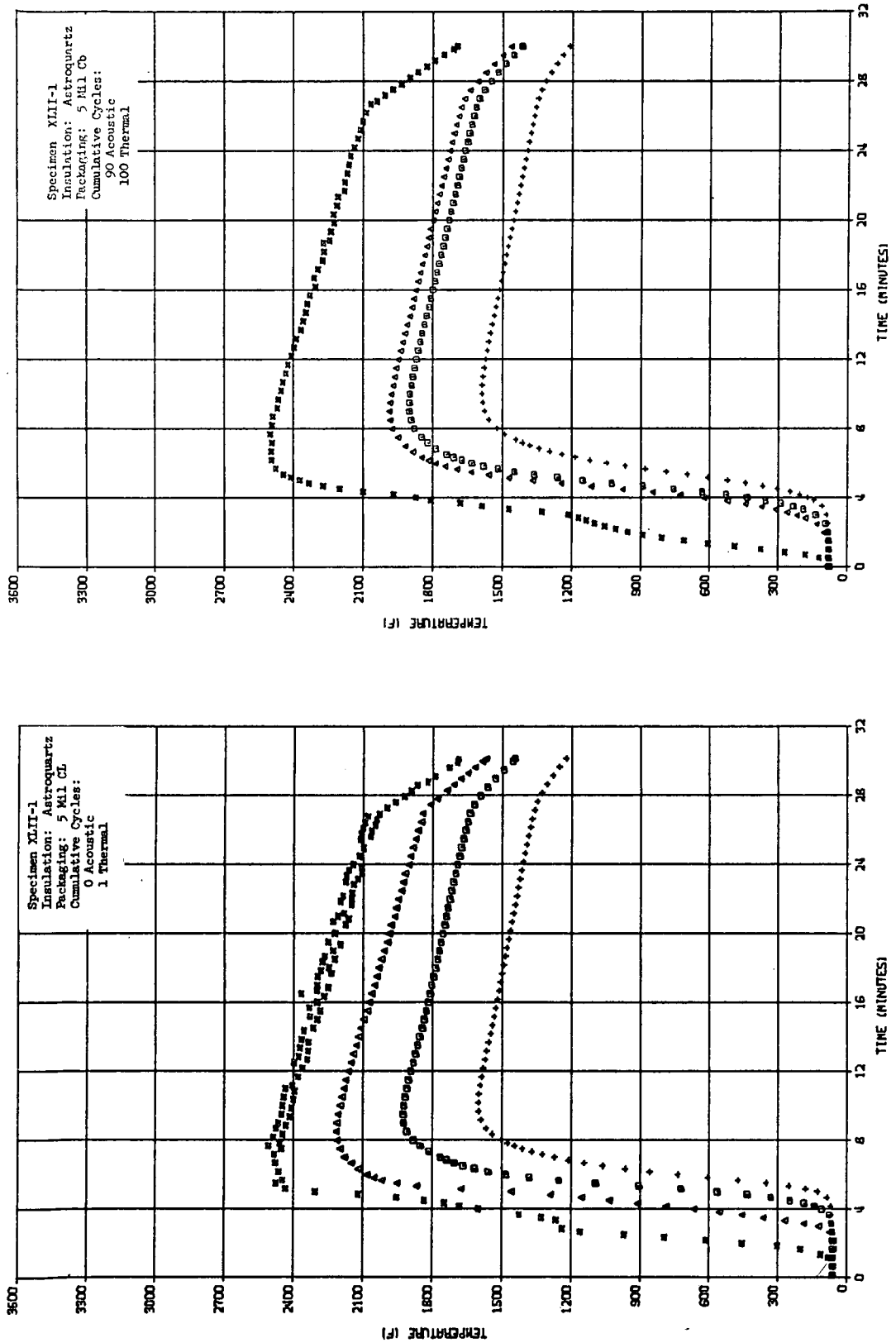

TIME–TEMPERATURE PROFILES – ASTROQUARTZ (4.3 LB/FT^3)
First and Last Thermal Cycles
2500°F Series

457-2764

Figure 52

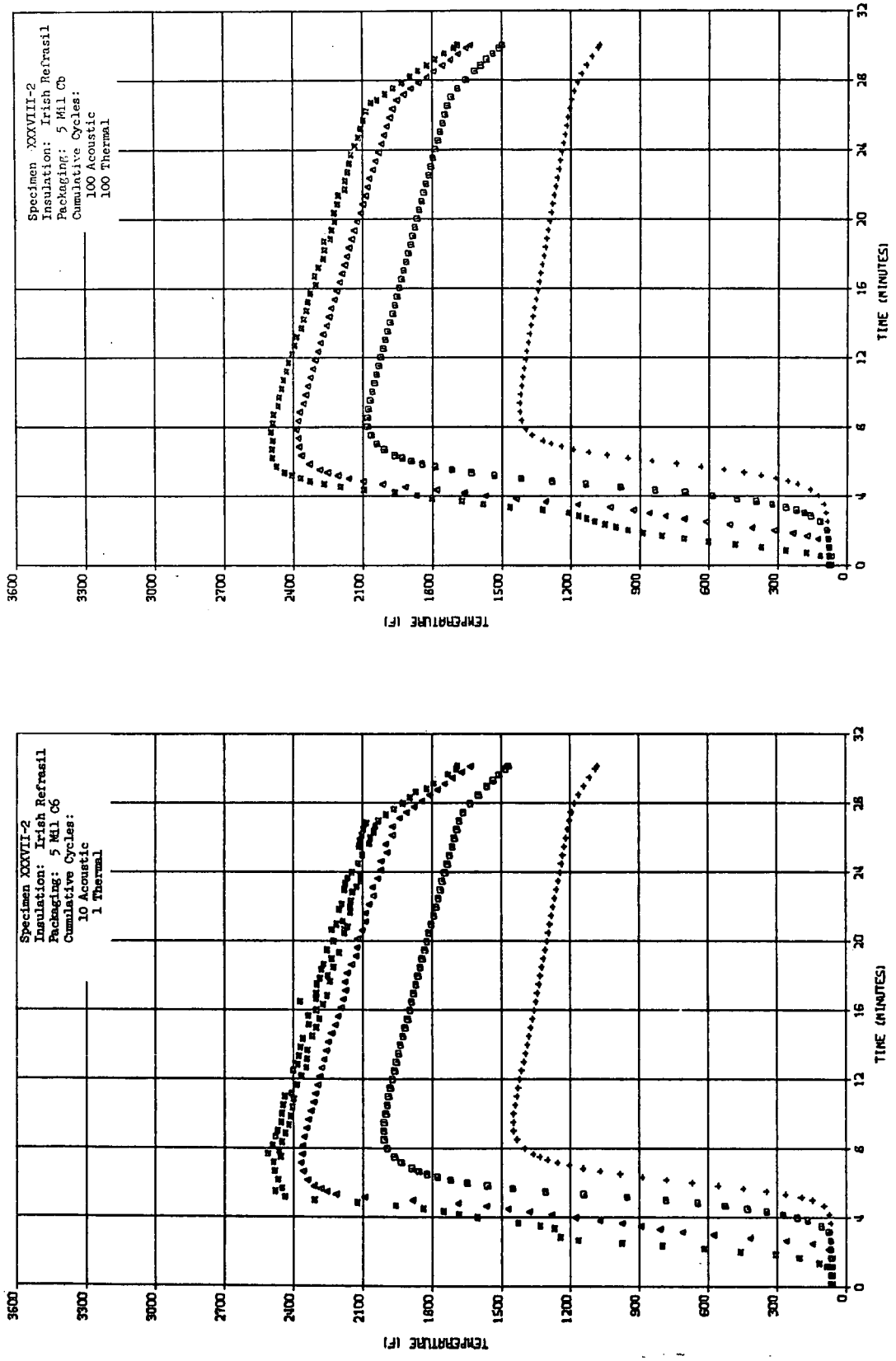

TIME–TEMPERATURE PROFILES – IRISH REFRASIL B-1576-1
First and Last Thermal Cycles
2500°F Series

457-2775

Figure 53

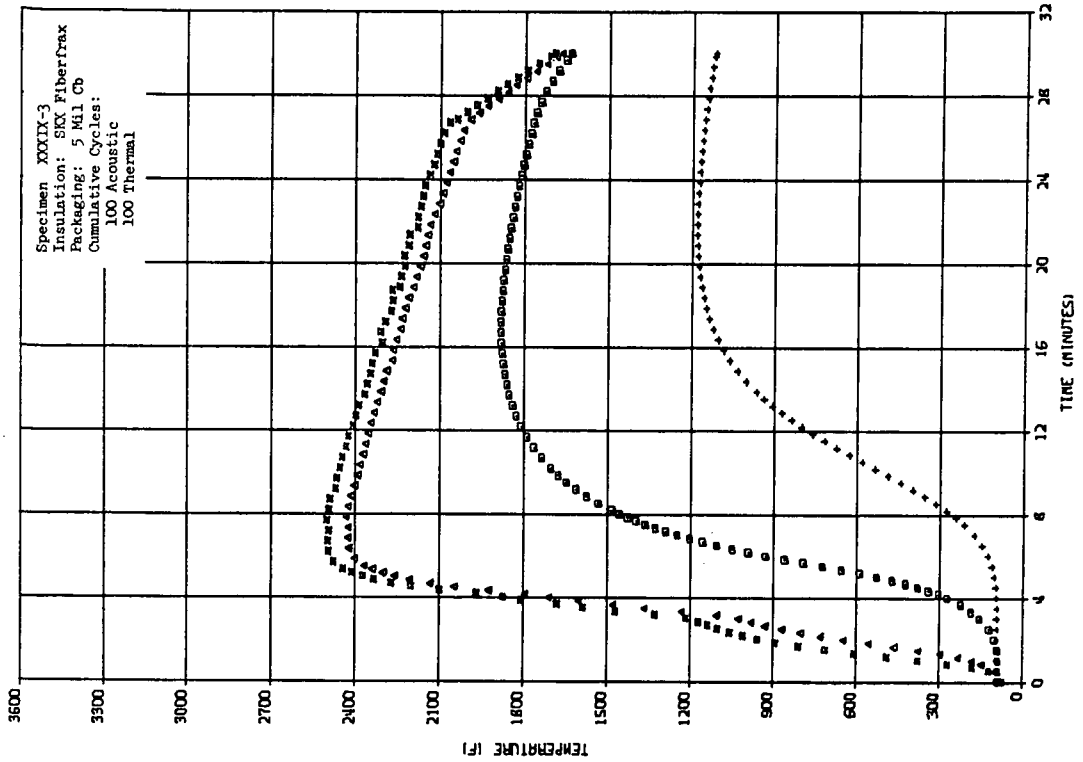

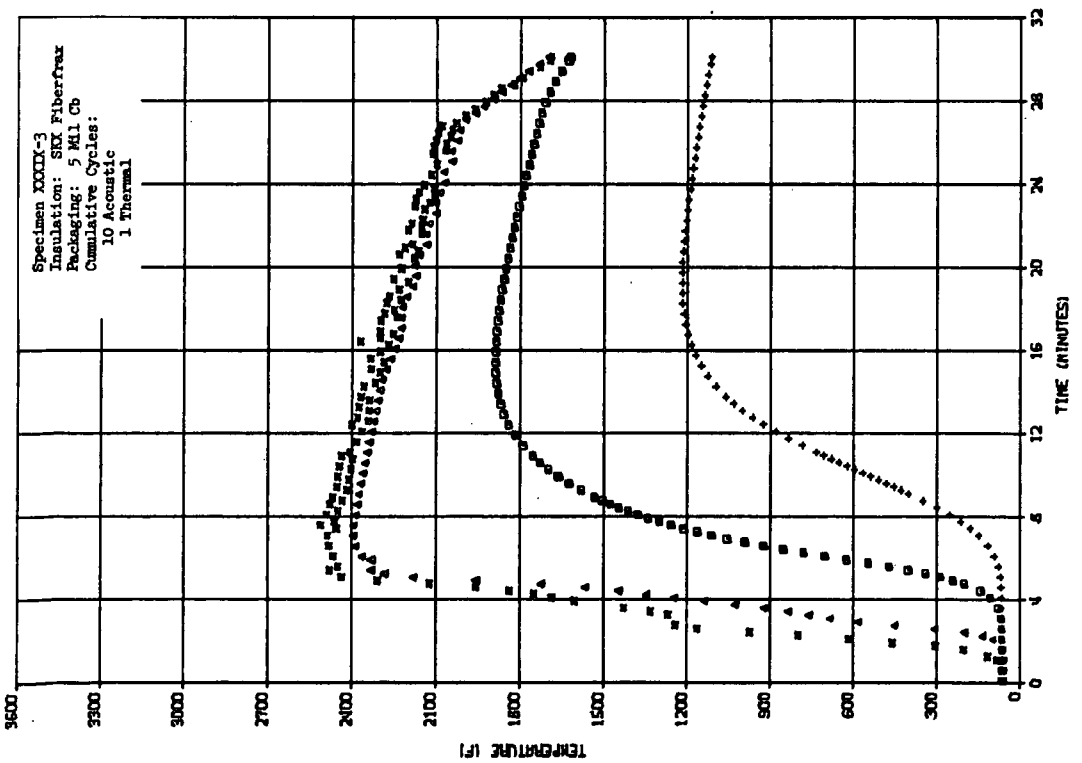

TIME–TEMPERATURE PROFILES – SKX FIBERFRAX
First and Last Thermal Cycles
2500°F Series

457-2765

Figure 54

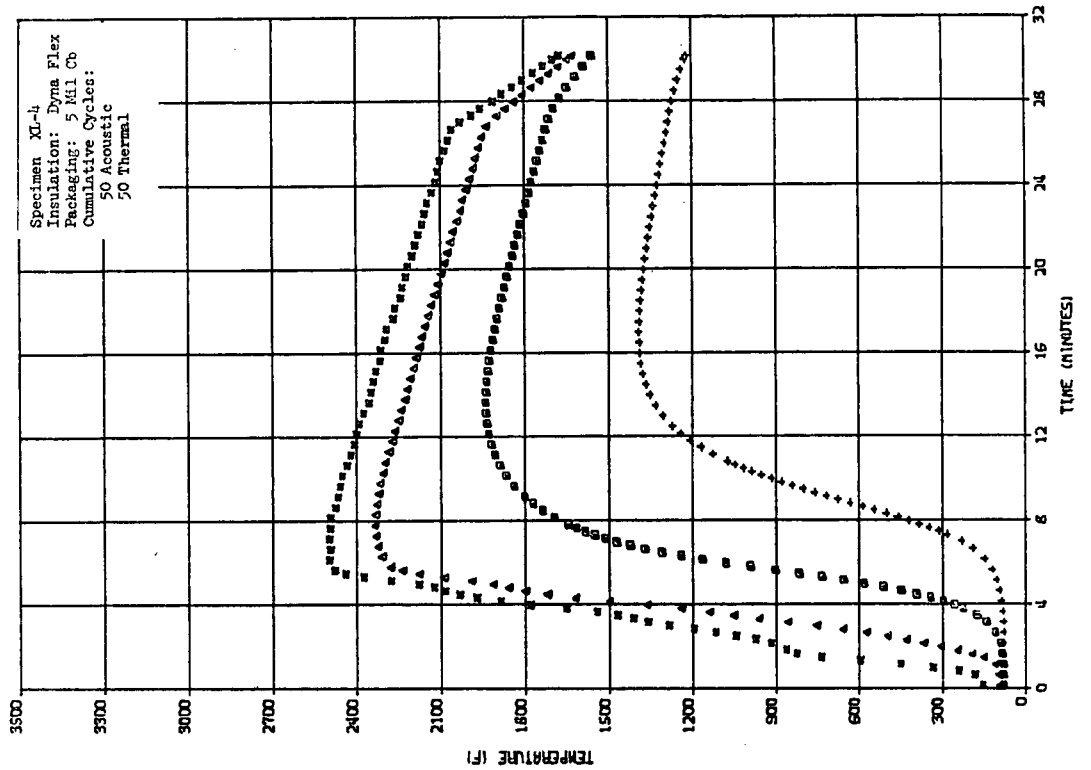

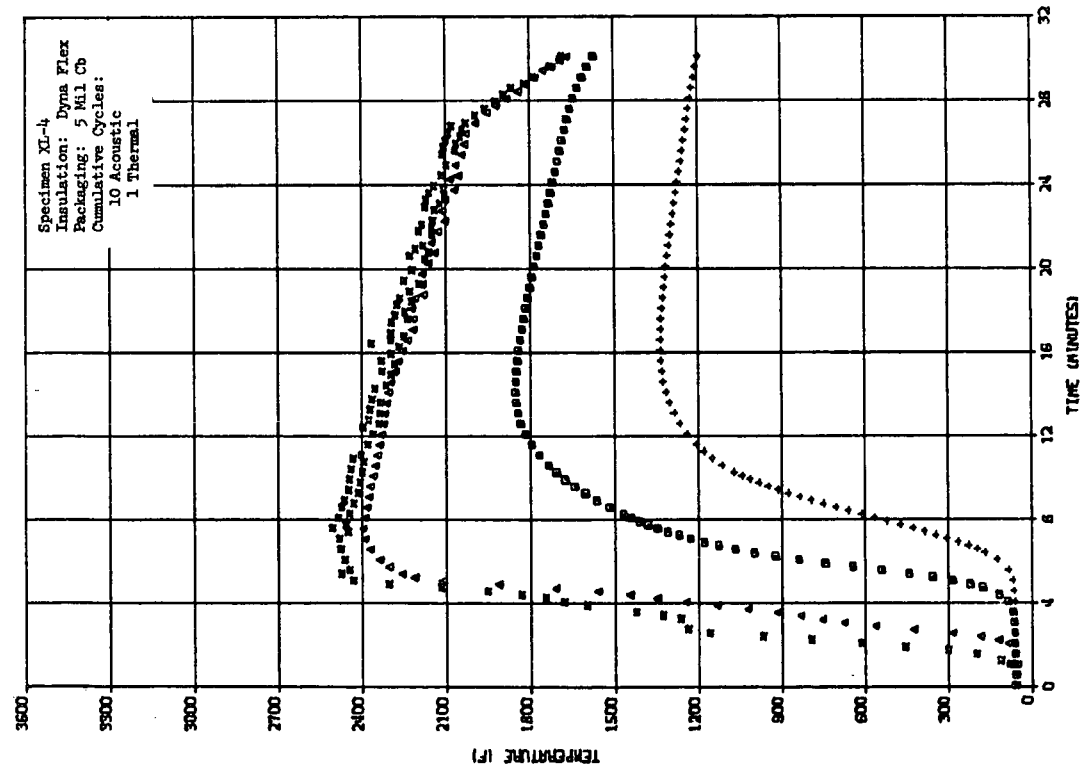

TIME-TEMPERATURE PROFILES – DYNAFLEX DF1200
First and Last Thermal Cycles
2500°F Series

457-2776

Figure 55

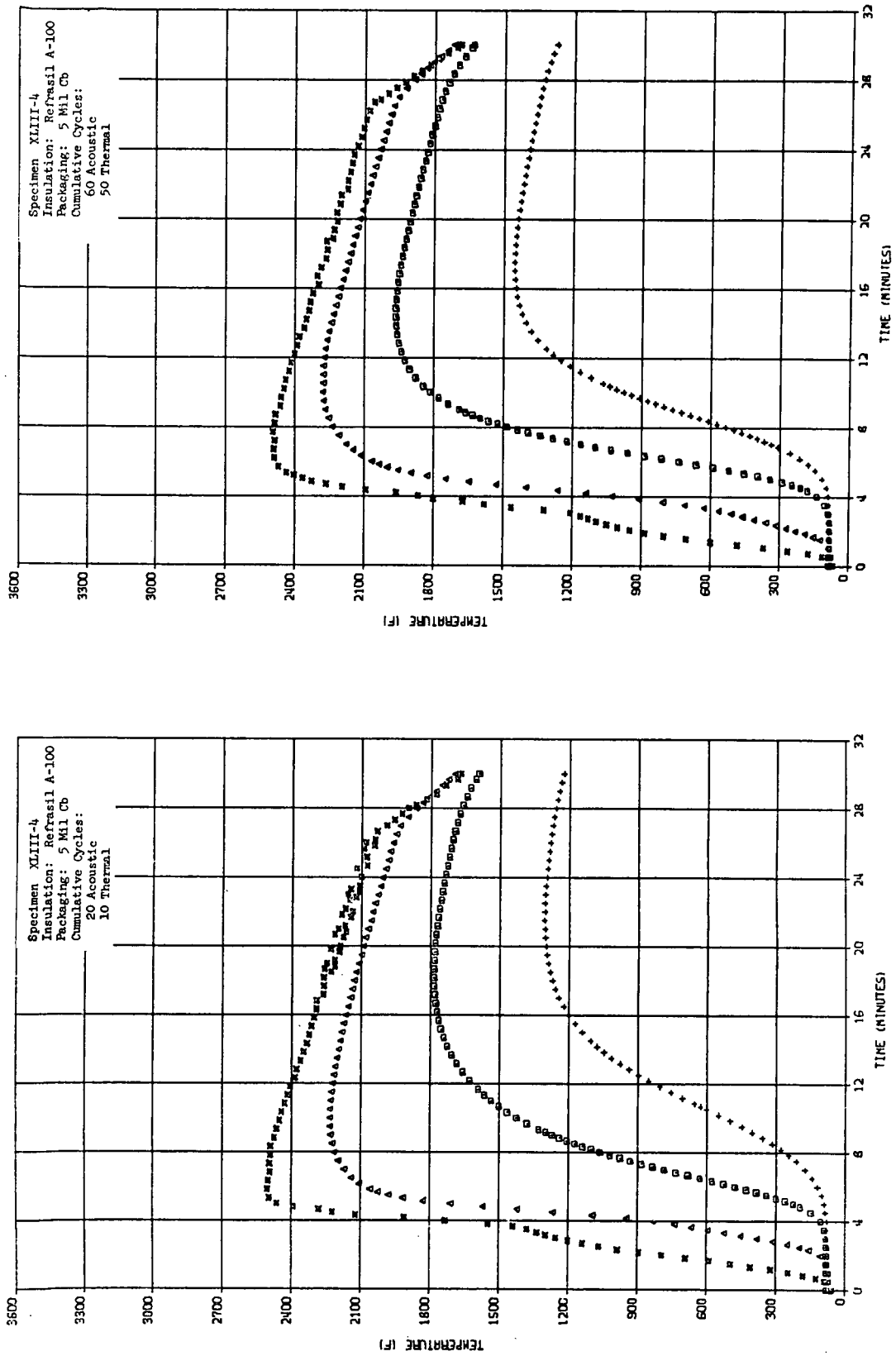

TIME-TEMPERATURE PROFILES - REFRASIL A-100
Early and Late Thermal Cycles
2500°F Test Series

457-2766

Figure 56

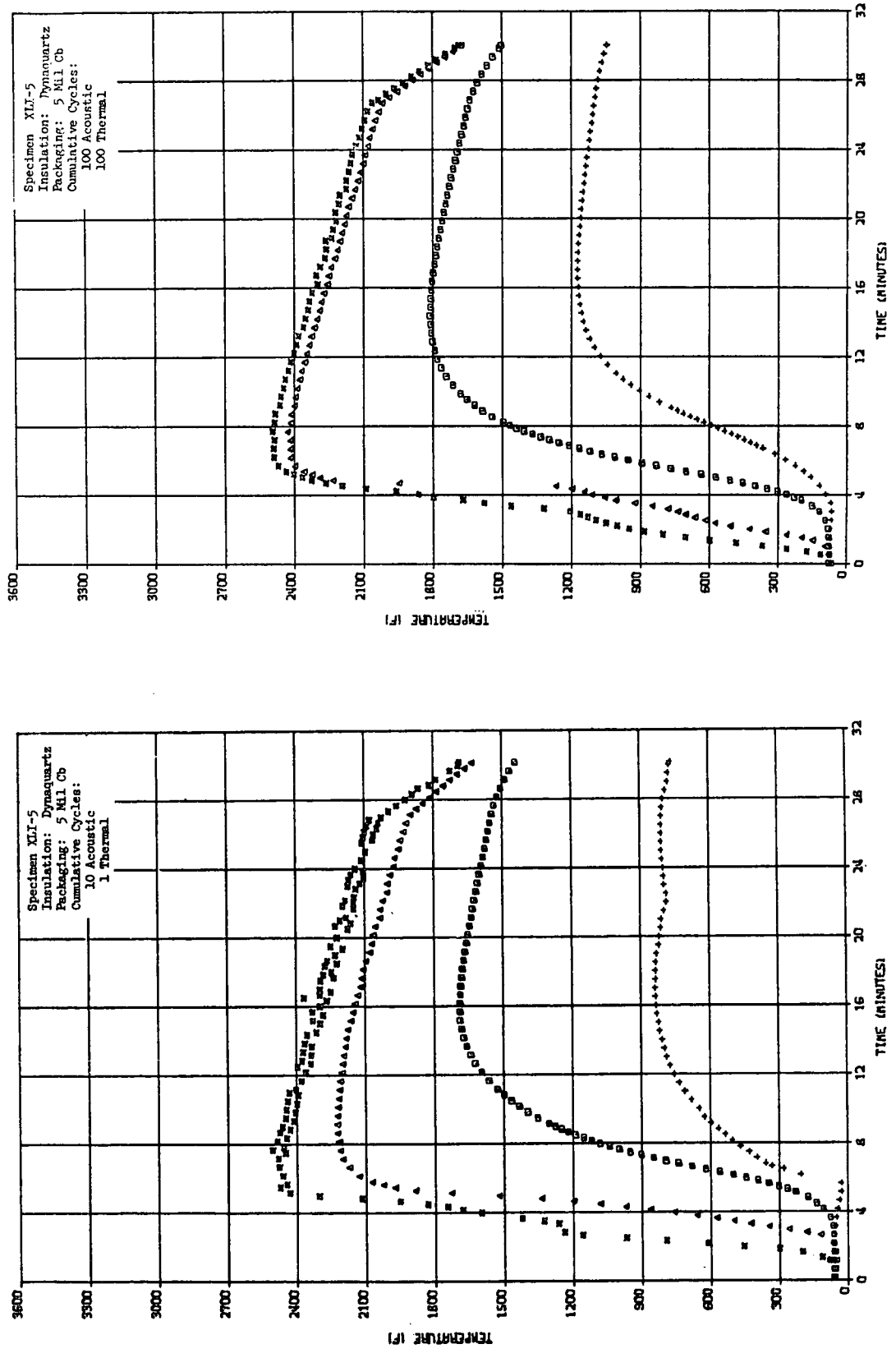

TIME–TEMPERATURE PROFILES – DYNAQUARTZ
First and Last Thermal Cycles
2500°F Series

457-2777

Figure 57

3.6 Flight Configuration Testing - The final thermal and acoustic testing of packaged insulations in this program consisted of larger-sized components designed to provide realistic thermal performance required by shuttle operations.

For design purposes the following was assumed:

- o The insulation would be required to protect aluminum structure, which is limited to a peak temperature of 300°F;
- o The outer skin temperature would peak out at 2000°F during reentry;
- o For purposes of simulation, the time-temperature profile used in our previous tests would be utilized, adjusted to 2000°F peak temperature.
- o Packages were to be 10 x 20-inches, to allow testing two at a time, and of appropriate thicknesses to provide the required cool side temperature response.
- o A total of six packages would be tested employing a range of thicknesses and surface densities.

As might be expected, the weight of insulation for the shuttle time-temperature profile is generally a function of the $k\rho$ product of the insulation. Minimum weight is therefore most likely to be achieved through minimum density insulations as they usually have the most favorable conductivity-density product. However, this also requires that space be available for the greater thickness of the lower density insulations. Recognizing that trade-offs in weight and space available are likely, the approach taken in our testing was to evaluate efficient insulations in low, intermediate, and high density categories.

The thermal design of the packages assumed emissivities of 0.8 for the interior of the vehicle skin (susceptor plate in our tests) and the hot face of the metal package, and 0.3 for the cool face of the metal package and aluminum structure. It was also assumed that the sole mode of heat transfer from the susceptor plate to the insulation package, and from the cool side of the package to the aluminum was by radiant interchange. For estimation of the thermal conductivity of the insulation, a 10 torr air pressure was assumed.

The six materials selected for test were:

Low density, high thickness

1. Astroquartz
2. Refrasil A-100/Astroquartz composite

Medium density, medium thickness

3. Refrasil A-100/FB-1 glass composite

4. Microquartz/FB-1 glass composite

High density, low thickness

5. Microquartz (10 pcf)

6. Min-K 2000

Specimen 2 listed above incorporated Refrasil at the hot surface to act as a partial radiation barrier, Specimens 3 and 4 were composites of high and low temperature insulations to take advantage of lower density and conductivity in the lower temperature regions. Specimen 5 represents a novel approach to obtain the low conductivity of Dynaquartz without the cracking problems associated with it; this specimen was formed by compressing 3.5 pcf Microquartz to three times its normal density.

Details of design and as-fabricated thickness, densities, and surface densities of the six specimens are presented in Table V, and photographs of the specimens prior to test are shown in Figures 58-61. The design of the first two packages incorporated "floating" hot surfaces and the remaining four were of simple box design except that the top corners were of 0.5-inch radius instead of sharp corners. The floating tops were of the configuration shown below and were intended to relieve thermal strains in the package.

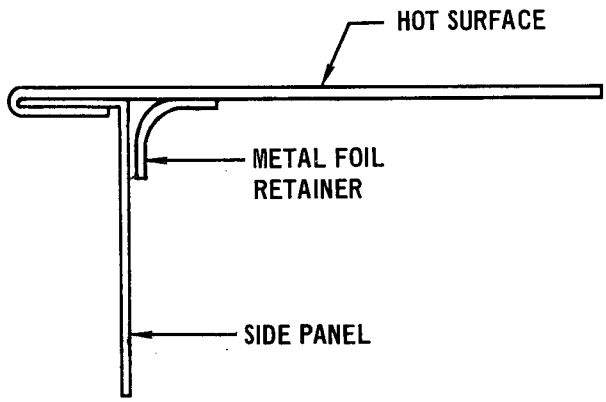

457-2778

This design is similar to the "floating" top tested previously (Ref 1), with the addition of the restrainer flap welded to the top cover. This was considered desirable because in previous testing, where it was not present, repressurization of the space chamber during cool-down between thermal cycles resulted in inward deformation of the package side panels.

For these tests the test fixture was modified to include an aluminum plate (0.080 inch thick) at the base of the test fixture to simulate aluminum tankage. The aluminum plate was also insulated on the side away from the test specimen

Table V

FLIGHT CONFIGURATION SPECIMENS

INSULATION	PACKAGE	INSULATION DENSITY		INSULATION SURFACE DENSITY		INSULATION AND PACKAGE SURFACE DENSITY LB/FT^2
		DESIGN LB/FT^3	AS FABRICATED LB/FT^3	DESIGN LB/FT^2	AS FABRICATED LB/FT^2	
1. ASTROQUARTZ - 6.75 IN.	INC 702/1.5 MIL	1.1	0.58	0.62	0.33	0.76
2. REFRASIL A-100 - 0.35 IN. ASTROQUARTZ - 5.75 IN.	INC 702/1.5 MIL	1.33	0.84	0.675	0.43	0.86
3. REFRASIL A-100 - 2.1 IN. FB-1 - 1.1 IN.	INC 702/1.5 MIL	4.03	4.9	1.07	1.31	1.65
4. MICROQUARTZ - 2.1 IN. FB-1 - 1.1 IN.	INC 702/1.5 MIL	3.0	3.0	0.80	0.80	1.31
5. MICROQUARTZ - 1.5 IN.	TD-NiCr/3 MIL	10	9.7	1.25	1.21	1.57
6. MIN-K 2000 - 0.75 IN.	INC 702/3 MIL	20	19.0	1.25	1.19	1.56

457-2767

with a 1.0 inch thickness of polyurethane foam so that the plate would have thermal characteristics similar to shuttle tankage that is internally insulated. The acoustic and thermal exposure of these specimens was limited to 40 cycles, conducted in groups of 10 successive cycles in each environment. This was considered adequate for this characterization, as most of the materials had been previously tested for longer durations.

3.6.1 Low Density Flight Configuration Test Results - The thermal tests were run in groups of 10 consecutive cycles; the maximum temperatures attained by aluminum plate with the first two specimens in place were:

Cycle No.	Aluminum Plate Peak Temperature °F	Plate Temperature Change During Cycle °F
1	292.5	223.3
5	324.5	217.4
10	331.3	216.3
11	289.8	221.0
20	304.2	203.6
21	285.8	217.4
30	316.8	213.6
31	288.9	220.5
40	343.9	232.0

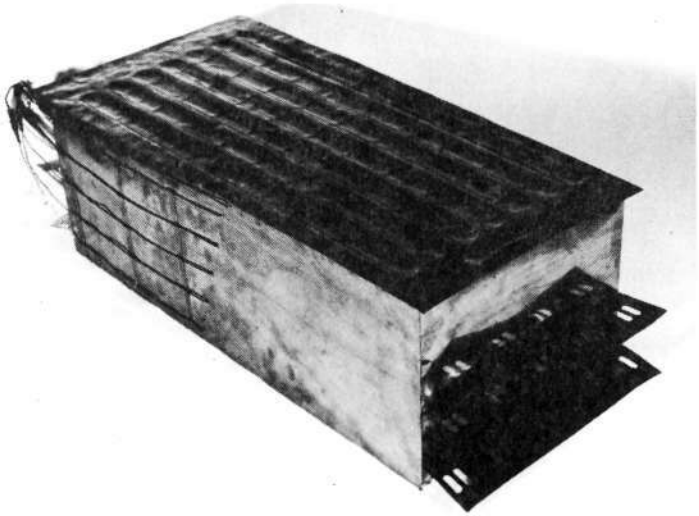

ASTROQUARTZ FLIGHT WEIGHT PACKAGE

457-2793

Figure 58

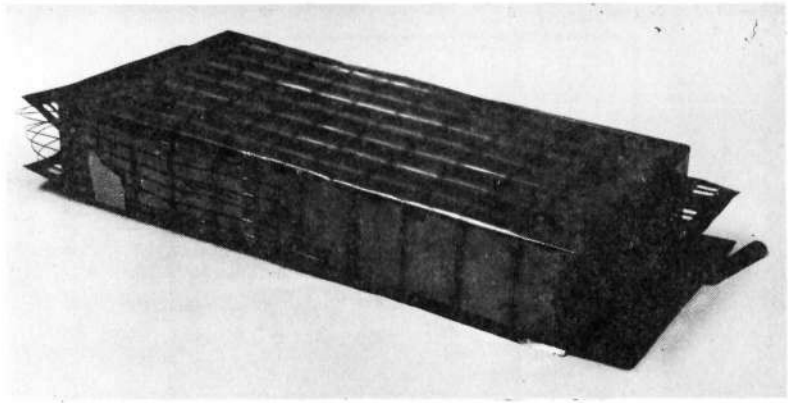

REFRASIL A-100/FB-1 FLIGHT WEIGHT PACKAGE.
(MICROQUARTZ/FB-1 SPECIMEN IS SIMILAR)

457-3122

Figure 59

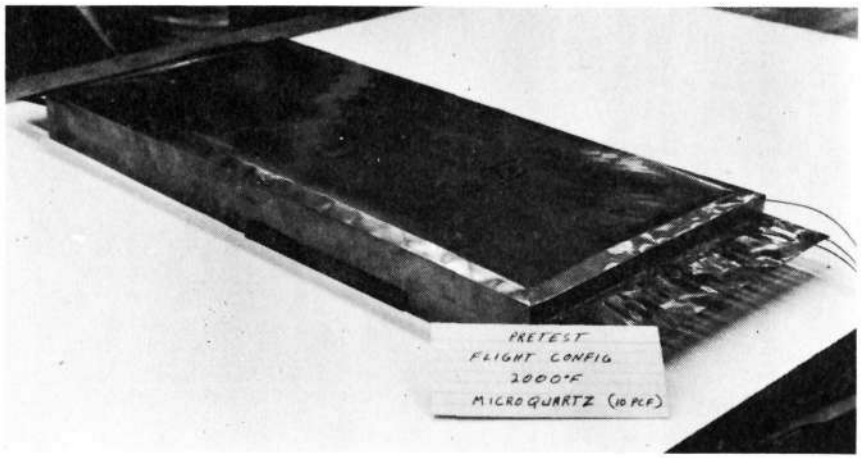

HIGH DENSITY MICROQUARTZ FLIGHT WEIGHT PACKAGE

457-2782

Figure 60

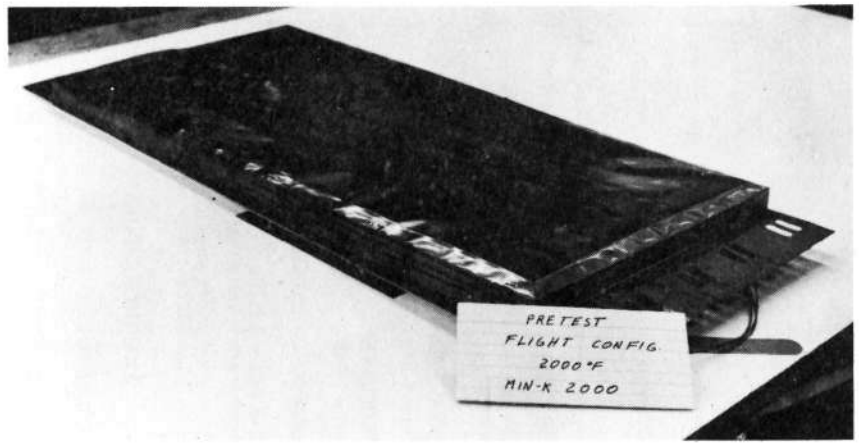

457-3123

MIN-K 2000 FLIGHT WEIGHT PACKAGE

Figure 61

In the first cycle of each group, the peak temperature averaged about 289°F; higher temperatures achieved in subsequent cycles in each group of 10 were due to insufficient cooling time between cycles, as illustrated by the data showing the relatively consistent temperature rise of the plate during the cycle.

After 10 thermal and acoustic cycles, tears were noted in the vertical corners of the packages, Figure 62. Before further testing, the corners were reinforced with additional foil (3 mil) spot welded in place. At the conclusion of the test, the packages and internal insulation were in good condition. No settling or shrinkage of the insulation was noted. Condition of the packages at the end of 30 cycles is shown in Figure 63, and the internal condition of the insulation after 40 cycles in Figures 64 and 65. Other than the tears at the corners, which were repaired after 10 cycles by local reinforcement, the Inconel 702, 1.5 mils thick, showed every indication of being adequate for 2000°F service. Compared to other results, the use of the "floating" top significantly reduced deformations of the package.

In retrospect, the calculated thickness of Astroquartz was fortuitous. At the time the package was designed, no data existed for the conductivity of 1 lb/ft^3 Astroquartz above 1000°F, and it had to be estimated by extrapolation using a curve for 3 lb/ft^3 Astroquartz (which did cover the higher temperature ranges) for guidance. However, subsequent conductivity tests of Astroquartz showed the estimation to be grossly optimistic. Apparently the estimates of the emissivities of the metal foil package, which remained much lower than anticipated, compensated for the low estimate of thermal conductivity.

3.6.2 Intermediate Density Flight Configuration Test Results - These packages incorporated moderate density high temperature insulations in conjunction with a lower density, and low cost glass felt in the cooler (1000°F and lower) areas of the package to form a composite insulation. These packages were made of the same metal foil employed for the low density insulation packages, but did not include the "floating" top (Figures 66 and 67).

It was necessary to suspend testing on the second group of flight configuration specimens at the end of 20 cycles when one of the specimens developed a large number of gross tears in the hot face of the metal package. The companion specimen, made of the same metal foil, and experiencing the same cycles simultaneously, had several minor tears in the foil. Cause of this failure is unknown. The metal foil was only very mildly oxidized, and there was no evidence of embrittle-

CORNER FAILURES IN PACKAGES OF LOW DENSITY FLIGHT CONFIGURATION PACKAGES REPAIRED BY REINFORCING

457-3124

Figure 62

ment or weakening of the metal. The tears were concentrated along seam welds (at right angles to the corrugation stiffeners), though the welds themselves do not appear to have failed. Some tears also occurred between the seam welds. The possibility that the tears resulted from an internal pressure within the package is discounted as a single rupture would relieve excess pressure. Another possibility is thermal expansion of the metal surface, which was corrugation stiffened to reduce flexure, or fatigue occurring in acoustic testing. The thinness of the metal foil (1.5 mil) may have been a contributing factor, though the two packages of the first group were made of the same foil and went through 40 cycles without

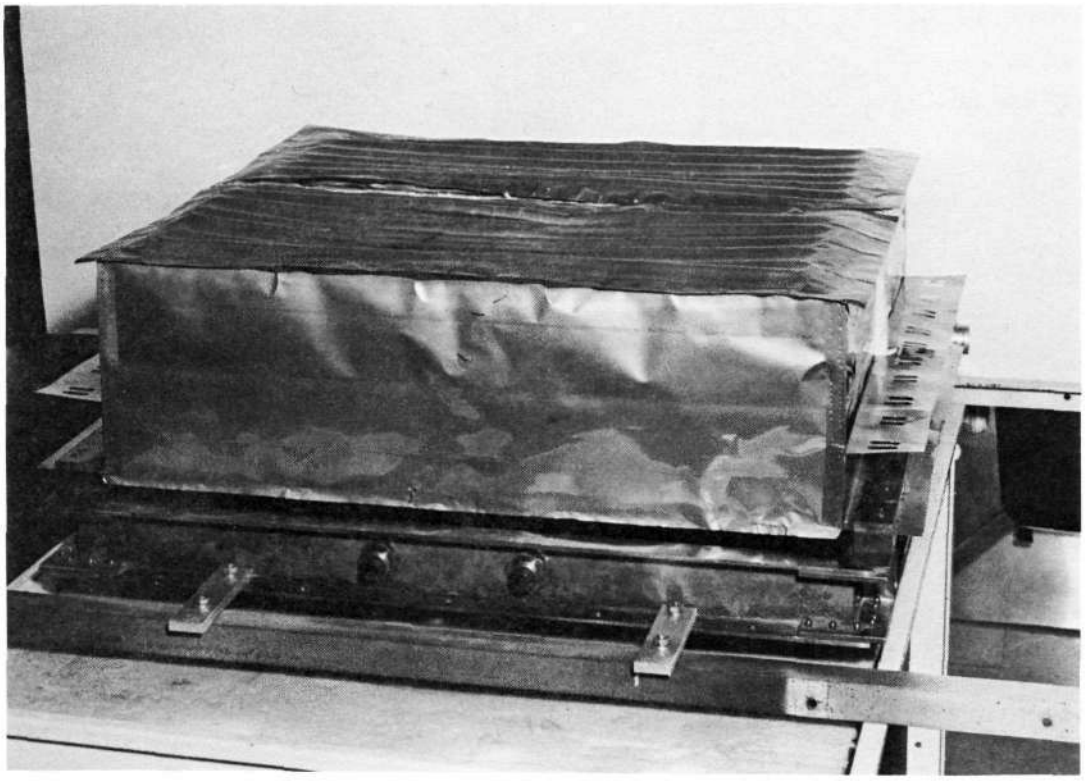

457-3125

GENERAL APPEARANCE OF LOW DENSITY FLIGHT CONFIGURATION SPECIMENS AFTER 30 CYCLES

Figure 63

difficulty. The failed package contained normal density Microquartz insulation and FB-1 glass insulation, but this does not appear to be a factor in the failure of the package.

Figures 66-73 show the conditions of the specimens as the test progressed. During the initial 10 thermal cycles, the package billowed out somewhat, but at that time there was no obvious physical damage (Figures 68 and 69). After the succeeding 10 acoustic cycles the damage to one package was apparent (Figures 70 and 71), and which worsened in the final 10 thermal cycles (Figures 72 and 73).

The hottest two layers of Microquartz (each layer 0.5 inch thick), shrunk about 0.4 inch in length (Figure 74). The Refrasil A-100 in the companion package (Figure 75) shrunk a similar amount, but over a smaller depth. The Microquartz shrinkage appears abrupt over the total thickness of the two layers affected. The Refrasil A-100 shrinkage has a more rounded appearance, possibly due to the much smaller thickness per layer ($\sim$0.18 inch).

The temperature of the aluminum plate reached 200°F in the first cycle in each group of ten cycles, and about 312°F in the 10th cycle. This increase, in this case, cannot be ascribed to heat buildup within the insulation as the initial

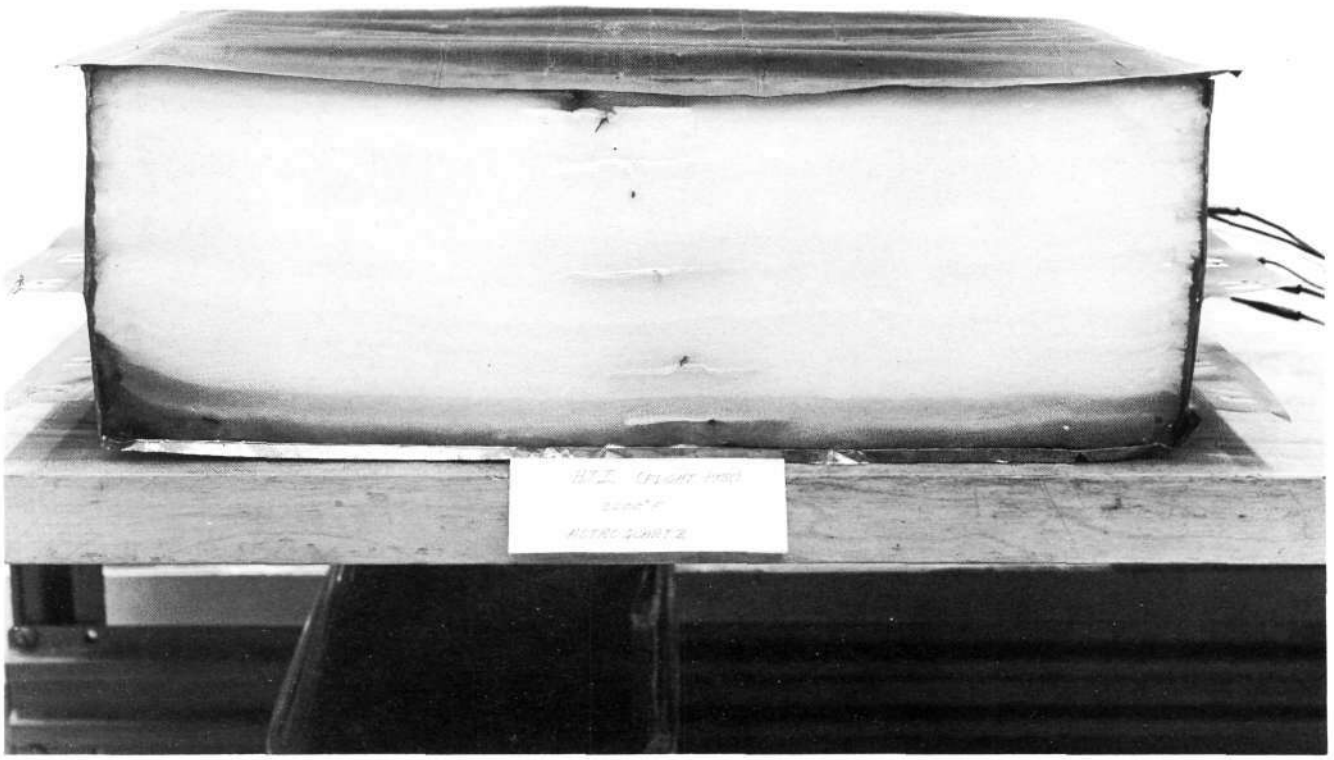

457-3126

ASTROQUARTZ FLIGHT CONFIGURATION PACKAGE AFTER 40 CYCLES

Figure 64

temperatures at the start of each thermal cycle were relatively constant.

3.6.3 High Density Flight Configuration Test Results - These specimens represent materials for potential use in areas that are volume limited. One specimen was Microquartz, compressed to about three times its nominal density of 3.5 lbs/ft^3, which was expected to yield a product with the thermal efficiency comparable to 10 lb/ft^3 Dynoquartz, without the hazards of cracking. The companion specimen was Min-K 2000.

Because of the greater dissimilarities in thermal performance and thickness of the two specimens, a modification was made in the test arrangement. In the previous flight configuration tests, a common aluminum plate had been used behind both specimens to represent tankage. In the high density series, the aluminum plate was cut-in-two to provide each specimen with its own

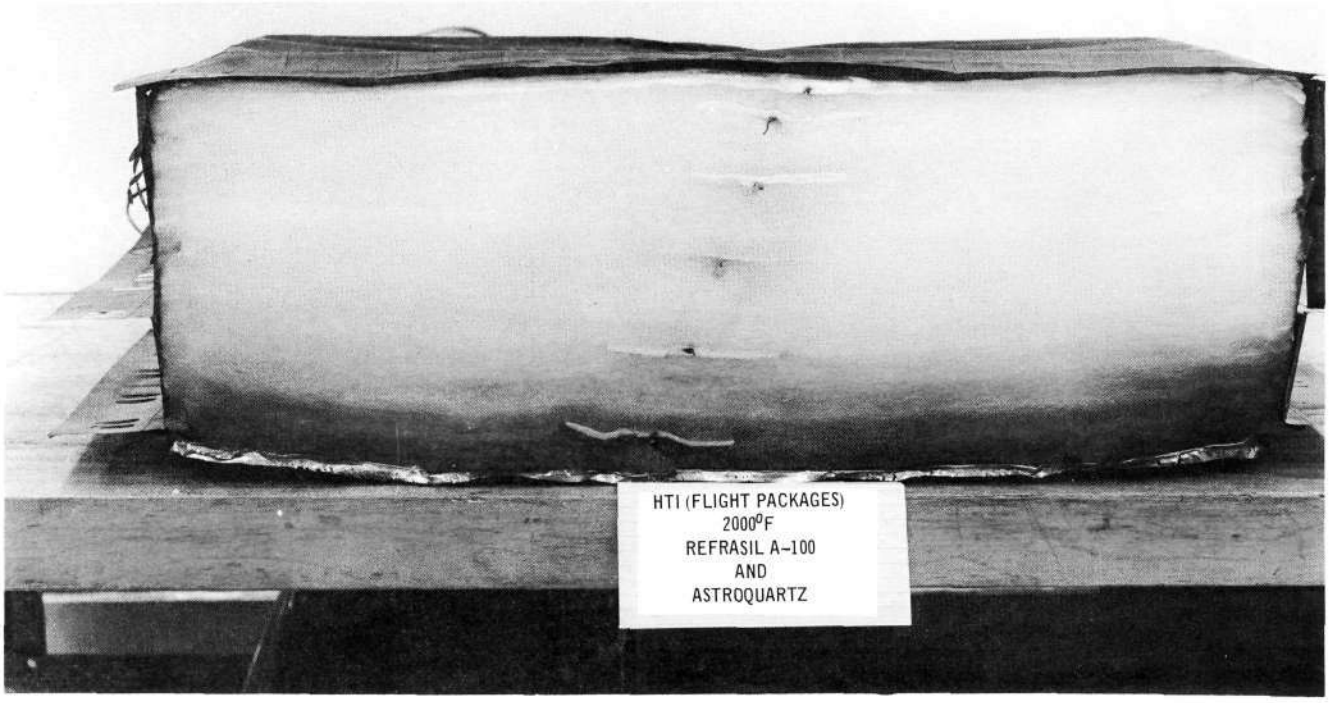

REFRASIL A-100/ASTROQUARTZ FLIGHT CONFIGURATION PACKAGE AFTER 40 CYCLES

457-3127

Figure 65

individual plate, and thus more independent temperature response. However, radiant interchange from the cool side of the packages to the adjacent aluminum plate could not be totally eliminated.

During the first acoustic cycle, some of the compressed Microquartz was expelled from the vent holes (30 - 1/4 in. dia. holes) in the cool face of the package. This specimen was opened up and the insulation replaced, but this time a layer of Stype 120 glass fabric was installed between the Microquartz and the cool face of the package. This specimen was then continued in test with no further problems. In compressing the felt, considerable force was required, possibly fracturing many of the fibers, and forming a relatively firm product. When subjected to acoustics, the dense felt apparently responded more vigorously, and coupled with possibly broken fibers, allowed some of them to be expelled through the open vent holes. However, the insertion of the layer of glass fabric between the Microquartz and the cool side of the package effectively prevented a repetition of the fiber loss.

In the first thermal cycle the susceptor plate temperature control failed, resulting in a temperature overshoot to 2200°F (instead of the programmed 2000°F) and the test was shut down at 700 sec, with no apparent damage to the specimens.

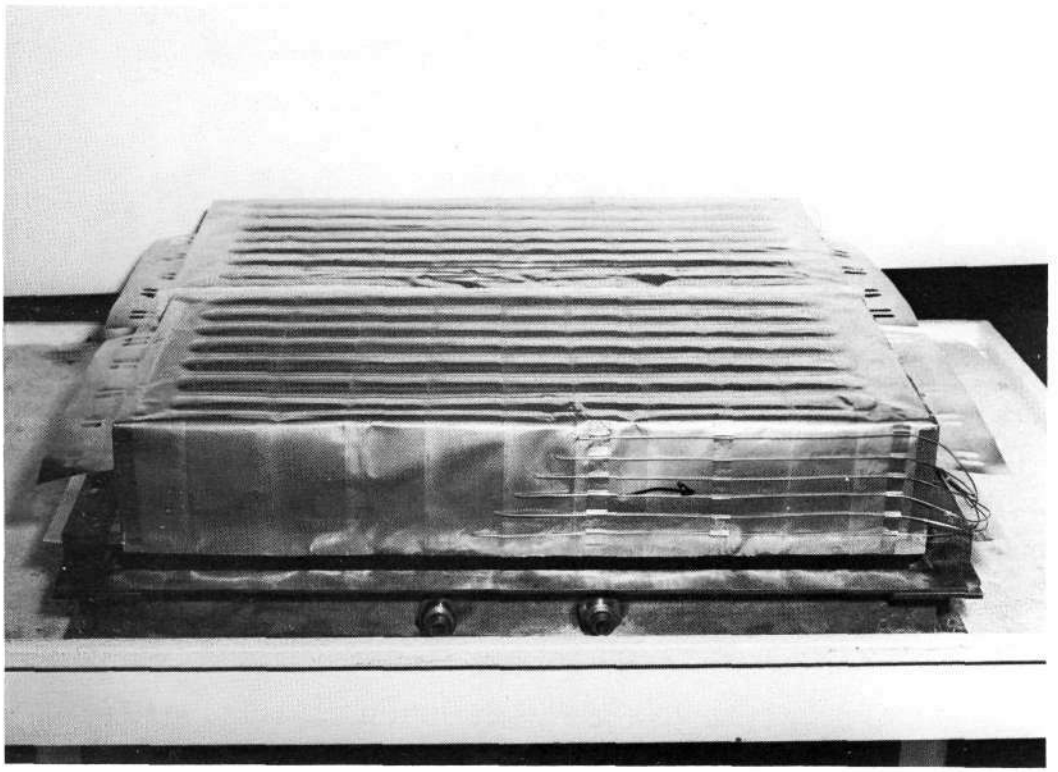

Figure 66

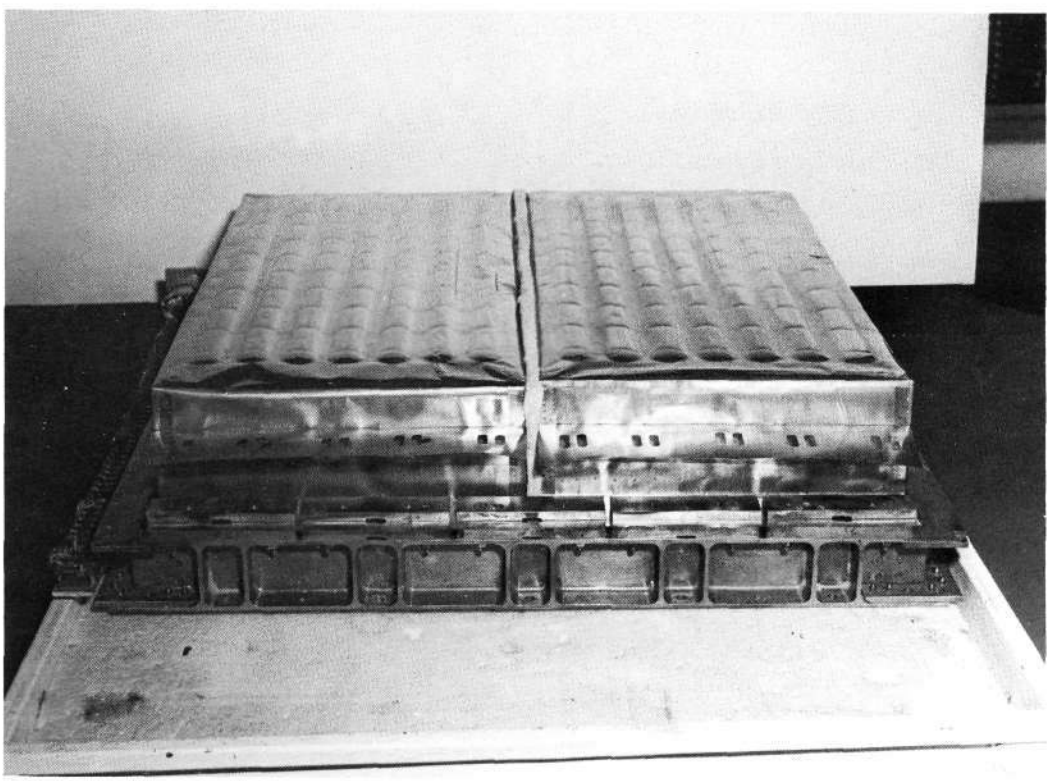

457-3128

INTERMEDIATE DENSITY FLIGHT CONFIGURATION SPECIMENS
PRE-TEST

Figure 67

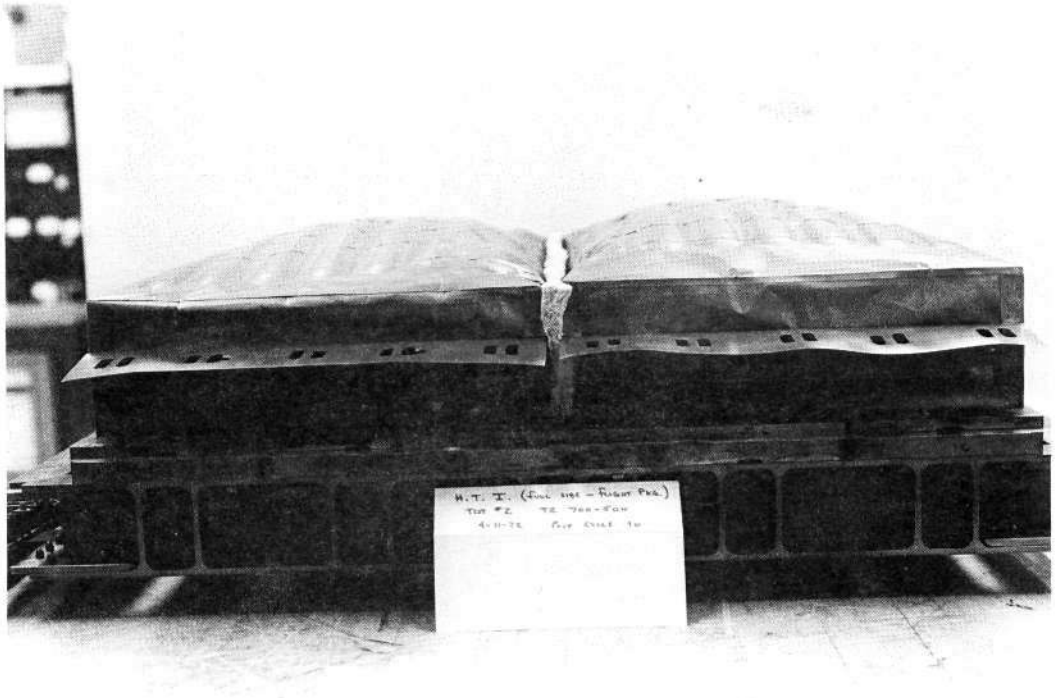

Figure 68

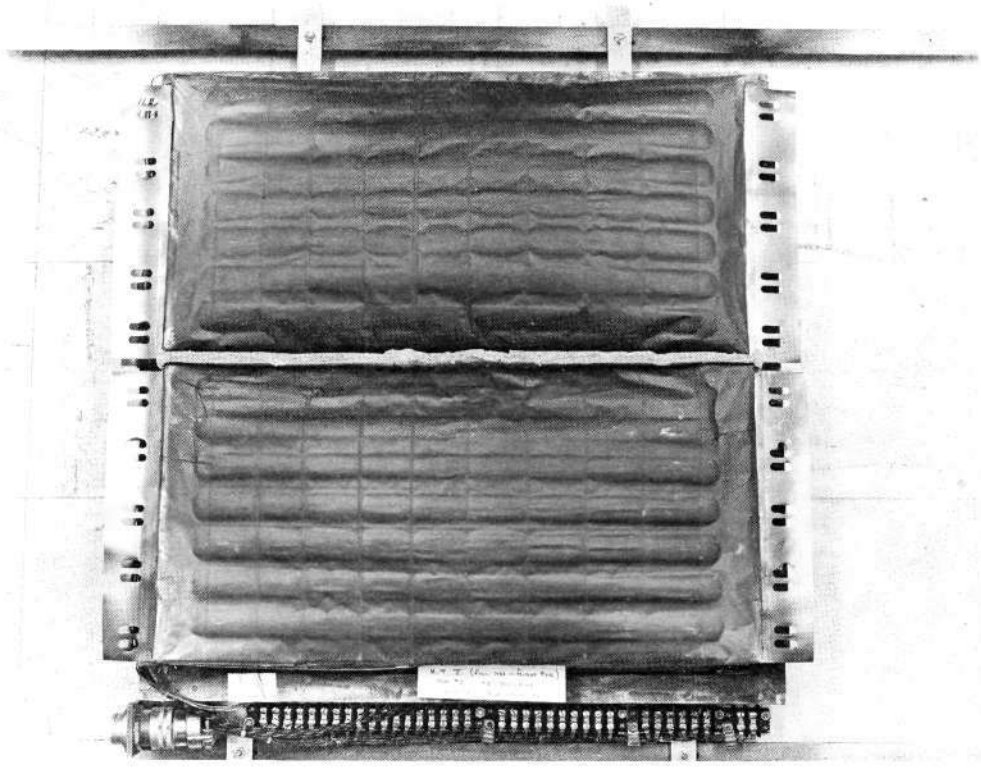

Figure 69

457-3129

INTERMEDIATE DENSITY FLIGHT CONFIGURATION TEST
AFTER 10 CYCLES ACOUSTIC/THERMAL EXPOSURE

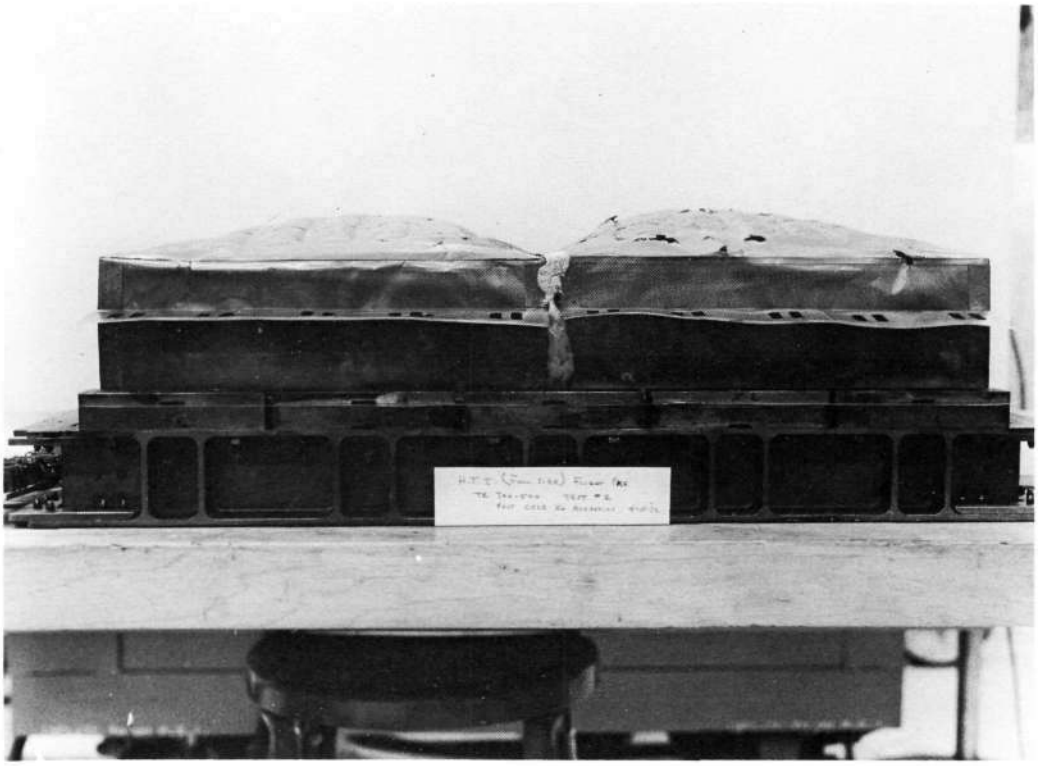

Figure 70

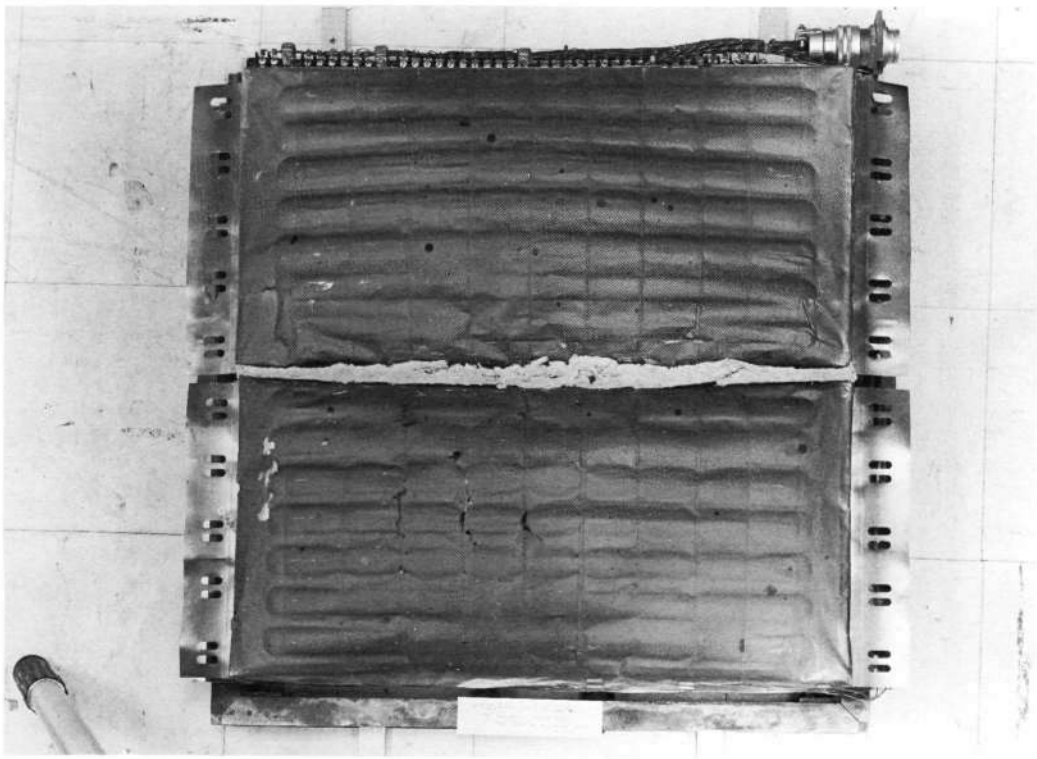

INTERMEDIATE DENSITY FLIGHT CONFIGURATION TEST
AFTER 20 ACOUSTIC AND 10 THERMAL CYCLES

Figure 71

457-3130

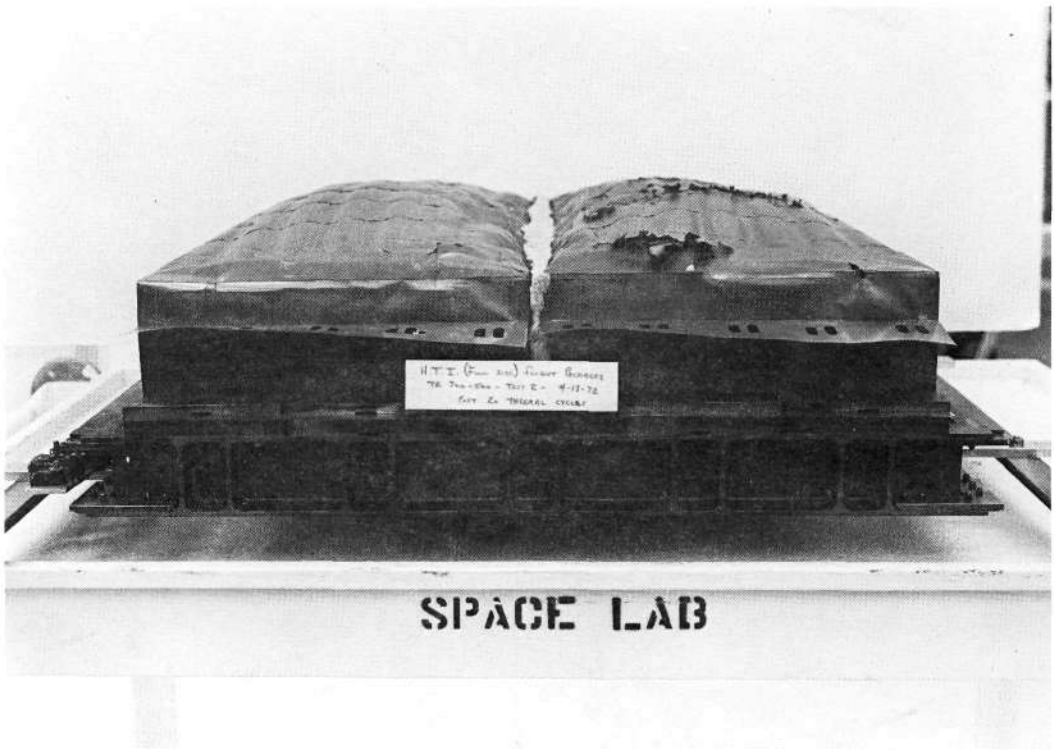

Figure 72

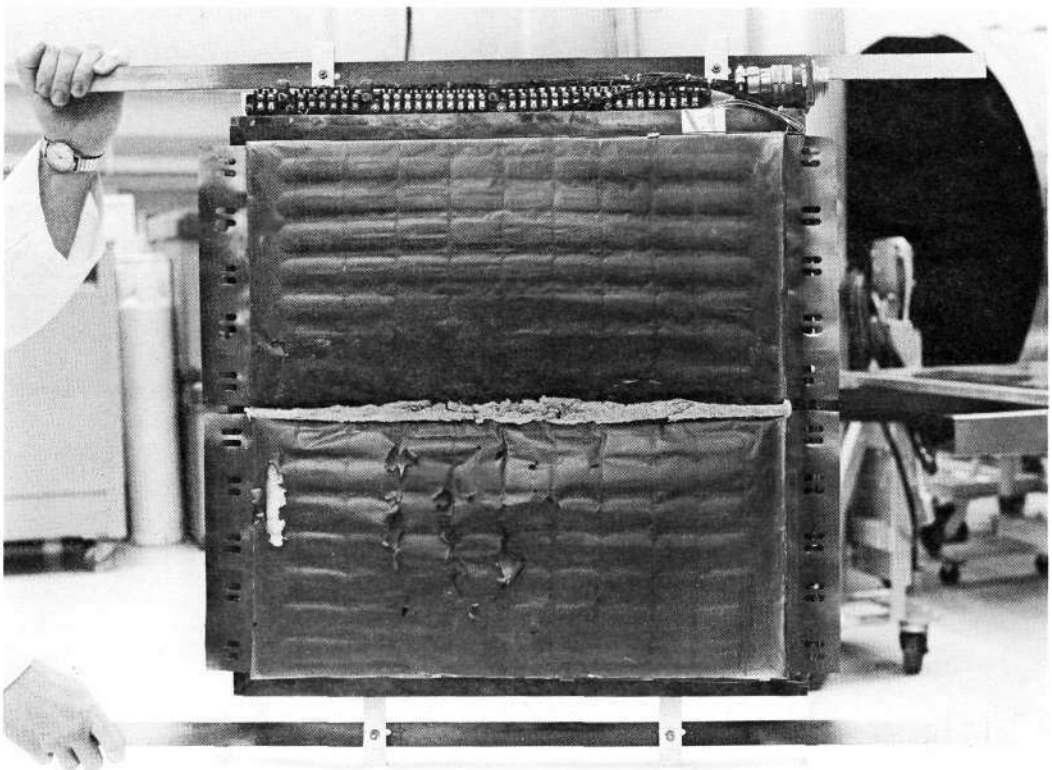

INTERMEDIATE DENSITY FLIGHT CONFIGURATION TEST
AFTER 20 ACOUSTIC AND 20 THERMAL CYCLES

Figure 73

457-3131

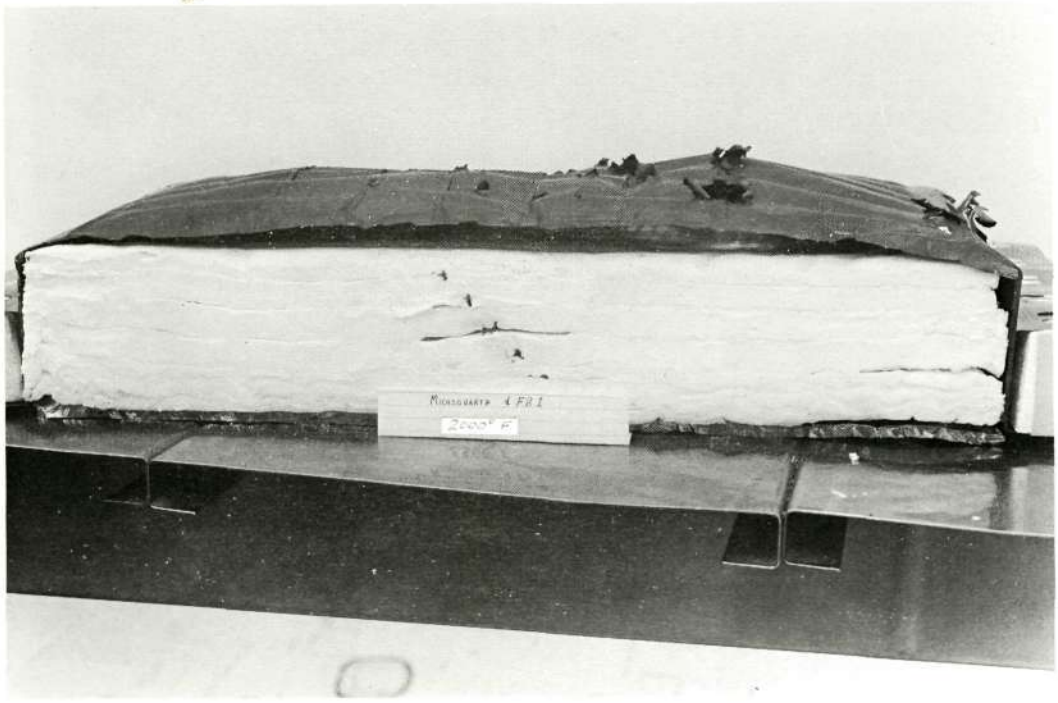

Figure 74

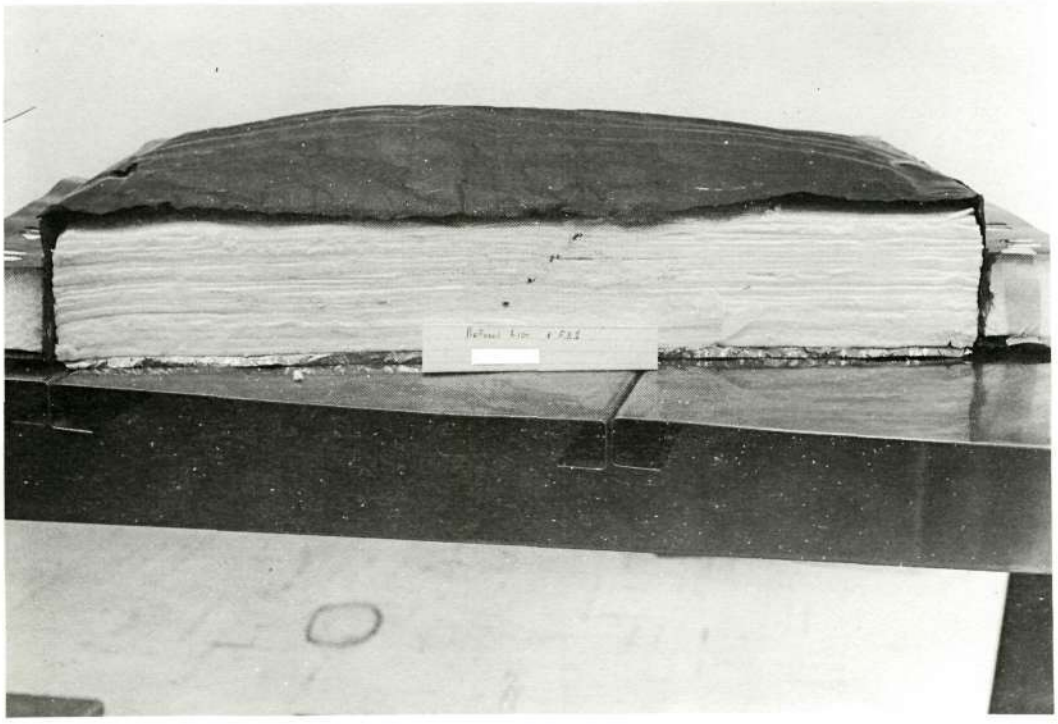

Figure 75

INTERMEDIATE DENSITY FLIGHT CONFIGURATION SPECIMENS INTERIOR INSULATION AFTER 20 ACOUSTIC/THERMAL CYCLES

457-3132

The total time the susceptor was in excess of 2000°F was about 70 seconds. The remainder of the 40 cycles was conducted without incident.

The condition of the test packages at the end of 30 cycles is shown in Figures 76 and 77, and the internal insulation at the completion of the 40 cycles in Figures 78 and 79. Cracks were numerous in the Min-K, and the joint at the center where thermocouples had been installed, opened up. The Microquartz, in its compressed condition, did not display any shrinkage such as it had in earlier tests at 1800°F or 2200°F.

The peak temperature at the cool face of the metal foil packages, and of the aluminum plate inboard of the insulation packages, are shown in Table VI, along with the temperature increases associated with those peak temperatures. The Microquartz gave results close to the design values, except for the 20th cycle. The Min-K 2000 insulating performance was considerably less than anticipated. The reasons for this are uncertain. One possibility is that the crack in the block (where internal thermocouples were installed) allowed direct radiation through to the cool side of the package. However, considering the small net thickness of Min-K employed (0.75 in.), this must still be considered good performance overall.

3.7 Thermal Performance of Packaged Insulations - In an attempt to "back out" effective thermal conductivity of the various packaged insulations as a function of service life, from their time-temperature responses, analyses were performed using thermal models of the test configuration and our General Heat Transfer Computer Program. Nominal reduced pressure thermal properties for the test specimens were used first in the computer model to determine their adequacy for correlating measured data. Next, thermal conductivity was reiterated to determine if a better correlation could be obtained.

This procedure has met with mixed success. The precise location of the thermocouples within the insulation has a profound effect on response, and requires a precision and stability greater than we have been able to achieve. The absorptivities and emissivities of the metal packages also have a large influence. The latter effect led to our measuring the room temperature emittances of many of the test packages, and which is reported separately. Movement of the thermocouples within the package introduced additional uncertainty.

The analysis of SKX Fiberfrax felt from the 2200°F test series was conducted for the first and 80th thermal cycle. Based on the center thermocouple within the specimen, the effective thermal conductivity was found to agree with the measured conductivity up to 800°F, where the effective conductivity began to deviate to

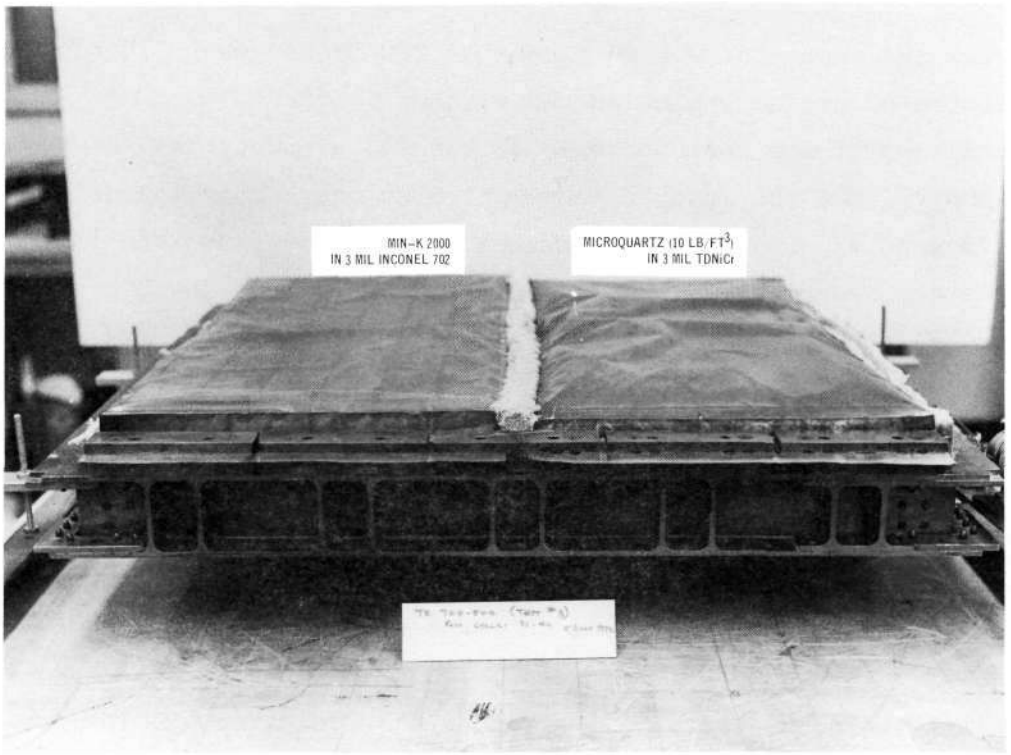

Figure 76

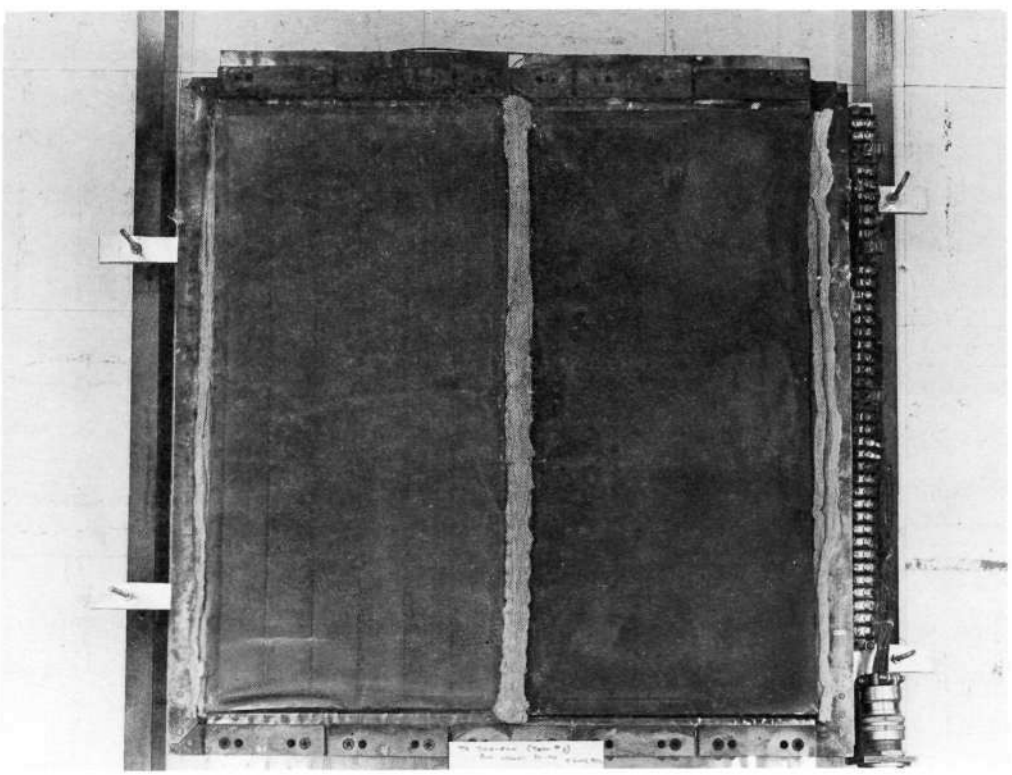

Figure 77

HIGH DENSITY FLIGHT CONFIGURATION SPECIMENS
AFTER 30 ACOUSTIC AND THERMAL CYCLES

457-3133

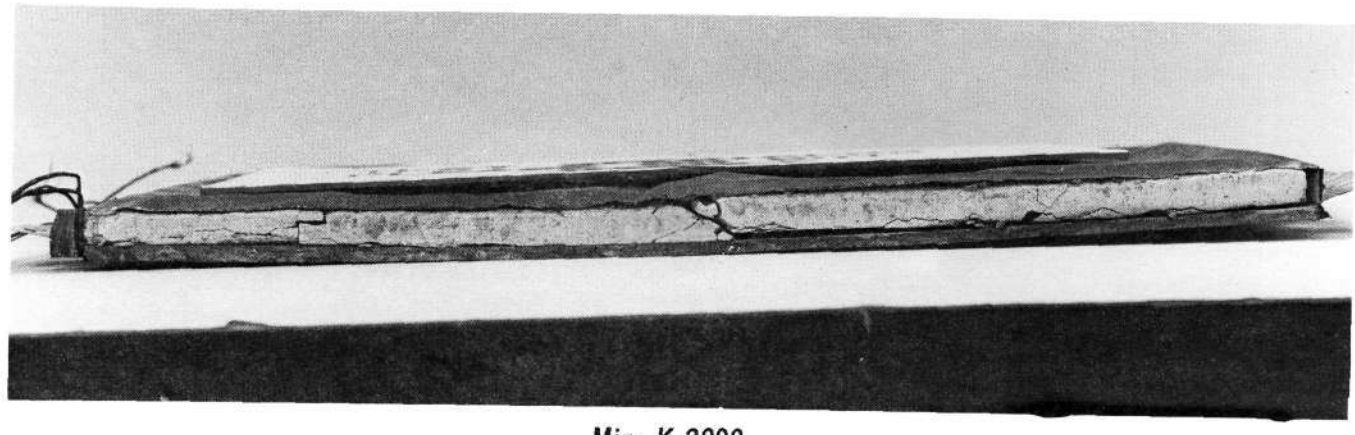

Min–K 2000

Figure 78

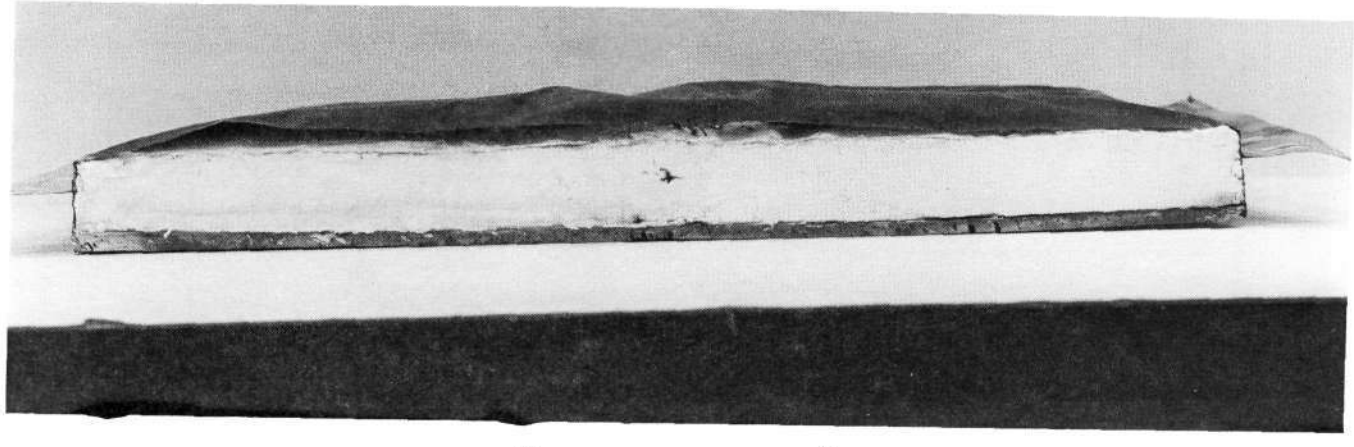

457–3134

Microquartz – 10 Lb/Ft^3

Figure 79

INSULATION CONDITION AT END OF 40 CYCLES HIGH DENSITY FLIGHT CONFIGURATION

higher values. The calculated thermal histories for the center thermocouple, based on the calculated effective conductivity, then showed excellent agreement with the measured data. However, similar agreement was not obtained for the other two thermocouples. The agreement was closer when effective, rather than nominal reduced pressure values of conductivity were used.

A study was also conducted to determine if the effective conductivity of SKX degraded between cycle 1 and cycle 80. The conclusion was that degradation was insignificant.

Similar studies conducted on the Astroquartz specimen from the 2200°F series resulted in anomalous results. The mid-point thermocouple could be correlated with test results only by assuming the effective conductivity was 24% of its nominal reduced pressure value. The maximum temperature of each thermocouple could be duplicated (assuming nominal conductivity) by assigning an emissivity to the cold

C-2

Table VI

PEAK TEMPERATURES AND TEMPERATURE INCREASES OF HIGH DENSITY FLIGHT CONFIGURATION TEST

CYCLE	MICROQUARTZ - 10 LB/FT^3				MIN-K 2000			
	PACKAGE COOL FACE		ALUMINUM STRUCTURE		PACKAGE COOL FACE		ALUMINUM STRUCTURE	
	T_{MAX} °F	Δt °F	T_{MAX} °F	Δt °F	T_{MAX} °F	Δt °F	T_{MAX} °F	Δt °F
2	502	442	270	206	775	714	512	447
5	530	437	333	242	798	705	561	466
10	534	436	342	246	812	718	576	478
11	488	423	312	247	784	722	537	473
20	686	596	526	436	789	696	558	462
21	495	430	330	263	645	581	394	326
30	496	392	340	238	639	539	411	308
31	398	343	275	211	576	516	313	249
40	466	381	325	238	613	526	377	289

457-3135

face of the package that was widely different from its measured value. Neither of these alternatives seemed likely.

It is believed that there were two inherent problems in the analysis of the response of Astroquartz. One was its very small heat storage capacity. The other problem was that it has high infrared transmission, and which in this particular case, was associated with low emissivity boundary surfaces. This enormously complicates the analysis.

Because of inconsistent results of this thermal modeling program, its use was not extended to the other specimens tested. It was also believed that thermal performance changes with service life could be as effectively evaluated by examining the changes in response of the thermocouples within the specimens.

Details of the thermal analyses conducted are presented in the sections following.

3.7.1 2200°F Mission Simulation - This study encompassed a thermal evaluation and analysis of two high temperature insulation packages subjected to a time -

temperature history profile that peaked at 2200°F, and simulating shuttle service conditions. The two test specimen materials evaluated and analyzed thermally were SKX-Fiberfrax and Astroquartz, each packaged in TD-NiCr (3 mil thickness), and results are based on thermal test cycle number 80. The objective of this study was to determine effective thermal conductivities that correlate with the temperature histories of three thermocouples placed in each test specimen and to document the sensitivity of the test configuration. Good thermal correlation was obtained for the SKX-Fiberfrax insulation whereas, the thermal analysis for Astroquartz did not achieve the same degree of correlation. The analyses were performed using thermal models of the test configuration and our General Heat Transfer computer program which computes the transient response of the model including the effects of conduction, heat storage, radiation and boundary heating conditions. Nominal thermal properties for the test specimen were used first in the computer model to determine their adequacy for correlating measured data. These so called nominal properties are based on published data and guarded hot plate measurements. Next thermal conductivity was iterated upon to determine if a better correlation could be achieved. The general heat transfer computer program determines constants for specified empirical thermal conductivity equation for the insulation. The program iterates on a specified temperature based on a family of curves input.

3.7.1.1 Test Specimens - The two test specimens studied were low density silica-fiber insulations in a 3 mil TD-NiCr foil package. The specimens were 3.85 inches wide, 20 inches long, and 1.5 inches thick. The metal foil packages had a rectangular box shape with tabs at ends of the hot and cold surfaces for mounting to the test fixture. A schematic of the insulation specimens is shown in Figure 80. Three thermocouples were installed in each insulation blanket near its longitudinal center. The thermocouples were positioned such as to have one at the center of the insulation, one near the hot face and the other near the cold face. After final assembly, each specimen was X-rayed to document thermocouple position. Five specimens were mounted in the test fixture for each test and a strip of guard insulation was placed between specimens to reduce lateral temperature gradients. The lateral temperature gradients were considered to be negligible.

3.7.1.2 Thermal Model - A one-dimensional thermal model (Figure 81) was constructed corresponding to the center of the test setup including the susceptor plate radiation gaps, metal packaging material and the water cooled backup structure. This 15 node model was employed to correlate the measured transient time - temperature profile experienced by the test specimen.

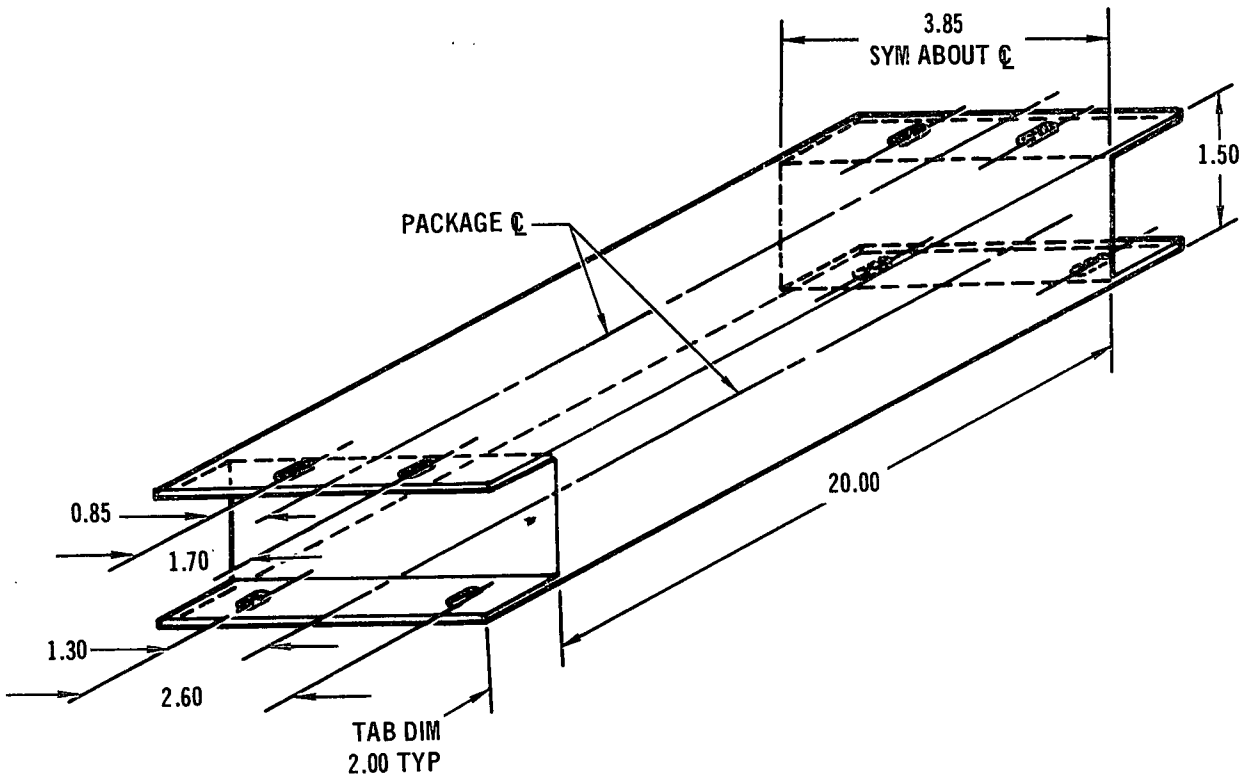

457-3136

HIGH TEMPERATURE SPECIMEN (FOIL ENCLOSED)

Figure 80

A one-dimensional thermal model of just the insulation was also employed for calculating effective conductivity. The boundary condition for this model were the temperature histories measured by the thermocouples at the hot and coolface of the insulation package. A schematic of this model is shown in Figure 82. These thermal models were used to analyze both SKX-Fiberfrax and Astroquartz test specimens.

3.7.1.3 SKX-Fiberfrax - A transient heat transfer analysis was conducted based on the results of thermal cycle 80. First, the nominal thermal conductivity and specific heat of 7.7 lb/ft^3 density SKX (Figure 83) were used to predict specimen thermal response. Figure 84 shows the comparison between measured temperature profiles for thermocouples 4, 5 and 6, and the analytically calculated temperature profiles of thermocouples 4, 5 and 6. These results show: thermocouple 4 test data to be lower (over the entire temperature history) than the calculated temperatures; thermocouple 5 slightly higher than calculated with reasonable profile agreement; thermocouple 6 higher than calculated profile but in fair agreement. The mismatch between measured and calculated temperatures could be due to several things, including sensitivity of thermocouple location, package surface emittance and the thermal conductivity of the SKX material. To illustrate the required relocation of the thermocouples, Figure 85 was constructed. The plot of maximum

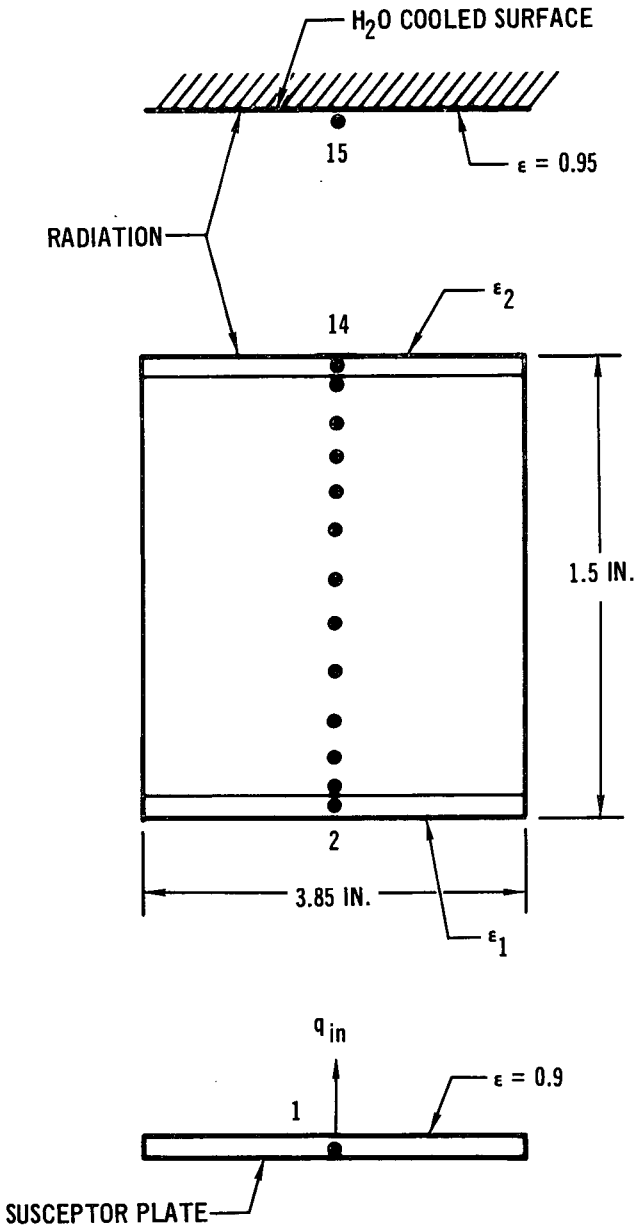

ONE DIMENSIONAL 15 NODE THERMAL MODEL

457-3137

Figure 81

temperature calculated through the insulation shows that the thermocouples would have to be recording temperatures as much as 0.10 inch away from their actual position. Consequently, it was concluded that relocating the thermocouples was not a plausible explanation. The measured surface emittances of the TD NiCr specimen package were essentially those which had been estimated and used in the thermal model.

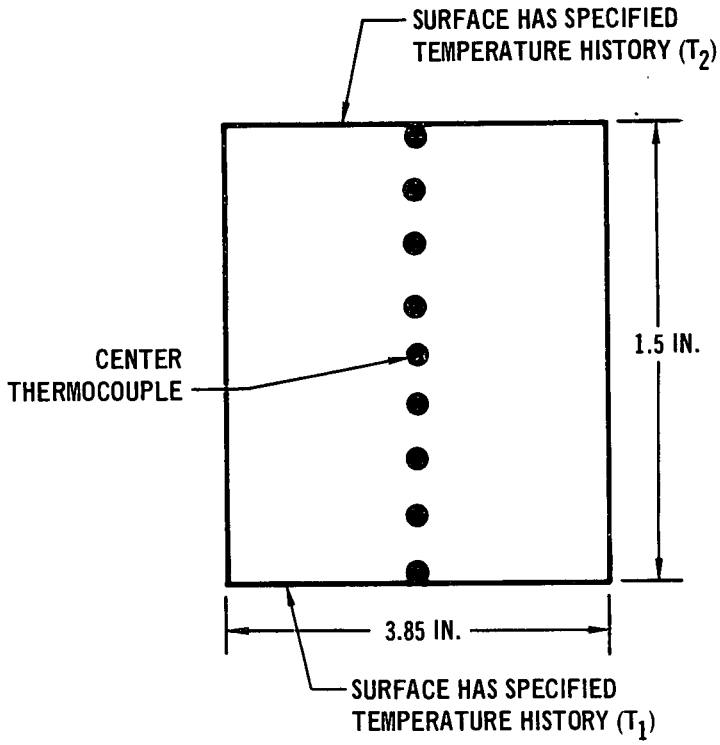

ONE DIMENSIONAL THERMAL MODEL FOR CALCULATING EFFECTIVE CONDUCTIVITY

457-3138

Figure 82

Because the calculated temperature histories are a direct function of thermal conductivity, the effective thermal conductivity for the test specimen was determined using the thermal model shown in Figure 82. The maximum temperature as measured by thermocouple 5 was utilized as a matching time-temperature history profile condition for determining the effective thermal conductivity. The resulting thermal conductivity produced a good correlation with the measured time-temperature curve for T/C5 (Figure 86). The nominal and effective thermal conductivity curves coincide to approximately 800°F and then the effective conductivity begins to deviate to higher values. At 1600°F the effective conductivity is approximately 16.3% higher than the nominal thermal conductivity. It should be noted that the full thermal model (Figure 81) was used for calculating Figure 86. As shown in Figure 86 thermocouple 5 test data is compared to profiles using nominal and effective conductivities and shows the profile using the effective conductivity to be in good agreement between measured and calculated temperatures. Thermocouples 4 and 6 do not agree as well as for T/C5, most likely because of boundary conditions. However, the

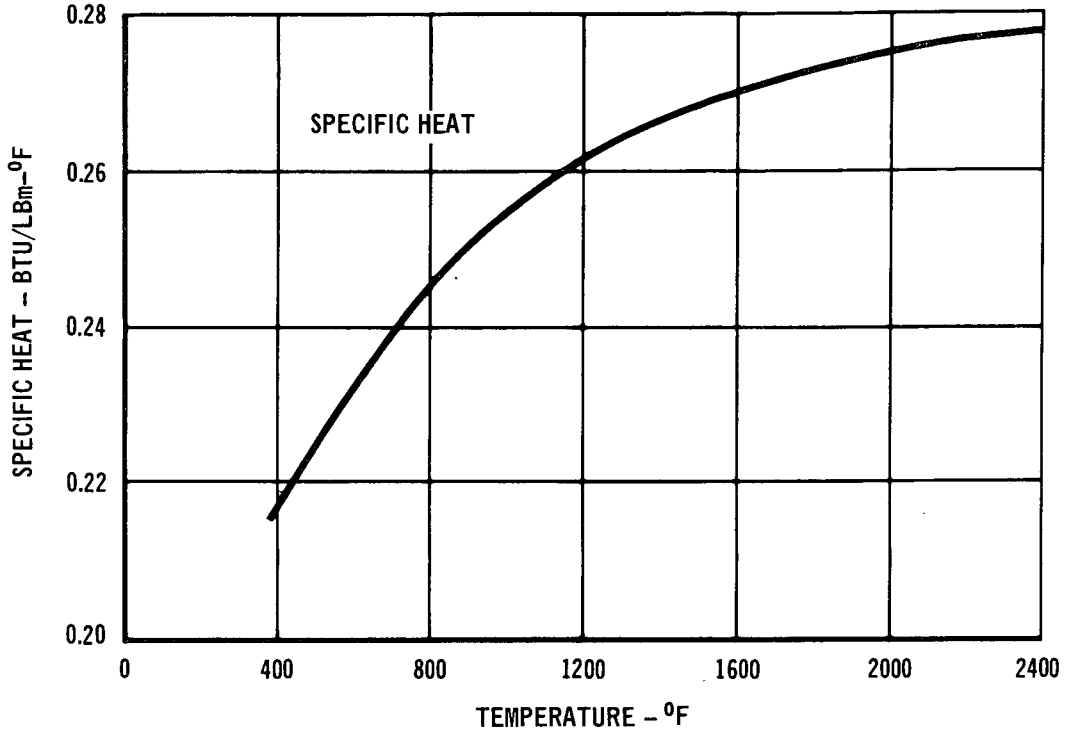

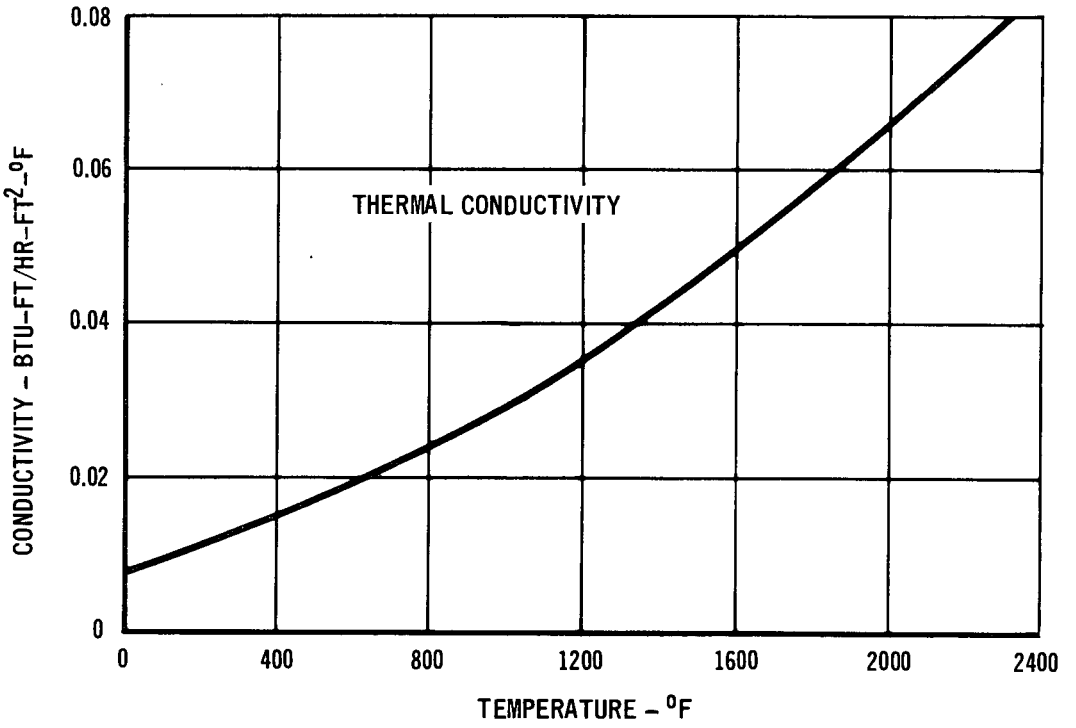

SKX-FIBERFRAX THERMAL PROPERTIES
Used In Analysis

- PRESSURE = 10 TORR
- DENSITY = 7.7 PCF

457-3139

Figure 83

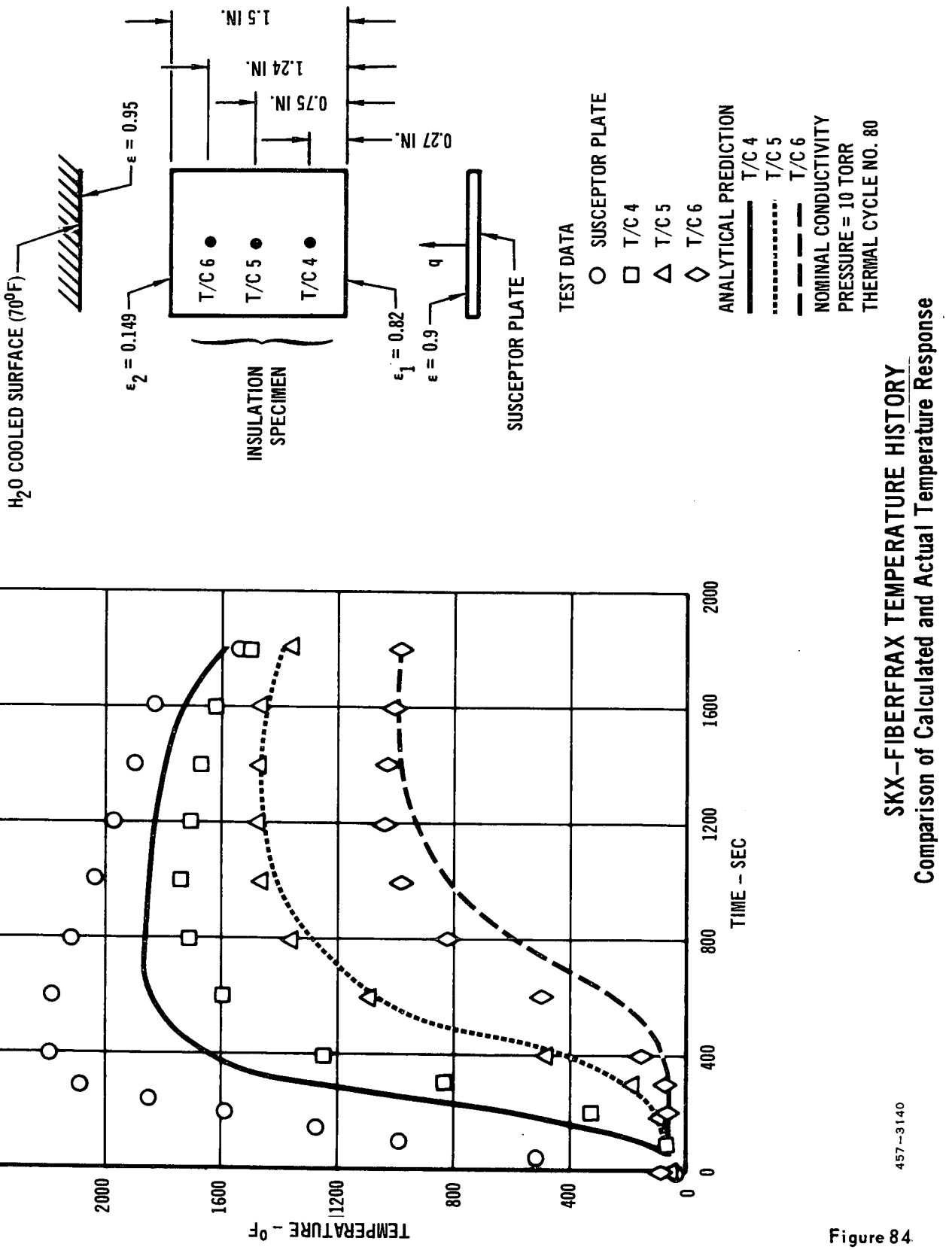

SKX–FIBERFRAX TEMPERATURE HISTORY
Comparison of Calculated and Actual Temperature Response

Figure 84

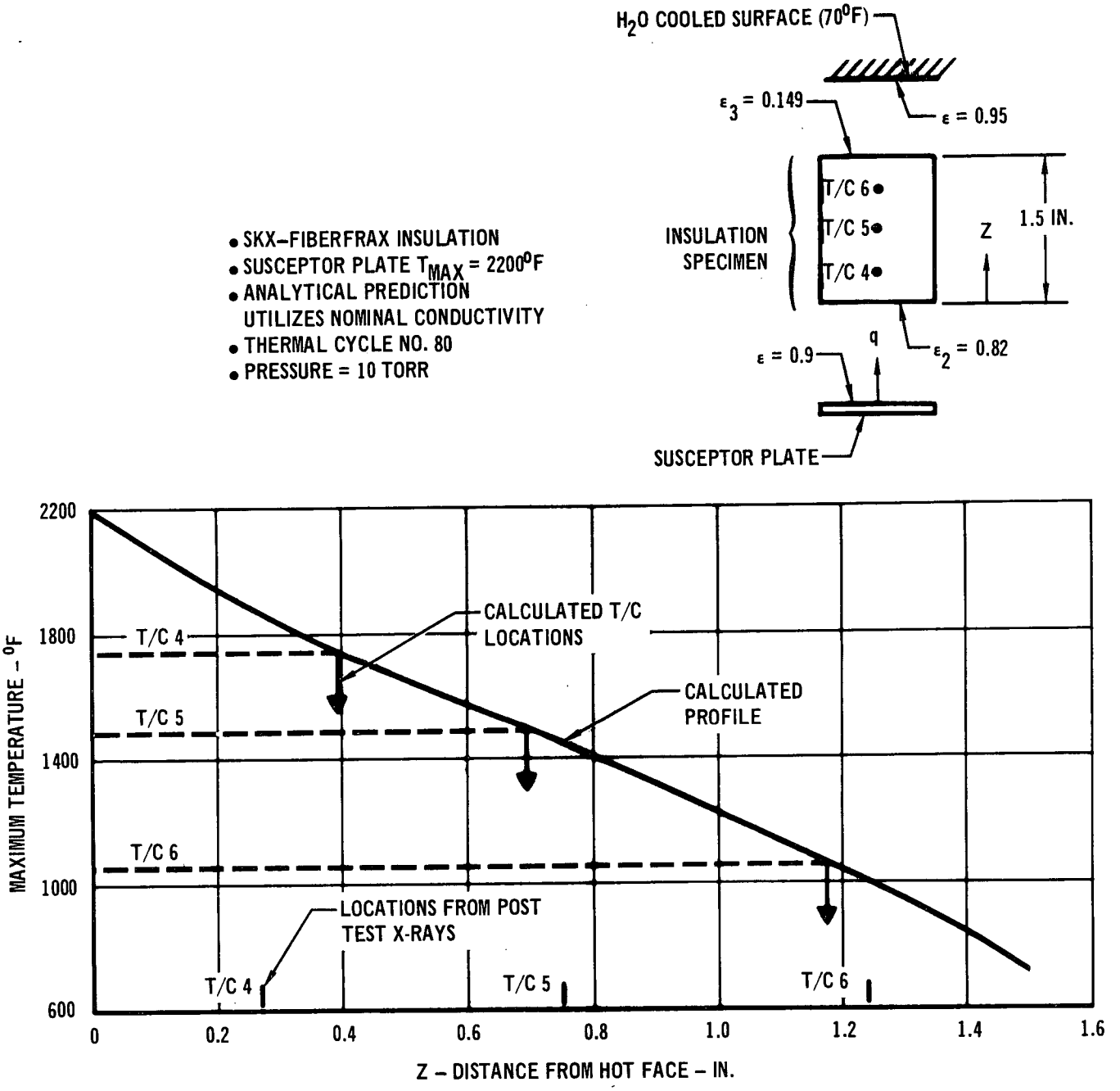

457-3141 THERMOCOUPLE LOCATION COMPARISON OF MEASURED AND ESTIMATED

Figure 85

agreement is closer using the effective thermal conductivity (Figure 86) than the nominal value (Figure 84).

A brief study was also conducted to determine if degradation of thermal conductivity occurred between thermal cycle 1 and 80. Figure 87 shows the comparison of the measured temperatures for both cycles and the calculated profile using the

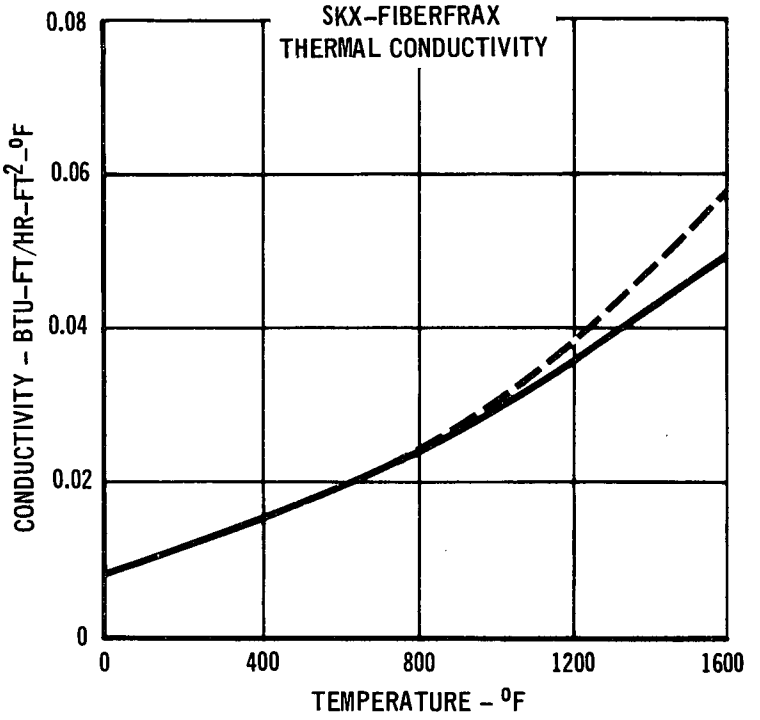

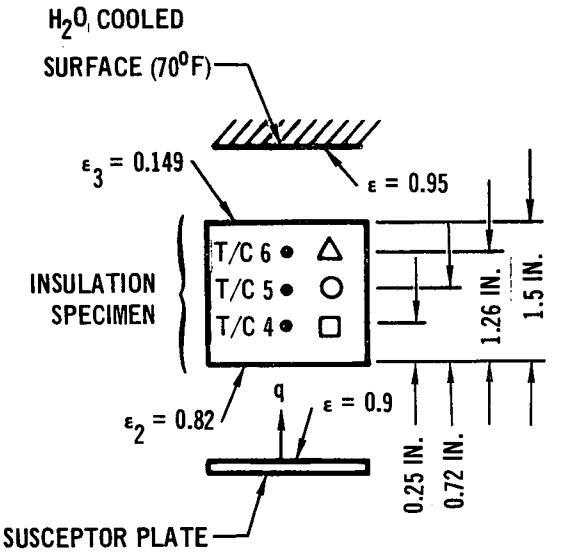

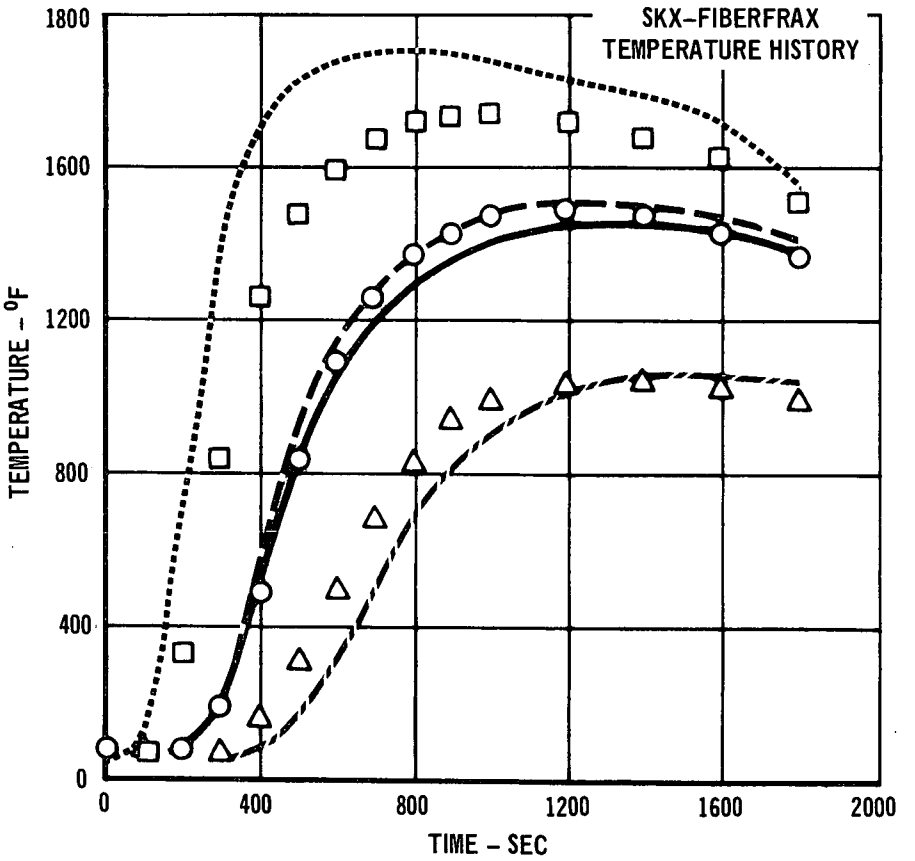

SYMBOLS - MEASURED TEST DATA
NOMINAL CONDUCTIVITY
EFFECTIVE CONDUCTIVITY
ρ= 7.7 PCF
PRESSURE = 10 TORR
THERMAL CYCLE NO. 80

457-3142

SKX-FIBERFRAX
Comparison of Temperature Response for Nominal and Effective Conductivities and Test Data

Figure 86

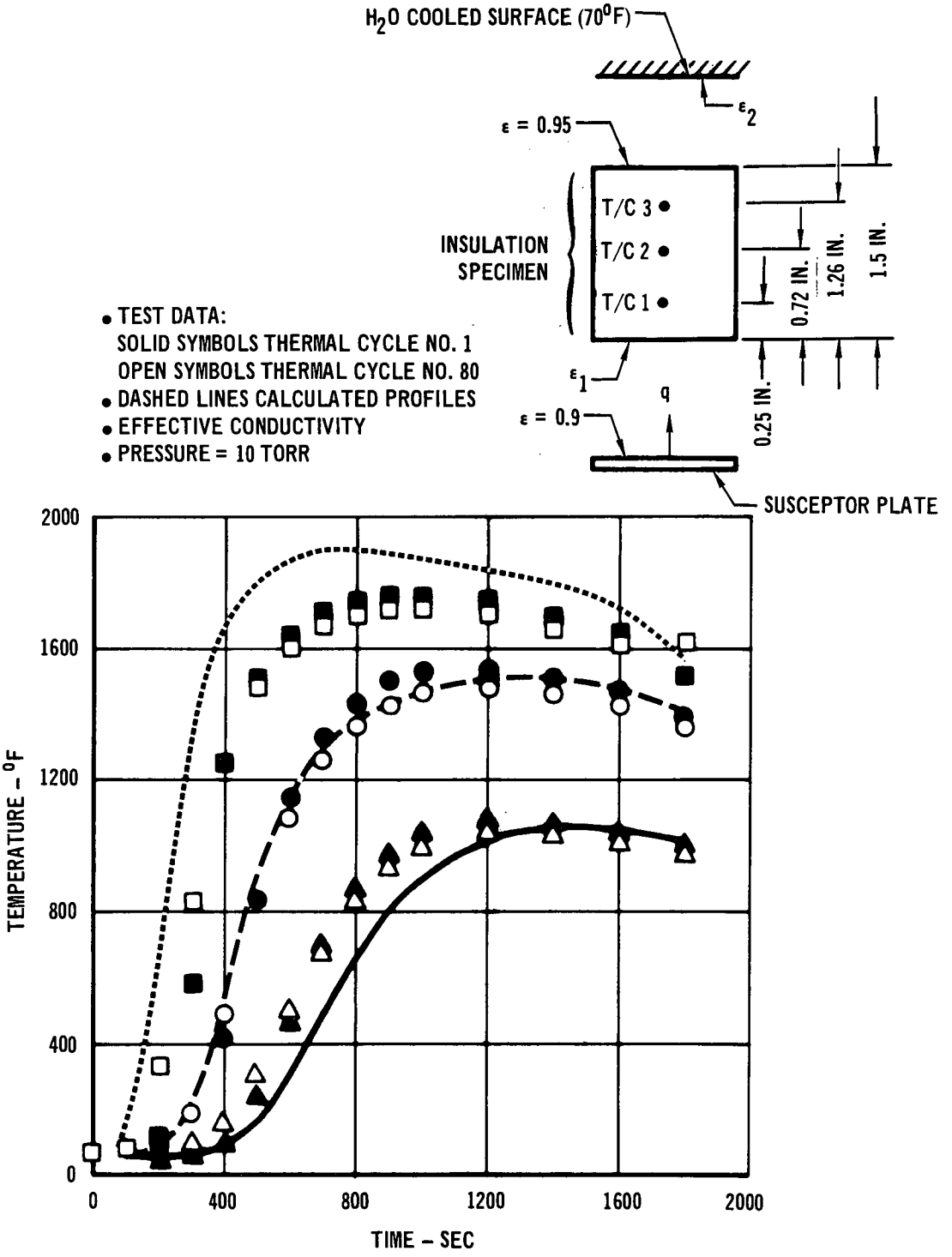

COMPARISON OF SKX–FIBERFRAX THERMAL RESPONSE BETWEEN CYCLES 1 AND 80 AND PREDICTED RESULTS

457–3143

Figure 87

effective conductivity. There was an insignificant difference in the measured profiles temperatures between the first and 80th cycles and correlation with the calculated profile (thermocouple 5) was very good. The conclusion was that thermal conductivity degradation over these 80 cycles is insignificant and the resulting effective thermal conductivity is valid for SKX-Fiberfrax for the 10 torr test condition.

3.7.1.4 Astroquartz - A transient heat transfer analysis was conducted based on the results of thermal cycle 80. First, the estimated nominal thermal conductivity and specific heat of 1.0 pcf density Astroquartz (Figure 88) were used to predict specimen thermal response. Figure 89 shows the comparison between measured temperature profile for thermocouples 1, 2 and 3, and the analytically calculated temperature profiles of thermocouples 1, 2 and 3. These results show the test data for the three thermocouples to be lower (over the entire temperature history) than the calculated temperature profiles. The mismatch between measured and calculated temperatures could be due to several things, including sensitivity of thermocouple location, package surface emittance, internal radiation and thermal conductivity of the Astroquartz material. To illustrate the required relocation of the thermocouples, Figure 90 was constructed. The plot of maximum temperature calculated through the insulation shows that the termocouples would have to be recording temperatures as much as 0.40 inch away from their actual position. Consequently, it was concluded that relocation of the thermocouples was not a valid explanation. The measured surface emittances of the TD NiCr specimen package agreed well with those used in the thermal model. With such a large difference it was anticipated that studies of the effective thermal conductivity, surface emissivity, and internal radiation would have to be conducted; sensitivity studies for thermal conductivity and surface emissivity were performed.

The thermal conductivity sensitivity analysis was conducted to determine if a reasonable effective conductivity, changed as a percentage of the nominal, for the purpose of obtaining the same maximum temperature as recorded from thermocouple 2, would provide a better fit to the test data. A temperature comparison is shown in Figure 91 of the test data, and three calculated profiles using thermal conductivity values of nominal, 78 percent of nominal and 50 percent of nominal. A 50 percent reduction in thermal conductivity results in approximately a 50 degree decrease in maximum temperature; to match the test data, a 120°F decrease in calculated temperature is required. Figure 92 shows the percentage of nominal conductivity value as a function of the maximum calculated temperature. The

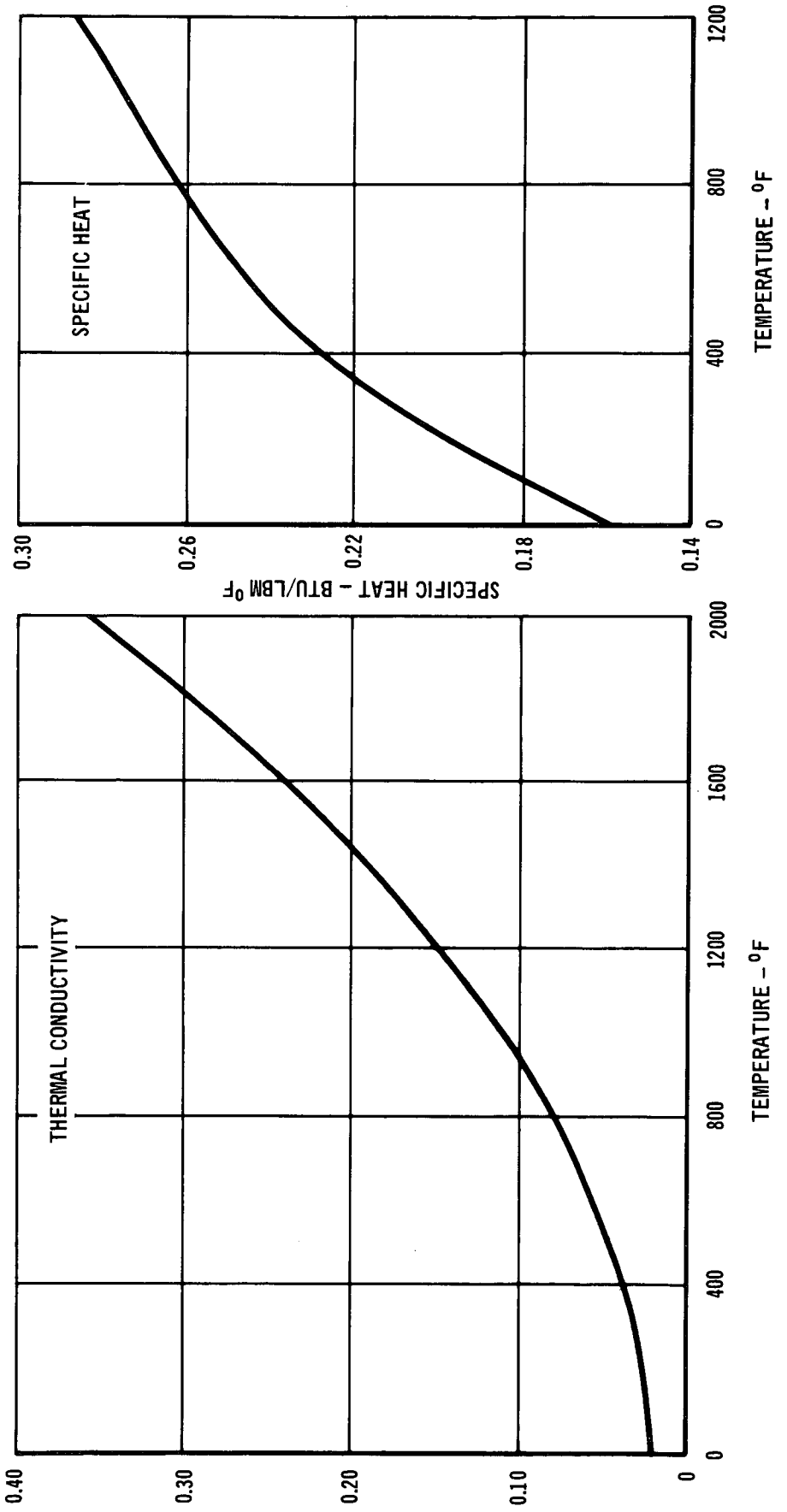

ASTROQUARTZ THERMAL PROPERTIES
Used In Analysis

457-3144

Figure 88

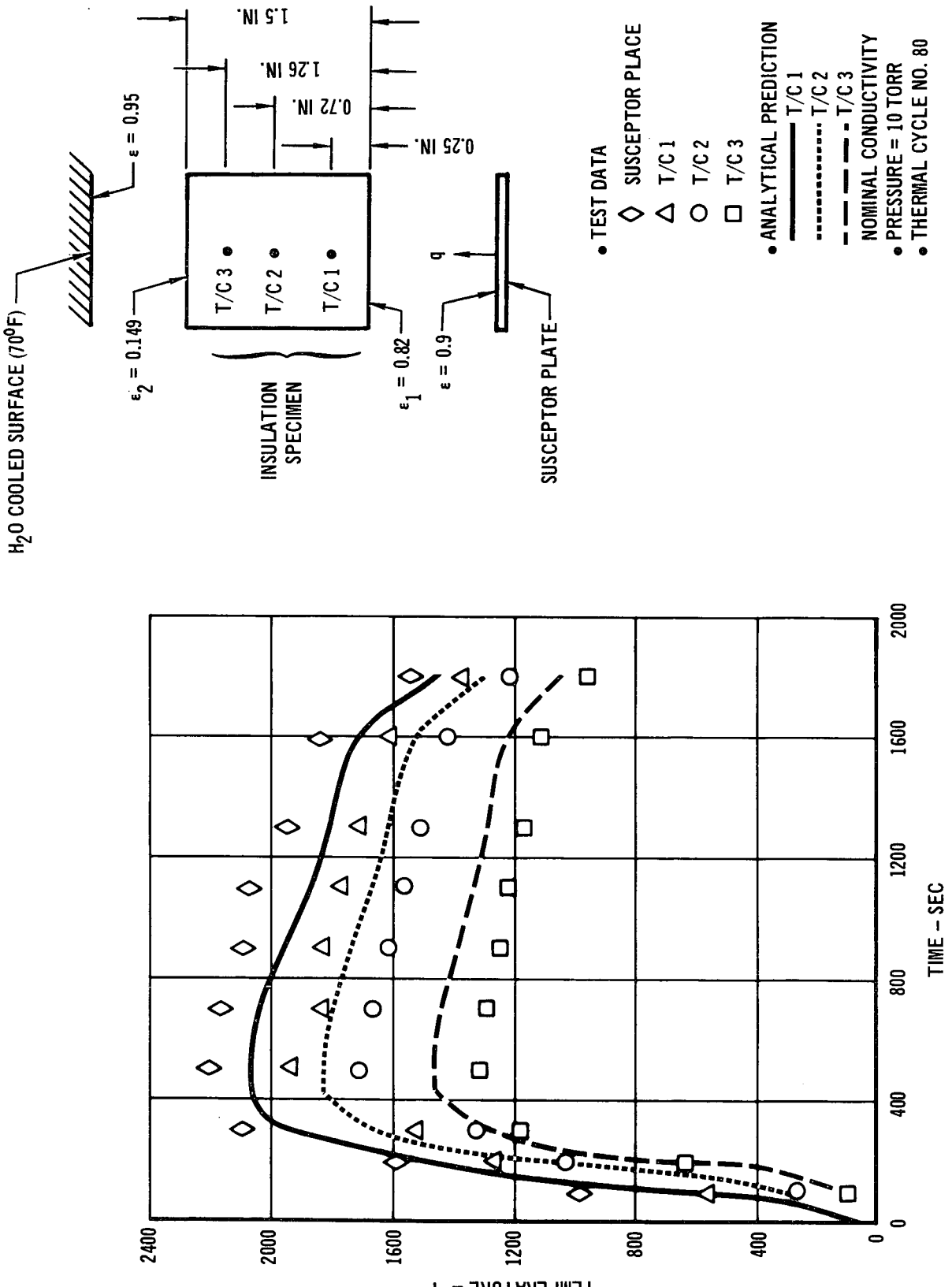

ASTROQUARTZ TEMPERATURE HISTORY

Figure 89

results of this sensitivity study indicate that a thermal conductivity value that is approximately 24 percent of the nominal thermal conductivity would be required to limit the thermal model mid-point temperature to a maximum of 1710°F. The nominal thermal conductivity value at 1710°F is approximately .27 BTU-FT/HR FT^2°F and a 24 percent value is .0648 BTU-FT/HR FT^2°F, which is not a reasonable value for this material and density. It should be noted that the heat storage capacity of this low density material makes it extremely sensitive to variations. Adjustment of thermal conductivity, we believe, does not explain the measured temperature discrepancies.

A hot and cold surface emissivity sensitivity analysis was also conducted for this specimen. This analysis generated constant temperature loci (Figure 93) as a function of surface emissivities to determine the emissivities necessary to correlate the measured temperatures of the three thermocouples. The constant temperature loci are for the maximum temperatures measured by thermocouples 1 (1940°F), 2 (1710°F) and 3 (1320°F). The results shown in Figure 93 indicate that a match between measured and calculated maximum temperatures requires emissivities for cold face and hot face to be approximately 0.16 and 0.08 respectively. The working curves used tc obtain Figure 93 are in Figures 94, 95, and 96. The measured emissivities for TD NiCr were 0.124 for the cold face and 0.46 for the hot face. The emittances for the cold side (0.124 measured and 0.16 analysis of test) are in reasonable agreement. However, the emittances for the heated side do not agree (0.46 measured and 0.08 analysis of test). It is very unlikely that the measurements are off by a factor of six. Consequently, adjusting the surface emittances used for the TD NiCr foil does not explain the measured temperatures. Resolution of these temperature discrepancies has not been possible at this time.

3.7.2 Flight Configuration Thermal Analysis - A thermal analysis was also conducted on the low density flight configuration insulation (Astroquartz) and attempted on the high density Microquartz flight configuration. In neither case was it possible to obtain effective conductivity data. The analyses conducted are described below.

3.7.2.1 Astroquartz Flight Configuration - A one-dimensional thermal model (Figure 97) was constructed corresponding to the center of the test setup including the susceptor plate, radiation gaps, and backup structure. This 60 node model was employed to correlate the measured transient time-temperature profile experienced by the test specimen.

The transient heat transfer analysis was conducted based on the results of

- ASTROQUARTZ INSULATION
- SUSCEPTOR PLATE T_{MAX} = 2200°F
- ANALYTICAL PREDICTION NOMINAL CONDUCTIVITY
- THERMAL CYCLE NO. 80
- PRESSURE = 10 TORR

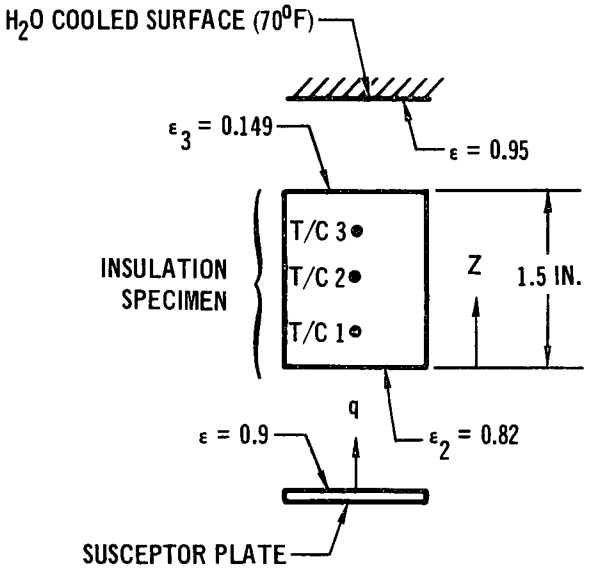

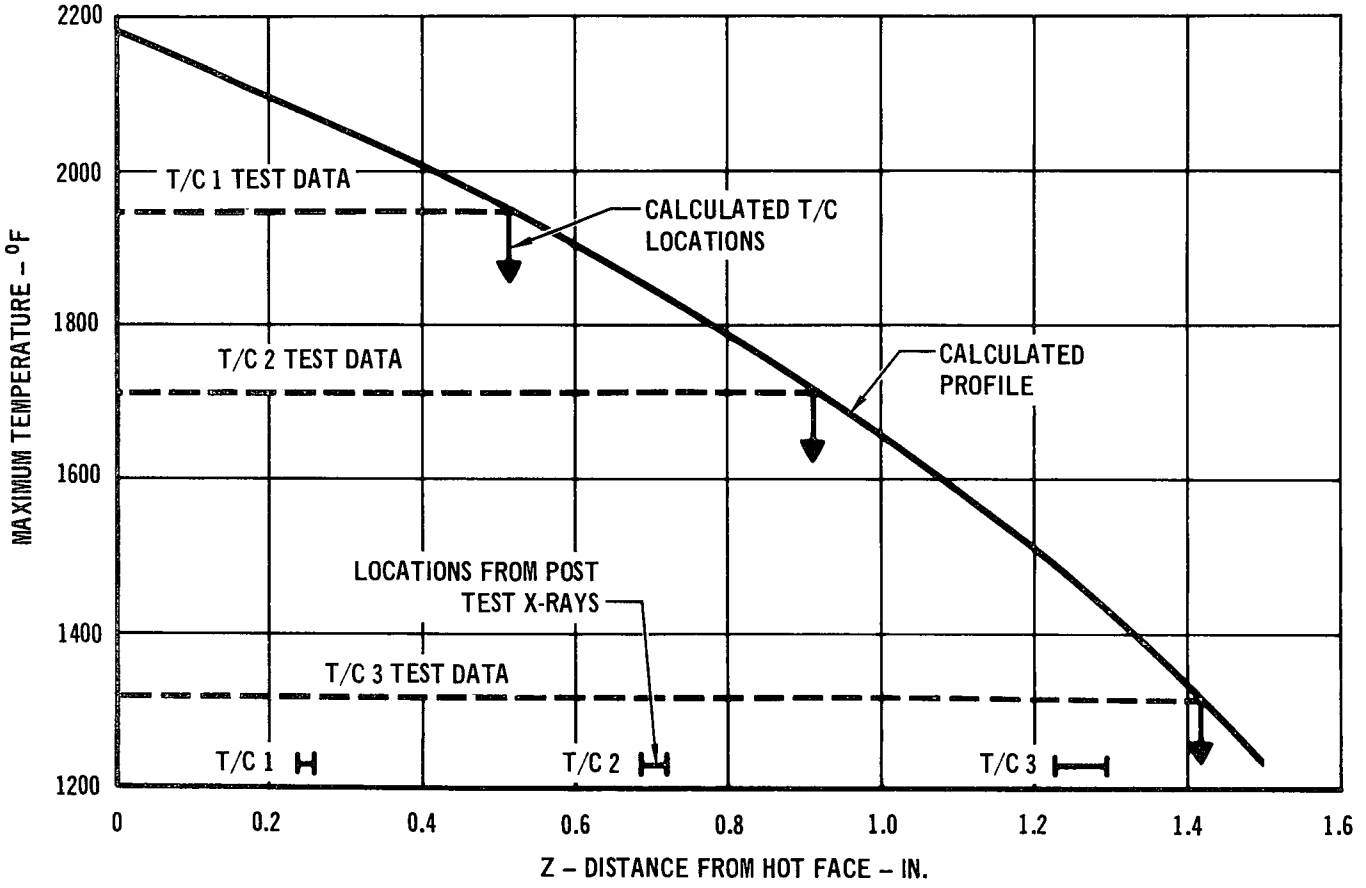

THERMOCOUPLE LOCATION COMPARISON OF MEASURED AND ESTIMATED

457–3146

Figure 90

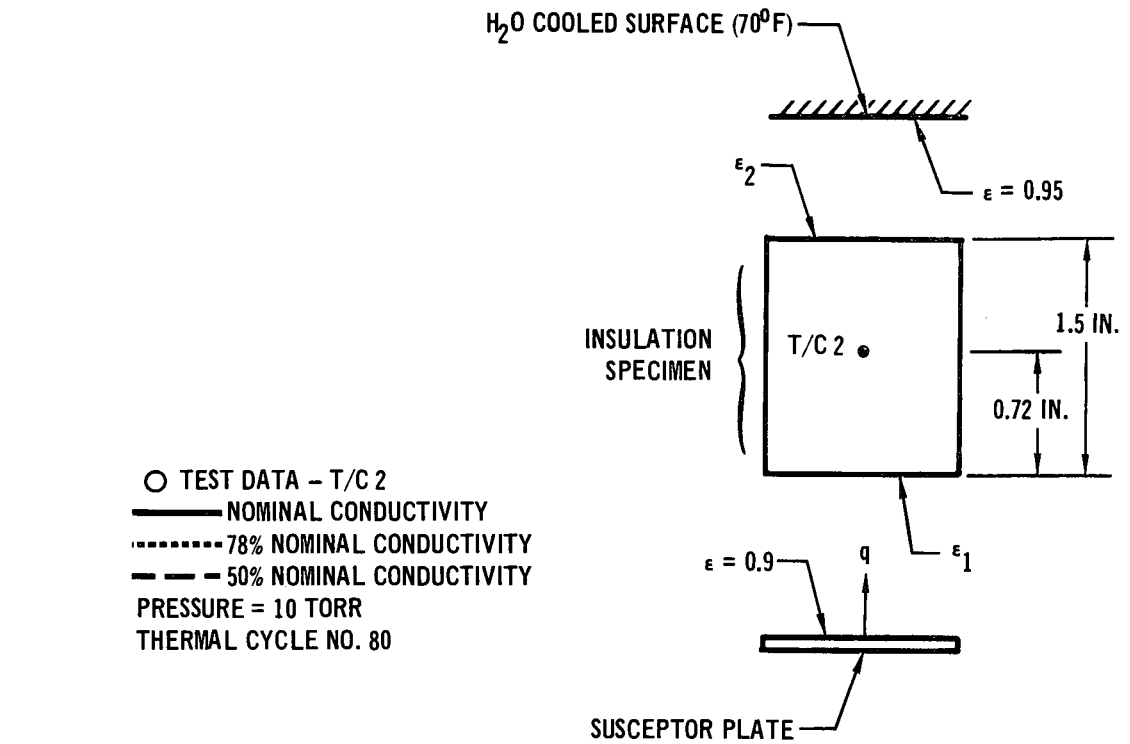

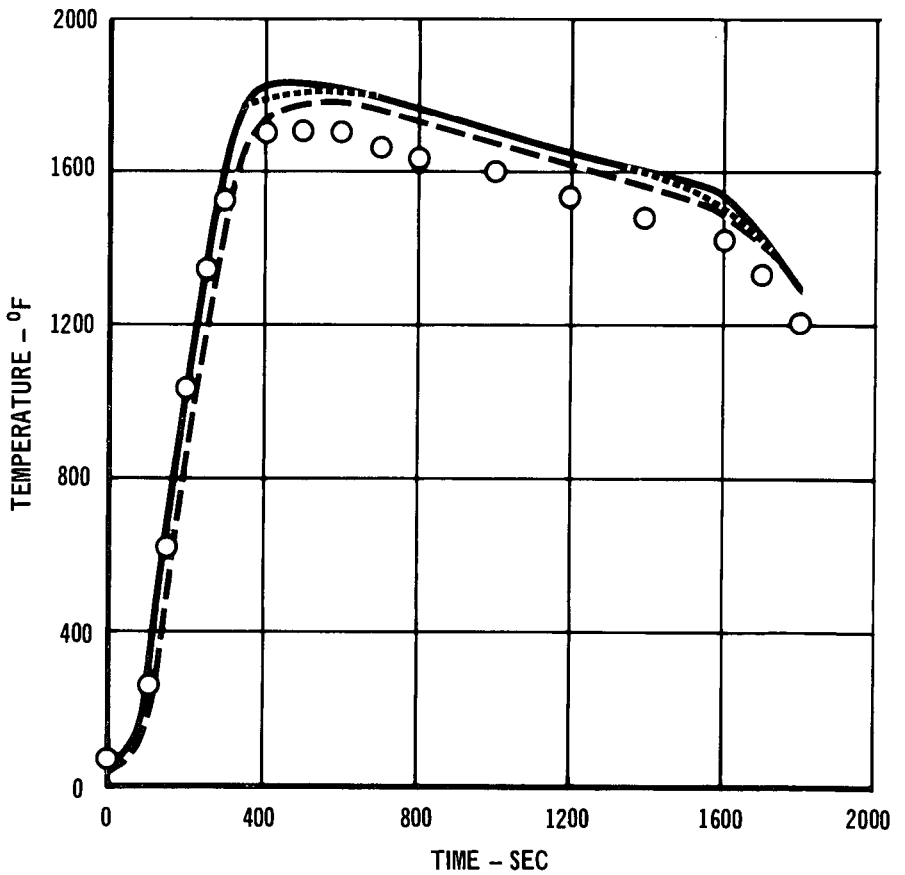

ASTROQUARTZ THERMAL CONDUCTIVITY SENSITIVITY

457-3147

Figure 91

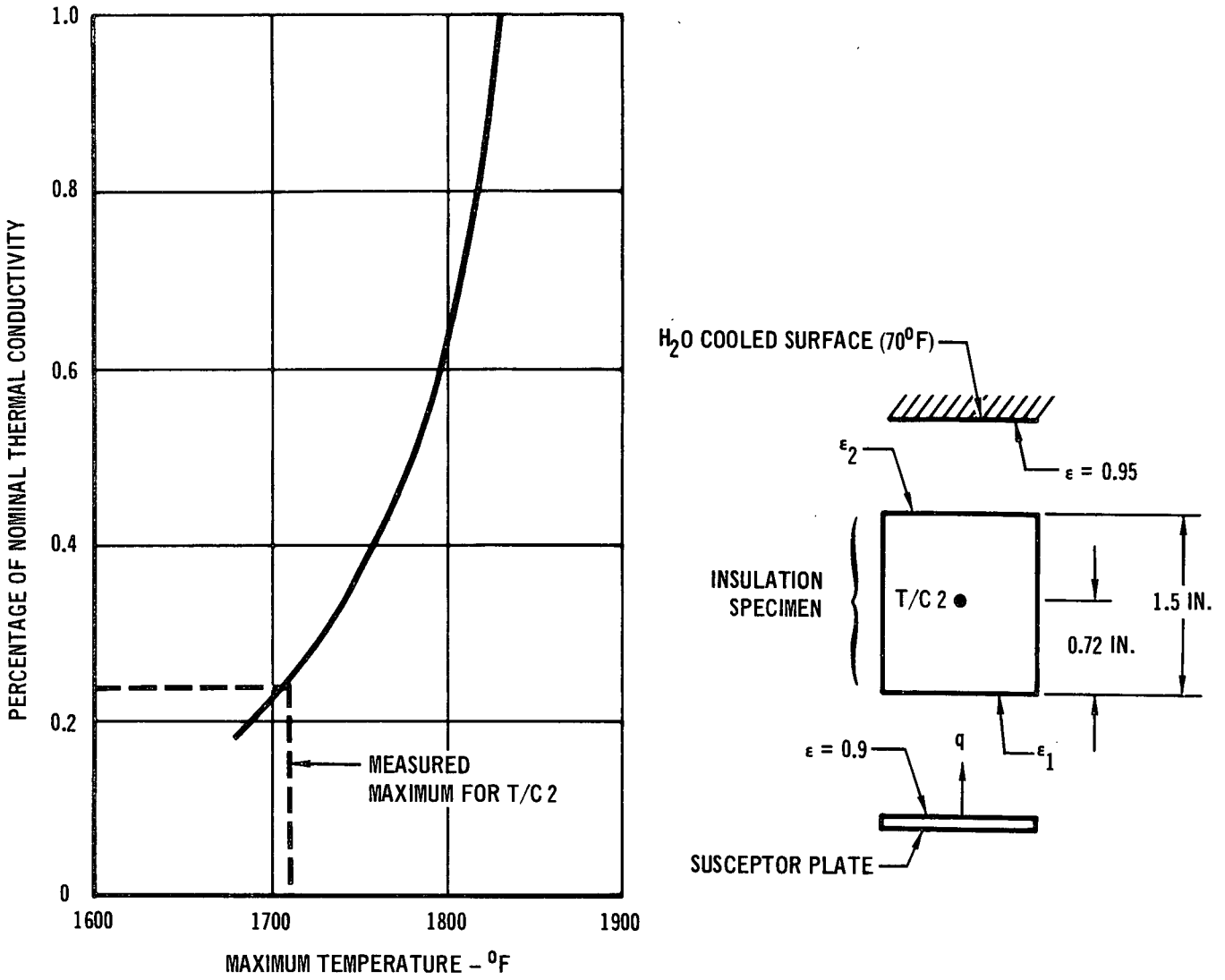

ASTROQUARTZ THERMAL CONDUCTIVITY SENSITIVITY

457-3148

Figure 92

thermal cycle 21. The nominal thermal conductivity and specific heat (Figure 88) of a 0.625 lb/ft^3 installed density of Astroquartz were used to predict specimen thermal response. The test specimen had six thermocouples located in the insulation at the locations shown in Figure 98. The comparison between measured and analytically calculated temperature profiles for thermocouples number 7 through 12 are also shown in Figure 98. These results show the test data for thermocouples 7, 8, 9 and 10 to be lower (over the entire temperature history) than the calculated profiles with maximum temperature differential of approximately 100 degrees; thermocouple 11 profile peaks at approximately the same temperature for both the test and calculated data at peak conditions, while thermocouple 12 (the coolest T/C) was as much as 200°F hotter than analytically calculated. This mismatch between

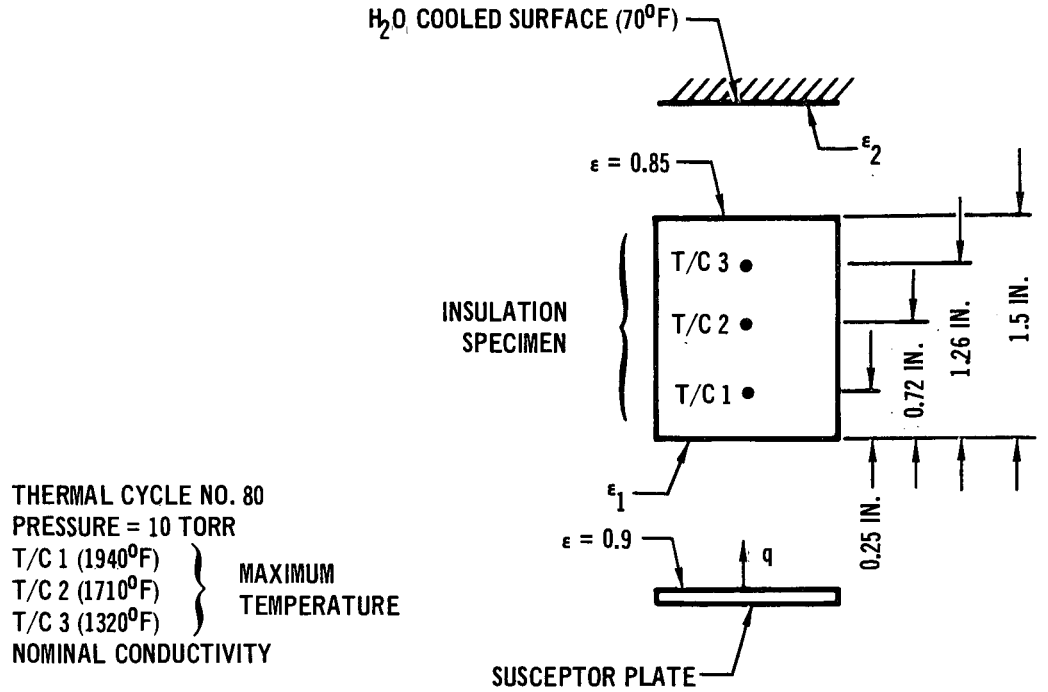

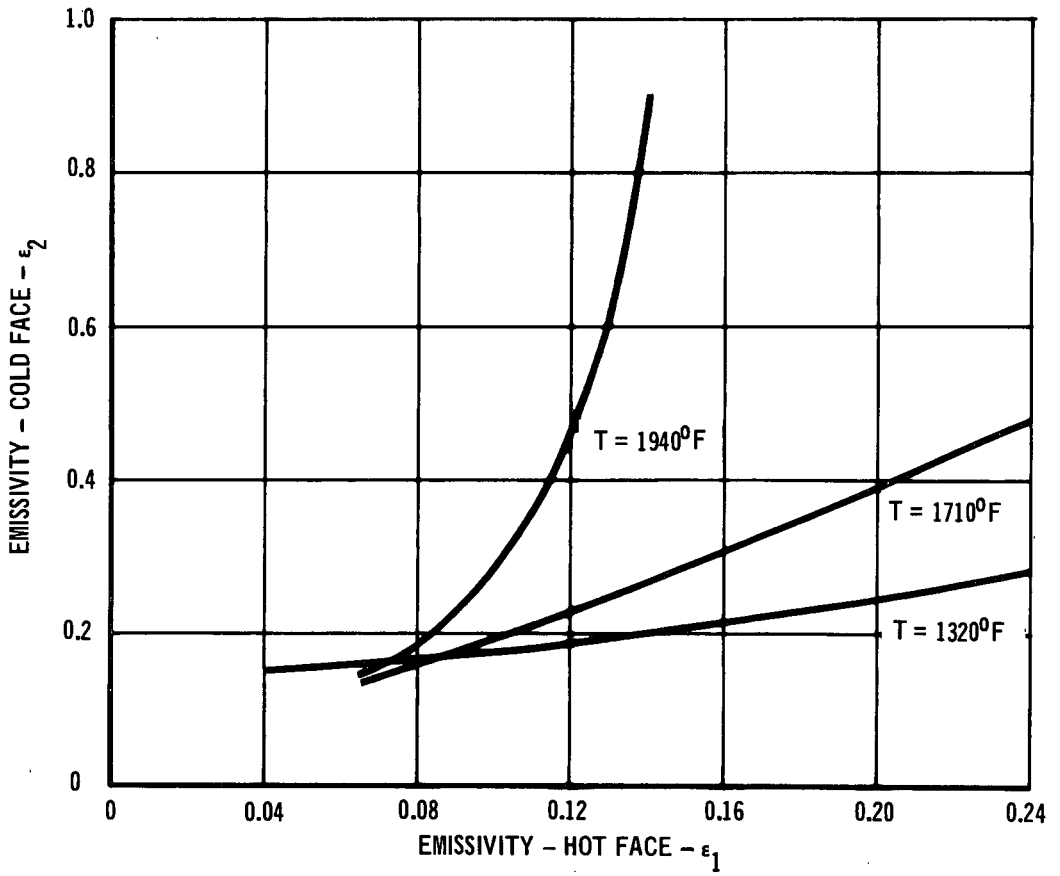

457-3149

TD-NiCr FOIL ON THE ASTROQUARTZ SPECIMEN
Emissivity Sensitivity Analysis

Figure 93

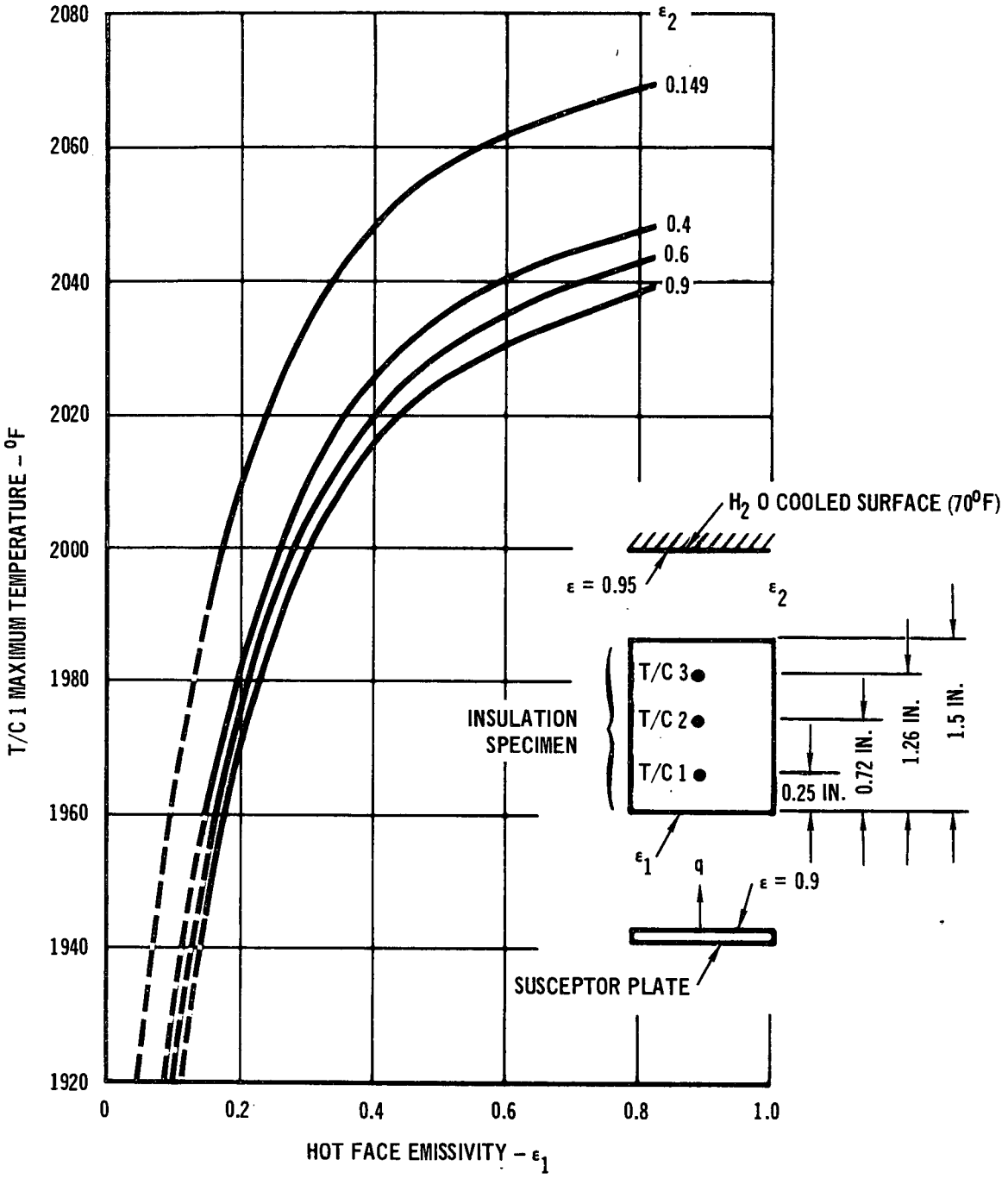

457-3150

ASTROQUARTZ EMISSIVITY ANALYSIS

Figure 94

measured and calculated temperatures could be due to several factors, including sensitivity of thermocouple location, package surface emissivity as a function of temperature, internal radiation and thermal conductivity of the Astroquartz

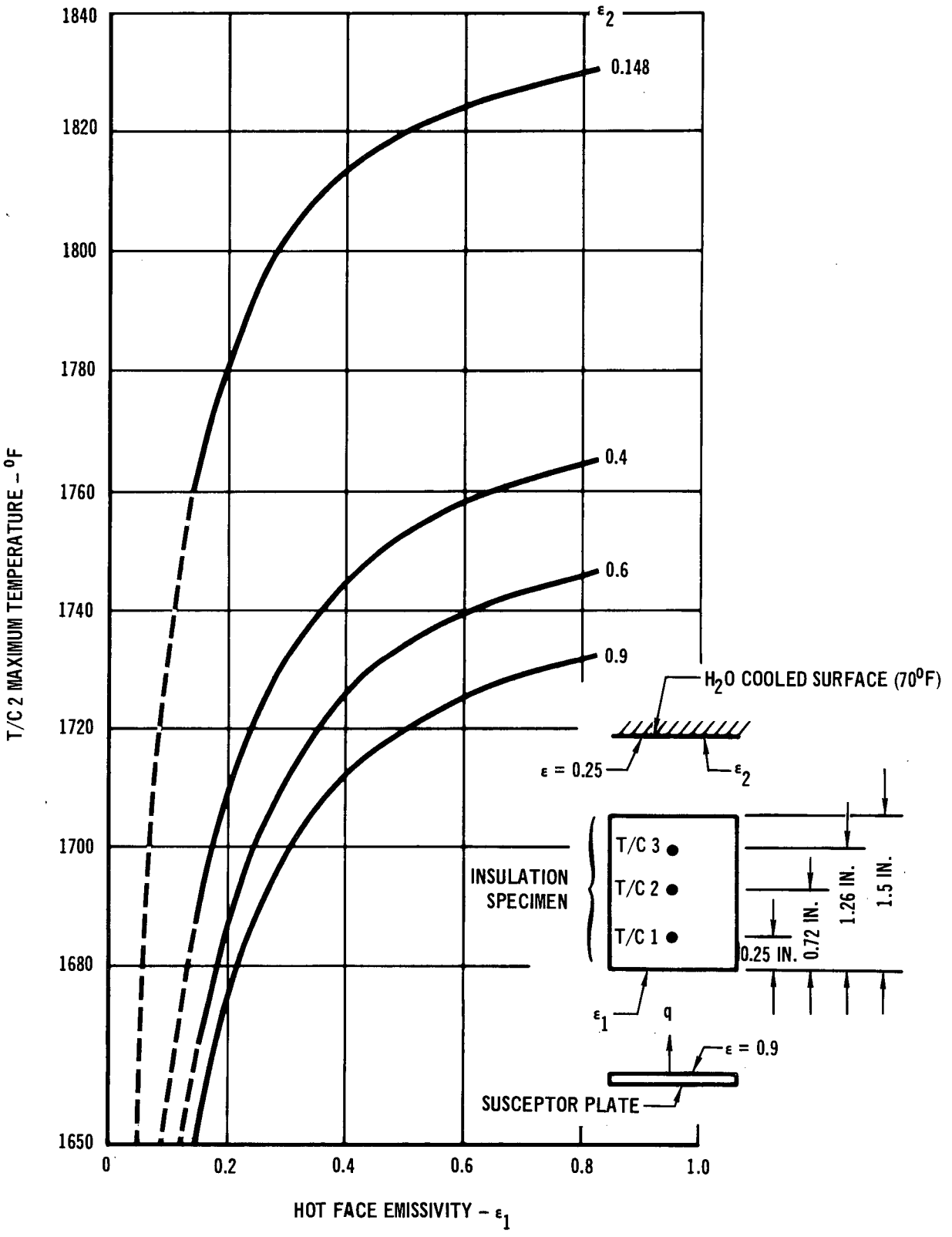

ASTROQUARTZ EMISSIVITY ANALYSIS

457-3151

Figure 95

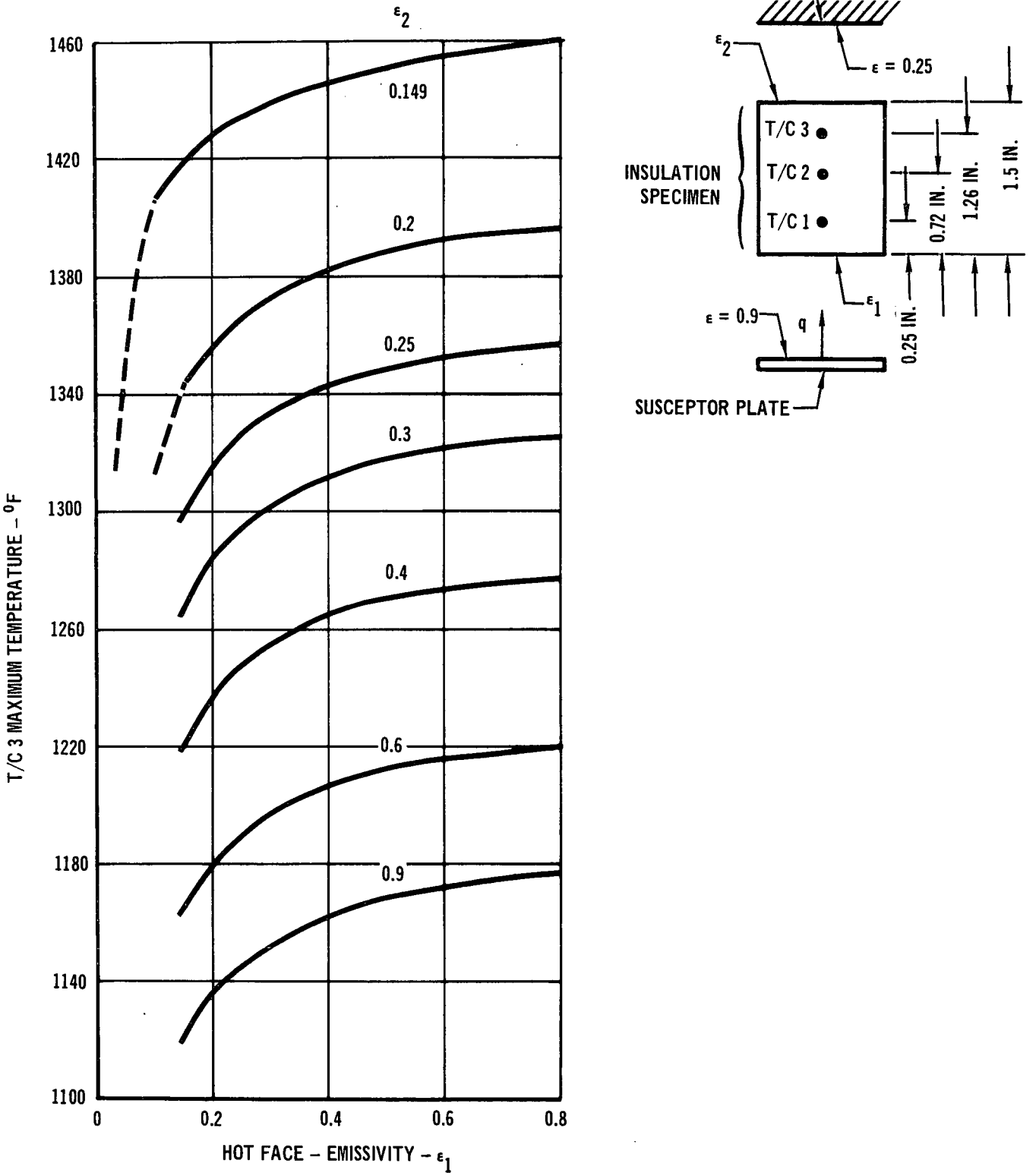

457-3152

ASTROQUARTZ EMISSIVITY ANALYSIS

Figure 96

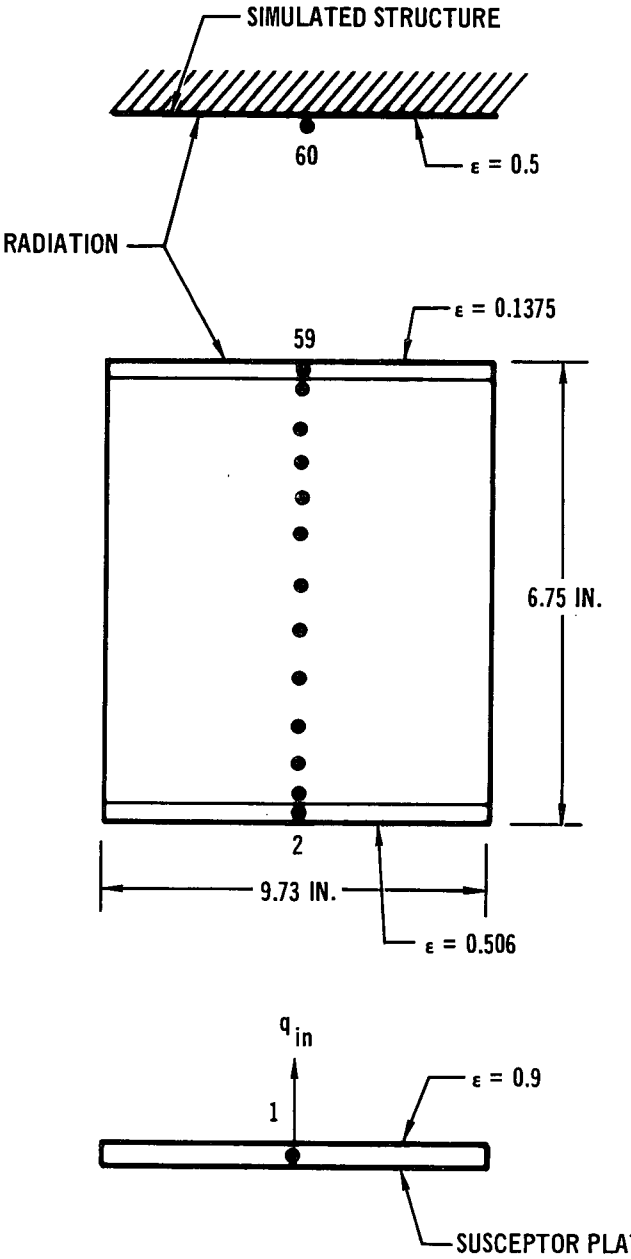

ONE DIMENSIONAL 60 NODE THERMAL MODEL OF FLIGHT CONFIGURED INSULATION PACKAGE

457-3153

Figure 97

material. To illustrate the required relocation of the thermocouples, Figure 99 was constructed. The plot of maximum temperatures calculated through the insulation shows that some thermocouples would have to be recording temperatures as much as 0.50 inch away from their actual positions, with only thermocouple 11 very near to its actual location. Consequently, with the majority of the thermocouples showing a large location discrepancy, it was concluded that errors in location of the

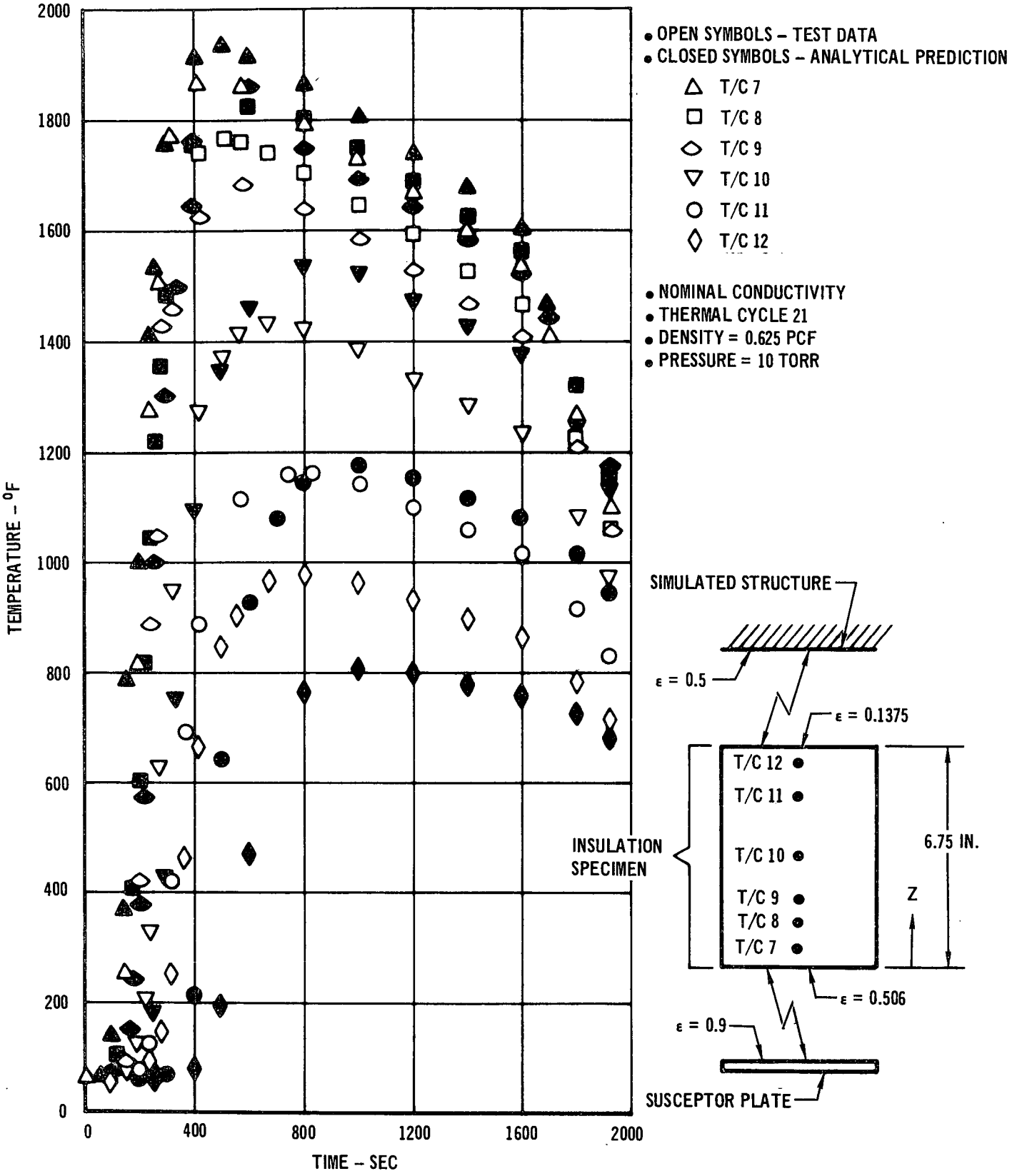

457–3154

ASTROQUARTZ TEMPERATURE HISTORIES FOR FLIGHT CONFIGURED PACKAGE

Figure 98

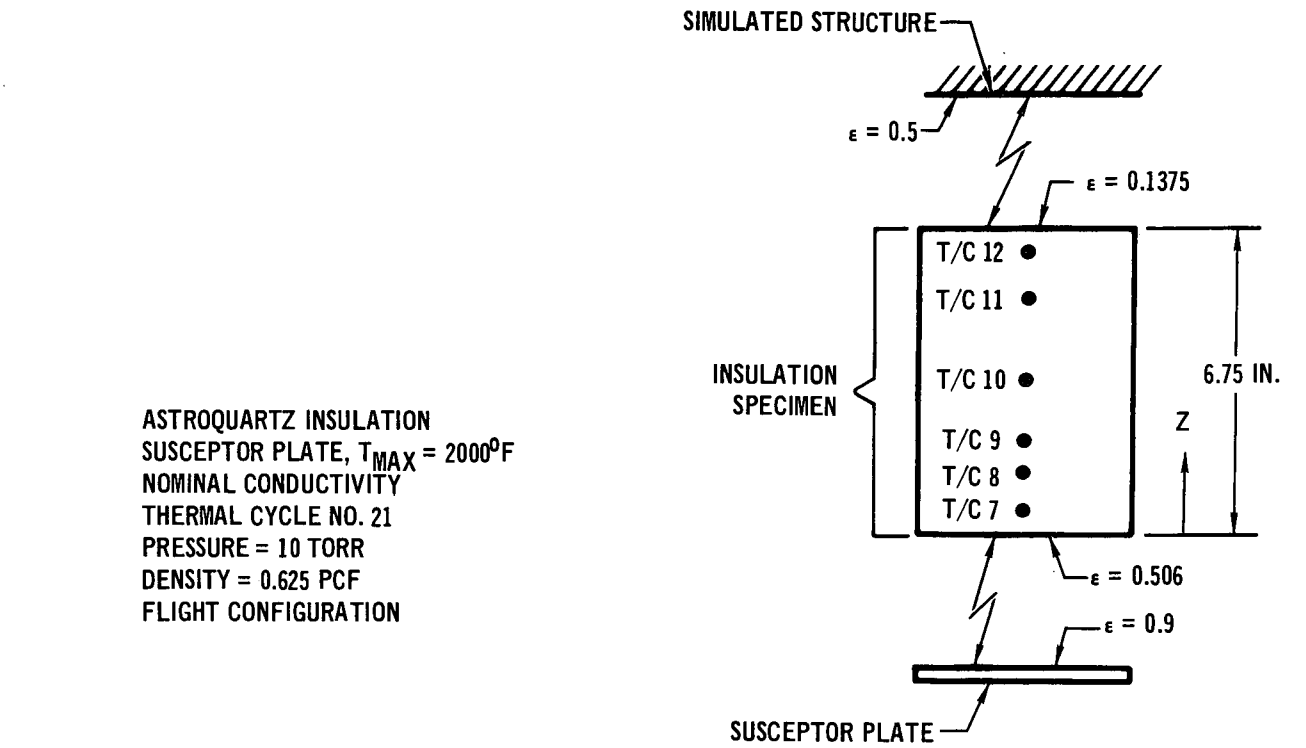

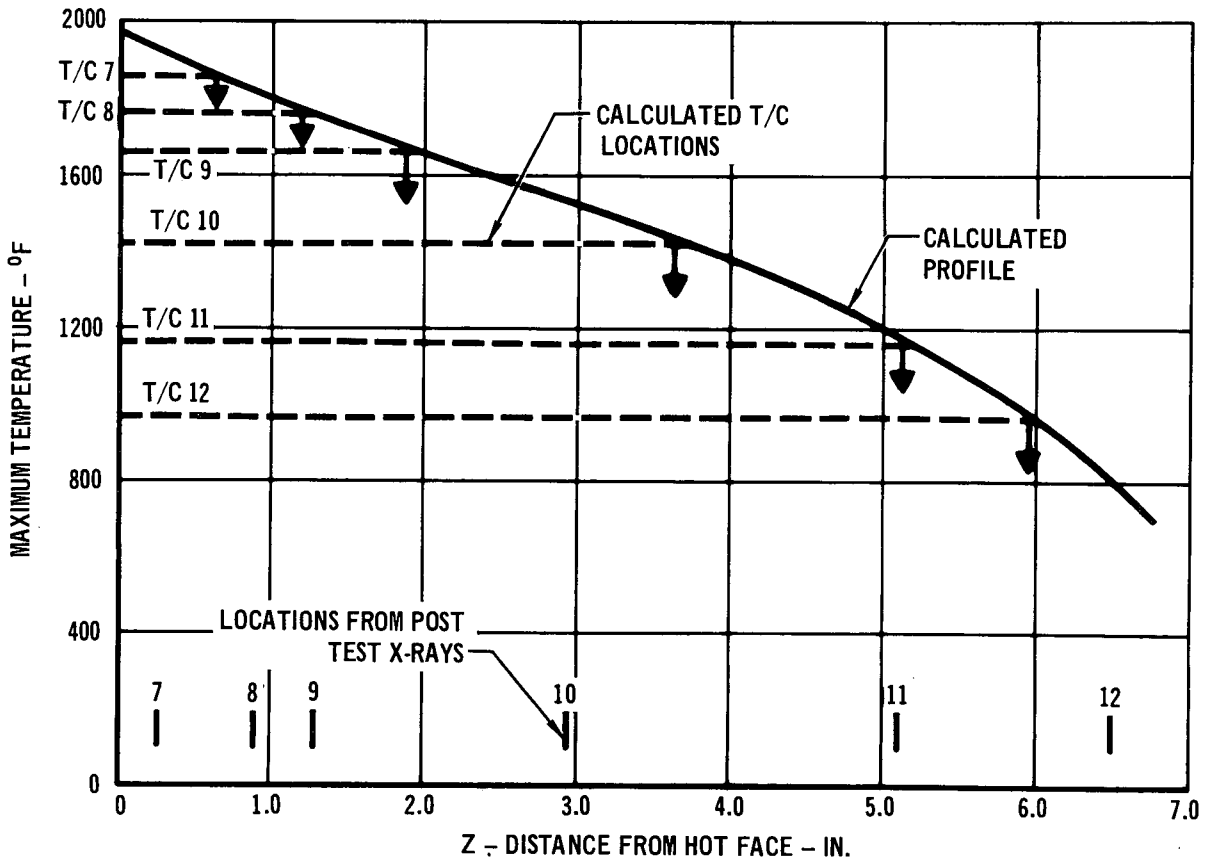

THERMOCOUPLE LOCATION COMPARISON OF MEASURED AND ESTIMATED

457-3155

Figure 99

thermocouples were not a valid explanation.

Previous thermal analysis conducted on a smaller Astroquartz insulation test specimen resulted in the conclusion that sensitivity studies of thermal conductivity and surface emissivities did not explain the measured temperatures. Because of the similarity in the calculated temperature profiles versus recorded temperature profiles for the two test specimens, the previously conducted thermal conductivity sensitivity study is applicable to the larger Astroquartz insulation test specimen. One of the primary objectives was to determine apparent thermal conductivity from this large test specimen. The difficulties encountered were that test data showed temperature differential between thermocouples to be too large for a mean temperature to reflect a conductivity value applicable to the two recorded end temperatures, and the distances between various thermocouples were very large. These conditions resulted in the inability to determine apparent thermal conductivity values as a function of temperature.

3.7.2.2 Microquartz Flight Configuration - A transient heat transfer investigation was conducted on the TD NiCr package High Density Microquartz Insulation test specimen. This specimen insulation consisted of 3.5 lb/ft^3 Microquartz felts compressed to a nominal density of 10 lb/ft^3. The actual measured density as installed was 8.8 lb/ft^3. A survey of peak temperatures for the thermal cycles showed that the simulated aluminum backup structure did not exceed 340°F for all cycles except one, where the aluminum structure attained a 526°F maximum, when the test specimen was subjected to a time-temperature history profile that peaked at approximately 2000°F, and simulating service conditions. Figure 100 is a tabulation of recorded peak temperatures showing this thermal protection configuration to perform satisfactorily with the exception of one thermal cycle.

A transient heat transfer analysis for calculating test data was not conducted on this specimen due to the inability to determine the location with reasonable accuracy of number 3 thermocouple from pre-test x-ray, and of all three thermocouples from post test x-ray. A survey of the thermal cycles showed cycles 2 to 10 and cycles 11 to 40 to have a significant change in peak temperature and the time at which peak temperature occurred (Figure 100) for thermocouples 1 and 2. Also, a significant change occurred in the shape of the time-temperature history profile for thermocouples 1 and 2. These two significant recorded data changes are definite indications that the thermocouples had moved from their original positions. The change in thermocouple response and the inability to determine the new positions led to the conclusion that a valid heat transfer analysis for

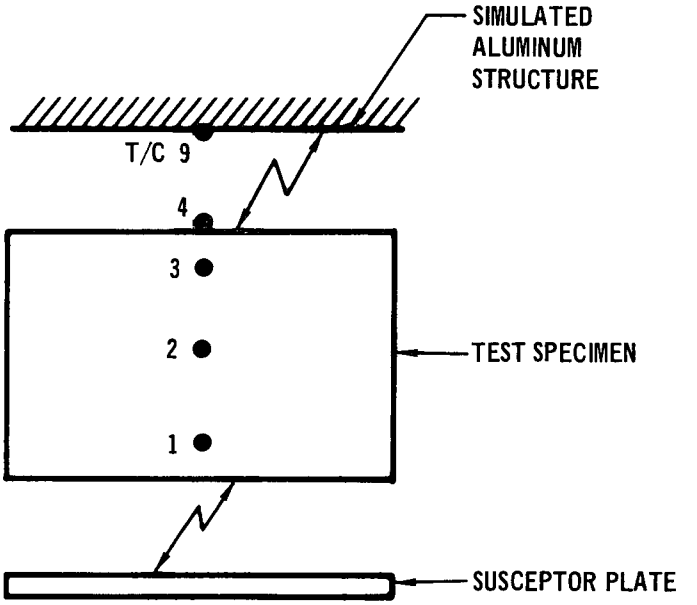

THERMAL CYCLE NO.	T/C 1 °F (MIN)	T/C 2 °F (MIN)	T/C 3 °F (MIN)	T/C 4 °F (MIN)	T/C 9 °F (MIN)
2	1590 (14)	1140 (28)	695 (30)	502 (30)	270 (32)
5	1620 (14)	1190 (30)	740 (32)	530 (30)	333 (32)
10	1620 (14)	1195 (30)	750 (31)	534 (30)	342 (32)
11	1270 (26)	1030 (31)	700 (32)	488 (30)	312 (32)
20	1280 (27)	1100 (30)	840 (31)	686 (23)	526 (32)
21	1140 (29)	970 (32)	680 (32)	495 (30)	330 (32)
30	1130 (30)	980 (32)	680 (32)	496 (30)	340 (32)
31	1020 (31)	960 (32)	540 (32)	398 (32)	275 (32)
40	1190 (30)	940 (32)	630 (32)	466 (32)	324 (32)

MICROQUARTZ FLIGHT CONFIGURATION TEST SPECIMEN

Peak Temperature and Time When Peak Occurred

457-3156

Figure 100

determining apparent thermal conductivity and degradation of insulation properties could not be conducted. The movement of thermocouple positions may have been caused by acoustic tests, foil package expansion during thermal testing, handling of the test specimen between tests or a combination of these conditions.

An occurrence that is consistent with TD NiCr Package/Microquartz Insulation test specimen during the tests was that the cold face thermocouple 4 (located on the back side of the foil package) recorded a higher temperature than did thermocouple 3 (located within the insulation close to the foil cold face) until both thermocouples reached approximately 300°F whereupon the condition reversed for the rest of the test. This occurrence can be attributed to the heat leak around the foil package, also the foil back face and cold side of the insulation are not in contact with each other. Therefore, at temperatures lower than 300°F conduction through the foil package is the predominant heat transfer mechanism; whereupon at temperatures higher than 300°F radiation exchange between the insulation and the foil package back face becomes the predominant heat transfer mechanism.

3.8 Emittance of Metal Foil Package Materials - To provide information necessary for the thermal analysis, the emittance was measured using specimens from previously cycled packages. A Gier-Dunkle DB-100 Emissometer was used to measure the total normal emittance at room temperature. The information shown in Figure 101 includes data for both internal and external faces of the hot and cold surfaces.

The measured emittance values are essentially what would be expected, considering their service exposure, with one exception. The internal face of the hot surface of the Inconel 702 package which contained the Astroquartz flight configuration specimen is much lower than other Inconel 702 specimens. No specific reason is known for this difference, nor is there any indication that the insulation (Astroquartz) contributed to the difference.

3.9 Salt Spray Resistance - To determine if the packaged insulations are susceptible to corrosion or other chemical attack from air-entrained salt spray environment, followed by high temperature exposure, a number of small packages were made incorporating various metal foil and insulation combinations. The specific combinations used were:

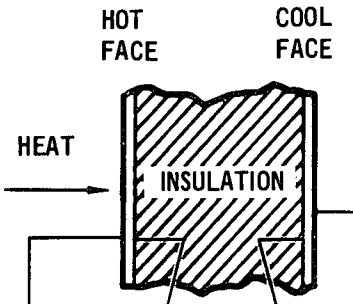

MATERIAL	THERMAL HISTORY (°F)	CYCLES	EMITTANCE			
TD-NiCr (DYNAFLEX)	2200	100	0.46	0.43	0.124	0.125
COATED Cb	2500	50	0.73	0.785	-	-
INCONEL 601 (DYNAFLEX)			-	-	0.2 → 0.115	0.195
TITANIUM (FB-1)	1000	80	0.18	0.175	0.130	0.125
INCONEL 702 (ASTROQUARTZ)	2000	40	0.505	0.275	0.130	0.130
INCONEL 702 REFRASIL A-100/FB-1	2000	20	0.46	0.585	0.140	0.140
INCONEL 702 MICROQUARTZ/FB-1	2000	20	0.53	0.625	0.135	0.130
ALUMINUM PLATE		100	0.11-0.24			

457-3157

TOTAL NORMAL EMITTANCE OF METAL FOILS AFTER SIMULATED SHUTTLE SERVICE

Figure 101

	Inconel 702 3 Mil	TD-NiCr 3 Mil	Titanium A-70 2.5 Mil
Astroquartz	X	X	
Microquartz	X	X	
Refrasil A-100	X	X	
Dynaflex	X	X	
Min-K 2000	X	X	
Fiberglas FB-1			X

Additional specimens, scheduled to be made of Hastelloy X, were discarded

after exposure to 2000°F, when it was found that titanium had been inadvertently substituted for the Hastelloy X.

It was estimated that a layer of salt 0.00006 in. thick would be deposited in a one year exposure in Florida, but ten times this amount is normally used to account for estimation errors and differences in location. A salt settling chamber was used for the deposition. A 7% synthetic sea salt water (ASTM D-1141-52) was sprayed into a 120°F chamber for 15 minutes, followed by a one hour period during which the salt settled out on the specimens. A total of 27 such cycles were required to produce a salt layer 0.0006 in. thick on the exposed face of the specimens. Vent holes were provided to allow infiltration of the salt into the insulation.

After the deposition was complete, the 4" x 4" x 1" specimens were placed into a furnace at 2000°F (1000°F for the titanium/fiberglass specimen) for 30 minutes. After the initial thermal exposure, one side (1" x 4") of each specimen package was additionally coated with 0.0006 in. layer of salt, and the thermal exposure repeated.

The Inconel 702 showed typical oxidation discoloration under a flaky layer of salt encrustation, with no apparent corrosion of the metal. However, after the second thermal exposure, the areas exposed directly to salt became embrittled and very weak. Areas not directly exposed were degraded to a lesser extent. The TD-NiCr was relatively unaffected in the same exposure, remaining strong and flexible. It also had a heavy layer of salt encrustation, and like the Inconel 702, the salt layer had a green coloration, indicating some diffusion of nickel or chromium. The titanium foil was unaffected by the salt exposure and subsequent heating to 1000°F.

The "cool side" of these packages which had not been directly exposed to the salt, but which had minor accumulations due to the atmosphere in the salt deposition chamber, showed much lower levels of corrosion. The insulations within the packages did not show any appreciable deterioration due to salt infiltration. Condition of the insulation was essentially that expected due to heating alone.

Photographs of the test specimens after the second thermal exposure are shown in Figures 102-106.

3.10 Guarded Hot Plate Thermal Conductivity Tests

There has been a general lack of thermal conductivity data at reduced pressures for most of the insulations of interest. Because the shuttle orbiter reentry heat pulse will occur mainly at high altitudes and low ambient pressures such data would

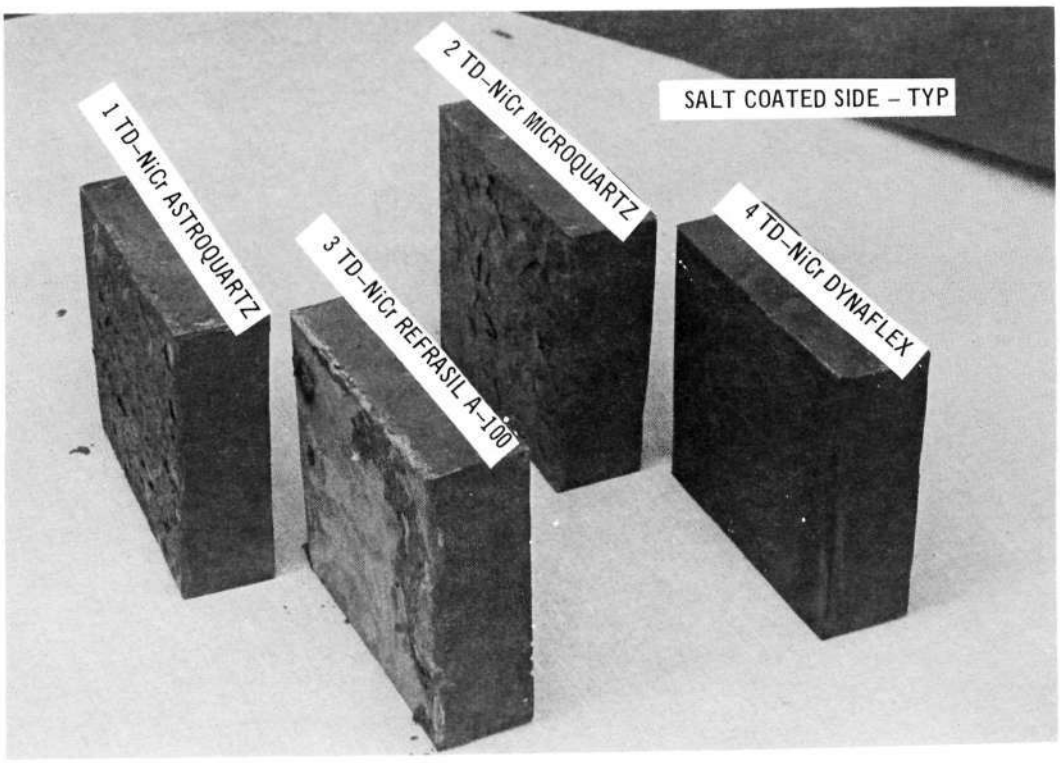

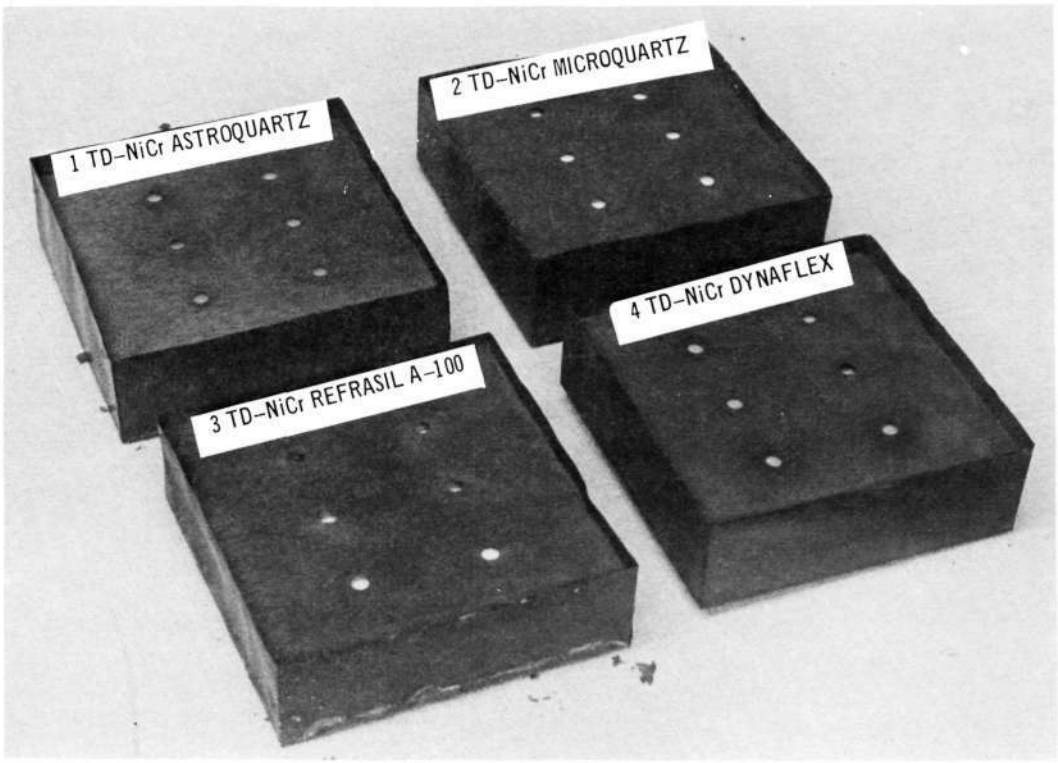

TD–NiCr PACKAGES CONTAINING VARIOUS INSULATIONS –
AFTER SALT SPRAY AND TWO THERMAL EXPOSURES

457–3158

Figure 102

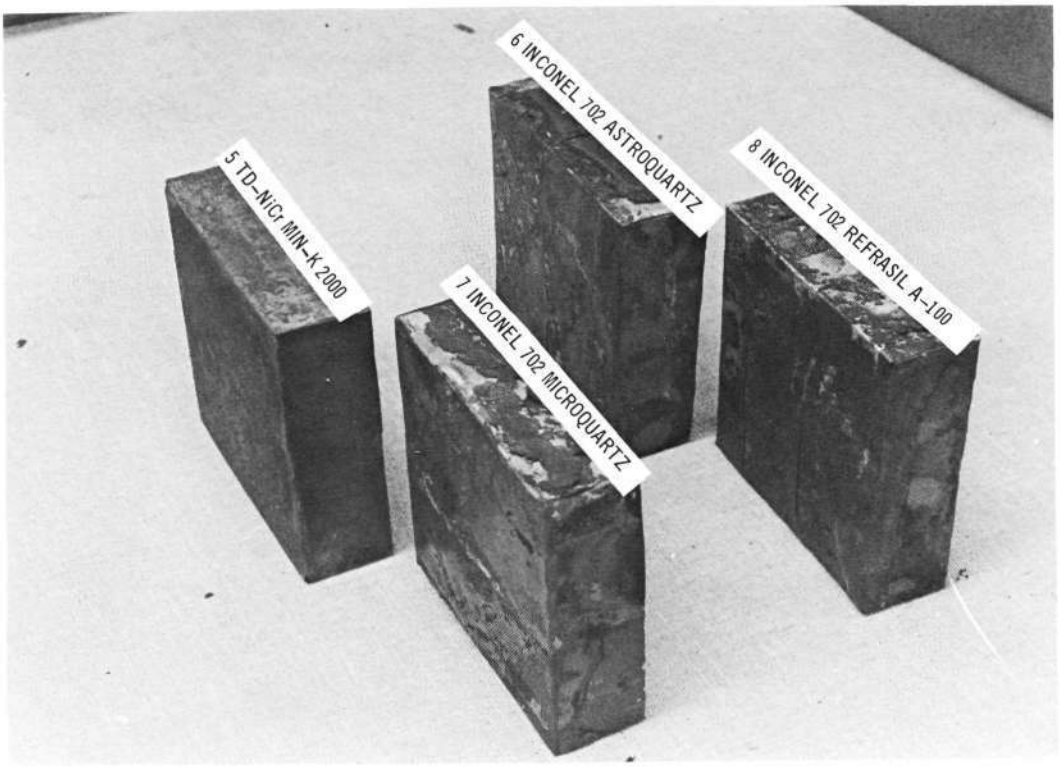

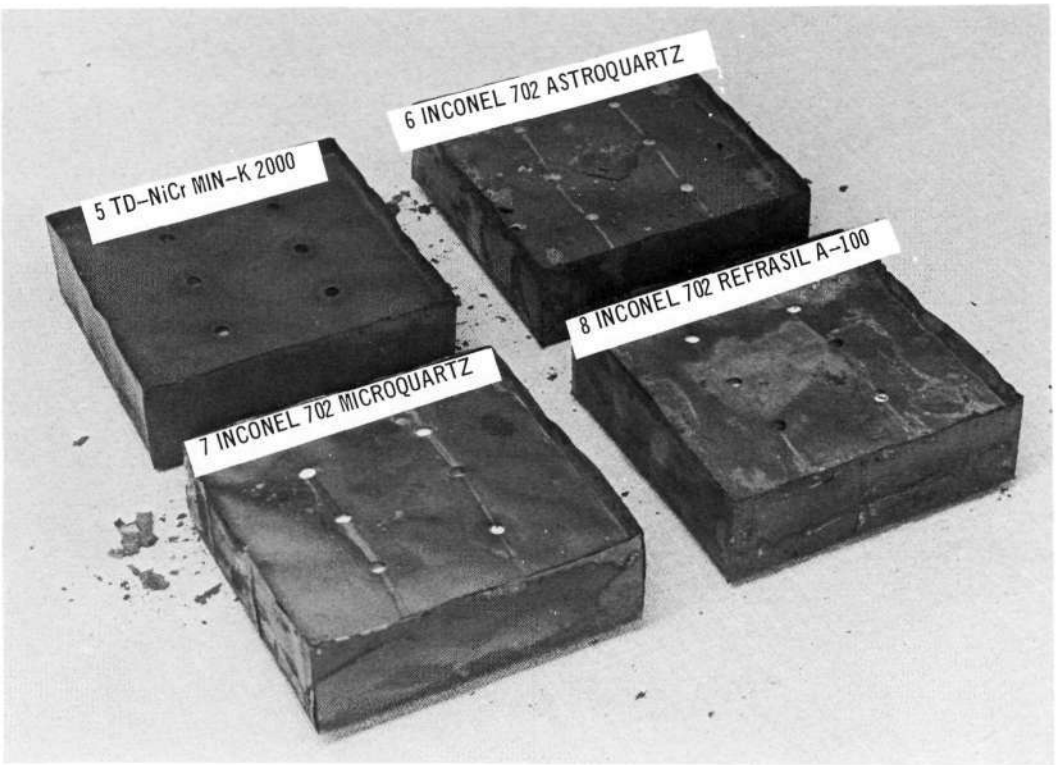

TD-NiCr AND INCONEL 702 PACKAGES CONTAINING VARIOUS INSULATIONS – AFTER SALT SPRAY AND TWO THERMAL EXPOSURES

457-3159

Figure 103

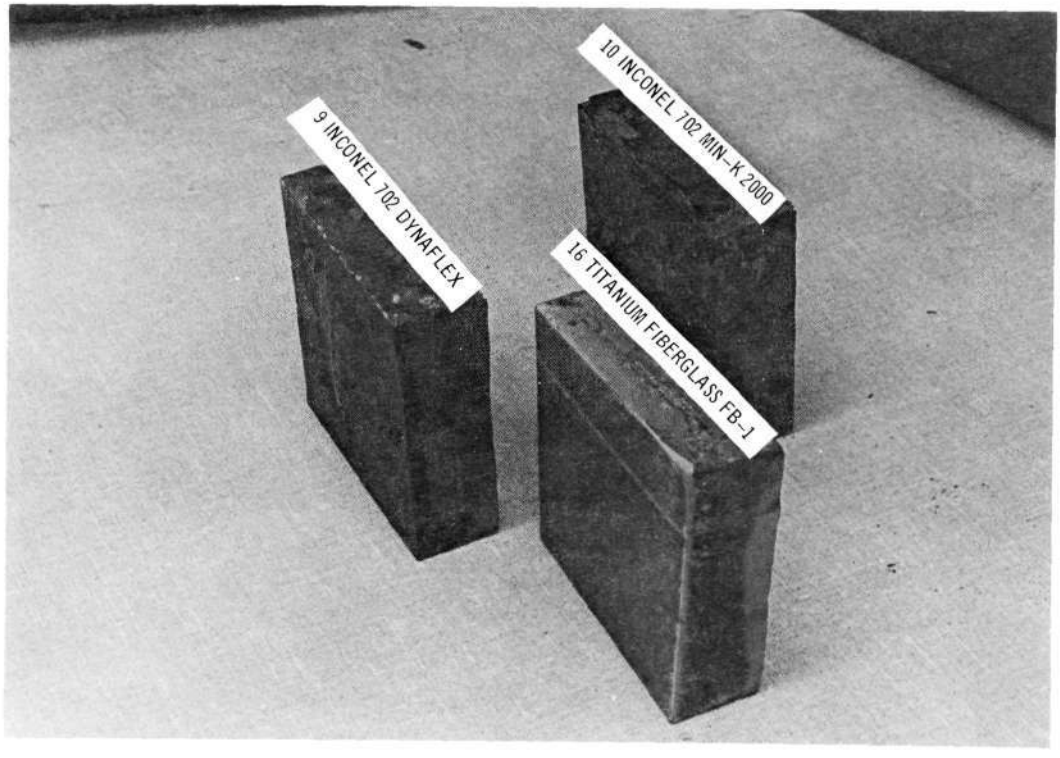

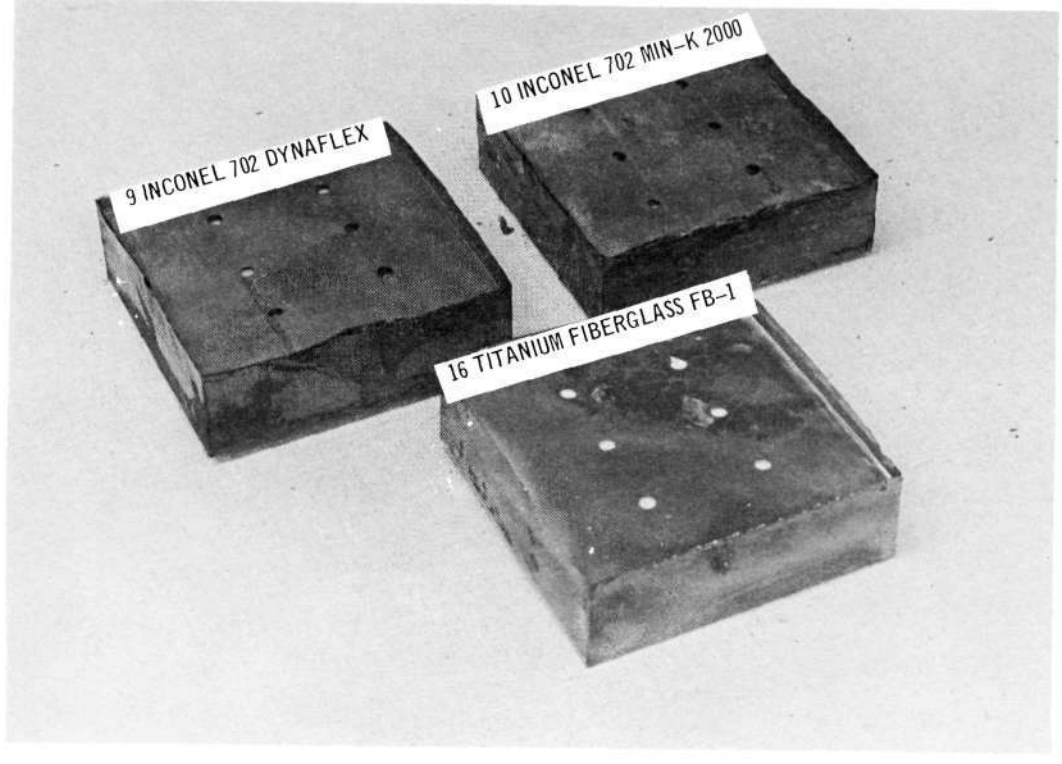

457-3160

INCONEL 702 AND TITANIUM PACKAGES CONTAINING VARIOUS INSULATIONS – AFTER SALT SPRAY AND TWO THERMAL CYCLES

Figure 104

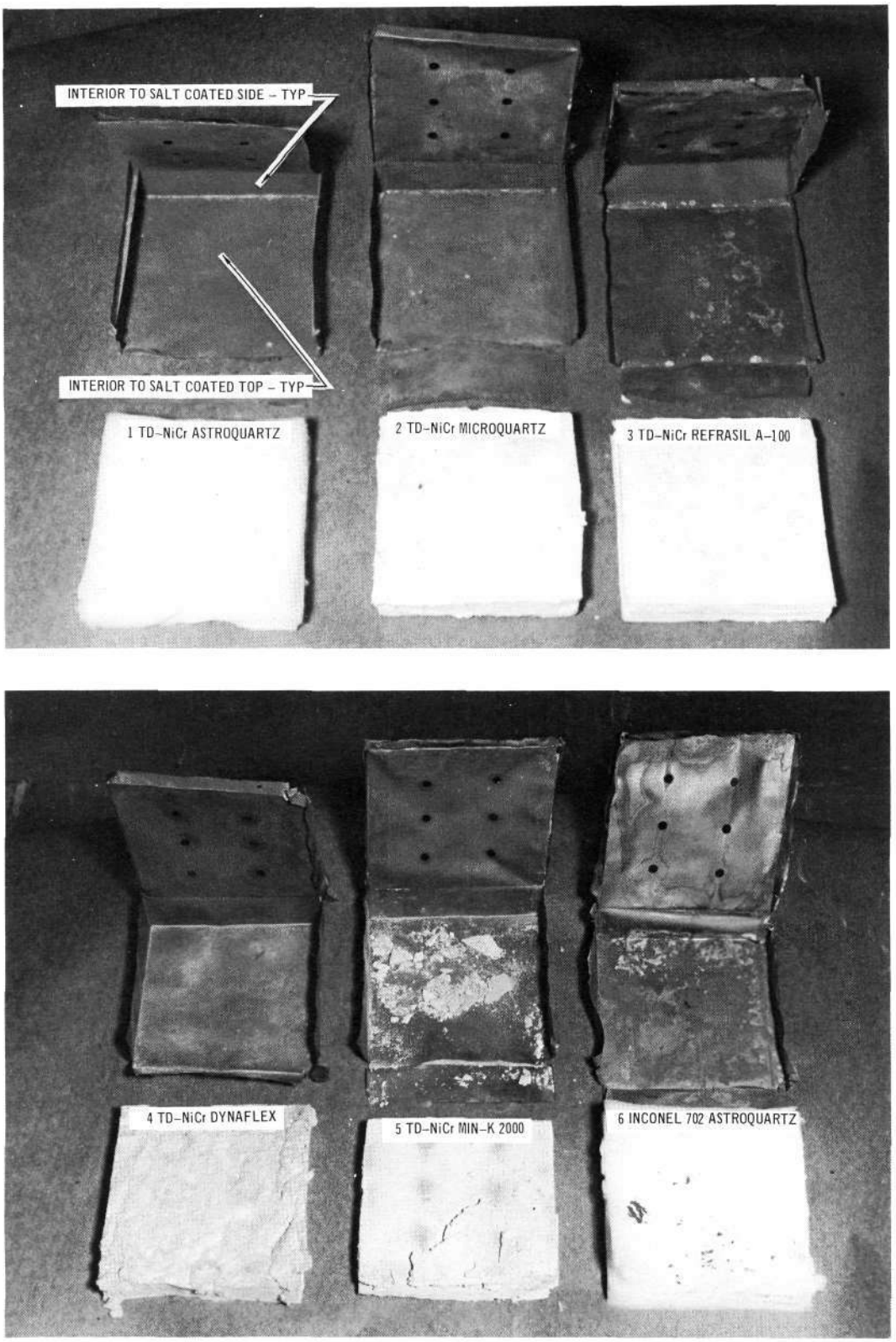

INSULATION AND INTERIOR OF METAL PACKAGES AFTER SALT SPRAY AND TWO THERMAL EXPOSURES

457-3161

Figure 105

Figure 106

INSULATION AND INTERIOR OF METAL PACKAGES AFTER SALT SPRAY AND TWO THERMAL EXPOSURES

457-3162

be needed for accurate sizing of the insulation. While a technique is available for estimating the effects of gas pressure on conductivity (Reference 7), it is primarily applicable to fibrous felts. It can also be applied to materials containing bulk fillers if some low pressure data is available. However, experimentally determined data is always preferable.

To provide such data, guarded hot plate thermal conductivity tests were run on a number of insulations, which might be used in shuttle service, in air at pressures ranging from 1 atmosphere to 1 torr and temperatures from 400 to 1600°F. The equipment used conformed to ASTM C-177. The tests were run on Astroquartz (1.1 lb/ft^3), Refrasil A-100 (7.3 lb/ft^3), Irish Refrasil B-1576-1 (4.8 lb/ft^3), SKX-Fiberfrax blanket (7.5 lb/ft^3), and two experimental HCF reuseable surface insulations. The experimental HCF's included one made with SKX fiber (1.6μ $Al_2O_3 \cdot SiO_2$) in place of the coarser mullite fibers, and one in which a fiber blend of mullite and fine diameter silica fibers was used. The latter composition (Mod V HCF) also did not include the coarse silica filler normally used in the HCF formulation.

The test results are shown in Table VII and Figures 107-112. A surprise was the very high conductivity of Astroquartz Mat. While a high conductivity had been anticipated for this material, due to its very low density, the results were still higher than expected. However, the high results were confirmed by calculating the radiation contribution to thermal conductivity as described in Section 5.3. This value was estimated from the infra-red back scattering coefficient using a representative temperature difference across the test specimen corresponding to the highest mean temperature at the lowest pressure employed in the guarded hot plate test. This value is shown on the graph for comparison. The meaning of this value is that the total thermal conductivity at any given mean temperature can never be lower than the radiation component, no matter how low the ambient air pressure. Similar points were also calculated for other materials for which back scattering data was available.

Table VII

THERMAL CONDUCTIVITY DATA FOR SEVERAL CANDIDATE INSULATIONS FOR SPACE SHUTTLE

MATERIAL	VENDOR	DENSITY (LB/FT^3)	ΔT (^{0}F)	PRESSURE (TORR)	MEAN TEMPERATURE (^{0}F)	k BTU IN. / HR-FT^2-^{0}F
ASTROQUARTZ	J.P. STEVENS & CO.	1.1	80	745	285	0.84
			101	97	299	0.66
			114	10	305	0.55
			101	745	679	2.00
			122	100	707	1.75
			128	10	709	1.56
			152	1	780	1.38
			157	0.2	837	1.34
			102	750	1074	3.48
			110	100	1083	3.16
			125	10	1092	2.92
			127	1	1101	2.73
			133	0.2	1137	2.68
			90	750	1415	6.24
			104	100	1410	5.84
			100	10	1415	5.58
			103	1	1421	5.36
			100	0.2	1424	5.22
REFRASIL A-100	HITCO	7.3	175	755	370	0.43
			185	100	383	0.39
			230	10	417	0.31
			350	1	542	0.24
			150	750	720	0.66
			170	100	730	0.59
			235	10	770	0.43
			385	1	850	0.27
			145	740	1124	0.92
			180	100	1141	0.78
			265	10	1185	0.53
			385	1	1254	0.35
			155	740	1428	1.11
			180	100	1444	0.97
			255	13	1483	0.69
			355	1	1532	0.50
IRISH REFRASIL B1576	HITCO	4.8	115	740	316	0.64
			130	102	419	0.57
			140	10	455	0.53
			190	1	479	0.39
			135	755	673	0.88
			150	100	680	0.81
			174	10	716	0.69
			200	1	760	0.60

457-3163

Table VII

THERMAL CONDUCTIVITY DATA FOR SEVERAL CANDIDATE INSULATIONS FOR SPACE SHUTTLE (Continued)

MATERIAL	VENDOR	DENSITY (LB/FT^3)	ΔT (^oF)	PRESSURE (TORR)	MEAN TEMPERATURE (^oF)	k $\frac{BTU\ IN.}{HR\text{-}FT^2\text{-}^oF}$
IRISH REFRASIL B1576 (Continued)	HITCO	4.8	150	745	1071	1.47
			160	100	1080	1.35
			195	10	1104	1.12
			210	1	1168	1.05
			150	740	1556	2.29
			155	100	1562	2.15
			180	11	1575	1.87
			205	1	1633	1.64
SKX FIBERFRAX	CARBORUNDUM	7.5	160	750	407	0.46
			170	102	416	0.43
			220	10	482	0.33
			320	1	548	0.22
			170	750	734	0.60
			200	100	755	0.54
			250	10	777	0.41
			355	1	836	0.29
			185	750	1151	0.92
			210	100	1166	0.82
			275	10	1203	0.63
			405	1	1275	0.42
			145	750	1490	1.52
			160	99	1498	1.40
			230	10	1541	0.95
			335	1	1600	0.64
SKX HCF	MDC	18.1	185	750	540	0.47
			203	100	560	0.42
			259	10	575	0.33
			290	1	550	0.28
			233	750	822	0.60
			257	100	820	0.55
			351	10	860	0.39
			381	1	875	0.35
			263	745	1046	0.71
			440	10	1228	0.43
			473	1	1250	0.39
			261	750	1527	0.99
			325	100	1570	0.85
			507	1	1632	0.50

457-3164

Table VII

THERMAL CONDUCTIVITY DATA FOR SEVERAL CANDIDATE INSULATIONS FOR SPACE SHUTTLE (Continued)

MATERIAL	VENDOR	DENSITY (LB/FT^3)	ΔT (^{0}F)	PRESSURE (TORR)	MEAN TEMPERATURE (^{0}F)	k BTU IN. / HR-FT^2-^{0}F
MOD 5 HCF	MDC	15.5	155	740	428	0.61
			155	100	438	0.58
			175	10	468	0.49
			155	740	761	0.75
			165	100	768	0.71
			205	10	790	0.58
			160	740	1109	1.07
			180	100	1124	0.98
			255	10	1160	0.70
			170	740	1451	1.39
			190	100	1470	1.26
			250	10	1502	0.95

457-3165

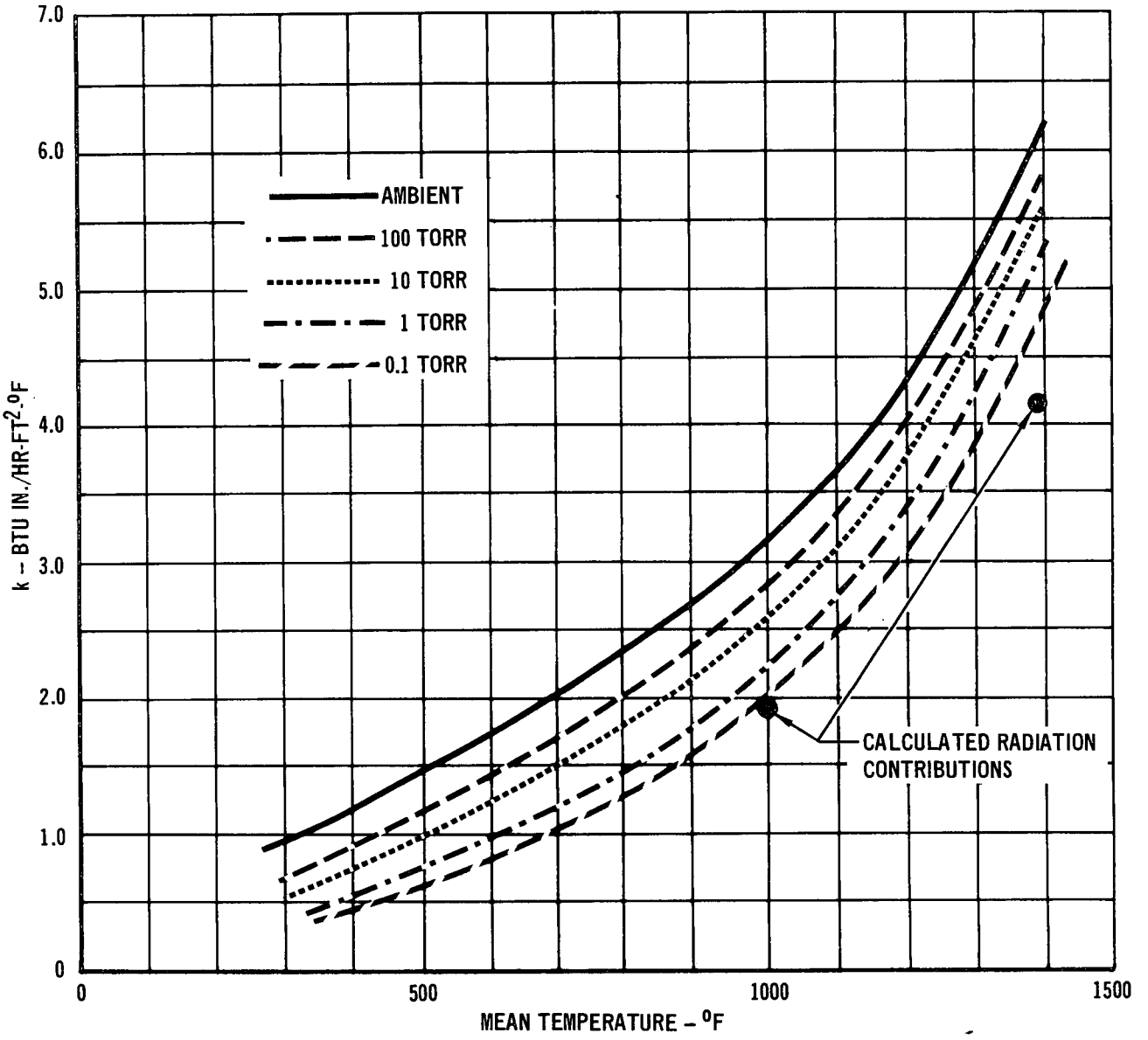

THERMAL CONDUCTIVITY OF ASTROQUARTZ AS A FUNCTION OF TEMPERATURE AND PRESSURE

$\rho = 1.1$ LB/FT^3

Figure 107

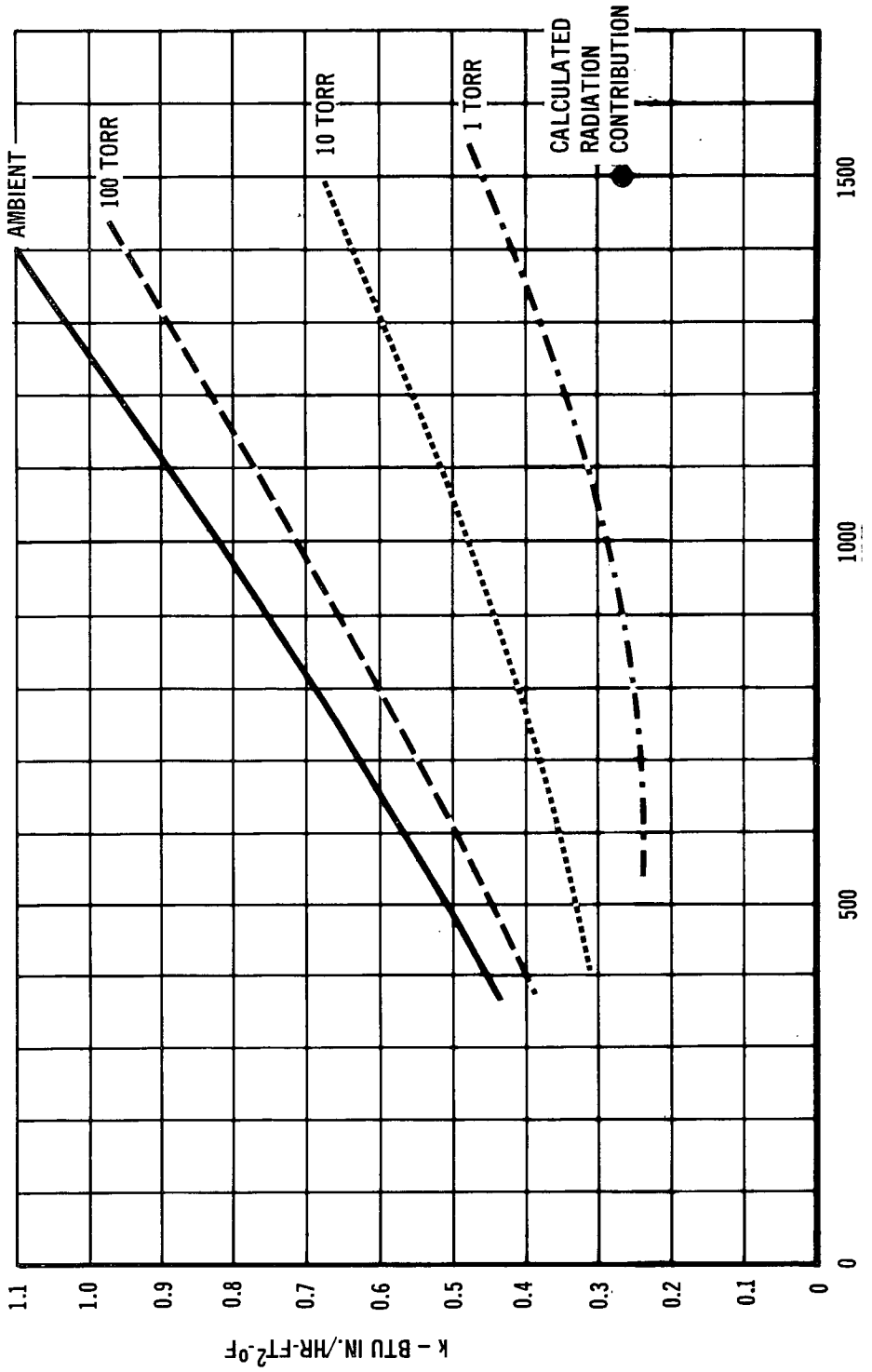

THERMAL CONDUCTIVITY OF REFRASIL A–100 AS A FUNCTION OF TEMPERATURE AND PRESSURE
ρ = 7.3 LB/FT^3

457–3167

Figure 108

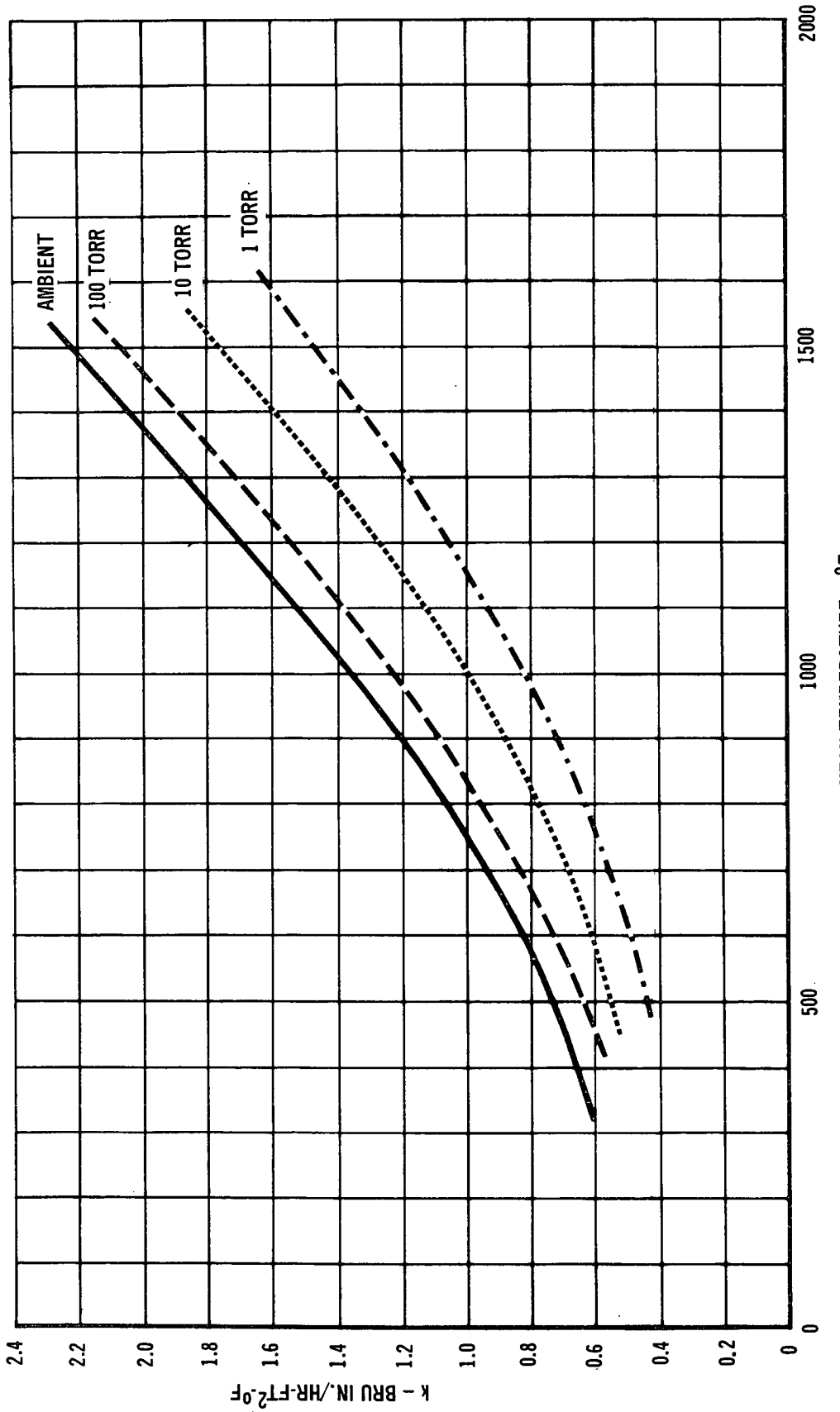

THERMAL CONDUCTIVITY OF IRISH REFRASIL B 1576 AS A FUNCTION OF TEMPERATURE AND PRESSURE

ρ = 4.8 LB/FT^3

457-3168

Figure 109

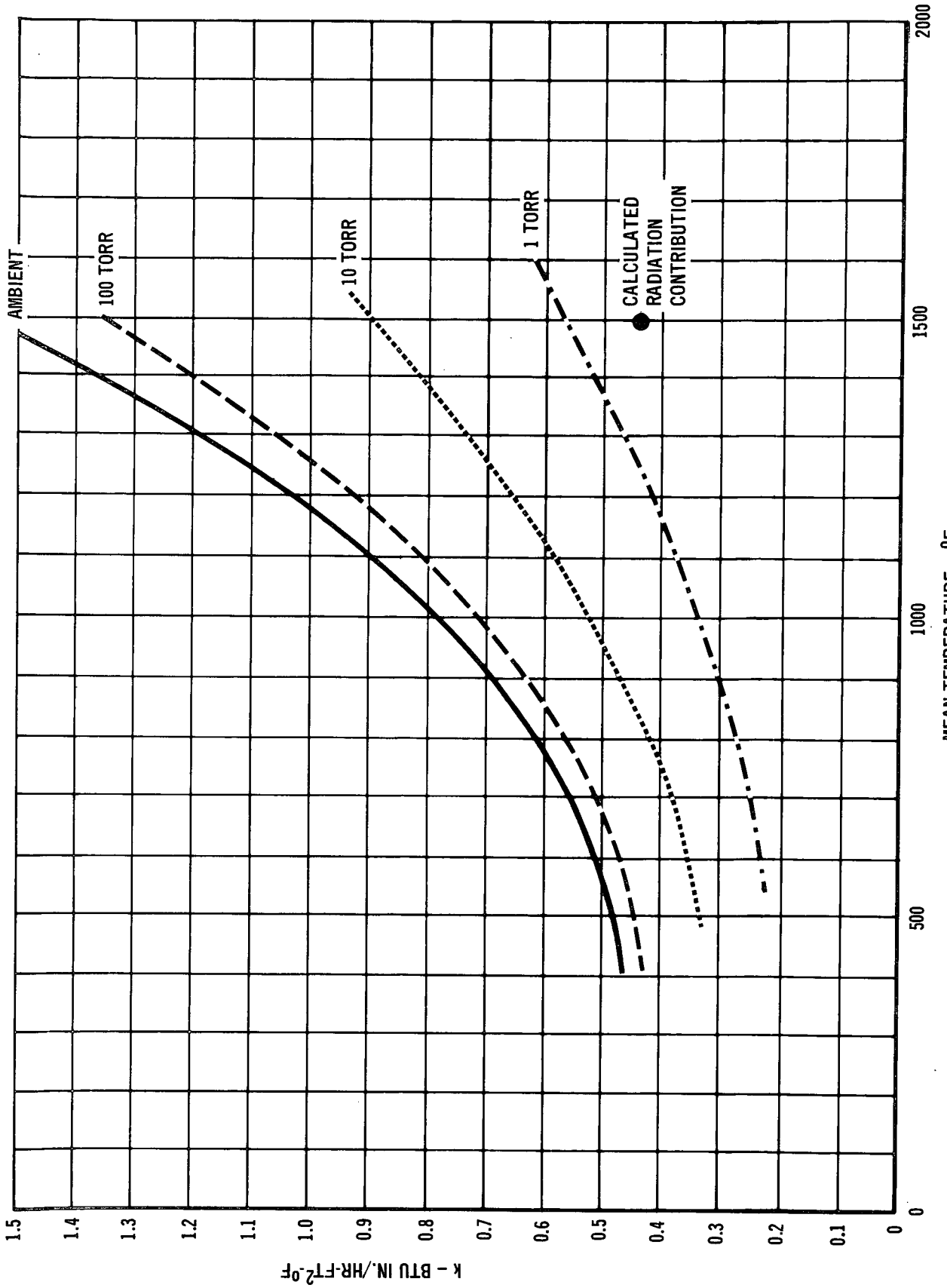
AMBIENT
100 TORR
10 TORR
1 TORR
CALCULATED
RADIATION
CONTRIBUTION
k - BTU IN./HR-FT²-°F
MEAN TEMPERATURE - °F
0
500
1000
1500
2000
0.1
0.2
0.3
0.4
0.5
0.6
0.7
0.8
0.9
1.0
1.1
1.2
1.3
1.4
1.5
THERMAL CONDUCTIVITY OF SKX FIBERFRAX AS A FUNCTION OF TEMPERATURE AND PRESSURE
ρ = 7.5 LB/FT³
457-3169

Figure 110

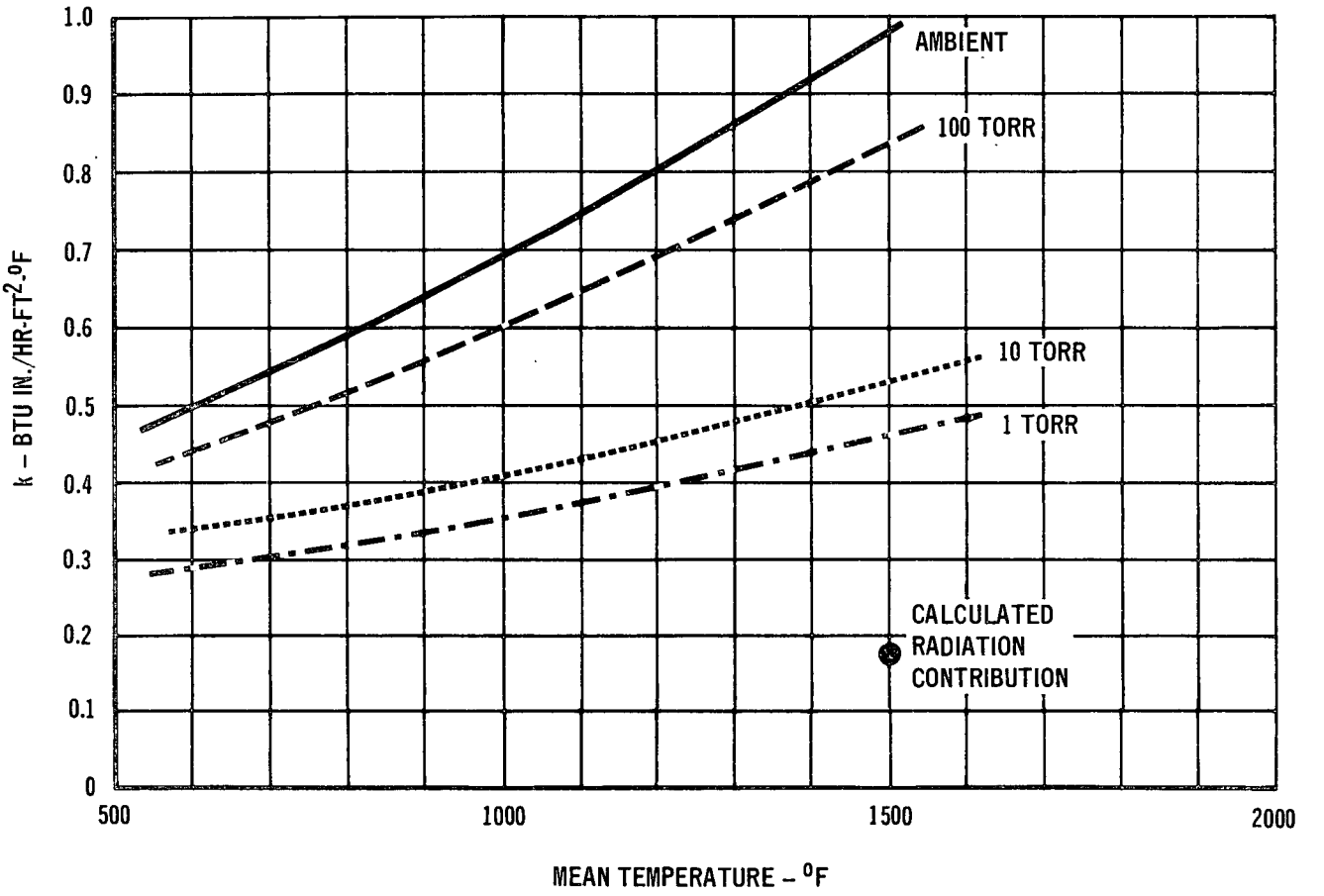

THERMAL CONDUCTIVITY OF SKX–HCF AS A FUNCTION OF TEMPERATURE AND PRESSURE
ρ = 18.1 LB/FT^3

457-3170

Figure 111

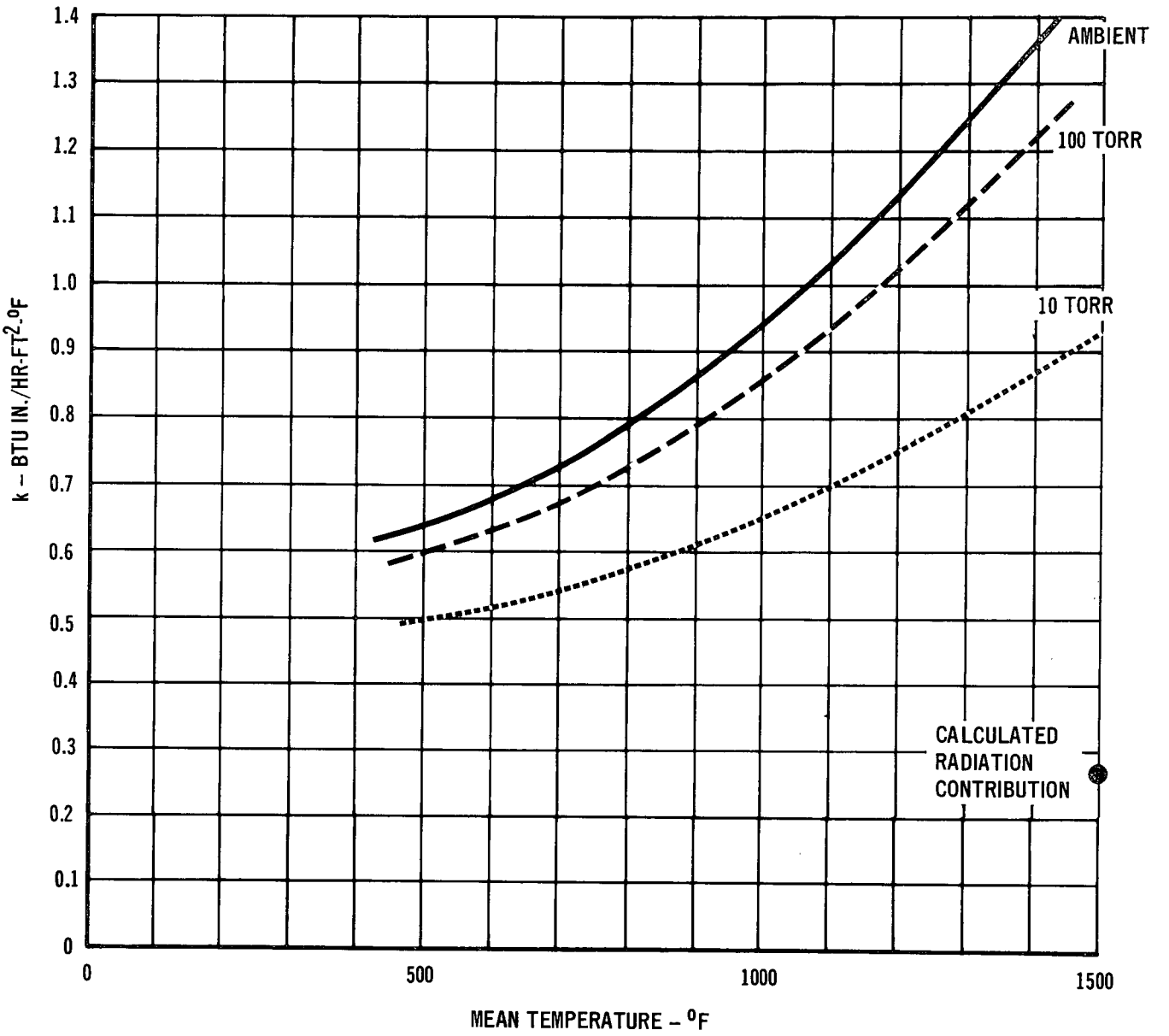

THERMAL CONDUCTIVITY OF MOD 5 HCF AS
A FUNCTION OF TEMPERATURE AND PRESSURE
ρ = 15.5 LB/FT^2

457-3171

Figure 112

4.0 HCF CONDUCTIVITY REDUCTION

The development of a reusable surface insulation for shuttle has taken two principal directions in the past, both with inherent advantages and disadvantages. One approach has employed fine diameter silica fibers which have provided good thermal conductance values, but which suffer from potential phase transformations and maximum temperature limitations. The other approach has employed mullite fibers, which provide a higher temperature capability, though at a sacrifice in thermal performance. In addition, service performance tests with mullite based material have not agreed with predictions based on measured thermal conductivity values. One of the objectives of this program was to explore means of reducing the thermal conductivity of mullite-based reusable surface insulation, using the MDAC-E HCF material as baseline. The reason mullite based materials have a higher thermal conductivity than silica based materials was believed to be high infrared transmission, due to lack of scattering by the comparatively coarse mullite fibers and/or the lack of opacity in the composition.

Our approach to this study was to determine the effects of additives to the base composition to reduce the I-R transmission, and which led to the initiation of I-R transmission studies. The latter work produced a significant amount of new and important data which is reported in Section 5.0; however, some data from that work is also reported in this section.

4.1 HCF Composition Modifications - The principal approach in reducing HCF thermal conductivity was to reduce the infra-red radiation component of the conductance mechanism. This can be accomplished by increasing internal scattering or absorption of radiant energy by adding opacifiers, or by using finer diameter fibers and fillers. Both techniques were employed. Initially HCF was made with 6μ diameter mullite fibers, and currently the standard HCF uses a 4.7μ mullite fiber. A 4μ mullite has also been made in very small quantities, and very recently a mullite fiber of about 2.5μ diameter has been made experimentally. However, neither of the latter two fibers has been available in sufficient quantity to afford anything more than exploratory work.

Another fiber approach was to blend mullite with fine diameter fibers such as Microquartz, Refrasil A-100 (1.3 micron diameter), or Fiberfrax SKX (1.6 micron). However, this approach might also degrade the high temperature capability of the HCF. Use of fiber blends was explored and resulted in some fabrication problems. Use of the intermediate diameter mullite fibers (4.7 microns) however, presented no problems and was investigated the fullest.

4.1.1 Torch Screening Tests - A number of HCF specimens were prepared incorporating various opacifiers at the 1%, 3% and 6% levels and evaluated by torch testing. The opacifiers used are shown in Table VIII. These specimens were all of approximately the same density (14.5 pcf) and were tested at essentially constant surface density (0.90 psf), though this was subject to some variation as surface density was measured in the as-coated condition. All specimens were coated to avoid differences in radiation cooling and provide similar hot surface temperatures. The torch test was conducted by pivoting an oxy-acetylene torch into a predetermined position to impinge on the coated surface of the specimen at a right angle, and to provide a 2250°F hot surface. The specimens were mounted in a reinforced plastic holder with the specimen hot surface flush with the end of the holder. Three 36 ga, type K, thermocouples were attached to the cool surface of the specimen which was bonded to a glass honeycomb support plate. Evaluation criterion was the time required for the cool face to be heated to 480°F.

Results of the torch test are shown in Table VIII. The greatest improvement over the control specimens (no opacifier) was provided by additions of either Co_3O_4, $ZrSiO_4$, and ZrO_2. It had been expected that there would be a trend of improvement with increasing opacifier content, but this was generally not true. This may have been a result of varying thickness or density of the test specimens. Some opacifiers such as carbon black, BN, and SiC were eliminated at this stage as their improvement was considered not sufficient to overcome potential problems in oxidation resistance.

Seven of the specimens used in the torch test were mounted in front of the columbium radiant heater (the same heater used for packaged insulation testing) and exposed to the initial heat up cycle (programmed heating to achieve 2200°F in 300 seconds). Results were comparable to those obtained in the torch test, as shown by the data below.

Specimen	Opacifier	Torch Test Time to 480°F - Sec.	Radiant Panel Test Time to 500°F - Sec.
23-1	None (control)	185	526
-2	None (control)	183	526
23-10	3% TiO_2	175	526
-11	6% TiO_2	204	543
23-12	1% Co_3O_4	214	565
-13	3% Co_3O_4	222	559
27-4	1% $ZrSiO_4$	236	577

Table VIII

TORCH TEST RESULTS
OPACIFIED HCF

SPECIMEN NO.	OPACIFIER	THICKNESS* IN.	TIME FOR COOL SURFACE TO REACH 480°F SEC	
23-1	NONE (CONTROL)	0.742	185	200
-2	NONE (CONTROL)	0.760	183	171
23-3	1% ZrO_2	0.821	224	217
-4	3% ZrO_2	0.794	218	162
-5	6% ZrO_2	0.774	195	207
23-6	1% NiO	0.806	188	
-7	3% NiO	0.748	205	
-8	6% NiO	0.716	172	
23-9	1% TiO_2	0.764	187	
-10	3% TiO_2	0.730	175	
-11	6% TiO_2	0.758	204	
23-12	1% Co_3O_4	0.779	214	
-13	3% Co_3O_4	0.760	222	
-14	6% Co_3O_4	0.703	197	
27-1	1% BN	0.813	219	
-2	3% BN	0.823	188	
-3	6% BN	0.766	200	
27-4	1% $ZrSiO_4$	0.842	236	
-5	3% $ZrSiO_4$	0.837	227	
-6	6% $ZrSiO_4$	0.780	194	
27-7	1% C	0.835	210	
-8	3% C	0.848	227	
-9	6% C	0.790	190	
27-10	1% Cr_2O_3	0.840	202	
-11	3% Cr_2O_3	0.816	216	
-12	6% Cr_2O_3	0.796	203	
27-13	1% SiC	0.841	236	
-14	3% SiC	0.826	194	
-15	6% SiC	0.818	207	
27-16	1% PKT**	0.750	168	
-17	3% PKT	0.809	218	
-18	6% PKT	0.791	206	
27-19	1% SnO	0.844	217	
-20	3% SnO	0.809	208	
-21	6% SnO	0.812	177	

* SURFACE DENSITY APPROXIMATELY 0.90 LB/FT^2
** PIGMENT GRADE-POTASSIUM TITANATE

457-1844

These specific specimens were selected to compare basic HCF (no opacifier) with the Mod I variation (3% TiO_2) with candidate opacifiers. These results indicated that the use of 3% TiO_2 opacifier may not make a significant improvement over unopacified HCF. This result is contrary to earlier results in another program which lead to the adoption of the Mod I formulation. Because of these anomalous results, further tests included the TiO_2 opacified HCF. Cobalt oxide was eliminated as a candidate because of its potential to act as a fluxing agent at elevated temperatures. Zircon, because of its effectiveness and relative inertness, appeared to be the best overall candidate.

Additional testing was conducted on compositions containing the intermediate diameter mullite fiber (4.7 micron) in comparison with previous compositions. Surface density in this test was placed under closer control and represented insulation surface density before coating. The surface density was approximately 1.3 lb/ft^2, instead of the 0.90 lb/ft^2 used previously. The data for tests on these specimens were:

Specimen	Opacifier	Density	Suface Density	Torch Test Time for Cool Surface to Reach 480°F	Radiant Panel Test Maximum Temperature on Cool Surface
		lb/ft^3	lb/ft^2	Sec.	°F
37-4A	1% $ZrSiO_4$ (6μ fibers)	14.37	1.287	358	540
123-A	3% TiO_2 (6μ fibers)	15.92	1.290	341	540
123-B	3% TiO_2 (6μ fibers)	14.93	1.300	363	520
41-1-A	1% $ZrSiO_4$ (4.7μ fibers)	14.74	1.297	436	440
41-2-A	3% $ZrSiO_4$ (4.7μ fibers)	13.87	1.301	501	410

The radiant panel test was conducted on these same specimens at 100 torr and 10 torr air pressure also, providing results in the same order as the data above. These tests indicated a significant improvement in performance with use of the 4.7μ fibers in comparison to 6μ (standard) fibers. Similar tests were also made on a group of specimens comparing combinations of 6.0μ and 4.7μ mullite fibers, silica filler and Cenosphere filler (fly-ash floaters, and essentially a mullite composition), and zircon and titania opacifiers. The results of this test again indicated the superiority of the finer diameter fiber, as well as the better performance of silica filler and zircon opacifier.

Alternate approaches examined included coating the filler material with platinum (via decomposition of a platinum resinate) and using a platinum boating beneath the water resistant/high emissivity coating. In the former case, the platinum was expected to add considerable internal reflection and scattering, and in the latter case, to reduce the emittance of the radiant energy source. Although the specimens were successfully made, these approaches provided no improvement in thermal performance.

Reduction of infra-red transmittance in HCF was also attempted through addition of finely divided nickel flakes to the HCF composition. It was expected that the high reflectivity of the flakes would significantly increase the back-scattering. An HCF specimen containing about 20% nickel flakes (-100, +325 mesh, International Nickel Co.) was formed, and fired in an inert gas atmosphere. The resulting block, however, was totally and uniformly black, indicating oxidation of the nickel. This was believed due to impurities in the argon atmosphere used in the furnace. Attempts to measure IR transmission provided no numerical results as even the thinnest slice was completely opaque to a black-body source at 1800°F. This could be due to either a very high scattering coefficient or to very high absorption, the latter more likely the case, judging by the black color in visible light. For reduced heat transfer, high absorption is not particularly desirable as the energy absorbed is also re-emitted, whereas, in scattering, the energy is not absorbed or re-emitted, but reflected or scattered back to its source.

The nickel flake specimen was tested for thermal performance in the graphite heater and found to be poorer than standard HCF, and compositions incorporating other modifications were superior. However, one unusual feature of the nickel flake composition was worthy of note: it was exceptionally strong and hard. Examination by scanning electron microscopy revealed considerable coating of the fibers and filleting at fiber intersections by the oxidized nickel. This indicated the possibility that other metal oxides formed in-situ might provide the added strength and conductivity reduction.

Following up on the lead provided by the nickel flakes, other metal additives were investigated which might provide added strength with oxidation in-situ, copied with high back-scattering of infrared. The metallic powders used are listed below along with the IR transmission test results on the specimens. All were used at the same composition level, about 6% metal, based on dry batch weight, except the nickel flake composition which was repeated at the 20% level. The nickel flake sample was fired in a vacuum furnace to avoid oxidation. This specimen had grayish

cast, indicating good success in avoiding oxidation. All of the other specimens were fired in air to intentionally form oxides. None of these derivatives had the obvious high strength that had been exhibited by the unintentional oxidation of the first nickel flake specimen, nor was there much of an improvement in back-scattering, as shown in the table below.

Metal Additive	Particle Size Microns	Back-Scattering N (1800°F) $(lb/ft^2)^{-1}$	Absorption P (1800°F) $(lb/ft^2)^{-1}$
None	--	88.9	0.2
Al	44	Not measurable	absorption high
Sn	1	98.8	0.1
Zn	1	110.8	0.1
Si	44	91.4	2.2
TiH_2	44	77.2	0.3
Zr	44	82.9	0.3
Mg	16	99.0	0.1
Ni (20%)	44	86.0	3.3

Other compositions that were tested for thermal performance in the graphite heater included alternate fibers, fiber blends and elimination of the coarse silica filler. The evaluation consisted of simultaneously exposing 3.3 inch diameter specimens of equal surface density to a programmed thermal cycle. The time required for the cool side of these specimens to reach 300°F is tabulated below, along with their corresponding scattering coefficients for comparison. The graphite heater tests were run at 5, 11, 100 and 760 torr. Data below is for the 11 torr test.

Composition	Time to Reach 300°F	Back Scattering Coefficient (N) 1800°F Source
	sec.	$(lb/ft^2)^{-1}$
Microquartz fiber, ziron opacifier, No Filler, 16.3 lb/ft^3	890	224
Mullite and silica fiber blend, ziron opacifier, No filler, 15.6 lb/ft^3	850	153
HCF Mod IIIA without filler, 15.2 lb/ft^3	840	82
Mullite, alumino-silica fiber blend, zircon opacifier, no filler, 17.2 lb/ft^3	780	--
HCF Mod IIIA, 14.5 lb/ft^3	705	84
Mullite fibers, Ni flakes, with filler, 16.9 lb/ft^3	690	--
Mullite and silica fiber blend, zircon opacifier, with filler, 16.3 lb/ft^3	680	77

The nickel flake composition shown here is the first nickel flake specimen which had oxidized in the impure argon atmosphere during firing.

The above thermal performance data should not be considered to show absolute relationships as the specimen densities varied from 14.5 to 17.2 lb/ft^3. As surface densities were held constant, thicknesses varied which introduced higher order perturbations to overall conductance.

Late in this evaluation program, many of the 3.3 in diameter specimens used in the radiant heater panel tests were instrumented with four internal thermocouples, in addition to the surface thermocouples. From the response of these thermocouples the effective thermal conductivity was extracted by means of a thermal performance analysis program. In this program an arbitrary thermal conductivity curve is used to predict the thermal response for the thermocouple midway through the specimen. The predicted response is then compared to the measured response, and the arbitrary thermal conductivity curve automatically modified, based on the results of the comparison. This process is reiterated until computed response matches measured response. Because the locations of these thermocouples can be measured with greater precision than was the case with packaged insulations, and are less subject to movement during test, this process provides relatively good results. This analysis has indicated that the effective conductivity of HCF Mod IIIA to be higher than the

value measured in guarded hot plate tests, and that the effective conductivity of the HCF made with the mullite-silica fiber blend (without filler) compares closely with the values obtained with the guarded hot plate measurement. This agrees with effects predicted from IR shine-through; with a high back scattering coefficient the infra-red component is lower and less sensitive to the temperature differences across the specimen.

4.2 Recommended Composition Changes for Low Conductivity Mullite HCF - Based on the work described in this section and the IR transmission studies described later, the following conclusions can be made on the reduction of thermal conductivity of mullite based HCF:

(a) Use of fine diameter silica fiber (1.3μ) or alumina-silica fiber (1.6μ) as a blend with the coarser varieties of mullite fiber will substantially reduce the conductivity.

(b) Use of 4μ mullite fiber would probably provide only a minor improvement over 4.7μ mullite fiber.

(c) Use of the 2.5μ mullite fiber is expected to provide a substantial reduction in conductivity without degradation of temperature limits. Availability of this fiber has been very limited to date, and only limited work has been performed with it. The sample we obtained, while purportedly 2.5μ nominal diameter, was indistinguishable in fiber diameter from Microquartz as judged by photomicrographs at 1000X.

(d) Use of selected powdered opacifiers can provide a minor improvement in thermal conductivity.

Some of the above recommendations have been incorporated in HCF. It has not been practical to incorporate all of them, in some cases due to a lack of availability of material which prevented fully characterizing the resulting product, and others are awaiting further tests to determine whether temperature capabilities will be degraded.

5.0 INFRARED TRANSMISSION STUDIES

In any form of insulation, a portion of the conductance can be attributed to radiant energy transport. Absorption, reemission and/or scattering by the constituent materials controls the radiation transport properties. An additional element of radiant heat transfer can occur when the insulation is partially transparent to infrared energy and can have serious consequences with high temperatures and large temperature differences. This is frequently referred to as shine-through, and results from lack of opaqueness and low scattering characteristics of insulation constituents at the wavelengths of interest.

In several HCF tests using radiant heat sources, the cool side temperature histories exceeded those predicted on the basis of known conductivities. This led to an assumption that shine-through was occurring and steps were initiated to reduce or eliminate it (i.e., opacifiers, greater scattering by finer diameter fibers). Also, HCF specimens were examined for direct transmission of near infrared energy.

The wavelengths of primary interest for the transmission studies are illustrated in Figure 113, where the spectral distribution of black body energy for the range of temperatures likely to be encountered by HCF is shown. It is apparent from Figure 113, that the wavelength range from about one to five microns covers the bulk of radiant heat transfer in which we are interested.

5.1 Integrating Sphere Infrared Transmissometer - Early in the present study of the infrared transmission of fibrous insulating materials, it was recognized that flux transmitted by the materials will emerge from the back surface at all angles with respect to the normal. Measurements made with detection systems which accept radiation only from a narrow angle will generate transmittance data of doubtful accuracy. The errors that can be introduced by improper collection optics are illustrated in Figure 114, which shows the spectral transmission curves obtained with a 0.05 in. thickness of Dynaquartz. The solid curve was obtained on Perkin-Elmer Model 137 prism spectrometer with a narrow field of view detector, the dashed curve was generated from an ellipsoidal mirror reflectometer. The collection angle of the prism spectrometer was less than 0.01 π steradians, while the ellispoidal mirror collected radiation over a solid angle of about π steradians. It is apparent from these curves that radiation in the 2 to 6 micron wavelength band is scattered extensively as it is transmitted through Dynaquartz, and is only detected by wide acceptance angle detectors. In contrast, the narrow angle detector measured only the radiation in a narrow band centered about 7 microns.

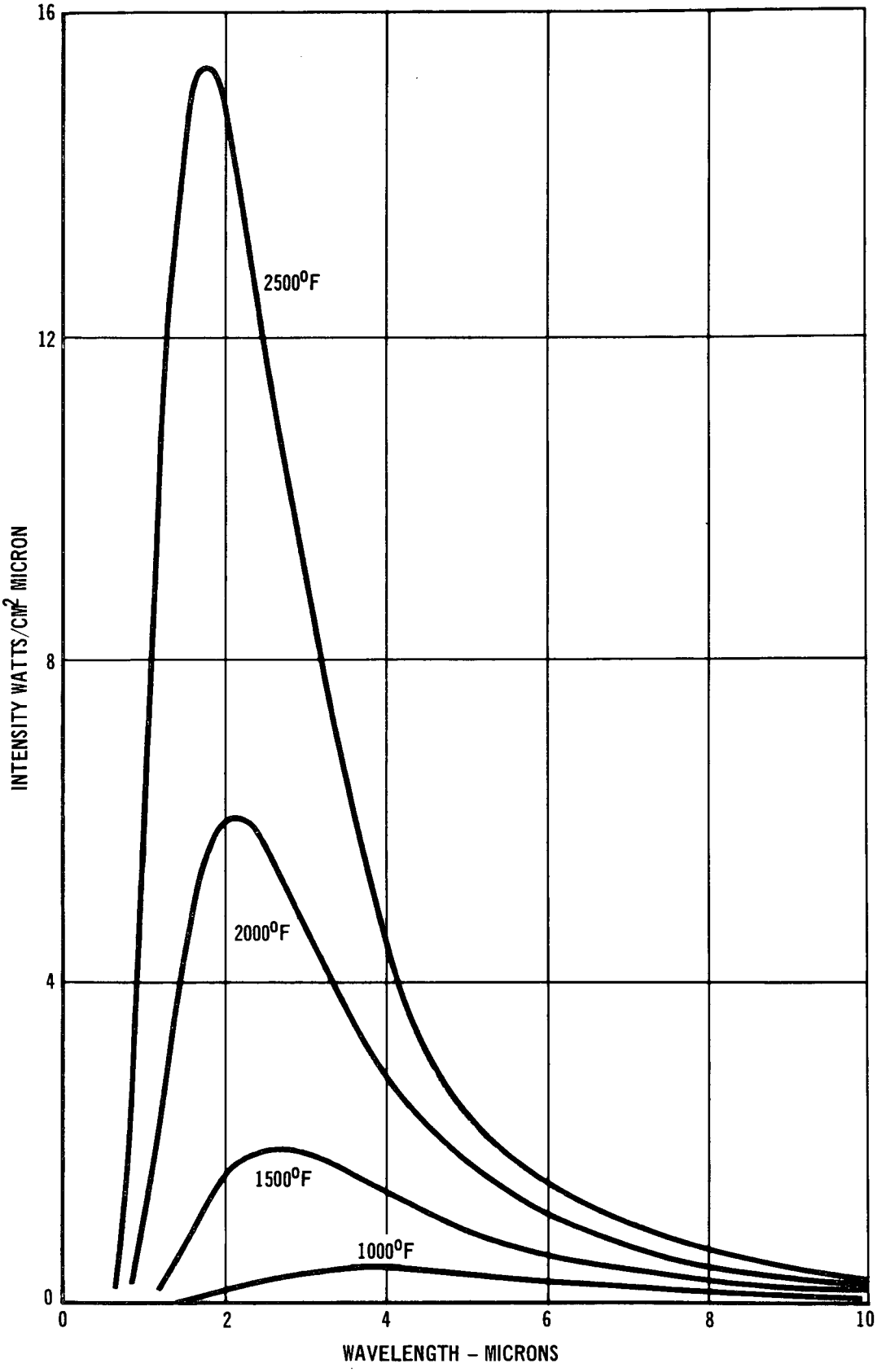

457-1840

BLACK BODY ENERGY DISTRIBUTION

Figure 113

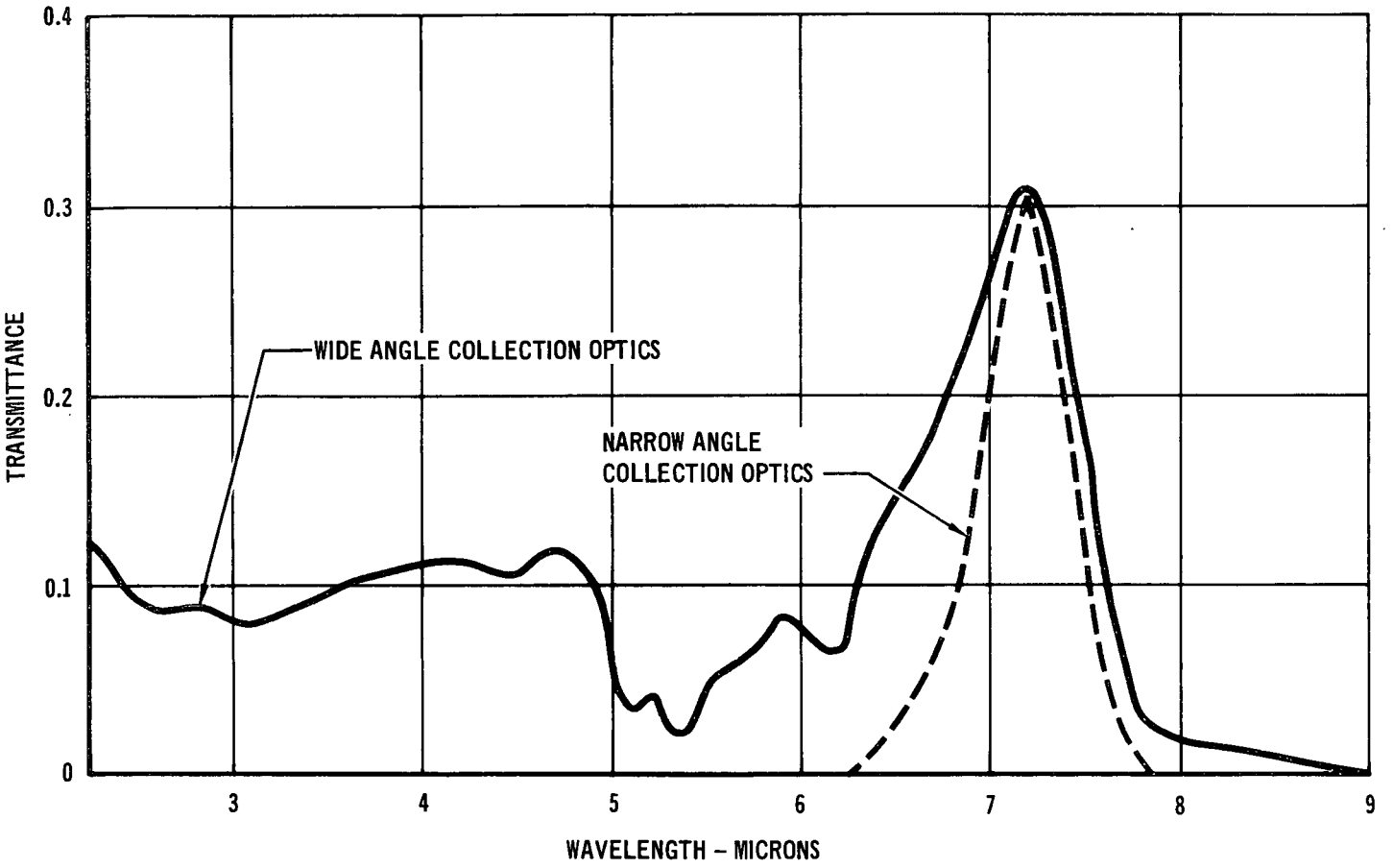

SPECTRAL TRANSMITTANCE OF DYNAQUARTZ

457-3172

Figure 114

(It should be noted that this "window" at 7 microns was observed with most silica based insulations, but not with fused silica bodies.) The significance of the data that should be recognized at this point is that wide-angle collection optics are imperative for valid experiments on the optical properties of insulations. All of the principal measurements in this program were made on equipment designed to collect all the radiation transmitted by the samples, i.e., over 2 π steradians.

The transmittance measuring equipment is shown in Figure 115. Black body radiation was generated by a cylindrical slug of oxidized Inconel which was inductively heated by a 450 kHz RF generator. The emittance of oxidized Inconel is about 0.9 and is relatively independent of wavelength; the slug was, therefore, a good gray body and the spectral distribution of the emitted radiation was essentially identical to that of a black body at the same temperature. A chromel-alumel thermocouple was spot welded to the slug for accurate temperature measurement. The radiation from the Inconel slug was chopped at 13 Hz and focused on the

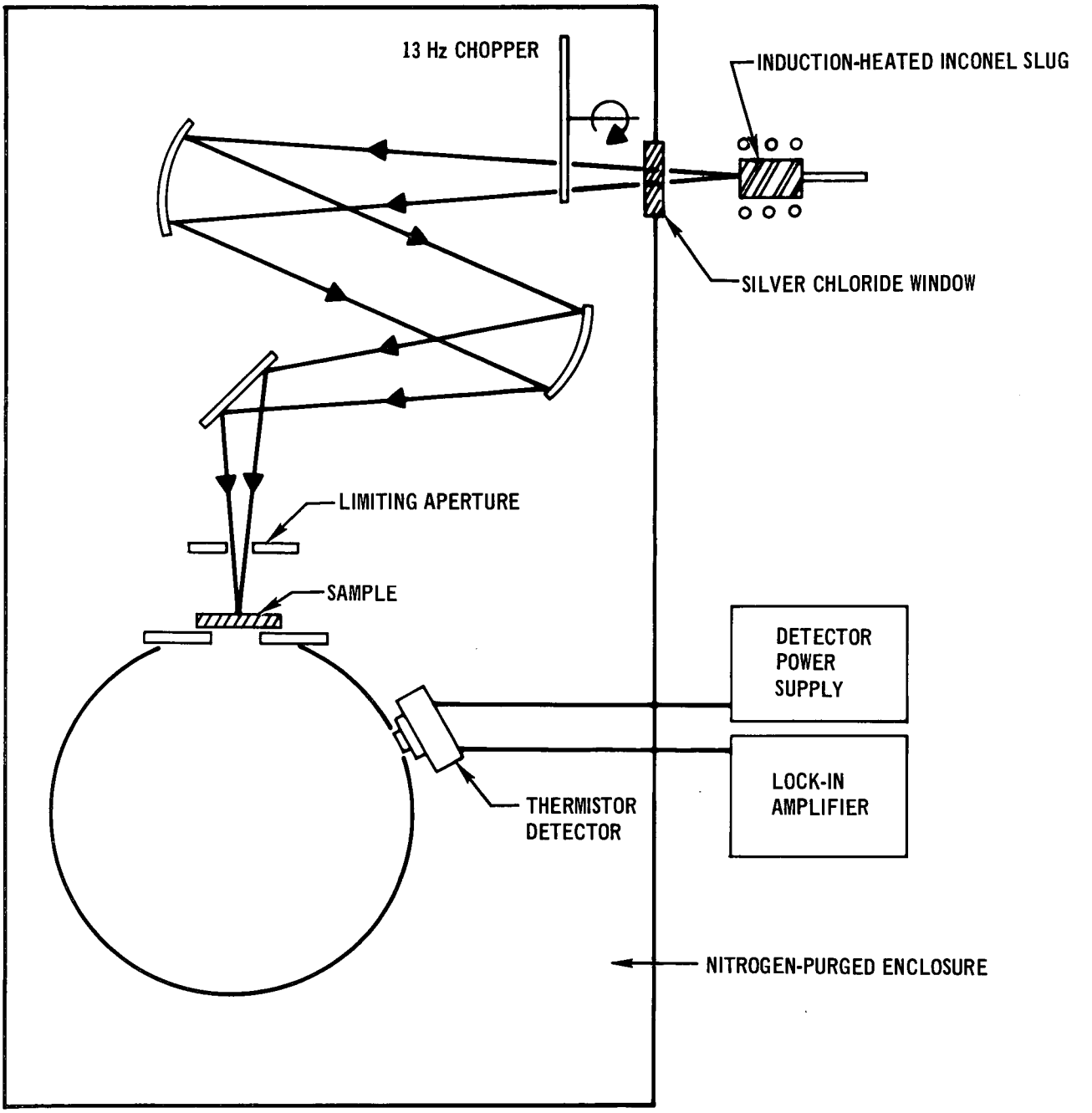

INFRA-RED TRANSMISSION MEASUREMENT

Figure 115

entrance aperture of the integrating sphere. To provide a highly reflective, diffuse surface on the interior of the sphere, the inner wall was sprayed with a suspension of 180-grit silicon carbide powder in epoxy resin, followed by a vacuum deposition of gold. The radiation entering the sphere was measured by a thermistor detector connected to a lock-in amplifier tuned to the 13 Hz modulation frequency.

With the exception of the heated Inconel slug, all of the optical equipment was enclosed in a nitrogen-filled plastic tent to reduce absorption of the radiation at selected wavelengths by atmospheric moisture and carbon dioxide. To preserve the integrity of the purge during frequent sample changes, plastic gloves were installed in the wall of the enclosure for sample handling. All optical components in the system, including the silver chloride window, the mirrors and the thermistor detector, were chosen for their uniform properties over the wavelength range of the experiment.

Transmittance was measured by the substitution method which involved three measurements, and was calculated from:

$$T = \frac{V_S - V_{BG}}{V_{100} - V_{BG}} \eta$$

where T = fraction transmitted

V_S = signal voltage with the specimen covering the aperture

V_{100} = signal voltage with the sphere entrance aperture uncovered

V_{BG} = signal voltage from background noise, obtained by blocking the source input to the optical transfer system.

η = sphere efficiency factor

If the detector in the sphere is not shielded from the aperture, a correction factor (η) is necessary to account for the change in reflective area of the integrating sphere when the specimen covers the aperture, and the reflectance of the surface of the sample facing the interior of the sphere. This was not recognized until late in this program, after most of the data had been accumulated, and the data has not been corrected for it. The transmission correction factor for our test equipment was found to be 0.88, which means that the reported interception (M) and backscattering (N) cross sections are slightly low, and the absorption cross section (P) slightly high.

To characterize the transmission properties of insulations, it is necessary to measure the percentage transmission for a series of specimens of varying thickness. The resultant data is analyzed by computer iteration to determine the constants M, N, and P which provide the best fit to the Larkin and Churchill equation (Ref 8):

$$I_{1(L)} = \frac{2\sqrt{M^2 - N^2}}{M + \sqrt{M^2 - N^2}} \; e^{-L\sqrt{M^2 - N^2}} \left[\sum_{n=0}^{n=\infty} (-1)^n \left(\frac{M - \sqrt{M^2 - N^2}}{M + \sqrt{M^2 - N^2}} \right)^n \; e^{-2nL\sqrt{M^2 - N^2}} \right] \qquad (1)$$

where $I_{1(L)}$ = intensity of forward scattered radiation at thickness (L) when source intensity $I_{1(0)} = 1$.

M = interception cross-section per unit volume $(\text{in.})^{-1}$

N = backscattering cross-section per unit volume $(\text{in.})^{-1}$

P = M - N = absorption cross-section per unit volume $(\text{in.})^{-1}$

NOTE: (In the reference cited, there are two typographical errors in the above equation. The form shown here is correct. The correctness was determined by independent derivation, and also by reviewing Larkin's original Ph.D. thesis which contains the correct version.)

According to Larkin and Churchill, when $L\,(M^2 - N^2)^{0.5} > 5$, the series within the bracket approaches unity. For the materials and temperature we are concerned with, this is generally true for sample thicknesses greater than 0.5 in. It is noteworthy that for those cases (thickness greater than 0.5 in.) the Larkin and Churchill equation takes the form of Lambert's Law:

$$I_{1(L)} = \frac{2\sqrt{M^2 - N^2}}{M + \sqrt{M^2 - N^2}} \; e^{-L\sqrt{M^2 - N^2}} \qquad \text{Larkin and Churchill} \qquad (2)$$

$$I_{1(L)} = A e^{-kL} \qquad \text{Lambert's Law} \qquad (3)$$

The Lambert absorption coefficient in terms of Larkin and Churchill constants is $k = \sqrt{M^2 - N^2}$, and:

$$A = \frac{2\sqrt{M^2 - N^2}}{M + \sqrt{M^2 - N^2}}$$

A plot of the Larkin and Churchill equation should, therefore, be asymptotic to Lambert's Law of thickness beyond about 0.5 in.

The units for M, N, and P are shown above as reciprocal length (in.^{-1}). For most of the experimental work, we have used an equivalent term -- the reciprocal of surface density $(\text{lb/ft}^2)^{-1}$. Measurements were made and are reported on the basis

of mass per unit area as that provided automatic compensation for variations in density of individual specimens of the same composition, and eliminated the problem of measuring the thickness of soft, low density felted products. For many applications, where it is desired to compare materials on a thickness basis, or for use in the equations presented here, the preferred unit is reciprocal length. The data can be readily converted by multiplying $(lb/ft^2)^{-1}$ by the density of the insulation to obtain reciprocal length.

The variation of transmittance by various thicknesses of HCF Mod III of an IR source at 3140°F is shown in Figure 116. This illustrates the comparison of experimental data with the Larkin and Churchill equation (Eq. 1) and with Lambert's Law.

5.2 IR Transmission Characteristics of Insulations - The backscattering coefficients for a number of insulations were measured as a function of source temperature and are shown in Figure 117, and tabulated in Table IX.

It will be seen from Figure 117 that the backscattering of fibers (mullite, Microquartz, Refrasil A-100, and Astroquartz) is influenced by both fiber diameter and composition, and also by the spectral distribution (temperature). As expected, the backscattering coefficient increased as the fiber diameter decreased within the range of diameters tested. The nominal diameters of these fibers were:

FIBER	COMPOSITION	NOMINAL AVERAGE DIAMETER (MICRONS)
Microquartz	Silica	1.3
Refrasil A-100	Silica	1.3
Astroquartz	Silica	7
Mullite, Coarse	Mullite	6
Mullite, Fine	Mullite	4

The reason for the disparity in backscattering results between Microquartz and Refrasil A-100 is unknown. Both are silica fibers of the same average diameter and about the same purity, though their manufacturing techniques are radically different. Scanning electron micrographs of these two fibers at 3000X and 10,000X do not reveal any visually apparent differences in surface texture or flaws. Two factors which might account for the difference, but which have not been measured, are the distribution of the fiber diameters, which make up the average diameter, and the average diameter of the specific materials tested.

Larkin and Churchill (Ref 8) demonstrated that for transmission by glass fibers at lower source temperatures (200°-800°F) there is an optimum fiber diameter for maximum backscattering for each source temperature. Glass fibers, smaller or larger than the optimum, resulted in greater IR transmission (lower backscattering).

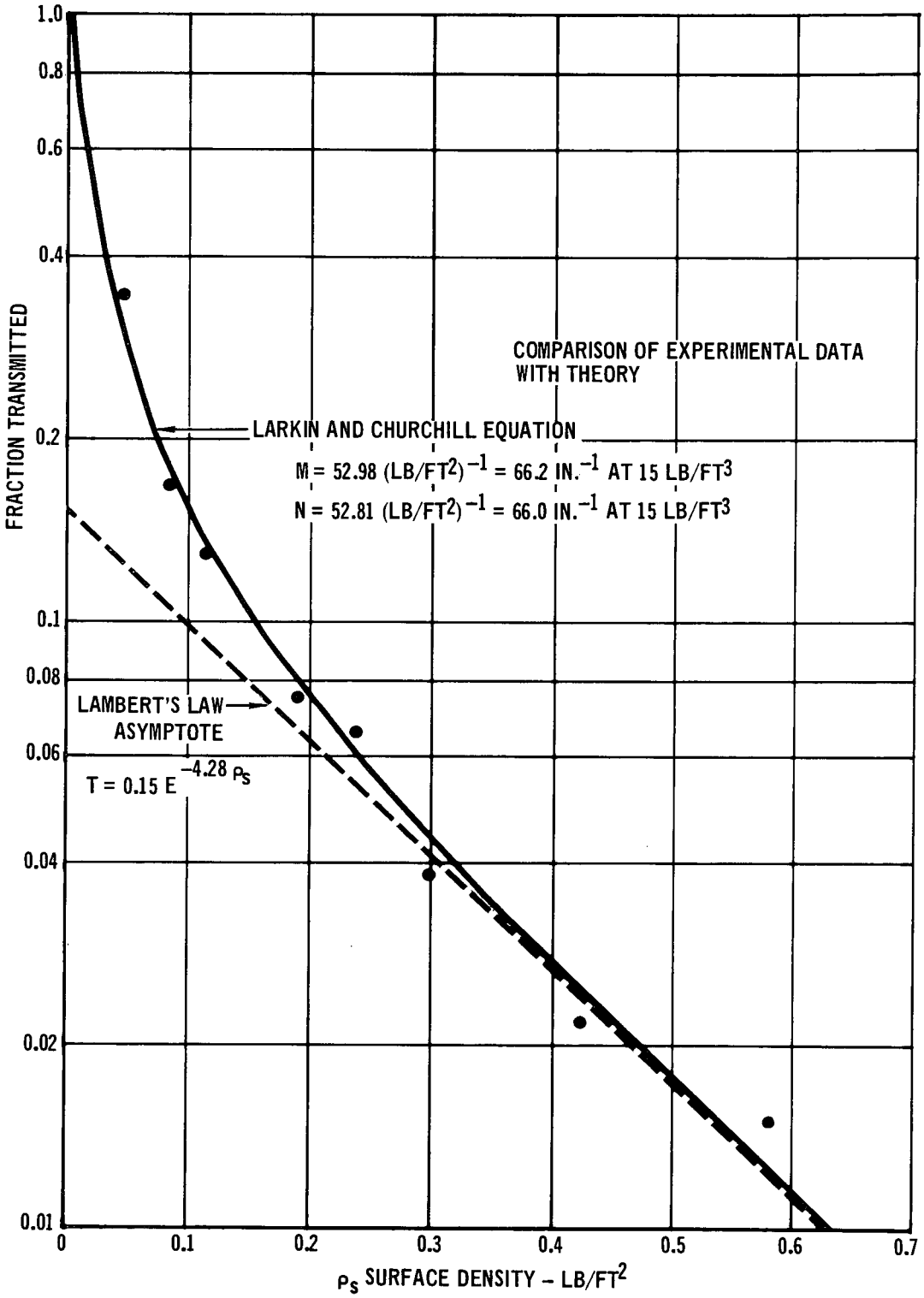

TRANSMITTANCE BY A 3140°F SOURCE OF HCF MOD III
Comparison of Experimental Data with Theory

457-2407

Figure 116

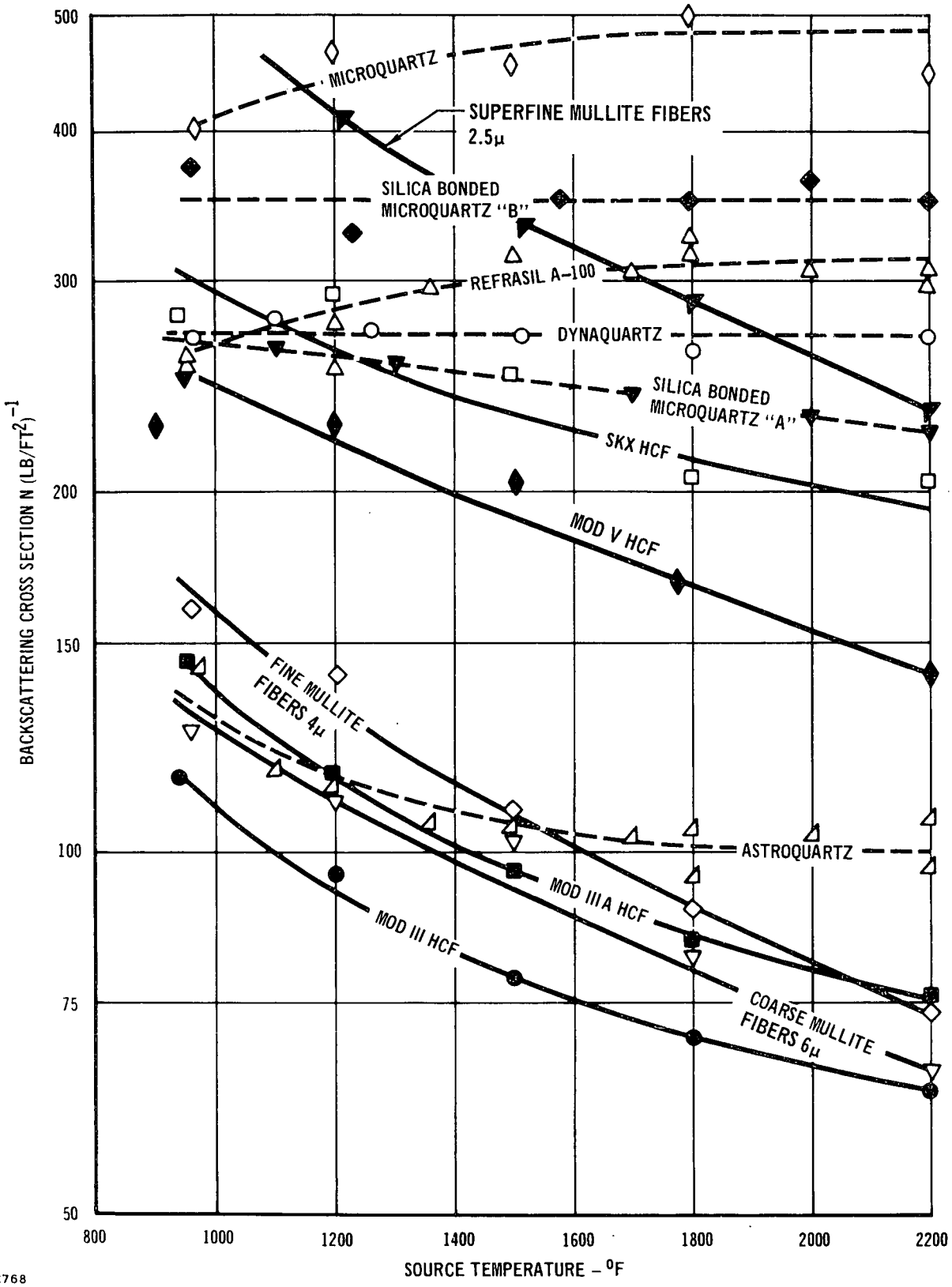

457-2768

BACKSCATTERING CROSS SECTIONS OF SEVERAL CERAMIC FIBROUS INSULATIONS

Figure 117

Table IX

INFRA-RED SCATTERING CHARACTERISTICS OF VARIOUS INSULATIONS

MATERIAL		CROSS SECTIONS – $(LB/FT^2)^{-1}$ SOURCE TEMPERATURE ^oF				
		950	1200	1500	1800	2200
HCF MOD III	M	114.4	96.4	80.1	68.2	62.0
	N	114.0	96.0	79.7	67.9	61.7
	P	0.4	0.4 (1300^o)	0.4	0.3	0.3
HCF MOD III A	M	145.1	126.0	104.5	88.3	76.6
	N	144.7	125.9	104.4	88.1	76.5
	P	0.4	0.1	0.1	0.1	0.1
HCF MOD V EXPERIMENTAL – BLEND OF 4.7 μ MULLITE FIBERS AND MICROQUARTZ – NO FILLER	M	228.5	228.4	204.6	167.5	141.3
	N	228.2	228.3	204.5	167.4	141.2
	P	0.3	0.1	0.1	0.1	0.1
SKX–HCF EXPERIMENTAL – SKX FIBERS 20% PKT	M	280.1	289.7	248.7	204.2	203.2
	N	279.6	289.4	248.5	204.0	203.0
	P	0.5	0.3 (1100^o)	0.2 (1300^o)	0.2 (1700^o)	0.2
SILICA BONDED MICROQUARTZ "A" 16.3 LB/FT^3	M	250.3	265.8	257.1	241.5	223.3
	N	249.5	265.3	256.6	241.2	223.0
	P	0.8	0.5	0.5	0.3	0.3
SILICA BONDED MICROQUARTZ "B" 8.8 LB/FT^3	M	371.9	330.7	350.0	349.4	346.7
	N	371.2	330.0	349.5	349.0	346.4
	P	0.7	0.7	0.5	0.4	0.3
MICROQUARTZ FELT	M	411.7	472.4	459.8	505.8	449.8
	N	397.4	463.2	451.8	500.6	444.2
	P	14.3	9.2	8.0	5.2	5.6
DYNAQUARTZ	M	269.4	272.5	269.4	259.0	267.5
	N	267.4	271.1	268.2	257.9	266.7
	P	2.0	1.4	1.2	1.1	0.8
REFRASIL A–100	M	261.7	259.0	270.0	315.3	295.3
	N	254.2	252.0	264.7	311.9	292.2
	P	7.5	7.0	5.3	3.4	3.1
ASTROQUARTZ	M	154.0	130.9	121.8	123.7	116.7
	N	142.0	112.4	103.2	105.2	97.2
	P	12.0	18.5	18.6	18.5	19.5
COARSE MULLITE FIBERS 6μ	M	126.5	110.5	101.1	82.1	65.2
	N	126.0	110.1	100.8	81.7	64.8
	P	0.5	0.4	0.3	0.4	0.4
FINE MULLITE FIBERS 4μ	M	160.6	140.3	109.5	89.6	73.1
	N	160.4	140.1	109.3	89.4	72.9
	P	0.2	0.2	0.2	0.2	0.2
SUPERFINE MULLITE FIBERS 2.5 μ	M		408.3	337.5	288.4	238.5
	N		408.2	337.4	288.8	238.4
	P		0.1	0.1	0.1	0.1

M = INTERCEPTION CROSS SECTION
N = BACKSCATTERING CROSS SECTION
P = ABSORPTION CROSS SECTION

457–3173

For the temperatures and materials of concern here, we are not certain where that optimum lies, but we believe it to be somewhere in the range of 1.0 to 1.5μ diameter.

HCF blocks made with mullite fiber show generally lower backscattering coefficients than the pure fibers. This would be expected as much of the weight of the blocks is made up of binder and low density coarse filler which are believed to be relatively inefficient scatterers. The substitution of SKX fiber (1.6μ $Al_2O_3 \cdot SiO_2$) for 4-6μ mullite fibers in HCF made a significant improvement in backscattering as shown in Figure 117.

The bonded Microquartz blocks also showed less backscattering than pure Microquartz, presumably due to binder content. The amount of binder in the bonded Microquartz is unknown, and though the binders are silica, their form is believed to be considerably different in the two products.

The possibility that the backscattering characteristics of an insulation might change with a change in specimen temperature was also considered. In tests with two materials (HCF and silica bonded Microquartz "A"), no change in transmission was noted as the specimen temperature was raised from room temperature to 1800°F. This test was performed with a modification to the transmission equipment described previously. The specimen was enclosed in a small furnace and in which the specimen was slowly rotated in and out of the beam. The detector output was fed through a lock-in amplifier tuned to the same frequency as the beam chopper. This was necessary to separate the transmission signal from the radiation of the heated specimen itself.

5.3 Correlation of IR Transmission with Radiation Contributions to Thermal Conductivity - Larkin and Churchill, in their derivation of the two flux model, assumed that the interception and backscattering coefficients were independent of radiant energy spectral distribution (i.e., source temperature) and wrote two differential equations:

$$\frac{dI_1(x)}{dx} = -MI_1(x) + NI_2(x) + P\sigma T_x^4 \qquad (1)$$

$$-\frac{dI_2(x)}{dx} = -MI_2(x) + NI_1(x) + P\sigma T_x^4 \qquad (2)$$

where I_1 = flux in the direction of increasing distance (x), hot to cold surface
I_2 = Flux in the opposite direction

M = Interception cross-section, unit area/unit volume

N = backscattering cross-section, unit area/unit volume

P = Absorption cross-section, unit area/unit volume

The first equation states that in traversing a slice of material (dx), the intensity of the radiant flux in the forward direction (I_1) is decreased by the amount of forward flux intercepted and increased both by the amount of backscattering of the flux from the reverse direction (I_2) and by reradiation of the flux absorbed. The second equation is the analogous balance for the flux in the reverse direction. They solved these equations for the case where absorption is negligible

$$P = M - N = 0$$

$$M = N$$

with appropriate boundary conditions, and derived an expression for the energy transmitted through the slab by radiation under a uniform temperature gradient:

$$q_r = \frac{\sigma\left[T_o^{\,4} - T_L^{\,4}\right]}{\frac{1}{\varepsilon_o} + \frac{1}{\varepsilon_L} - 1 + NL} \qquad (3)$$

where ε_o and ε_L are the emittances of the hot and cold faces of the slab and L the thickness.

The assumption that M and N are independent of temperature of the source (there are two sources: the hot boundary and the cold boundary) has been shown to be incorrect by our recent measurements. Indeed, Larkin and Churchill's results also showed a wide variation for glass fibers. Therefore, the last equation cannot be used with confidence. In order to generate a more accurate expression for q_r, a fresh approach to the model was formulated.

The new approach might aptly be called the "four-flux model." With materials for which $P \cong 0$, the radiation within the slab must have originated from either the opaque hot or cold surface of the slab as internal radiation from individual fibers must also be negligible if their absorption is negligible. Radiation from each of these two sources is characterized by the temperature of the appropriate surface and will be attenuated by the scattering cross-section corresponding to that surface temperature. The net radiant heat flow through the slab is the balance between the radiation originating at the hot surface, x = 0, which penetrates the slab to the cold surface, less the radiation emitted by the cold surface, x = L, which reaches the hot face. As each of these components is scattered in accordance with the cross-sections associated with its source temperature, which we identify as N_o

and N_L, we have considered each source separately and have written four equations for the hot face radiation, I, and the cold face radiation, J:

$$\frac{dI_1(x)}{dx} = -M_o I_1(x) + N_o I_2(x) + P_o \sigma T_x^4 \tag{4}$$

$$-\frac{dI_2(x)}{dx} = -M_o I_2(x) + N_o I_1(x) + P_o \sigma T_x^4 \tag{5}$$

$$\frac{dJ_1(x)}{dx} = -M_L J_1(x) + N_L J_2(x) + P_L \sigma T_x^4 \tag{6}$$

$$-\frac{dJ_2(x)}{dx} = -M_L J_2(x) + N_L J_1(x) + P_L \sigma T_x^4 \tag{7}$$

These equations can be simplified as when P = 0, M = N. The boundary conditions used in their solution are:

for x = 0

$$I_1(0) = \sigma \varepsilon_o T_o^4 + (1 - \varepsilon_o)\, I_2(0)$$

$$J_1(0) = (1 - \varepsilon_o)\, J_2(0)$$

for x = L

$$I_2(L) = (1 - \varepsilon_L)\, I_1(L)$$

$$J_2(L) = \sigma \varepsilon_L T_L^4 + (1 - \varepsilon_L)\, J_1(L)$$

These boundary conditions are illustrated in Figure 118.

The solution of these sets of equations for a uniform temperature gradient yields:

$$q_r = \frac{\sigma T_o^4}{\frac{1}{\varepsilon_o} + \frac{1}{\varepsilon_L} - 1 + N_o L} - \frac{\sigma T_L^4}{\frac{1}{\varepsilon_o} + \frac{1}{\varepsilon_L} - 1 + N_L L} \tag{8}$$

For the case where $NL >> \frac{1}{\varepsilon_o} + \frac{1}{\varepsilon_L} - 1$, Equation (8) reduces to:

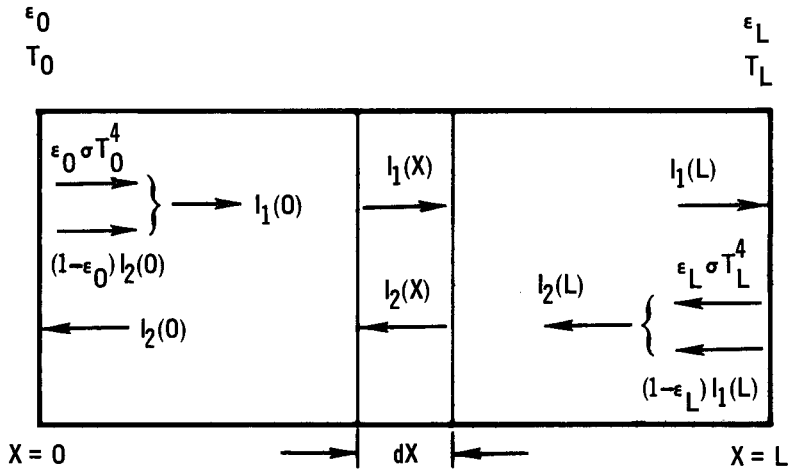

$q_r = I_1(X) - I_2(X)$

Two Flux Model

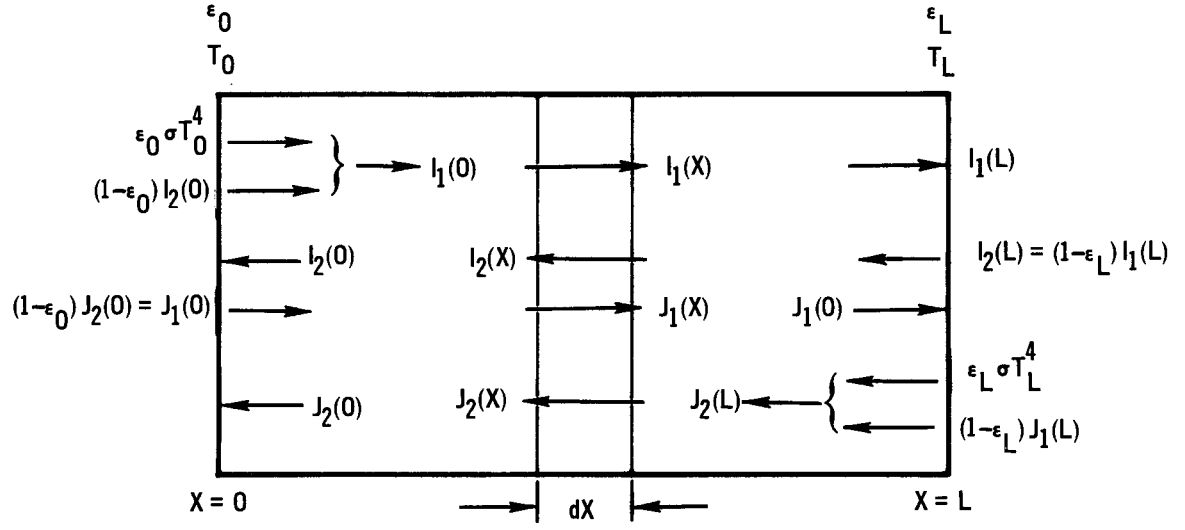

$q_r = I_1(X) - I_2(X) + J_1(X) - J_2(X)$

Four Flux Model

457-2850

BOUNDARY CONDITIONS

Figure 118

$$q_r = \frac{\sigma}{L}\left[\frac{T_o^4}{N_o} - \frac{T_L^4}{N_L}\right] \tag{9}$$

and the radiation contribution to thermal conductivity is:

$$k_r = \frac{q_r L}{\Delta T} = \frac{\sigma}{T_o - T_L}\left[\frac{T_o^4}{N_o} - \frac{T_L^4}{N_L}\right] \tag{10}$$

When $N_o = N_L$, Equations (8), (9) and (10) reduces to the equivalent expressions in Ref 8.

Equation (10) indicates that the radiative shine-through is a function of the hot and cold boundary temperatures and the backscattering coefficients associated with each of these temperatures. If the backscattering coefficients are essentially unchanged by variations in source temperature ($N_o = N_L$), then the simpler expression:

$$k_r = \frac{4\sigma Tm^3}{N} \tag{11}$$

is a close approximation* of the radiative contribution to total thermal conductivity.

*The exact expression is $k_r = (4 + \alpha^2)\,\sigma\,\frac{Tm^3}{N}$, where $\alpha = \frac{\Delta T}{Tm}$ and Tm = mean temperature.

This last equation is a convenient one for making several generalizations about the radiative component of total thermal conductivity. It indicates that the radiative shine-through is directly proportional to the cube of the mean temperature, and is inversely proportional to the backscattering coefficient. The effect of the source temperature (and its associated backscattering coefficient) on the radiative component of the thermal conductivity of HCF Mod III at various mean temperatures has been estimated using Equation (11) and is shown in Figure 119. The source is assumed to be the high emittance coating applied to the insulation. In an actual situation, the radiation contribution would be slightly higher than shown in Figure 119, due to the fact that the backscattering coefficient for this material (and many others) decreases with increase in source temperature. This has the effect of reducing the internal radiation away from the cool surface, while increasing the radiation from the hot surface to the cool surface. This can be readily seen by comparing Equation (11) with Equation (10).

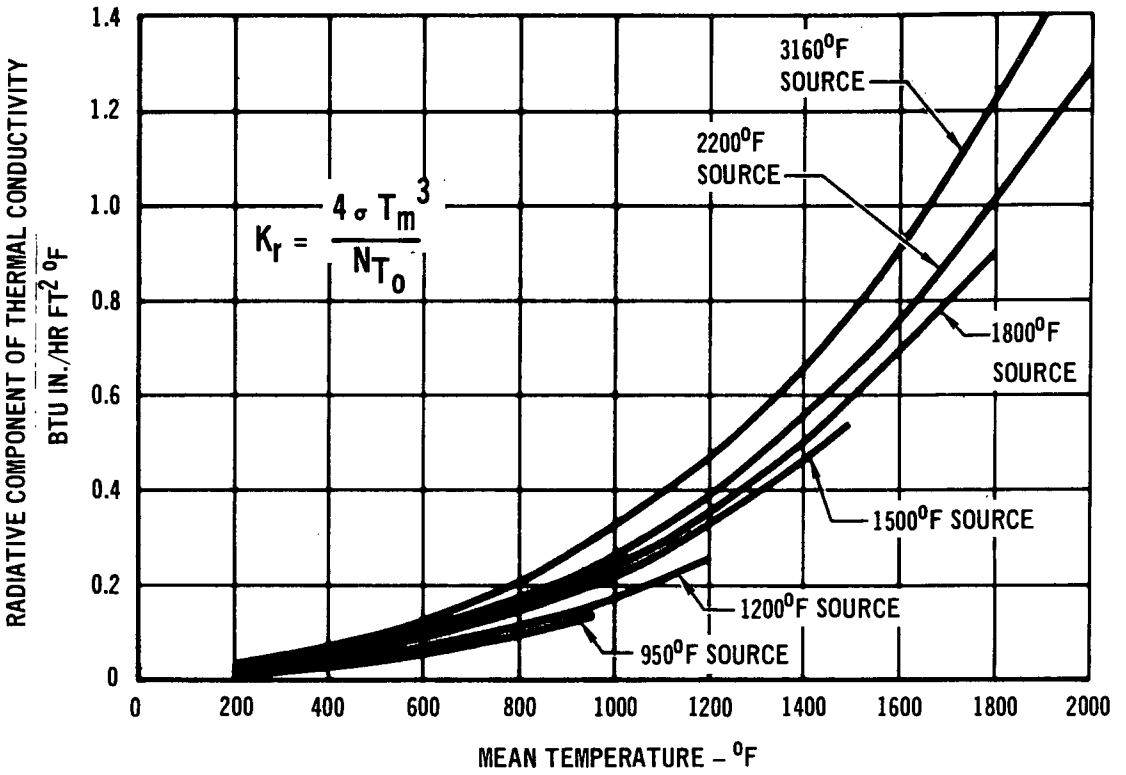

457-2408

HCF MOD 3 RADIATIVE COMPONENT OF THERMAL CONDUCTIVITY Figure 119

The illustration used in Figure 119 is for a material which has a fairly low backscattering coefficient. The radiative contribution to other materials, for which data was available, was illustrated in Section 3.10, in comparison with their measured total conductivity values. In Section 3.10, the radiation contribution was calculated from Equation (10), using the hot and cold plate temperatures.

Examination of Equation (10) indicates that when N is independent of temperature, conductivity measurements should be valid irrespective of the temperature difference across the specimen. However, when N varies with temperature, the apparent conductivity realized in service can be different than that measured in guarded hot plate tests any time the temperature difference across the specimen is different from the test conditions. This will be found to be especially critical in transient heat flow cases.

It is interesting to note from inspection of Equations (3) and (8), that when no insulation is present (NL = 0), the equations are then identical to the usual equation describing radiant interchange between two parallel plates.

6.0 CONCLUSIONS AND RECOMMENDATIONS

The results of this program have provided much needed data on the merits and weaknesses of many of the insulations and packaging materials that could be used behind a metallic radiative TPS. Our suggestions and comments on the most appropriate materials for various temperature regimes are presented below. No "best" material was found for any service; any recommendation or selection must be premised on acceptance of some weaknesses or tradeoffs.

6.1 Package Design - The use of a floating top, or some means of divorcing the hot surface of the package is desirable with many metals, and mandatory with some, particularly at temperatures of 2000°F and higher. Inconel 702 falls in the latter category, and TD-NiCr approaches it.

6.2 Venting - Vent openings totaling about 0.023% of the insulation surface area will be required per inch of thickness of insulation, to reduce package hot surface deflections to about 0.25 inch under ascent pressure changes. This assumes a 20 x 20 inch package with a corrugation stiffened surface. To inhibit entry of liquid moisture, the vent holes should be covered with 400 x 400 mesh wire cloth (0.001 inch wire diameter). The required vent area should then be corrected for the net open area of the wire cloth. Excessive moisture accumulation was never a problem when vent openings were screened, even under cryopumping conditions.

6.3 2500°F Service

6.3.1 Packaging - Coated columbium was the only material evaluated, and at the thickness used (5 mil Cb, prior to coating) provided about 50 cycles of simulated service. It is believed that 100 cycles would have been possible had heavier metal foil (7-8 mil) been used, along with a heavier coating. An alternate approach, which has not been tested, would be to use the metallic heat shield as the package hot face.

6.3.2 Insulations - Many of the insulations appeared to fare better in 2500°F exposure than in 2200°F service, possibly as a result of greater hardening in service. Normally such hardening is accompanied by excessive shrinkage, but such was not the case in this environment. SKX-Fiberfrax provided excellent performance; Dynaflex gave good performance also, at a 9 lb/ft^3 density. Astroquartz had excellent dimensional stability. Irish Refrasil also had good dimensional stability, but its performance must be tempered by the fact that it lacked dimensional stability in the 2200°F tests.

6.4 2200°F Service

6.4.1 Packaging Materials - TD-NiCr (3 mil) provided good service for 100 cycles and is the preferred material. Inconel 702 might provide service for a

reduced number of cycles, but would require a floating top design. It is expected that coated columbium could also be used in this temperature range, though it was not tested at 2200°F. Use of coated columbium would provide greater insurance against temperature overshoots.

6.4.2 Insulations - The SKX-Fiberfrax, Astroquartz, and higher density Dynaflex (> 9 lb/ft^3) all had good dimensional stability over 100 cycles. Irish Refrasil displayed excessive settling, and Refrasil A-100 some shrinkage over the 100 cycles. In the previous year's work (Reference 1) Flexible Min-K exhibited good mechanical stability, and would be a preferred material for volume limited areas. Microquartz at 6 lb/ft^3, which was also evaluated in the earlier work, showed a slight amount of shrinkage over 40 cycles. The amount of heat leak caused by small amounts of shrinkage would not be expected to be serious. The use of densified Microquartz (8-10 lb/ft^3), while not specifically evaluated at 2200°F (but was tested at 2000°F), could offer some advantages in volume limited areas.

6.5 2000°F Service

6.5.1 Packaging Materials - Either Inconel 702 or TD-NiCr may be used for 2000°F service, and a floating top design is suggested, especially for the Inconel 702. While thicknesses of Inconel as low as 1.5 mils were used successfully in our 2000° tests, (40 cycles), this results in a rather flimsy package in the larger size packages. It is recommended that 2-3 mil minimum thickness be employed. In any application of Inconel 702, its sensitivity to attack by heavy salt concentrations must be borne in mind. It would be appropriate to further study this effect with decreased amounts of salt, representing fewer years of exposure.

6.5.2 Insulations - Comments made for 2200°F insulations are applicable.

6.6 1800°F Service

6.6.1 Packaging Materials - A wider variety of metals was found satisfactory for use at 1800°F. These included Hastelloy X (2 and 5 mils thick), Inconel 702 (2 and 5 mils thick), and Inconel 601. Simple box designs were adequate at this temperature level.

6.6.2 Insulations - Flexible Min-K, Refrasil A-100, and Astroquartz were dimensionally stable at this temperature. While Microquartz at 3.5 lb/ft^3 density displayed a slight amount of shrinkage at this temperature, it was not considered sufficient to make it unacceptable for this temperature range. Dynaflex at 3 lb/ft^3 density was unacceptable due to excessive settling in the package.

6.7 1000°F Service

6.7.1 Packaging Material - Only titanium was evaluated for this service and was found acceptable.

6.7.2 Insulations - Felts of either AA glass fibers of 1.0 lb/ft^3 or greater density, or B glass fibers of 2.0 lb/ft^3 or greater density, provided good dimensional stability and thermal resistance.

6.8 Conductivity Reduction in Reusable Surface Insulations - The best approach to improvement of the thermal conductivity of mullite fiber block insulations is through the use of the small diameter fibers, preferably in the range of 1-2.5 micron diameter.

6.9 Heat Transfer Calculations - For those insulations in which radiation shine-through has prevented accurate estimations of heat transfer, use of radiation transport equations described in this report is suggested. Analytical techniques for using this approach in transient heat flow cases are required and are being investigated.

7.0 REFERENCES

1. High Temperature Insulation Materials for a Reradiative Thermal Protection System, Year End Summary Report, MDAC-E Report MDC E0449, 10 August 1971, Contract NAS8-26115 (NASA CR-119950).

2. ASSET, Aeroelastic and Dynamic Experiments, Flight Results and Correlation (U), McDonnell Aircraft Company, AFFDL TR-65-31, Vol. 13, Contract AF 33(616)8106, (Confidential)

3. Coe, Charles F., Buffet and Aerodynamic Noise, NASA-Ames, Presented at the Space Transportation System Technology Symposium, NASA-Lewis Research Center, 15-17 July 1970, NASA TM-X-52876, Vol. 2.

4. Cox, B. G., Thermal Testing Techniques for Space Shuttle Thermal Protection System Panels, Presented at IES/AIAA/ASTM Sixth Space Simulation Conference, New York, N.Y., 1-3 May 1972.

5. Hansen, Constitution of Binary Alloys, Second Edition, Page 256, McGraw-Hill, New York, 1958

6. Levin, E. M., Robbins, C. R., McMurdie, H. F., Phase Diagrams for Ceramists, Page 125, American Ceramic Society, Columbus, Ohio, 1964.

7. Hughes, T. A., A Technique for Estimating Thermal Conductivity of Insulations at Low Pressures, MDAC-E Report E0285, 8 January 1971.

8. Larkin, B. K., and Churchill, S. W., Heat Transfer By Radiation Through Porous Insulations, AIChE Journal, 5 (4), 467, (1959).

APPENDIX

Reference is made in this report to certain products using registered trade marks. The owners of these trade marks are noted below.

DYNAFLEX
DYNAQUARTZ
MIN-K
Johns-Manville Corp.
Denver, Colorado

ASTROQUARTZ
J. P. Stevens and Co.
New York, New York

REFRASIL
IRISH REFRASIL
HITCO
Gardena, California

FIBERFRAX
Carborundum Co.
Niagra Falls, New York

INCONEL
Huntington Alloy Products Div. of
International Nickel Co.
New York, New York

HASTELLOY
Union Carbide
New York, New York